

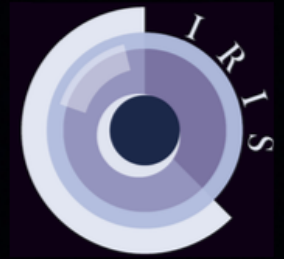
# Project IRIS

Information Relay InfraStructure for translunar communication

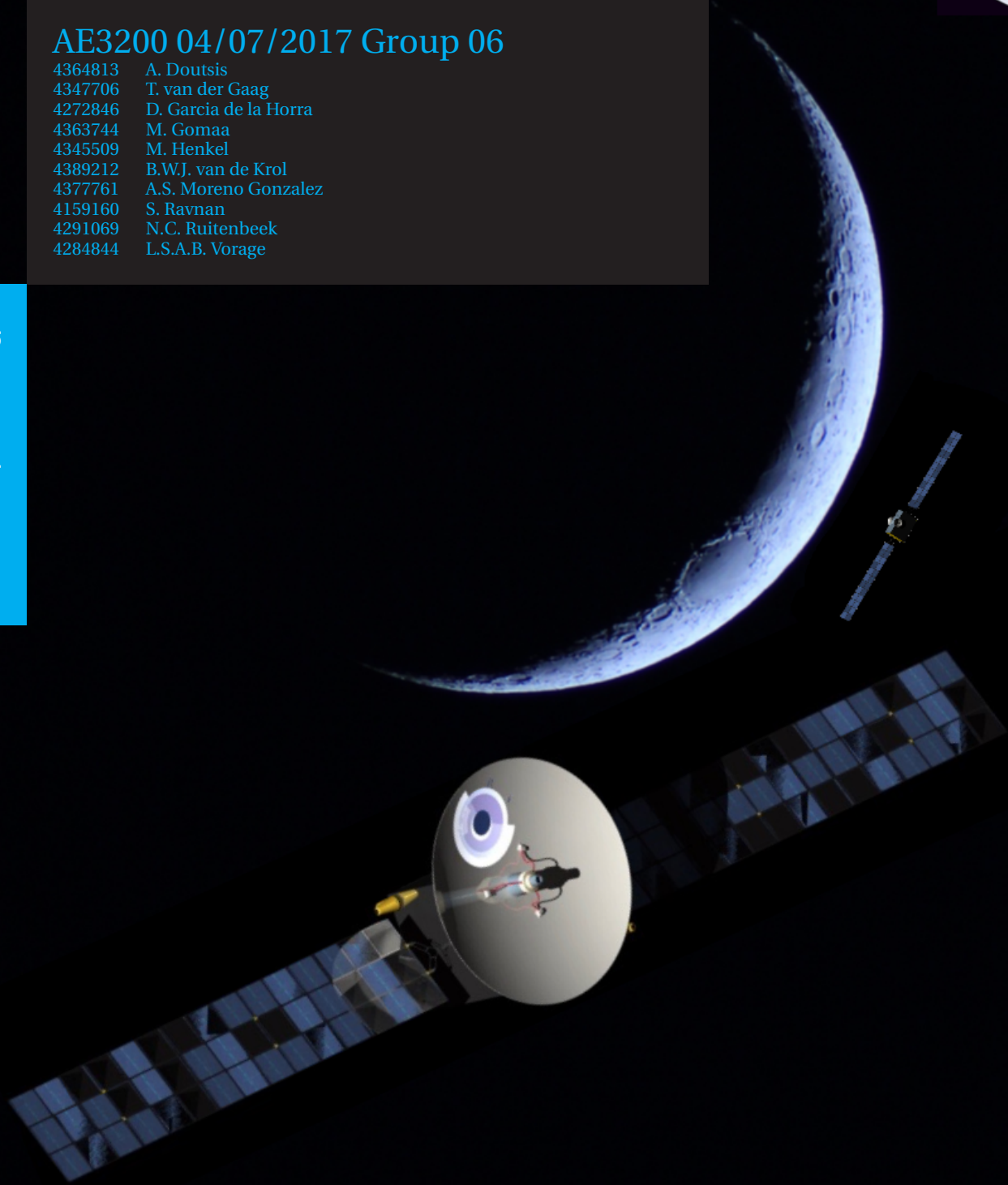
## DSE Final Report

AE3200 04/07/2017 Group 06

4364813	A. Doutsis
4347706	T. van der Gaag
4272846	D. Garcia de la Horra
4363744	M. Goma
4345509	M. Henkel
4389212	B.W.J. van de Krol
4377761	A.S. Moreno Gonzalez
4159160	S. Ravnan
4291069	N.C. Ruitenbeek
4284844	L.S.A.B. Vorage



Delft University of Technology





## PREFACE

Project IRIS is the product of a team of 10 students working in the context of the DSE (Design Synthesis Exercise), as part of their Bachelor of Aerospace Engineering at the Technical University of Delft. The mission objective is to produce a preliminary design for a constellation of communication satellites around the Moon. So far, the technical management plan, requirement analysis and trade-off on concepts have been presented. At this point in the project, a final conceptual design has been made. This fourth and final report provides a briefing on the results of the design process of the chosen concept, while underlining recommendations to improve it in the future.

We would like to personally thank our tutor ir. B.C. Root for his assistance, counsel and support as well as the time he made available to us. We would also like to thank our coaches J. Maas and S.S. Mestry whose perspectives proved invaluable to the progress of Project IRIS.

We would like to express our gratitude to Jeroen Rotteveel, CEO of ISISpace, for taking the time to review our concepts and answering our many questions. Furthermore we want to thank from TU Delft aerospace engineering research staff J. Bouwmeester, F.Topputo, D. Dirks, E.J.O Schrama and B. Zandbergen for their input and advice. Lastly we would like to thank Abhinaya Gnana for assisting us greatly with designing the IRIS logo and the IRIS project poster.



## EXECUTIVE SUMMARY

Lunar exploration initially started as a race between two superpowers to see who had the highest technical capabilities to send a human onto the Moon's surface. Until recently, the frequency of Moon missions has been in decline, but in the last couple years there has been an increasing interest in returning. Scientific studies and observations will be performed and will give humanity a better understanding of the solar system and our place in it. As a result there will be a need for a direct communication line between the lunar surface and Earth, such that rovers can be controlled in real-time and immediately relay their data back, independent of their location on the Moon.

The goal of this final report is to develop the concept chosen in the Midterm report into a comprehensive conceptual design. This concept was chosen from three possible options of which the trade-off table can be seen in [Table 1](#). Concept one used a direct transfer to establish a satellite network in a Walker delta formation around the Moon. Concept two used a low-thrust transfer to establish a Walker delta constellation and in addition to the first concept, a High Moon Orbit relay around the Moon. Concept three used a low-energy transfer to establish a relay network in a halo orbit around the first Earth-Moon Lagrangian point and a direct transfer to establish a frozen-orbit around the Moon. The third concept - involving a halo orbit - was further developed in this final report as it outperformed the other two concepts in terms of overall performance and cost.

Table 1: Final trade-off of the three concepts in the midterm report.

	Performance				Risk level	Cost	Time
	Satellite mass	Trans. eff.	$\Delta V$ Orb. maint.	Ecl.			
<b>C1</b>	1217.4 kg <i>yellow</i>	17.3 <i>yellow</i>	300 m/s <i>blue</i>	.253 <i>blue</i>	42.9% <i>green</i>	€893 million <i>yellow</i>	11.7 day <i>green</i>
<b>C2</b>	830.4 kg <i>blue</i>	1.3 <i>green</i>	300 m/s <i>blue</i>	.238 <i>blue</i>	50.0% <i>blue</i>	€898 million <i>yellow</i>	4.06 years <i>red</i>
<b>C3</b>	437.8 kg <i>green</i>	11.2 <i>blue</i>	150 m/s <i>green</i>	.159 <i>green</i>	71.5% <i>yellow</i>	€552 million <i>green</i>	205 days <i>blue</i>

The final concept consists of two different launches. One launch consists of the relay deployment vehicle with six relay satellites, which will head to the Earth-Moon first Lagrange point through a low-energy transfer. This will take about 347 days and after successful insertion into a halo orbit around the Earth-Moon first Lagrangian point, the second launch is initiated. This launch contains two network deployment vehicles in one launcher with 24 network satellites each. Through a direct transfer these deployment vehicles will arrive on the Moon after which they will both conduct three different right ascension of ascending node changes and deploy eight satellites for each orbital plane, totalling 48 satellites in the constellation distributed over six orbital planes. This constellation has a Walker delta configuration consisting of a family of frozen, circular orbits at an orbital altitude of 1,629 km. From launch to deployment this process will take 10 days.

During operations, signals from vehicles on the lunar surface will be picked up by the Walker delta network, which will send it to the relay satellites which send and receive signals from Earth.

This executive summary of the IRIS system presents the results of each part of the mission.

### TRAJECTORY DESIGN

Firstly, The relay satellites are brought to the Earth-Moon first Lagrange point using a low-energy trajectory, which is split up in three parts that were simulated separately to break down the complexity of the problem. The three parts are chosen such that they can be matched relatively easily to come up with the complete trajectory. The different parts of the trajectory are visualised in [Figure 3.1](#), including the different burns. The first part (point 1 to 3) is defined from Earth LEO (500 km) into a halo orbit around the Sun-Earth L2 point. This manoeuvre would be identical for going towards Sun-Earth's L1 and L2 points. In this case it is chosen to go towards the L2 region. A thermal analysis showed that the temperature ranges between 4 °C to 35 °C in the worst case [1, p. 42]. Furthermore, moving away from the Sun for roughly  $2 \times 10^6$  km decreases the irradiance by only 3 %, which is not a problem since most of the communication subsystem is not operational during the transfer. Therefore a transfer through L2 is chosen over L1 since the radiation received from the Sun is slightly less. Also, the L2 ballistic transfer is used more often than the L1 transfer, so there is more literature on a L2 transfer available. The second part (point 3-4) is defined from the halo orbit around the Sun-Earth L2, where the spacecraft is given a small kick, such that it falls back towards the Earth-Moon system. The second part stops when the satellite crosses the Earth inertial y-axis. The third part (point 4-5) deals from crossing this y-axis until the spacecraft reaches its final destination, a Earth-Moon L1 orbit.

The total required  $\Delta V$  for this low-energy transfer is  $3,376 \text{ m s}^{-1}$ , compared to a  $\Delta V$  of  $3,780 \text{ m s}^{-1}$  of a direct transfer to the Lagrange point.

Not only the reduced amount of  $\Delta V$  is advantageous, especially the fact that after leaving LEO, no large burns (above  $150 \text{ m s}^{-1}$ ) are required. This means that no big propulsion systems are needed on the relay deployment vehicle or the relay satellites, which would only increase the mass and volume of these vehicles.

A downside of the low-energy trajectory is that it takes 347.5 days to complete, while a direct transfer would only take around 5 days. However, this increase is acceptable as time is not of high importance. Of the 347.5 days, 116.2 are spent in part 1, 54.1 days are spent in the Sun-Earth L2 orbit, 122.1 days are spent in part 2 and 55.1 are spent in part 3.

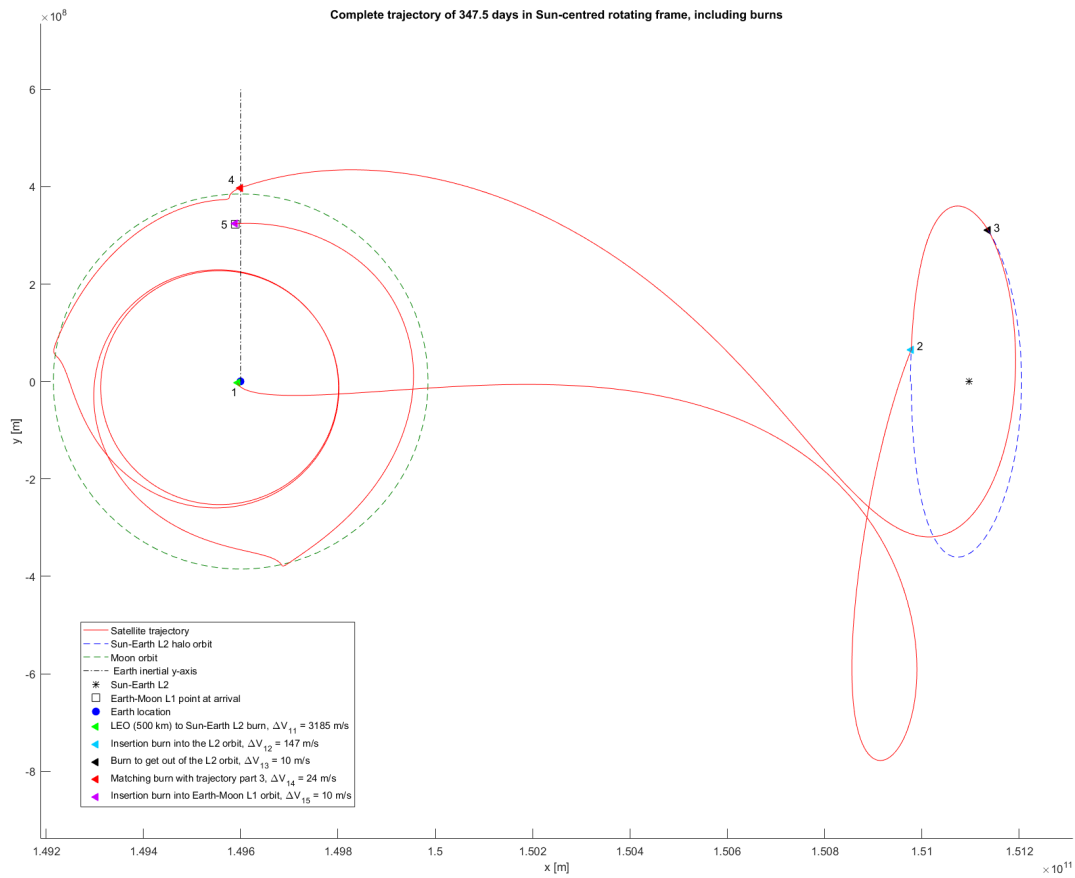


Figure 1: Complete low energy transfer trajectory in Sun-centred rotating frame.

The network satellites are taken to the Moon in two separate deployment vehicles in a single launch using a direct transfer. A Falcon 9 rocket will launch two identical deployment vehicles and insert them in a transfer orbit to the Moon. After the 107.9 hour transfer shown in [Figure 2](#), the deployment vehicles will perform a burn of  $1,360 \text{ m s}^{-1}$ , which injects them into lunar orbit with the desired inclination of  $46^\circ$ . After this, right argument of the ascending node (RAAN) changes are conducted alternating with satellite deployments in different orbits. These manoeuvres together will take about  $2,330 \text{ m s}^{-1}$  for each network deployment vehicle.

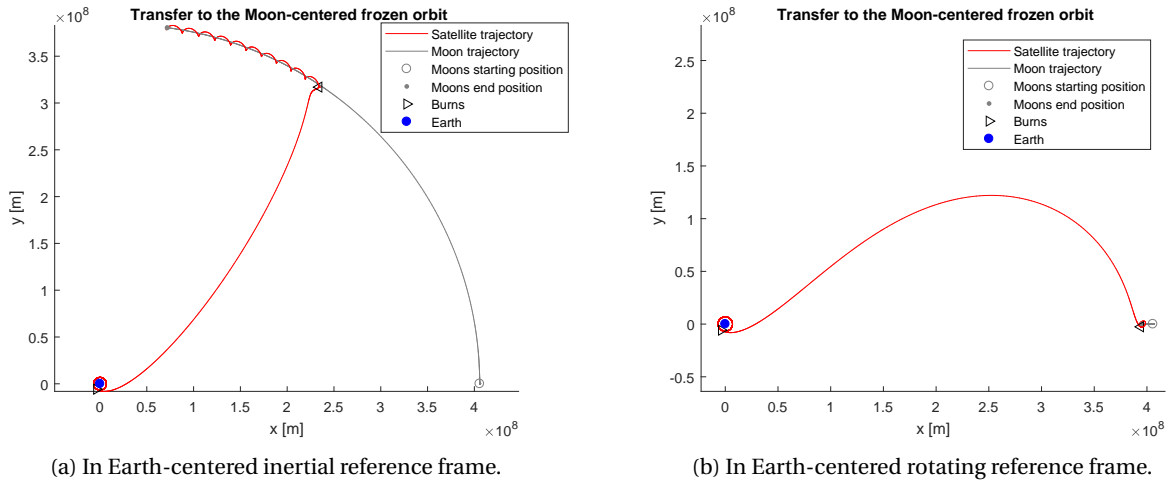


Figure 2: Direct transfer to frozen Moon-centered orbit.

Once the deployment vehicles are in the correct orbits, the deployment sequence begins. The vehicle will be rotating around its longitudinal axis ( $45^\circ \text{s}^{-1}$  rotation rate), aligned normal to the orbital plane. The satellites are then deployed in the orbital plane with a 3 second delay time between successive deployments, using a spring based mechanism. With these parameters, the minimum distance within one orbital period (2.5 hours) between the satellites is 360 m.

### CONSTELLATION DESIGN

As mentioned, the constellation consists of two parts: a network and a relay. Six relay satellites are present in two different halo orbits around the first Earth-Moon Lagrange point. These two near-circular halo orbits, mirrored in the Earth-Moon plane with a semi-major axis of 44,000 km and period of 12.25 days are chosen to guarantee full visibility of the network by the relay satellites. Each halo orbit has 3 relay satellites which are equally phased with a  $120^\circ$  angle and the two planes have a relative phasing of  $60^\circ$ .

For the network, a family of circular, frozen orbits are chosen with an altitude of 1,629 km and an inclination of  $50.2^\circ$ . The network constellation has a Walker delta configuration, which is a constellation type that has an optimised phasing difference between the orbital planes for coverage. The chosen Walker delta constellation consists of six orbital planes with a RAAN difference of  $60^\circ$ . In each constellation eight satellites are present, of which six are active and two act as spares. The six operational satellites have an equally distributed phasing of  $60^\circ$ . The complete constellation can be seen in Figure 3.

This constellation guarantees coverage by at least two satellites everywhere on the Moon at all times. To prove this, a visibility check is conducted of which the results can be seen in Figure 4.

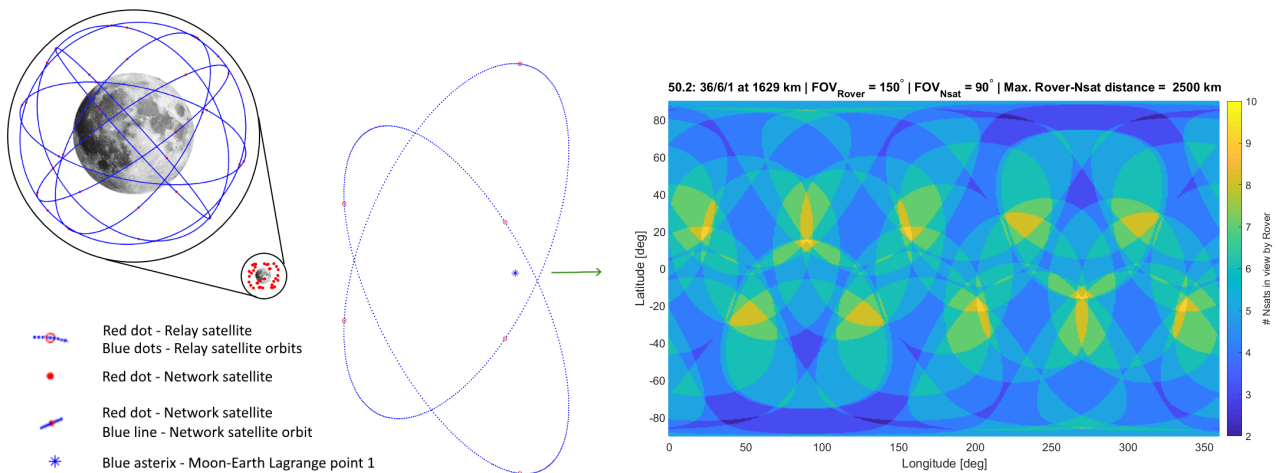


Figure 4: 2D visibility map: The amount of network satellites that are in view by the rovers on the Moon.

Figure 3: Final constellation: 36 network satellites in a Walker Delta constellation and 6 relay satellites in two halo orbits around Earth-Moon L1.

To maintain the constellation, orbit maintenance has to be conducted. For the network satellites this consists of a series of three burns every 27 days, which requires a  $\Delta V$  of  $15 \text{ ms}^{-1} \text{year}^{-1}$ . For the relay satellites, a value of  $50 \text{ ms}^{-1} \text{year}^{-1}$  is found.

When a satellite reaches its end of life stage, it will conduct an end of life manoeuvre. The network satellites will arrive in a circular orbit with a 1,200 km radius with an inclination of  $52.2^\circ$  after a  $105 \text{ m s}^{-1}$  burn. This orbit will decay until the satellite collides with the lunar surface within 14 years. The relay satellites will be disposed at their end of life by inserting them in a heliocentric orbit, which requires a  $\Delta V$  of  $100 \text{ m s}^{-1}$ .

### SPACECRAFT DESIGN

Two different designs were made for the relay and network satellites.

#### NETWORK SATELLITE DESIGN

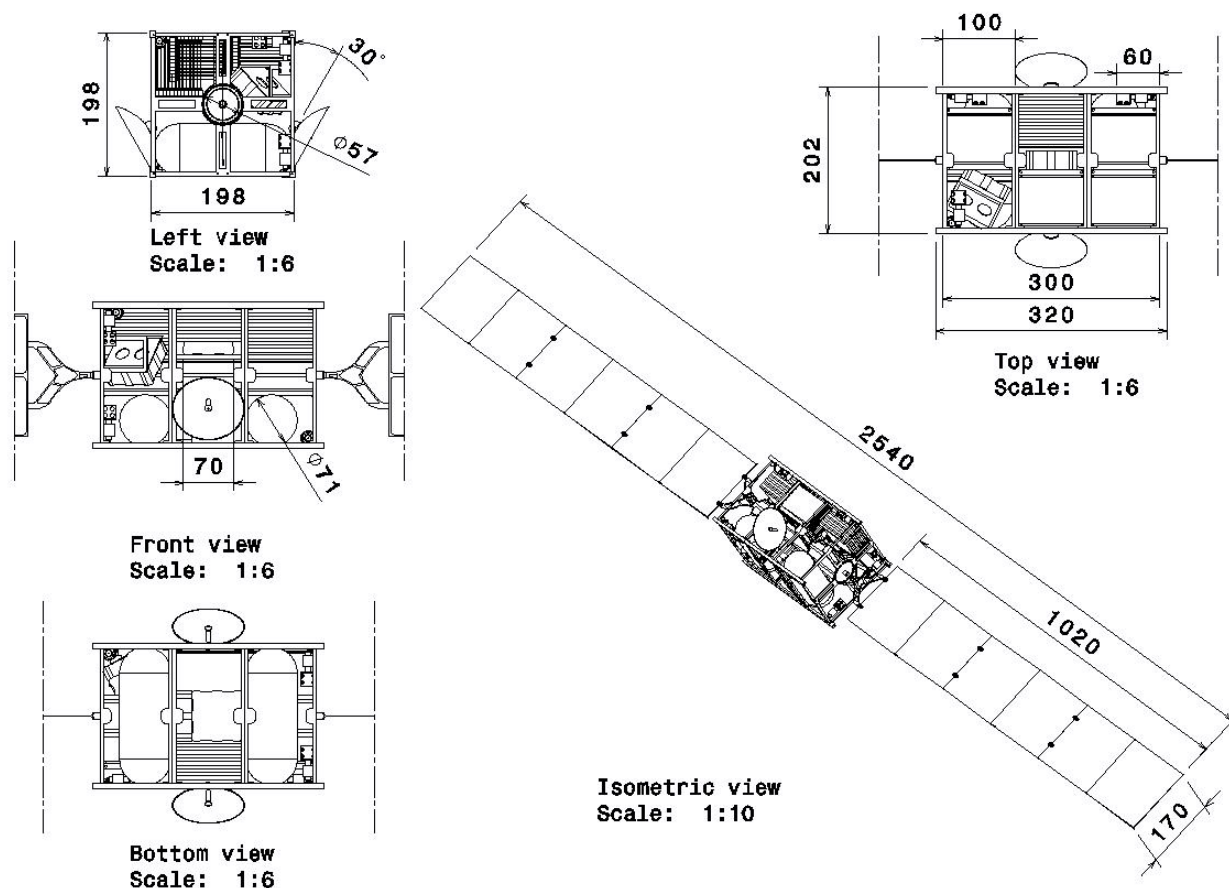


Figure 5: Conceptual layout of the network satellite with dimensions in mm.

A network satellite can be seen in [Figure 5](#). It is a 12 unit micro satellite with exterior structural dimensions of 20x20x30 cm. It is calculated that the network satellites will need  $75 \text{ m s}^{-1}$  for orbit maintenance over the five-year lifetime, which is achieved using green fuels. A fully passive thermal systems utilising only black paint and goldised kapton foil is used to ensure thermal stability. Three axis control stabilisation is required due to high accuracy requirements. This is ensured with the use of reaction wheels and momentum-dumping thrusters which allow for translation. An on-board oscillator enables the satellites to perform tracking and down-link in one go through one-way tracking. The network satellites make use of two phased array to make contact with the Moon surface and the relay satellites. In this way they can guarantee the field of view requirement for full coverage while at the same time reducing spacecraft weight due to the lack of pointing mechanisms or severe pointing requirements on the ADCS. In addition to the phased arrays, the network satellites utilise two parabolic antennas, mounted on a  $30^\circ$  angle, for the inter satellite links. The high gain of the parabolic antenna and the possibility to have it fixed, allow the increase of data rates. As a power supply, two solar arrays are present with a symmetrical layout. To satisfy the power requirements, both the arrays require six deployable panels with four solar cells each. The solar cells are chosen to be conventional triple junction InGaP/GaAs/Ge solar cells. To be able to provide power during eclipse and to accommodate peak loads, a secondary Li-ion battery is used.

#### RELAY SATELLITE DESIGN

The relay satellite utilises similar propulsion mechanisms, ADCS and green fuels similar to the network satellites. The thermal control is also completely passive, using aluminised kapton foil with the aluminium turned towards the satellite for cooling purposes. The relay satellites use parabolic antennas to make connections to the network satellites. The high gain of the parabolic antenna is needed to close the link at a data rate of  $500 \text{ kbits}^{-1}$  with a 3 dB margin.

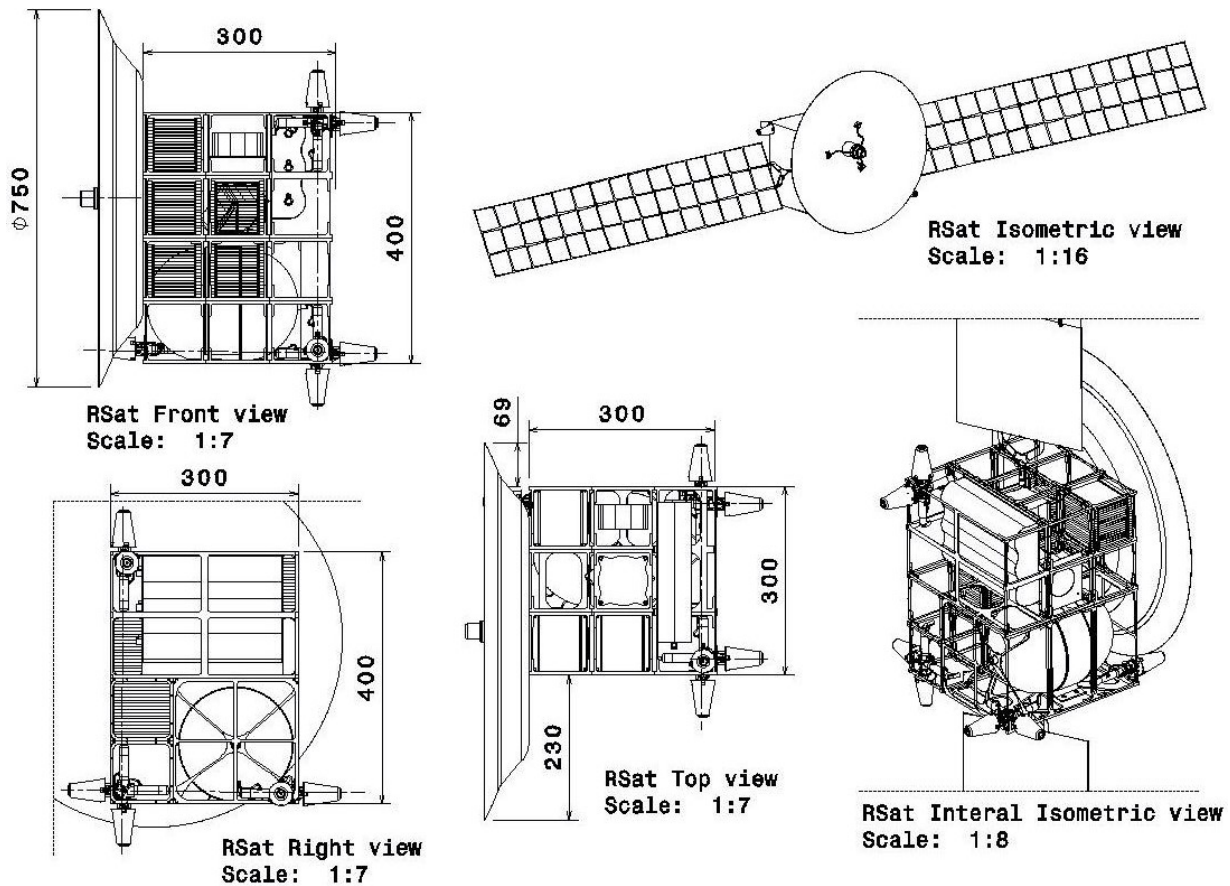


Figure 6: Conceptual layout of the relay satellite with dimensions in mm.

Pointing of the antenna is done by slewing the relay satellite using its ADCS. To connect to Earth the relay satellite uses a phased array, which minimises pointing losses even at unfavourable geometries and allows for data rates as high as  $2 \text{ Mbit s}^{-1}$ . The power subsystem consists of two solar arrays of five panels each with nine triple junction solar cells per panel.

The designs described above ensure that all communication links are able to close with at least a 3 dB margin and a data rate of  $500 \text{ kbit s}^{-1}$  available to each rover between the rover and operators on Earth. The overview of the designed vehicles can be seen in [Table 2](#).

Table 2: Vehicle parameter overview

	Amount	Mass [kg]	$\Delta V [\text{m s}^{-1}]$	Peak power [W]	Continuous power [W]
Network satellite	48	14.97	215.01	112.1	28.5
Relay satellite	6	31.13	400	145.1	94
Network deployment	2	1394	3802.18	602	79.13
Relay deployment	1	86.89	156.8	210.6	76.3

The total cost of the IRIS system is estimated to be  $\text{€}791.9 \pm 63.4$  Million in Financial Year 2017 for five years operational time from 2030 onwards. A price for IRIS service (continuous data rate of  $500 \text{ kbit s}^{-1}$ ) costs  $\text{€}86,800$  per day, which can be asked while remaining financially attractive for the customer. With a minimum of 10 lunar rovers or satellites (customers), a Return On Investment of 100% can be obtained in 5 years, where the break even point is met after 2.5 years of operations.



# LIST OF SYMBOLS AND ABBREVIATIONS

## ABBREVIATIONS

Abbreviation	Definition
ADCS	Attitude Determination and Control System
BIM	Brinbaum Importance Measure
C&DH	Command & Data Handling
CER	Cost Estimation Relationship
COM	Communication sub-system
CPF	Cost Per Function
cg	Centre of gravity
DeVe	Deployment Vehicle
DR	Data rate
DSE	Design Synthesis Exercise
ECSS	European Cooperation for Space Standardization
EIRP	Equivalent Isotropically Radiated Power
EPS	Electrical Power System
FEM	Finite Element Model
FOV	Field of view
FY[2010]	Financial Year 2010
GTO	Geostationary transfer orbit
HMO	High Moon Orbit
HLO	High Lunar Orbit
ICRF	International Celestial Reference Frame
LEO	Low Earth Orbit
LLO	Low Lunar Orbit
LRO	Lunar Reconnaissance Orbiter
LTE	Long-Term Evolution
L1-L5	Lagrange point 1-5
MDR	Mission Definition Review
MPPT	Maximum Power Point Tracker
NDeVe	Network Deployment Vehicle
Nsat	Network Satellite
Nloc	Network Satellite location
P5	People, Planet, Prosperity, Process, Product
PECE	Predict–Evaluate–Correct–Evaluate
PROP	Propulsion sub-system
PRA	Probabilistic Risk Analysis
PSLV	Polar Satellite Launch Vehicle
RAAN	Right Ascension of the Ascending Node
REE	Rare Earth Elements
RDeVe	Relay Deployment Vehicle
ROI	Return On Investment
Rsat	Relay Satellite
RTG	Radioisotope Thermo-electric Generator
Rx	Receiver
SE&I	Systems Engineering and Integration
SLOC	Source Lines of Code
SMAD	Space Mission Analysis and Design
SME	Space Mission Engineering
SNR	Signal-to-Noise ratio
Sloc	Spare network satellite location
$S_{Nsat}$	Spare network satellite
$S_{Rsat}$	Spare relay satellite
SRR	System Requirement Review
SSE	Sum of the Squares of Errors
STR	Structural sub-system
THR	Thermal sub-system
TLI	Trans-Lunar Injection
TMI	Trans-Mars Injection
TRK	Tracking sub-system
TT&C	Telemetry, Tracking & Control
Tx	Transmitter

## SYMBOLS

Symbol	Definition	Unit
<b>a</b>	Acceleration vector	$[\text{m s}^{-2}]$
<i>a</i>	Semi-major axis	[m]
<i>A</i>	Cross-sectional area	$[\text{m}^2]$
<i>A<sub>sol</sub></i>	Solar absorptivity	[-]
<i>A<sub>u</sub></i>	Average user activity	[days/year]
<i>c</i>	Speed of light	$[\text{m s}^{-1}]$
<i>C<sub>op</sub></i>	Sum of yearly operation costs	[€]
<i>C</i>	Specific heat	$[\text{J kg}^{-1} \text{K}]$
<i>C<sub>s</sub></i>	System capacity	[-]
<i>cg</i>	Centre of gravity	[m]
<i>d<sub>Earth</sub></i>	Diameter of Earth	[km]
<i>E</i>	Young's Modulus	[GPa]
<i>EC</i>	Electrical current	[A]
<i>e</i>	Eccentricity	[-]
<b>F</b>	Force vector	[N]
<i>F</i>	Force	[N]
<i>F</i>	Phasing parameter	[-]
<i>F<sub>ij</sub></i>	View factor	[-]
<i>F<sub>c</sub></i>	Centrifugal force	[N]
<i>f</i>	Fundamental frequencies	[Hz]
<i>F<sub>Nsats</sub></i>	Phasing parameter for Walker delta constellation	[-]
<i>f</i>	Probability density	[-]
<i>f<sub>t</sub></i>	Transmission frequency	[Hz]
FOV	Field of View	[°]
<i>G</i>	Universal gravitational constant: $6.67408 \times 10^{-11}$	$[\text{m}^3 \text{kg}^{-1} \text{s}^{-2}]$
<i>g</i>	Gravitational acceleration	$[\text{m s}^{-2}]$
<b>h</b>	Angular momentum vector	$[\text{kg m}^2 \text{s}^{-1}]$
<i>h</i>	Height	[m]
<i>h</i>	Hazard rate	[-]
<i>h<sub>rw</sub></i>	Reaction wheel angular momentum	$[\text{kg m}^2 \text{s}^{-1}]$
<i>h<sub>ij</sub></i>	Effective conductance	[S]
<i>I</i>	Initial investment cost	[€]
<i>I</i>	Second moment of area	$[\text{m}^4]$
<i>i</i>	Inclination	[°]
<i>i<sub>I</sub></i>	Initial inclination	[°]
<i>i<sub>F</sub></i>	Final inclination	[°]
<i>I<sub>sp</sub></i>	Specific Impulse	[s]
<i>k</i>	Spring constant	$[\text{N m}^{-1}]$
<i>k</i>	Interest rate	[-]
<i>L</i>	Length	[m]
<i>L<sub>f</sub></i>	Solar cell degradation factor	$[\text{year}^{-1}]$
<i>m</i>	Mass	[kg]
<i>M</i>	Bending Moment	[Nm]
<b>n</b>	Normal vector to the orbital plane	[m]
<i>N<sub>u</sub></i>	Expected number of customers	[-]
<i>P</i>	Power	[W]
<i>P<sub>crit</sub></i>	Critical buckling load	[N]
PRx	Receiver power	[W]
PTx	Transmission power	[W]
<i>Q</i>	Internal heat generation	[J]
<i>q</i>	Shear flow	$[\text{N m}^{-1}]$
<i>R</i>	Radius	[m]
<i>R</i>	Reliability	[-]
<b>r</b>	Position vector	[m]
<i>r</i>	Radius	[m]
RAAN	Right ascension of the ascending node	[°]
<i>R<sub>E</sub></i>	Radius of the Earth: 6371.0	[km]
<i>S</i>	Shear force	[N]
<i>T</i>	Period of an orbit	[s]
<i>T<sub>Nsats</sub></i>	Total amount of satellites	[-]
<i>t</i>	thickness	[m]

$t_D$	Skin thickness	[m]
$T_D$	Disturbance torque	[Nm]
$T_{Eclipse}$	Satellite eclipse time	[s]
$T_s$	Solar radiation pressure torque	[Nm]
$\mathbf{U}$	Rotation matrix	[-]
$\mathbf{u}$	Position vector	[m]
$V$	Voltage	[V]
$\mathbf{v}$	Velocity vector	[ms <sup>-1</sup> ]
$V_\theta$	Circumferential velocity	[ms <sup>-1</sup> ]
$v_x$	velocity in x	[ms <sup>-1</sup> ]
$v_y$	velocity in y	[ms <sup>-1</sup> ]
$v_z$	velocity in z	[ms <sup>-1</sup> ]
$\alpha$	Weibull relative weight parameter	[-]
$\alpha_{VIS}$	Reference angle visibility tool	[°]
$\beta$	Weibull shape parameters	[-]
$\beta_{VIS}$	Reference angle visibility tool	[°]
$\Delta V$	Change in velocity	[ms <sup>-1</sup> ]
$\gamma$	Reference angle visibility tool	[°]
$\epsilon$	Emissivity	[-]
$\eta$	Weibull scale parameters	[days]
$\theta$	True anomaly	[°]
$\theta_S$	Solar incidence angle	[°]
$\mu$	Standard gravitational parameter	[m <sup>3</sup> s <sup>-2</sup> ]
$\Phi$	Solar constant adjusted for distance	[Wm <sup>-2</sup> ]
$\Phi_r$	Relative inclination	[°]
$\varphi$	Solar incidence angle	[°]
$\rho$	Density	[kgm <sup>-3</sup> ]
$\hat{\rho}$	Range-rate measurement error	[m]
$\sigma$	Normal stress	[Pa]
$\sigma_b$	Stefan-Boltzmann constant: $5.670367 \times 10^{-8}$	[Wm <sup>-2</sup> K <sup>-4</sup> ]
$\tau$	Shear stress	[Pa]
$\omega$	Argument of periapsis	[°]
$\omega_r$	rotation rate	[°s <sup>-1</sup> ]
$\Omega$	Right argument of the ascending node	[°]

In Table 5 astronomical constants of the Moon, Earth and Sun are stated, which are used throughout the report.<sup>1 2 3</sup>

Table 5: Astronomical constants of the Moon, Earth and Sun

	Moon	Earth	Sun
Mass [kg]	$7.346 \times 10^{22}$	$5.9724 \times 10^{24}$	$1.988500 \times 10^{30}$
$\mu$ [km <sup>3</sup> s <sup>-2</sup> ]	$4.90 \times 10^3$	$3.9860 \times 10^5$	$1.32712 \times 10^{11}$
Volumetric mean radius [km]	1,737.4	6,371.0	695,700.0
Distance from Earth [km]	$3.844 \times 10^5$	0	$1.4960 \times 10^8$
Orbit eccentricity [-]	0.0549	0.0167	-
Ellipticity (Flattening) [-]	0.0012	0.00335	0.00005
Sidereal rotation period [days]	27.32	0.997	25.38

<sup>1</sup><https://nssdc.gsfc.nasa.gov/planetary/factsheet/moonfact.html> Accessed on 26.06.2017

<sup>2</sup><https://nssdc.gsfc.nasa.gov/planetary/factsheet/earthfact.html> Accessed on 26.06.2017

<sup>3</sup><https://nssdc.gsfc.nasa.gov/planetary/factsheet/sunfact.html> Accessed on 26.06.2017



# CONTENTS

<b>Preface</b>	<b>iii</b>
<b>Executive Summary</b>	<b>v</b>
<b>List of Symbols and Abbreviations</b>	<b>xi</b>
<b>1 Introduction</b>	<b>1</b>
<b>2 Mission Overview</b>	<b>3</b>
2.1 Rsats: Low-Energy Transfer to Moon-Earth L1 Halo Orbit . . . . .	3
2.2 Nsats: Direct Transfer to Frozen Moon Orbits . . . . .	3
2.3 Launcher Selection . . . . .	4
<b>3 Trajectory Design</b>	<b>5</b>
3.1 Low-Energy Transfer . . . . .	5
3.2 Direct Transfer . . . . .	10
<b>4 Constellation Design</b>	<b>15</b>
4.1 Design Process . . . . .	15
4.2 Communication flow and architecture . . . . .	16
4.3 Nsat constellation design . . . . .	16
4.4 Rsat constellation design . . . . .	17
4.5 Final constellation description . . . . .	19
4.6 Orbit Maintenance . . . . .	19
4.7 Disposal procedure . . . . .	20
4.8 Spares system . . . . .	20
4.9 Constellation Reliability Analysis . . . . .	20
<b>5 Link Design</b>	<b>23</b>
5.1 Design Process . . . . .	23
5.2 Data Flow . . . . .	25
5.3 Link Performance . . . . .	27
<b>6 Network Satellite Design</b>	<b>29</b>
6.1 Network Satellite Layout . . . . .	29
6.2 Electrical Power System . . . . .	29
6.3 Command and Data Handling . . . . .	34
6.4 Tracking and Orbit Determination . . . . .	36
6.5 Propulsion and Tank Sizing . . . . .	38
6.6 ADCS Design . . . . .	40
6.7 Thermal Design . . . . .	41
6.8 Primary Structure Design . . . . .	45
<b>7 Relay Satellite Design</b>	<b>47</b>
7.1 Relay Satellite Layout . . . . .	47
7.2 Electrical Power System . . . . .	49
7.3 Command and Data Handling . . . . .	50
7.4 Tracking and Orbit Determination . . . . .	51
7.5 Propulsion and Tank Sizing . . . . .	51
7.6 ADCS Design . . . . .	51
7.7 Thermal Design . . . . .	52
<b>8 Network Deployment Vehicle Design</b>	<b>53</b>
8.1 Network Deployment Vehicle Layout . . . . .	53
8.2 Electrical Power System . . . . .	54
8.3 Command and Data Handling . . . . .	55
8.4 Tracking and Orbit Determination . . . . .	55
8.5 Propulsion . . . . .	56
8.6 ADCS Design . . . . .	56
8.7 Thermal Design . . . . .	58
8.8 Structures Design . . . . .	58
8.9 Deployment Procedure Design . . . . .	60

<b>9 Relay Deployment Vehicle Design</b>	<b>61</b>
9.1 Relay Deployment Vehicle Layout . . . . .	61
9.2 Electrical Power System . . . . .	61
9.3 Command and Data Handling . . . . .	62
9.4 Tracking and Orbit Determination . . . . .	62
9.5 Propulsion Design . . . . .	62
9.6 ADCS Design . . . . .	63
9.7 Thermal Design . . . . .	64
9.8 Structure Design . . . . .	64
<b>10 Technical Budget Management</b>	<b>65</b>
10.1 Concurrent Engineering Strategy . . . . .	65
10.2 Engineering Budgets . . . . .	65
10.3 Administrative budgets . . . . .	67
<b>11 Sensitivity Analysis</b>	<b>69</b>
11.1 Changing Network Orbital Altitude . . . . .	69
11.2 Changing the Number of rovers to be serviced . . . . .	70
<b>12 Operations and Mission Planning</b>	<b>73</b>
12.1 Operations . . . . .	73
12.2 Mission Planning . . . . .	73
12.3 Strategy for extending mission duration . . . . .	74
<b>13 Manufacturing, Assembly and Integration Plan</b>	<b>75</b>
<b>14 Calculation Tools</b>	<b>77</b>
14.1 Trajectory Simulation Tool . . . . .	77
14.2 Rotating frame tool . . . . .	79
14.3 Plane change tool . . . . .	81
14.4 Deployment Movement Simulation . . . . .	84
14.5 Structural Sizing Nsat (Support) Structure . . . . .	86
14.6 Structural sizing of deployment ring . . . . .	88
14.7 Structural sizing of the Nsat primary structure . . . . .	90
14.8 Weibull processor . . . . .	92
14.9 Monte Carlo Simulation: Adjacent plane failure analysis . . . . .	92
14.10 Monte Carlo Simulation: In-plane Failure Analysis . . . . .	94
14.11 Disturbance torques calculator . . . . .	95
14.12 Reaction wheels and thrusters sizing tool . . . . .	97
14.13 Power Sizing and Monitoring tool . . . . .	98
14.14 Orbit perturbation simulation . . . . .	100
14.15 Thermal analysis tool . . . . .	103
14.16 Visibility Check Tool . . . . .	105
<b>15 Verification and Validation Procedure</b>	<b>109</b>
15.1 Key and Driving Requirement verification . . . . .	109
15.2 Validation of Requirements . . . . .	110
<b>16 Financial Analysis</b>	<b>113</b>
16.1 Cost Estimation . . . . .	113
16.2 Market Analysis . . . . .	114
16.3 Return on investment . . . . .	115
<b>17 Technical risk impact analysis</b>	<b>117</b>
<b>18 Sustainable Development Strategy</b>	<b>119</b>
18.1 Social Impact . . . . .	119
18.2 Environmental Impact . . . . .	120
<b>19 Post-DSE Planning</b>	<b>121</b>
<b>20 Recommendations</b>	<b>123</b>
<b>21 Conclusions</b>	<b>125</b>
<b>Bibliography</b>	<b>127</b>
<b>A Functional Flow Diagram</b>	<b>129</b>
<b>B Functional Breakdown Structure</b>	<b>135</b>
<b>C Technical risk register</b>	<b>141</b>
<b>D Requirements</b>	<b>145</b>
<b>E Post-DSE Gantt Chart</b>	<b>151</b>

# 1

## INTRODUCTION

Project IRIS is established within the context of the DSE created by Delft University of Technology, of which the end goal is to propose a finalised, conceptual design. Implementing the project is considered to be out of the scope of the DSE though may be considered once concluded. This is left to the discretion of project team.

Returning to the Moon has been at the heart of many space and research institutes for many different reasons. NASA gathered over 200 lunar objectives that resulted from the global exploration strategy process <sup>1</sup>. These proposed objectives aim at achieving broader goals defined by one of the following exploration themes, human civilisation, economic expansion, exploration preparation, global partnerships, scientific knowledge and public engagement. The main reasons lunar missions are limited at the time being, are that they are costly and complex. However, with recent technological developments, several governments and private companies are planning on sending missions to the Moon <sup>2 3</sup>. Furthermore, this increasing interest in returning to the Moon is visible in the rising number of planned Moon mission in the near future (2030).

With this surge in curiosity for our largest natural satellite, there will be need for a reliable 24/7 communication infrastructure linking operators on Earth and the Lunar surface. This will simplify the communication subsystem of all future lunar missions, resulting in a significant reduction in mass. Which will therefore reduce the cost of the vehicle under consideration whether it is a lunar lander, habitat, orbiter or rover. This implied need is captured in the mission need statement for Project IRIS:

*The growing need for Lunar exploration will be facilitated through the implementation of an economically viable communication infrastructure between the Earth and the Moon from 2030.*

This need is fulfilled by the project objective statement adopted by Project IRIS:

*To conceptually develop an economically viable, 24/7 communication system between at least 10 Lunar vehicles anywhere on the Moon and Earth-based operators, within a budget of 1 billion Euros, by 10 students in 10 weeks.*

This paper constitutes the final report, and is the successor of the project plan [4], the baseline report [5] and the midterm report [1]. In the baseline possible concepts for fulfilling the project objective statement were generated. Three concepts were generated for the trajectory and three for the constellation. The nine possible combinations of these concepts are displayed in [Figure 1.1.\[5\]](#)

---

<sup>1</sup>[https://www.nasa.gov/exploration/home/why\\_moon\\_objectives.html](https://www.nasa.gov/exploration/home/why_moon_objectives.html) Accessed on 26.06.2017

<sup>2</sup><http://www.space.com/28809-china-rocket-family-moon-plans.html> [2] Accessed on 26.06.2017

<sup>3</sup><http://Lunar.xprize.org/teams> [3] Accessed on 26.06.2017

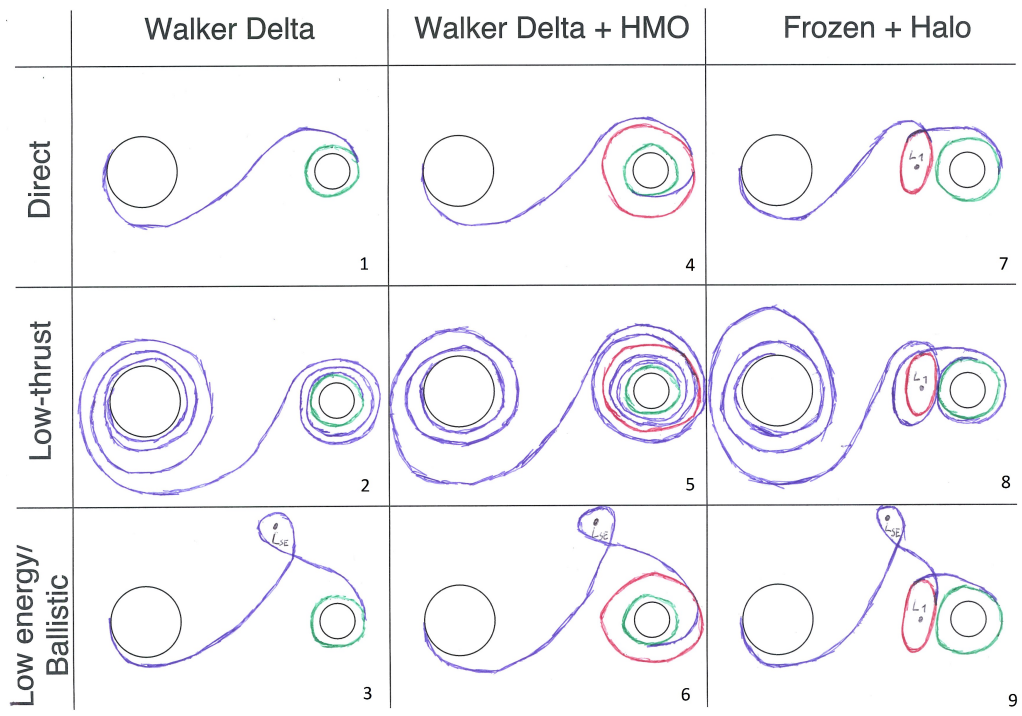


Figure 1.1: The possible combinations of the concepts for the constellation and the trajectory.

These nine concepts were reduced to three using an intuitive trade-off: a Walker-delta constellation with a direct transfer, a Walker-delta and High Moon Orbit constellation with a low-thrust transfer and a frozen orbit and halo constellation with a low-energy transfer. In the midterm [1] the concept with a frozen orbit and halo constellation with a low-energy transfer was chosen as the best concept. This concept was chosen out of the three possible concepts, as it performed the best in terms of performance, risk, cost and time. This trade-off is summarised in Table 1.1 [1].

Table 1.1: Final trade-off of the three concepts in the midterm report.

	Performance				Risk level	Cost	Time
	Satellite mass	Trans. eff.	$\Delta V$ Orb. maint.	Ecl.			
<b>C1</b>	1217.4 kg <i>yellow</i>	17.3 <i>yellow</i>	300 m/s <i>blue</i>	.253 <i>blue</i>	42.9% <i>green</i>	€893 million <i>yellow</i>	11.7 day <i>green</i>
<b>C2</b>	830.4 kg <i>blue</i>	1.3 <i>green</i>	300 m/s <i>blue</i>	.238 <i>blue</i>	50.0% <i>blue</i>	€898 million <i>yellow</i>	4.06 years <i>red</i>
<b>C3</b>	437.8 kg <i>green</i>	11.2 <i>blue</i>	150 m/s <i>green</i>	.159 <i>green</i>	71.5% <i>yellow</i>	€552 million <i>green</i>	205 days <i>blue</i>

To improve this design first an overview of the mission is given in chapter 2. After that, the design of the transfer trajectories and the design of the constellation are described in chapter 3 and chapter 4. This constellation design is closely linked with the link design discussed in chapter 5. To accommodate these links, the designs of the network satellites (Nsats) and relay satellites (Rsats) are explained in chapter 6 and chapter 7. The deployment vehicles are designed in chapter 8 and chapter 9. Furthermore, an overview of the technical budgets is given in chapter 10. To test the robustness of the design, a sensitivity analysis is performed in chapter 11. Then, the operations and planning of the mission is detailed in chapter 12. After which the manufacturing, assembly and integration of the different system elements is examined in chapter 13. The tools which are used to come up with the design are described, verified and validated in chapter 14. Moreover, the verification and validation procedures are outlined in chapter 15. In chapter 16, chapter 17 and chapter 18 an analysis is performed in terms of finance, risk and sustainability respectively. The planning of the activities after the DSE is described in chapter 19. Lastly, recommendations for future development are given in chapter 20 and the report is concluded in chapter 21.

## MISSION OVERVIEW

An overview of the mission is given in order to provide a framework for the design of the technical aspects of the system. The mission will have two different launches, one for the Relay satellites (Rsats) toward the first Moon-Earth Lagrangian point and one launch for the Network satellites (Nsats) toward frozen orbits around the Moon. A schematic overview of the mission is given in [Figure 2.1](#), including preliminary launch dates, where the system should be operational at the 3rd of October 2029. The full functional flow diagram and functional breakdown structure of this mission is included in [Appendix A](#) and [Appendix B](#).

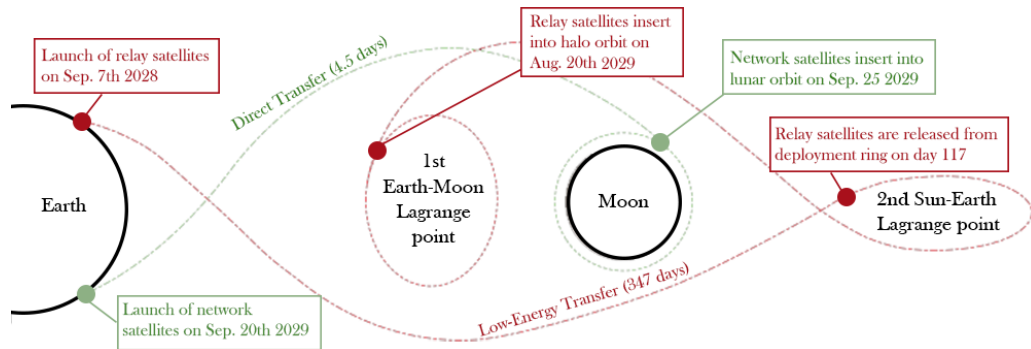


Figure 2.1: Schematic overview of the mission with preliminary launch dates (figure not to scale), where system is planned to be operational on the 3rd of October 2029

### 2.1. RSATS: LOW-ENERGY TRANSFER TO MOON-EARTH L1 HALO ORBIT

First, the launcher will bring the Rsats, with their Deployment Vehicle (DeVe), into a 500 km LEO orbit ( $\Delta V_{10}$ ) from where the launcher will conduct a burn into a transfer orbit towards the second Sun-Earth Lagrangian point ( $\Delta V_{11}$ ). Once arriving at the Sun-Earth L2 point, the DeVe will insert itself in a halo orbit around it ( $\Delta V_{12}$ ). After spending a certain amount of time in this halo orbit, where the Rsats are deployed, a small kick will cause the Rsats to fall back to the Earth-Moon system ( $\Delta V_{13}$ ). Back in the Earth-Moon system, another small kick will insert the satellites into trajectories towards the required halo orbits ( $\Delta V_{14}$ ). Then, the satellites will insert themselves in their desired halo orbits around the first Earth-Moon Lagrangian point ( $\Delta V_{15}$ ). Lastly, phasing manoeuvres are performed ( $\Delta V_{16}$ ). In [Table 2.1](#) all the different burns are summarised for this low-energy trajectory.

Table 2.1: Burns performed during the low-energy transfer (first trajectory), where  $\Delta V_{1x}$  stands for the x'th burn of the low-energy transfer

Identifier	Performed by	Description
$\Delta V_{10}$	Launcher	Launch from the surface to LEO
$\Delta V_{11}$	Launcher	Insert into transfer orbit to Sun-Earth L2
$\Delta V_{12}$	DeVe	Insert into halo orbit around Sun-Earth L2
$\Delta V_{13}$	Rsat	Insert into trajectory back to Earth-Moon system
$\Delta V_{14}$	Rsat	Insert in trajectory towards required halo orbits and perform preliminary phasing
$\Delta V_{15}$	Rsat	Insert into halo orbit around Earth-Moon L1

Once the Rsats are in their specified halo orbit around the Earth-Moon L1 point and are operational, the launch of the Nsats is a go. This is done to minimise the risk.

### 2.2. NSATS: DIRECT TRANSFER TO FROZEN MOON ORBITS

As for the Rsats, the launcher will bring the Nsats with their two DeVe's into a 500 km LEO orbit ( $\Delta V_{20}$ ) from where the launcher will insert them into a direct transfer orbit towards the Moon ( $\Delta V_{21}$ ). The DeVe's will be separated during the transfer and will obtain a small phase shift, such that they safely can perform the insertion into the desired orbit around the Moon as well as the desired inclination change at the same time ( $\Delta V_{22}$ ). Once in orbit around the Moon, both DeVe's will do a relatively small RAAN change in opposite direction. Once they are in their new plane they will deploy the first batch of Nsats, after which they perform a larger RAAN change and deploy a new batch of Nsats. Both DeVe's deploy three batches of Nsats. Therefore, both DeVe's perform one smaller and two larger RAAN change manoeuvres. ( $\Delta V_{23}$ ). A batch is defined as six operational Nsats and two spare Nsats, which are in the same orbital plane. Once the satellites are deployed they will perform a phasing manoeuvre. In [Table 2.2](#) the different burns are summarised for this direct Lunar trajectory.

Table 2.2: Burns performed during the direct transfer (second trajectory), where  $\Delta V_{2y}$  stands for the y'th burn of the direct transfer

Identifier	Performed by	Description
$\Delta V_{20}$	Launcher	Launch from the surface to LEO
$\Delta V_{21}$	Launcher	Insert into transfer orbit to the Moon
$\Delta V_{22}$	Deployment Vehicle	Insert into desired orbit around the Moon and change to desired inclination
$\Delta V_{23}$	Deployment Vehicle	Change of the Right Ascension of the Ascending Node (RAAN)
$\Delta V_{24}$	Satellite	Phasing manoeuvre

In Figure 2.2 the sequence of launches and manoeuvres are displayed in a flow diagram. Note that the dotted line resembles the command of successful operational Rsats in halo orbit for launch 2.

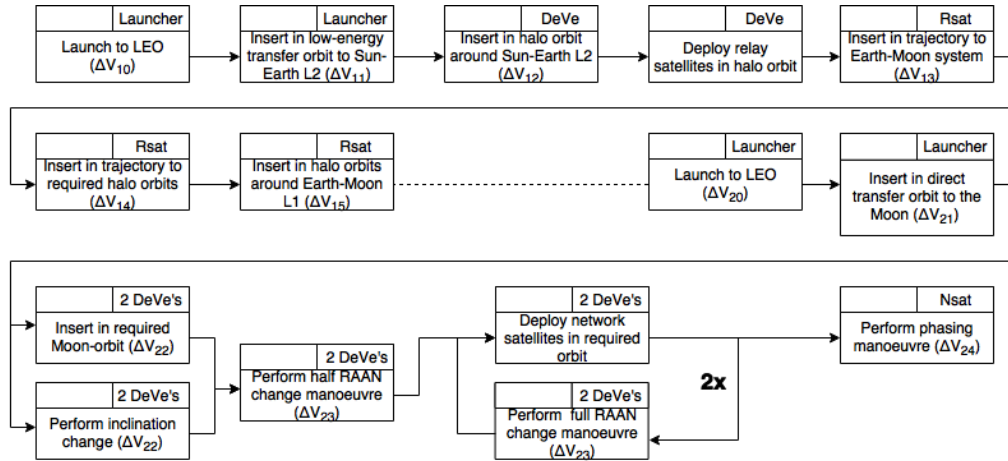


Figure 2.2: Overview of the mission in terms of manoeuvres of both trajectories.

### 2.3. LAUNCHER SELECTION

The launcher selection was first of all based on the launcher capabilities in terms of payload bay volume and if it can get the system (payload) into its desired orbit. For the low-energy transfer this is a minimum of 300 kg and for the direct transfer a minimum of 3,600 kg as payload. It is assumed here that if a launcher can bring a certain amount to Trans Mars Injection (TMI), it can perform at least the same for Trans Lunar Injection (TLI). Contact with the launcher supplier should be made to obtain further exact information about payload capabilities to TLI. Next to this, the cost of the launcher and its reliability where considered. Current and upcoming rockets were investigated<sup>1</sup>. For the Low-Energy transfer the Minotaur V rocket and PSLV-XL were identified as potential candidates. For the direct transfer the Long March 5 and Falcon 9 Full Thrust launcher were identified. In Table 2.3 these four launchers are presented including their payload capabilities to LTI or TMI, their cost and reliability based on number of successful over total launches.

Table 2.3: Information about identified launcher options.

Launcher	Manufacturer	Payload capabilities [kg]	Cost [Million's of \$]	Reliability [%]
Minotaur V	Orbital Sciences (USA)	342 [6] (TLI)	46 <sup>2</sup>	100 <sup>2</sup> (1/1)
PSLV-XL	ISRO (Indian)	1,350 (TMI) <sup>3</sup>	15 <sup>4</sup>	100 <sup>3</sup> (17/17)
Long March 5	CALT (Chinese)	8,200 [7] (TLI)	unknown	50 <sup>5</sup> (1/2)
Falcon 9 Full Thrust	SpaceX (USA)	4,020 (TMI) <sup>6</sup>	62 <sup>6</sup>	94 <sup>7</sup> (33/35)

Using the information in Table 2.3, the PSLV-XL was chosen to be used for the low-energy transfer due its lower cost compared to the Minotaur V and its high reliability. The Falcon 9 Full Thrust was chosen for the direct transfer, based on its relative low-cost per kg and its high reliability compared to the Long March 5. The lack of information on Long March 5 aided to this decision, as well as the lack of specified launch loads, which are present for the Falcon Nine [8]. These launch loads are needed for the Deployment Group and are also available for the PSLV-XL [9].

Note that in this trade-off no third-party unencumbered launchers are considered. So no piggy-back launches are considered, which could potentially decrease the overall launch costs of the system.

<sup>1</sup>[https://en.wikipedia.org/wiki/Comparison\\_of\\_orbital\\_launch\\_systems](https://en.wikipedia.org/wiki/Comparison_of_orbital_launch_systems) Accessed on 26.06.2017

<sup>2</sup><https://oig.nasa.gov/audits/reports/FY11/IG-11-012.pdf> Accessed on 26.06.2017

<sup>3</sup><http://www.isro.gov.in/launchers/pslv> Accessed on 26.06.2017

<sup>4</sup><http://www.thehindubusinessline.com/news/science/pslvc21-sends-french-spot-6-japanese-satellite-into-orbit/article3877021.ece> Accessed on 26.06.2017

<sup>5</sup>[https://en.wikipedia.org/wiki/Long\\_March\\_5](https://en.wikipedia.org/wiki/Long_March_5) Accessed on 02.07.2017

<sup>6</sup><http://www.spacex.com/about/capabilities> Accessed on 26.06.2017

<sup>7</sup>[https://en.wikipedia.org/wiki/List\\_of\\_Falcon\\_9\\_and\\_Falcon\\_Heavy\\_launches](https://en.wikipedia.org/wiki/List_of_Falcon_9_and_Falcon_Heavy_launches) Accessed on 26.06.2017

As described in [chapter 2](#) Project IRIS uses two trajectories. First, the Rsats are taken to their halo orbits using a low-energy transfer as described in [section 3.1](#). Once the Rsats are in orbit, the Nsats are brought to their frozen orbits using the direct transfer described in [section 3.2](#).

### 3.1. LOW-ENERGY TRANSFER

The low-energy transfer uses the influence of the Sun to reduce the amount of  $\Delta V$  necessary for the transfer, as discussed in the midterm [1]. The design of the low-energy trajectory is split up in three parts, which will make doing the calculations easier and doable in the time-frame of the DSE. The three parts are chosen such that they can be matched relatively easily to come up with the complete trajectory. The different parts of the trajectory are visualised in [Figure 3.1](#), including the different burns. The first part (point 1 to 3) is defined from Earth LEO into halo orbit around the Sun-Earth L2 point. This manoeuvre would be identical for going towards Sun-Earth's L1 and L2 points. In this case it is chosen to go towards the L2 region. A thermal analysis showed that the temperature ranges between  $4^\circ\text{C}$  to  $35^\circ\text{C}$  [1, p. 42] in the worst case. Furthermore, moving away from the Sun for roughly  $2 \times 10^6$  km decreases the irradiance with only 3 %, which is not a problem since most of the communication subsystem is not operational during the transfer. The radiation received from the Sun is slightly less in L2 compared to L1. Also, the L2 ballistic transfer is used more often than the L1 transfer, so there is more literature on a L2 transfer available. Based on the aforementioned points a transfer through L2 is chosen over L1. The second part (point 3-4) is defined from the halo orbit around the Sun-Earth L2, where the spacecraft is given a small kick, such that it falls back towards the Earth-Moon system. The second part stops when the satellite crosses the Earth inertial y-axis. The third part (point 4-5) deals from crossing this y-axis till the spacecraft reaches its final destination, an Earth-Moon L1 orbit.

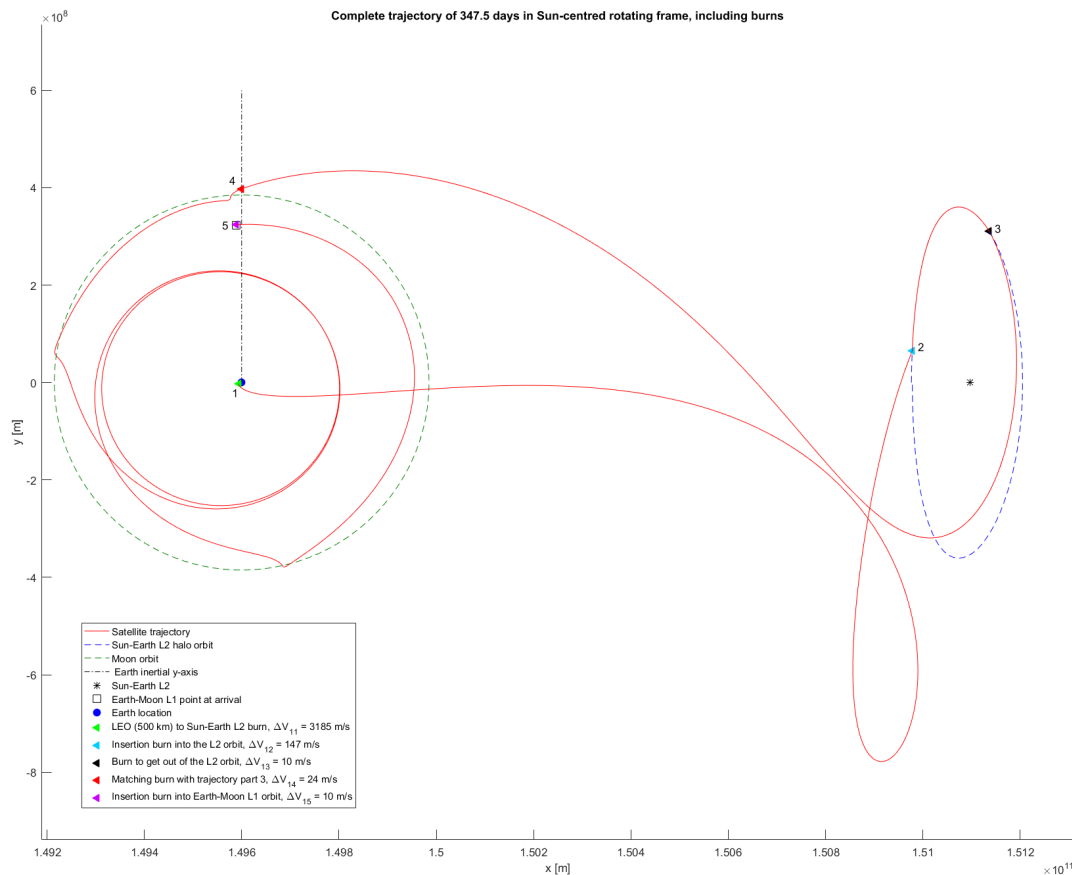


Figure 3.1: Design of the complete trajectory of the low-energy transfer of the Rsats in a Sun-centred, Earth-fixed rotating frame.

The total required  $\Delta V$  for this low-energy transfer is  $3,376 \text{ m s}^{-1}$ , whereas a non-optimal direct transfer ( $\approx 5$  days) from

500 km LEO would need approximately  $3,780 \text{ ms}^{-1}$  [10, p. 139]. An optimised direct transfer would need around  $3,470 \text{ ms}^{-1}$ . The current design of the low-energy transfer has not been optimised, but it already shows the advantage in  $\Delta V$  compared to a direct transfer.

Not only the reduced amount of  $\Delta V$  is advantageous, especially the fact that after leaving LEO, no burns above  $150 \text{ ms}^{-1}$  are needed anymore. This means that no big propulsion systems are needed on the RDeVe or the Rsats, which would only increase the mass and volume of these vehicles.

A downside of the low-energy trajectory is that it takes 347.5 days to complete, while a direct transfer would only take around 5 days. Of those 347.5 days, 116.2 are spent in part 1, 54.1 days are spent in the Sun-Earth L2 orbit, 122.1 days are spent in part 2 and 55.1 are spent in part 3.

The low-energy transfer is very susceptible to errors in position and velocity determination as it is designed in a chaotic system. According to section 6.4 the maximum errors are 6 m in position and  $3.6 \times 10^{-4} \text{ ms}^{-1}$  in velocity. To investigate the effect of these errors the maximum errors are added to the initial conditions of the intermediate halo orbit which are propagated for one day. After this day the position error increased to 31.7 m and the velocity error decreased to  $3.6 \times 10^{-4} \text{ ms}^{-1}$ . It is determined that this is acceptable, as long as the orbit is corrected at least once a day. This is taken into account in the propellant budget of the Rsats.

In the next sections all 3 parts of trajectory are discussed in more detail, especially why they were chosen. The  $\Delta V_{11}$  and the preliminary phasing of the Rsats done during  $\Delta V_{14}$  won't be discussed here. Due to the fact that the launcher will perform the  $\Delta V_{11}$  and is not influencing the rest of the trajectory. Also the phasing of the Rsats could partially be done by their deployment procedure, see also chapter 20.

### 3.1.1. TRAJECTORY PART 1

The design of the first part of the trajectory is performed by first creating a halo orbit around Sun-Earth L2 in the x-y plane of the Sun-Earth system. This is done using the tool described in section 14.1. The halo orbit is established using a trial and error approach. The initial position is estimated from the ISEE-3 mission profile<sup>1</sup>. The initial position is assumed to be 120,000 km towards Earth from Sun-Earth L2. The initial conditions in terms of velocity are guessed by adding a small amount of velocity to the velocity of the Sun-Earth L2. The halo orbit with these initial conditions is then propagated, using the tool described in section 14.1, until the trajectory crosses the x-axis again (in the rotational frame). If the trajectory crosses the x-axis more towards Earth than the initial position velocity is added to the initial conditions. If the trajectory crosses the x-axis more towards the Sun-Earth L2 than the initial position the initial velocity is reduced. This is done until a halo orbit is established which is semi-stable for more than four periods. The initial conditions for this orbit are determined to be  $[x, y, z, vx, vy, vz] = [1.5098 \times 10^{11} \text{ m}, 0 \text{ m}, 0 \text{ m}, 1.06749 \text{ ms}^{-1}, 3.0211 \times 10^4 \text{ ms}^{-1}, 1.260005700065 \text{ ms}^{-1}]$ . The trajectory which is achieved after propagating these initial conditions is displayed in Figure 3.2. Note that the reason for this many digits is to ensure the correct initial conditions and correct use in calculations. It is known that this accuracy is not realistic.

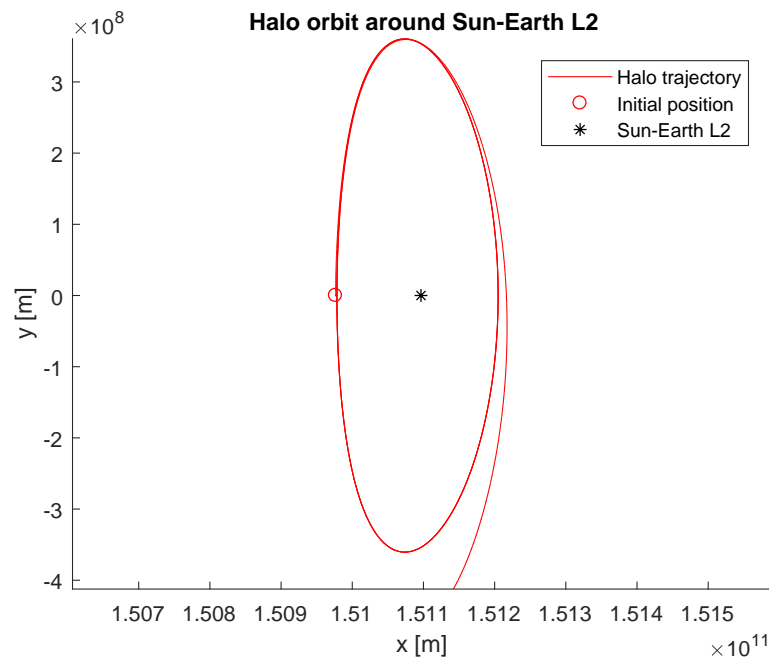


Figure 3.2: Intermediate halo orbit around the Sun-Earth L2 used during the low-energy transfer of the Rsats in a Sun-centred rotating reference frame.

To design the trajectory from Earth to the halo orbit, the initial conditions of the halo orbit are taken and integrated

<sup>1</sup><https://directory.eoportal.org/web/eoportal/satellite-missions/i/isee-3> Accessed on 26.06.2017

back in time. This is done for varying initial conditions to simulate the application of a burn to insert in the halo orbit. Furthermore, the burn is simulated to be applied at multiple positions in the halo orbit by changing the simulated time spent in the halo orbit.

The variation in the initial conditions is done using nested loops and the trajectories are first optimised to come within the closest distance possible to Earth. After optimisation, it is discovered that some trajectories hit the Earth. After that discovery, the trajectory is optimised with respect to the required  $\Delta V_{12}$  to minimise the requirements on the RDeVe. Which yields the possibilities displayed in [Figure 3.3](#).

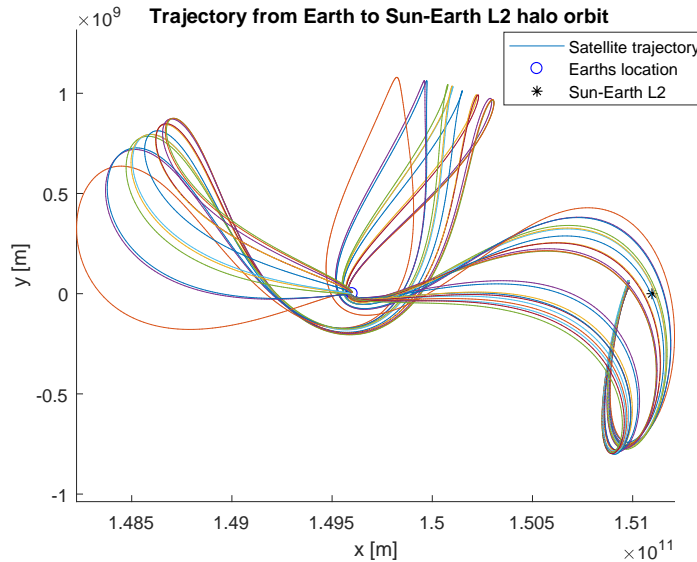


Figure 3.3: Possible trajectories from Earth to the intermediate halo orbit around the Sun-Earth L2 in a Sun-centred rotating reference frame.

As displayed in [Figure 3.3](#), there are some trajectories which take an indirect route to the halo orbit around Sun-Earth L2. It is decided that these trajectories are undesirable due to the vast increase in transfer time (in the order of 100s of days). These optimisation decisions result in the transfer displayed in [Figure 3.1](#) from point 1 to 2. This transfer orbit requires a burn of  $-86.0 \text{ ms}^{-1}$  and  $-119.0 \text{ ms}^{-1}$  in the x- and y-direction respectively to insert in the halo orbit. This results in a  $\Delta V_{12}$  of  $146.82 \text{ ms}^{-1}$ . This part of the low-energy transfer trajectory takes 116 days.

The burn required to insert in this trajectory from a circular 500 km altitude LEO is computed by comparing the velocities in the two trajectories at the point where the transfer trajectory and circular trajectory intersect. The difference between these velocities is the  $\Delta V_{11}$  needed to insert in the transfer orbit. The computation of these velocities is done using the tool described in [section 14.1](#) and is determined to be  $-3,111.6 \text{ ms}^{-1}$  and  $678.51 \text{ ms}^{-1}$  in x- and y-direction respectively. This means a  $\Delta V_{11}$  of  $3,184.8 \text{ ms}^{-1}$  is required to insert in the transfer orbit.

### 3.1.2. TRAJECTORY PART 2

The second part of the trajectory takes the spacecraft from the halo orbit around the Sun-Earth L2 point back to the Earth-Moon system. This is done by propagating the initial conditions of the halo orbit found in [subsection 3.1.1](#) forward in time using the tool described in [section 14.1](#). The multiple possible trajectories are found by applying a small kick of  $10 \text{ ms}^{-1}$  at different locations throughout the halo orbit in the opposite direction of the velocity. In other words the spacecraft is slowed down such that it falls back to the Earth-Moon system. In [Figure 3.4](#) a variety of these trajectories is displayed, but in fact there are infinitely many of them.

As can be seen in [Figure 3.4](#), trajectories cross the Earth inertial y-axis from  $1 \times 10^8 \text{ m}$  to  $5 \times 10^8 \text{ m}$ . Not all of these trajectories are equally suitable for the purposes of Project IRIS. The Moon is located at  $3.844 \times 10^8 \text{ meter}$  ([Table 5](#)) away from the centre of the Earth, it was chosen to only consider trajectories crossing the Earth inertial y-axis above  $3.95 \times 10^8 \text{ meter}$ , because at 10000 km away from the Moon centre its gravity influence is limited.

The decision of the final trajectory of part 2 is based on the combined transfer time with part 3 as well as how well it matches in terms of their relative position and velocities (required  $\Delta V$ ), [subsection 3.1.4](#) is devoted to this trade off. The final chosen trajectory of part 2 is displayed in [Figure 3.1](#) from point 3 to 4.

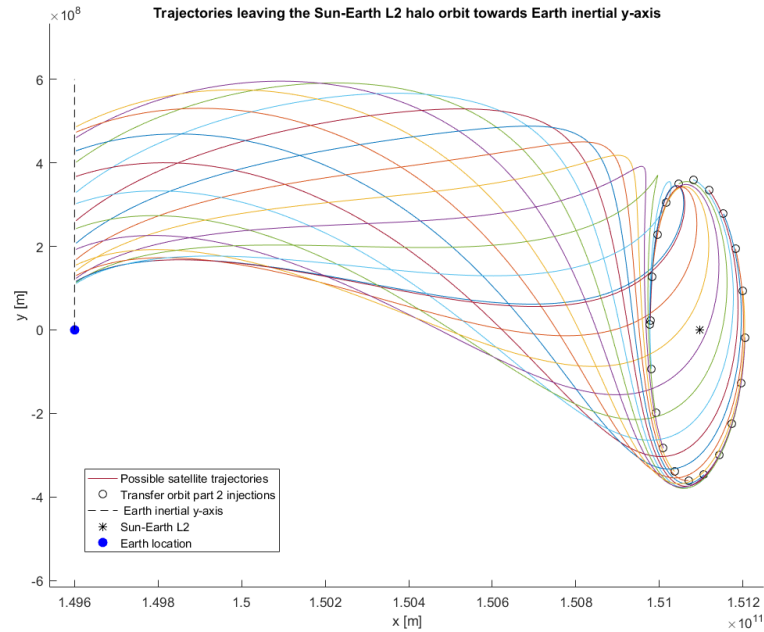


Figure 3.4: Trajectories from Sun-Earth L2 halo orbit to the Earth inertial y-axis in Sun-centred rotating frame with a kick of  $-10 \text{ m s}^{-1}$  applied in the halo orbit.

### 3.1.3. TRAJECTORY PART 3

Trajectory part 3 brings the spacecraft from crossing the inertial y-axis of the Earth till the spacecraft reaches its final destination, the Earth-Moon L1 halo orbit. This trajectory is modelled by first obtaining a stable halo orbit at an orbital height of 44,000 km as is preferred by the Constellation Group. The initial conditions for this orbit are determined to be  $[x, y, z, vx, vy, vz] = [3.2338 \times 10^8 \text{ m}, 0 \text{ m}, 44,000,000 \text{ m}, 0 \text{ m s}^{-1}, 1.0948 \times 10^3 \text{ m s}^{-1}, 0 \text{ m s}^{-1}]$ , see Figure 3.5 (the blue trajectory). During iterations of the design of the IRIS system it was decided to add an extra halo orbit, this is done because it gives better visibility of the Nsats by the Rsats. This second halo is mirrored in the XY-plane and has initial conditions  $[x, y, z, vx, vy, vz] = [3.2338 \times 10^8 \text{ m}, 0 \text{ m}, -44,000,000 \text{ m}, 0 \text{ m s}^{-1}, 1.0948 \times 10^3 \text{ m s}^{-1}, 0 \text{ m s}^{-1}]$ , see also Figure 3.5 (the orange trajectory). Both orbits have an orbital time of 12.25 days.

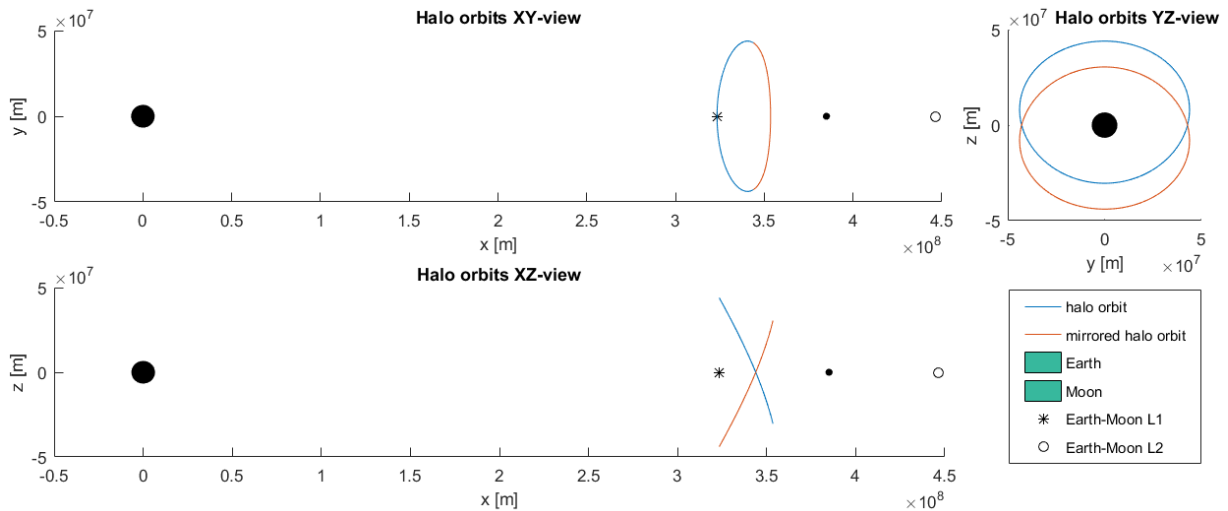


Figure 3.5: Design of the halo orbits around L1 Earth-Moon point, with Earth at the origin.

The trajectory of part 3 is found using the same approach as in subsection 3.1.1, by integrating back in time and applying a small kick at different locations, but now in an Earth-Moon L1 orbit. In Figure 3.6 different possible trajectories of part 3 are displayed, as well as the locations where the insertion burn of  $10 \text{ m s}^{-1}$  is performed. As can be seen in the figure there are multiple ways to arrive in the L1 orbit. There exists trajectories which take a direct route (Figure 3.6, the light blue line) and there are trajectories which performs multiple Moon swing by's (Figure 3.6, the orange line). The trade off on how the final trajectory of part 3 is chosen is discussed in subsection 3.1.4 and is based on the com-

bined transfer time and the required  $\Delta V$ . The final chosen trajectory of part 3 is displayed in Figure 3.1 from point 4 to 5, which is the same trajectory as the orange line in Figure 3.1, but now in Sun-centred rotating frame.

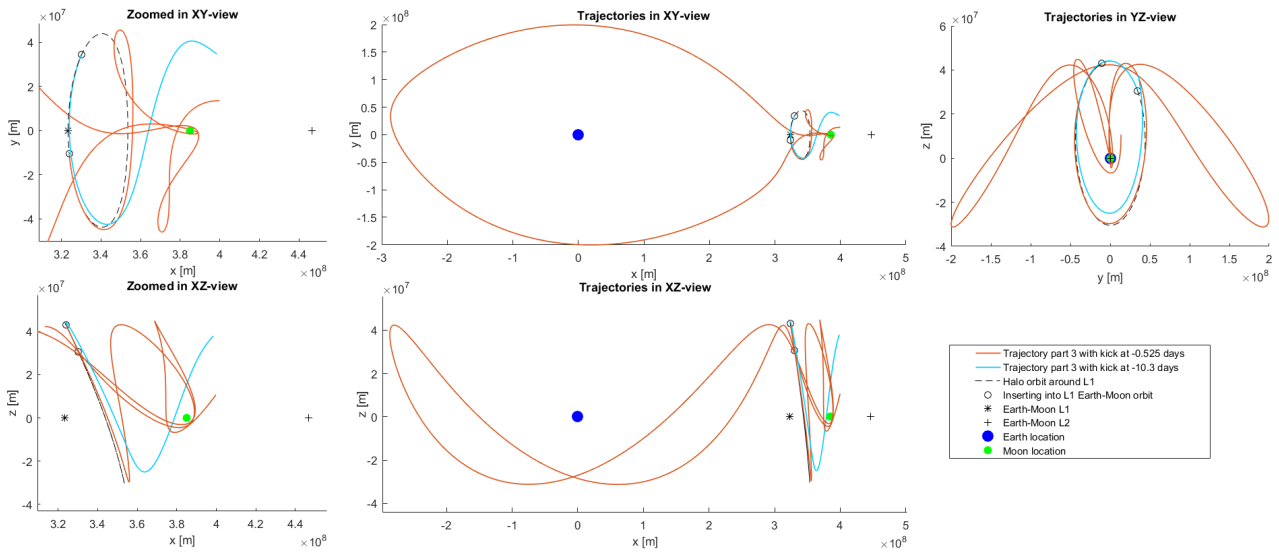


Figure 3.6: Possible trajectories from the inertial y-axis of the Earth to injection in the desired halo orbits around the Earth-Moon L1.

### 3.1.4. MATCHING TRAJECTORY PART 2 WITH PART 3

The matching between trajectory part 2 and 3 is based on how much  $\Delta V$  is needed to 'glue' them together and how long the combined transfer time is. For this trade-off the  $\Delta V$  has the main priority, because it would highly influence the design of the Rsats in terms of propulsion system. While time is influenced by the requirement to be operational before 2030. In Figure 3.7 the arrival/departure locations at the Earth inertial y-axis are plotted against the velocities in the x and y-direction for trajectories of both part 2 and 3. The black asterisks corresponds to the trajectories in Figure 3.4, but now more trajectories are considered (1800 to be precise). The coloured lines corresponds to the trajectories in Figure 3.6 with two extra possible trajectories plotted.

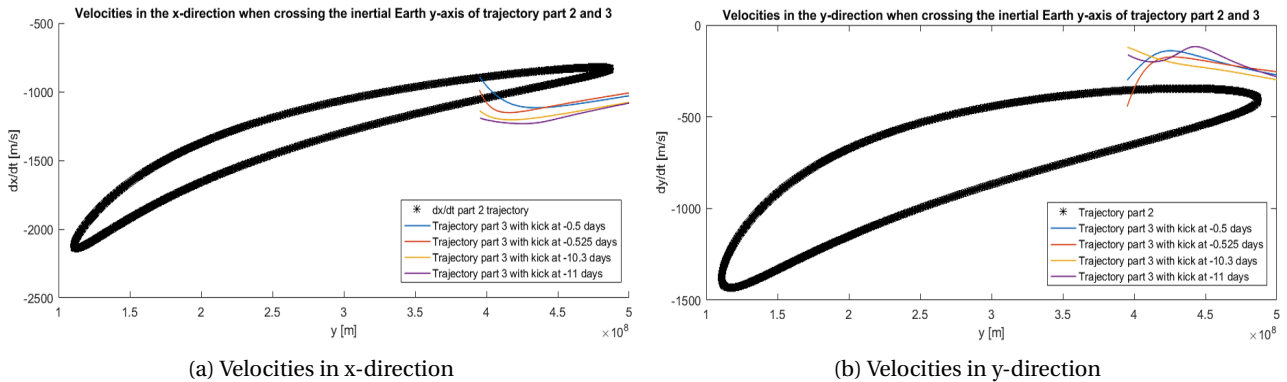


Figure 3.7: Velocities in x and y-directions when crossing the inertial Earth y-axis.

As can be seen from Figure 3.7a and Figure 3.7b, the orange line of trajectory part 3 with a kick at -0.525 days crosses the range of options from part 2 in both cases. Therefore this option was investigated in more detail, see Figure 3.8. From here the required  $\Delta V$ 's for matching the lines at different locations on the Earth inertial y-axis were investigated. It was found that a minimum  $\Delta V$  was found at  $y = 3.978726194287806 \times 10^8$  m, where the absolute difference in velocity is only  $24.0 \text{ ms}^{-1}$ , of which  $18.1 \text{ ms}^{-1}$  is in x-direction and  $15.8 \text{ ms}^{-1}$  is in y-direction. Note that these numbers are required to reproduce the trajectories, in reality this accuracy is not achievable. The downside of this combined trajectory is that it takes 177.2 days, this is mainly due to the fact that part 3 takes 55.1 days, due the 3 Moon swing-by's, as can be seen Figure 3.1.

To decrease the transfer time, a more direct route should be chosen for part 3, for example the light blue trajectory in Figure 3.6. Now the transfer time for part 3 is only 10.8 days. Combining this with new trajectories from part 2, it gives a total combined transfer time of  $133 \pm 5$  days, dependent on which height the inertial y-axis of the Earth is crossed ( $3.98 \times 10^8$  m to  $4.90 \times 10^8$  m). But a  $\Delta V$  of  $252 \pm 4 \text{ ms}^{-1}$  is needed for matching part 2 and 3. These amounts of  $\Delta V$  turned out to be too high for the Deployment group, that it would drive the design of the Rsats DeVe to the unfeasible

domain. Therefore it was chosen to go for a longer transfer time of 177.2 days, but a relative low  $\Delta V$  of  $24.0 \text{ m s}^{-1}$ .

Note that in this trade-off the z-direction of the position and velocity are not considered at the Earth inertial y-axis. For further optimisation of the trajectory these should be considered, see also [chapter 20](#).

Note that during this section only arrival in the blue halo Earth-Moon L1 orbit of [Figure 3.5](#) is considered. For the mirrored orbit (orange trajectory in [Figure 3.5](#)) it is assumed that using the same methodology a trajectory for part 2 and 3 can be found, with an equivalent  $\Delta V$  budget for the Rsat. This will need to be investigated in further design iterations if this could be done, see also [chapter 20](#).

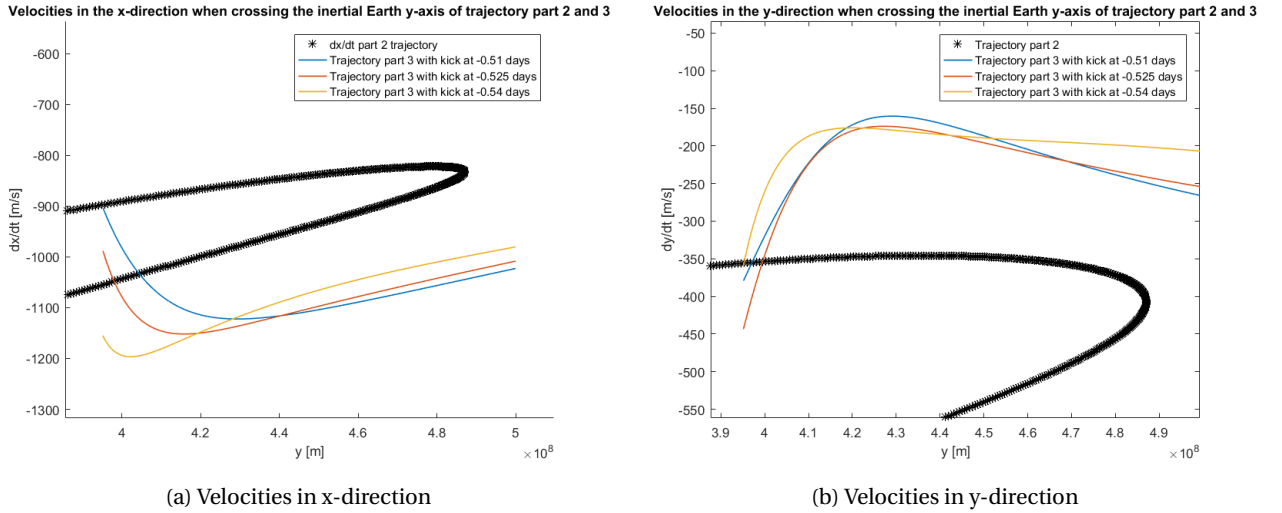


Figure 3.8: Velocities in x and y-directions when crossing the inertial Earth y-axis (zoomed in).

## 3.2. DIRECT TRANSFER

A basic design of the direct transfer was made in the midterm report [1, p. 41-43]. This basic design includes an initial burn at a 500 km altitude LEO which is  $3,059.9 \text{ m s}^{-1}$ . Then, a burn of  $1,285.0 \text{ m s}^{-1}$  is applied to insert the NDeVe in a circular frozen orbit around the Moon at 1,629 km altitude. After it is inserted, a  $894.8 \text{ m s}^{-1}$  burn is applied to change the inclination to  $50.2^\circ$ . Then, the first batch of Nsats is deployed which perform a phasing manoeuvre requiring a maximum of  $29.08 \text{ m s}^{-1}$  per Nsat. Following the deployment of the first batch of Nsats the NDeVe performs five plane changes in terms of RAAN, which takes a total of  $1,726.0 \text{ m s}^{-1}$ . This design of the direct trajectory has a total of 9.96 days of transfer time.

The basic design described above was not optimised yet, to improve this design, several steps are taken. First, the eccentricity of the orbit of the Moon is introduced in the model to obtain a more accurate simulation of the transfer. Then, it is decided that the orbit insertion and inclination change are done in the same burn ( $\Delta V_{22}$ ). Furthermore, the transfer is optimised to minimise  $\Delta V_{22}$ , to minimise the amount of  $\Delta V$  required for the NDeVes. This optimisation is done by changing the relative location along the starting orbit and the magnitude of the first burn ( $\Delta V_{21}$ ). Lastly, the different plane change manoeuvres computed by the tool described in [section 14.3](#) are included in the direct transfer tool described in [section 14.1](#).

### 3.2.1. ECCENTRICITY OF THE MOON'S ORBIT

Instead of the circular orbit used to create the basic design, the Moon's orbit is modelled to have its real eccentricity of 0.0554. This is done by changing the initial conditions of the Moon's orbit in the tool described in [section 14.1](#). This ensures that the trajectory which is designed for the direct transfer of the Nsats is more accurate. The optimisation of the transfer orbit is done for two scenarios: the Moon is assumed to be at the pericentre or apocentre of its orbit as  $\Delta V_{21}$  is applied.

### 3.2.2. OPTIMISATION OF THE TRANSFER

The optimisation of the direct transfer is twofold: optimisation of the location and optimisation of the magnitude of  $\Delta V_{22}$ . The aim is to minimise the  $\Delta V$  required by the NDeVes.

The relative location of  $\Delta V_{22}$  along the starting orbit is defined by the angle  $\theta$  with respect to the x-axis from the origin of the Earth through the origin of the Moon at starting conditions. For each  $\theta$  the assumed  $\Delta V_{21}$  is applied in the direction of the velocity. The trajectory is then propagated using the tool described in [section 14.1](#). When the trajectory crosses the desired orbit around the Moon, the simulation is halted. Then, the required  $\Delta V_{22}$  to insert in the 1,629 km,  $46.0^\circ$  frozen orbit is computed for that particular trajectory.

The magnitude of  $\Delta V_{21}$  is increased and decreased by  $100 \text{ m s}^{-1}$  from the magnitude of  $\Delta V_{21}$  in the midterm design with a step-size of  $1 \text{ m s}^{-1}$ . These  $\Delta V_{21}$ 's are applied at all the different locations and propagated using the tool described in [section 14.1](#). When the trajectory crosses the desired orbit around the Moon, the simulation is halted and the required  $\Delta V_{22}$  is computed.

The optimisation of  $\Delta V_{22}$  by changing the two parameters as described before are done in a nested loop, to make sure all possible combinations are tested. This yields the graphs displayed in [Figure 3.9](#) and [Figure 3.10](#) which only include trajectories which cross the desired orbit.

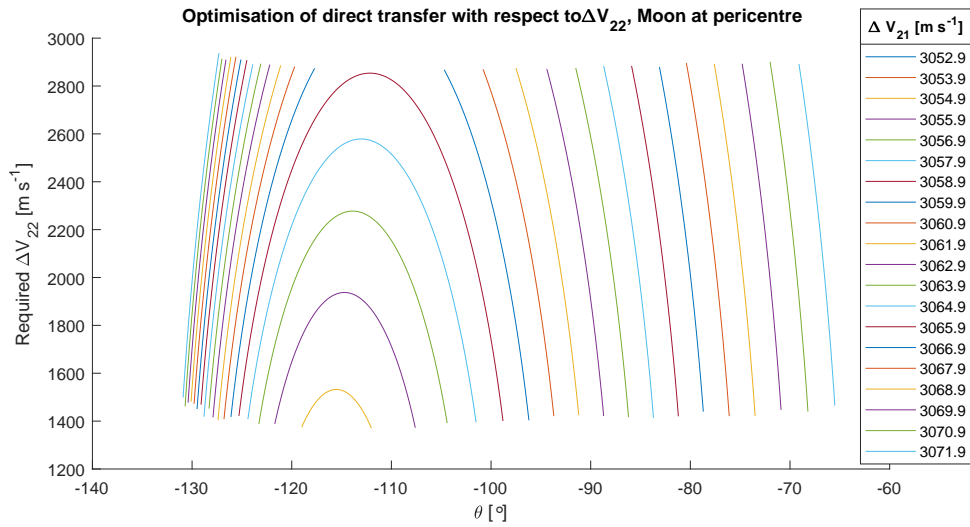


Figure 3.9:  $\Delta V_{22}$  required, for changing location and magnitude of  $\Delta V_{21}$  with the Moon at its pericentre.

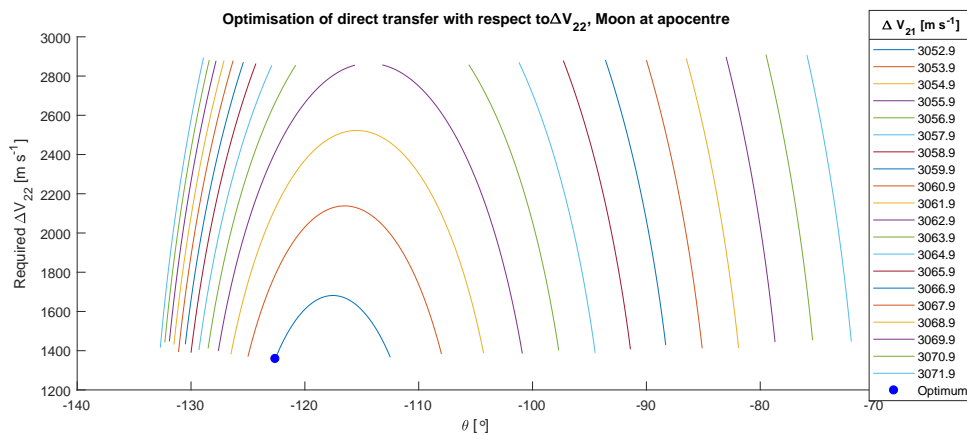


Figure 3.10:  $\Delta V_{22}$  required, for changing location and magnitude of  $\Delta V_{21}$  with the Moon at its apocentre.

The resulting minimum  $\Delta V_{22}$  of  $1,358.43 \text{ m s}^{-1}$  is achieved for a  $\theta$  of  $-122.6^\circ$  and a  $\Delta V_{21}$  of  $3,059.93 \text{ m s}^{-1}$ , with the Moon at its apocentre at  $t=0$ . This yields the trajectory displayed in [Figure 3.11](#). This trajectory takes 107.9 hours from  $\Delta V_{21}$  to  $\Delta V_{22}$ .

### 3.2.3. MANOEUVRES

As described in [section 2.2](#), after the NDeVe is in orbit multiple manoeuvres are performed. These manoeuvres are split in manoeuvres performed by the NDeVe and manoeuvres performed by the Nsats.

#### PLANE CHANGES BY THE NDEVE

Both NDeVes have to perform three manoeuvres, which are the same in magnitude for both vehicles. First, the NDeVes need to get into the respective planes of the first batches of Nsats. This means a change in inclination from  $46.0^\circ$  to  $50.2^\circ$  and simultaneously a RAAN change from  $-75.7^\circ$  to  $-45.7^\circ$  and from  $-75.7^\circ$  to  $-105.7^\circ$  respectively. This manoeuvre was computed by the tool described in [section 14.3](#) to require  $472.88 \text{ m s}^{-1}$  per NDeVe. This tool also computed the location and direction of this manoeuvre which was given as input to the tool described in [section 14.1](#) to create a simulation which is displayed in [Figure 3.12a](#).

Once the two NDeVes performed the first RAAN change manoeuvre, the first batches of Nsats are deployed. Then, the two NDeVes perform a RAAN change from  $-45.7^\circ$  to  $14.3^\circ$  and from  $-105.7^\circ$  to  $-165.7^\circ$  respectively. Again, the tool described in [section 14.3](#) is used to compute this manoeuvre. It is determined that  $927.44 \text{ m s}^{-1}$  is needed for this manoeuvre per NDeVe. The simulation of this manoeuvre is shown in [Figure 3.12b](#).

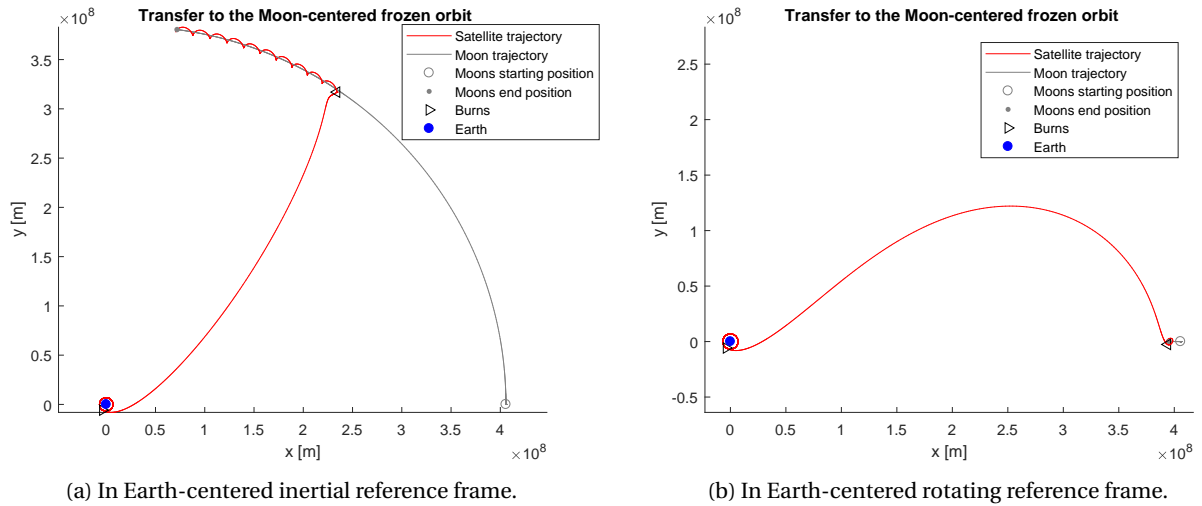


Figure 3.11: Direct transfer to frozen Moon-centered orbit.

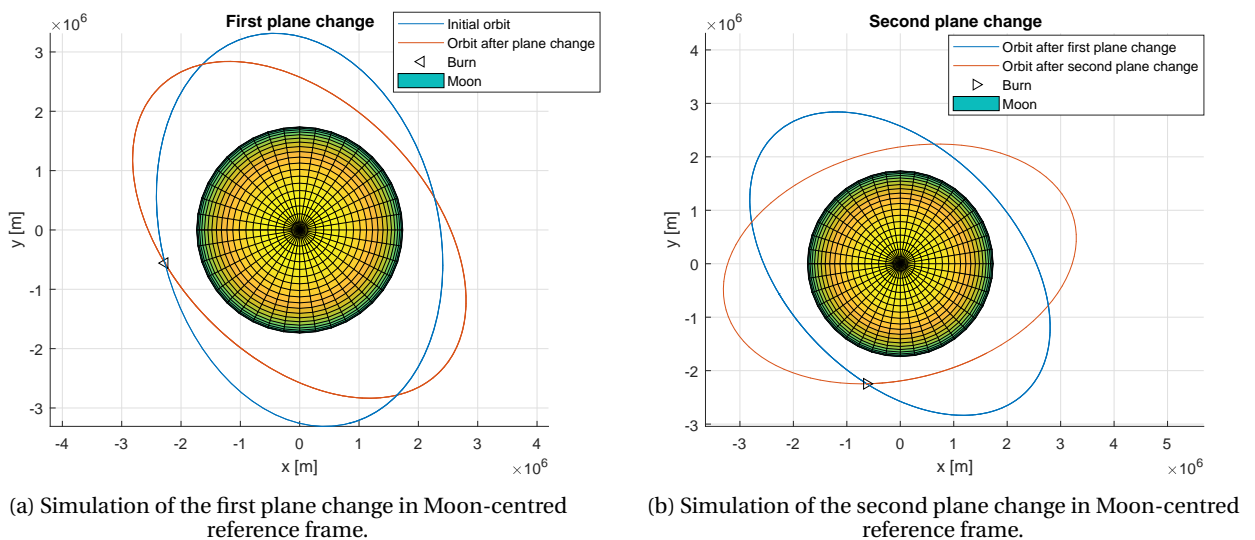


Figure 3.12: Simulations of the plane changes performed after orbit insertion in Moon-centred reference frame.

Following the deployment of the second batches of Nsats, the last RAAN change manoeuvres are performed by the NDeVes. These are RAAN changes from  $14.3^\circ$  to  $74.3^\circ$  and from  $-165.7^\circ$  to  $134.3^\circ$  respectively. This manoeuvre is equal to the previous manoeuvre and requires  $927.44 \text{ ms}^{-1}$  per NDeVe.

These plane changes combined require a  $\Delta V_{23}$  of  $2,327.8 \text{ ms}^{-1}$  per NDeVe. The changes over time are displayed in Figure 3.13. In the same figure the dotted lines indicate the desired values for the Keplerian elements. The deviations mainly originate due to the influence of the Earth. This is particularly visible in the plots of the eccentricity and the semi-major axis. These manoeuvres take a total of 33.95 hours from orbit insertion to the insertion in the last plane.

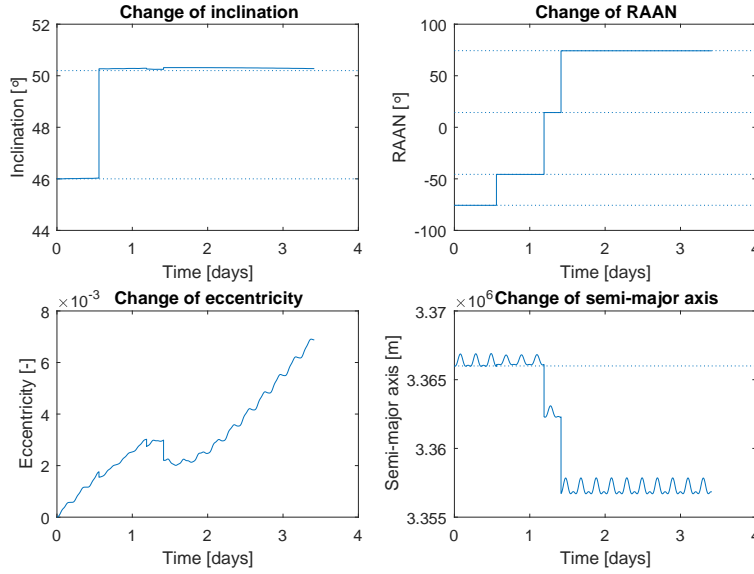


Figure 3.13: Changes in the Keplerian elements during the simulation of the plane change manoeuvres.

PHASING MANOEUVRES BY NSATS

Once the Nsats are deployed, they perform a phasing manoeuvre. This manoeuvre is the same for the different planes. The only difference between the Nsats is the magnitude of the phase change to be performed. The maximum phase change to be performed is 150° to space the Nsats evenly over the planes. To do this, an elliptic phasing orbit is used. This phasing orbit can be sized to minimise the required  $\Delta V_{25}$  at the cost of a longer manoeuvring time, and vice versa. It is assumed that the Nsats will spend ten periods in the phasing orbit. This means that the change in phase has to be 15° per period in the phasing orbit.

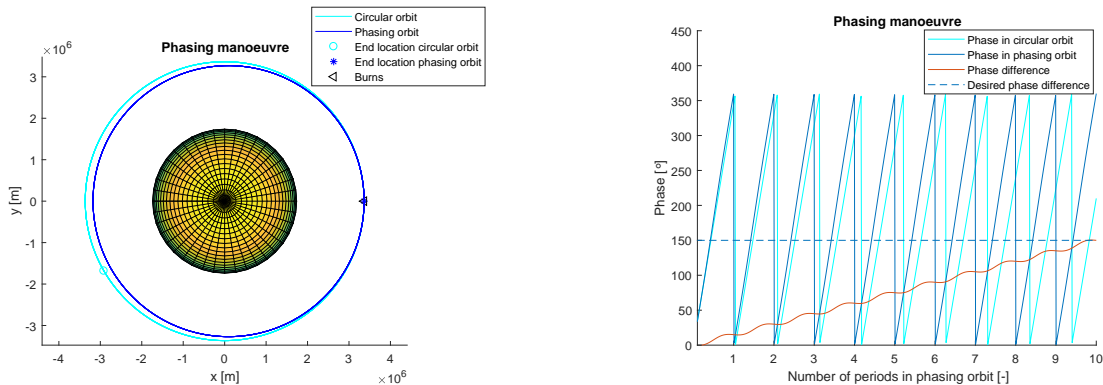
The period of an orbit is determined by Equation 3.1 [11, p.200]. The velocity of the satellite at the point where the elliptic phasing orbit intersects with the circular orbit is computed using the Vis Viva equation displayed in Equation 3.2 [11, p. 201].  $T$  is the period in s,  $a$  is the semi-major axis in m and  $\mu$  is the standard gravitational parameter of the Moon in  $m^3 s^{-2}$ ,  $V$  is the velocity in  $m s^{-1}$  and  $r$  is the radius in m. The period of the constellation orbit is determined to be 17,524 s. Therefore, the period of the phasing orbit is determined by:  $T_{phase} = \frac{360-15}{360} \cdot T = 16,794$  s. Consequently, using the inverse of Equation 3.1, the semi-major axis of the phasing orbit is 3,271.8 km. The velocity in the circular starting orbit is computed using the Vis Viva equation where the semi-major axis is equal to the radius, displayed in Equation 3.3. This means that the required  $\Delta V_{25}$  for phasing equals  $2 \cdot 1206.88 - 1189.38 = 35.00$   $m s^{-1}$ . This manoeuvre takes 46.65 hours to complete.

$$T = 2\pi \sqrt{\frac{a^3}{\mu}} \quad (3.1)$$

$$V^2 = \frac{2\mu}{r} - \frac{\mu}{a} \quad (3.2)$$

$$V^2 = \frac{\mu}{r} \quad (3.3)$$

The  $\Delta V_{25}$  computed above is introduced in an adaptation of the tool described in section 14.1. This yields the simulation displayed in Figure 3.14a. The change of the relative phase over time is displayed in Figure 3.14b.



(a) Simulation of phase change in Moon-centred frame.

(b) Change of relative phase over time.

Figure 3.14: Maximum phase change for the Nsats after deployment.



The process of designing the constellation used by Project IRIS is described in this chapter.

## 4.1. DESIGN PROCESS

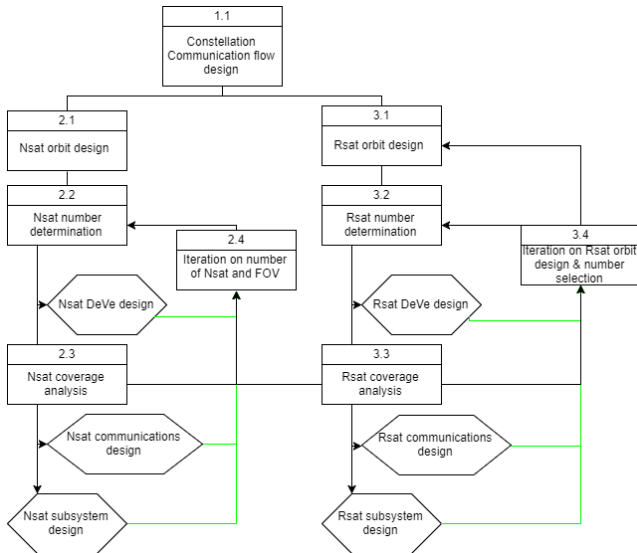


Figure 4.1: Constellation general design chart. (green lines are influences on the design origination from other design groups.

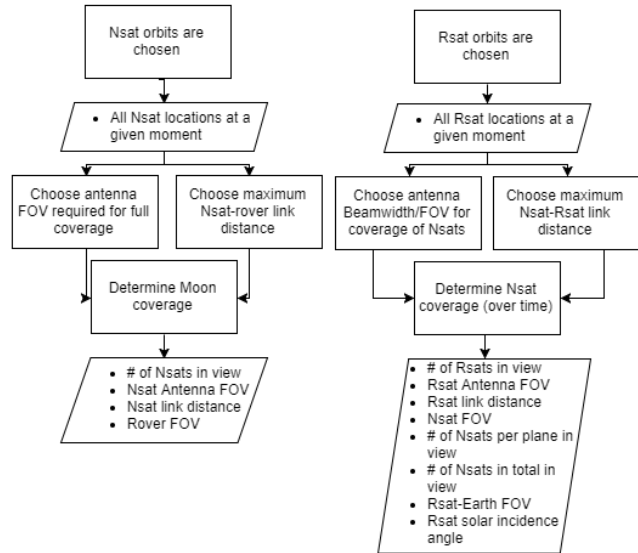


Figure 4.2: Nsat coverage design chart(left), Rsat coverage design chart(right)

The overall design process for the constellation is shown in Figure 4.1. The first step is to look at the overall communication flow of signals through the constellation (section 4.2). For example, how a signal from a rover travels through the constellation to Earth. The second step is to design the orbits of the Nsats and their required numbers (section 4.3). The third step is to design the orbits and number of Rsats that are required (section 4.4).

For the design of the Nsat constellation, the orbits chosen during the midterm are used and were taken from literature [12, p.61]. After the orbits are set (2.1), a number of Nsats per orbit is chosen according to the Walker delta notation (2.2), the first number of required Nsats was found during the midterm phase and is 24 Nsats [1, p.43]. Further analysis in terms of coverage is performed on this constellation (2.3). The outputs from this are used in the communication design. If the option does not work, a reiteration on the number of Nsats and the Field of View (FOV) of the Nsats is required (2.4). Once a Nsat constellation is found that satisfies the requirements and that works for the communication subsystem it is to be used for the Rsat constellation design and Nsat design.

The initial estimate made during the midterm for the halo orbit around the Earth-Moon L1 is used (3.1) [1, p.43]. The initial number of Rsats is equal to one, which is taken from the midterm (3.2). This Rsat constellation can then be used for further coverage analysis (3.3). From the coverage analysis there could also be some iteration required for the Nsat constellation design. The last step is to check whether the outputs of this coverage analysis meet the requirements. Furthermore, it is checked whether the chosen constellation works for the communication subsystem design. If this is not the case an iteration on the orbit, the number of Rsats and the Rsat FOV is performed (3.4). If the requirements are met with respect to the communication design, the design can be passed on to the Rsat design, again iteration can be done if necessary.

### 4.1.1. ASSUMPTIONS

For coverage analysis the Moon-Earth system is assumed as in Figure 4.3. Since the halo orbits are within the Moon-Earth plane and since the visibility tool works with a Moon fixed centred frame, there is a rotation of  $6.69^\circ$  around the y-axis applied to the halo orbit. It is assumed the Rsats have equal tangential velocity within their orbits. If this was not the case, it would influence the phasing of the Rsats within the halo orbits. It is currently unknown what the actual velocity profile of a satellite in halo orbit is, but since it is near circular, the assumption is suspected to be reasonable. Other assumptions for coverage analysis are as stated in section 14.16.

### 4.1.2. NSAT COVERAGE ANALYSIS

The Nsat coverage analysis is done according to Figure 4.2. Using the chosen Nsat orbits, the Nsat locations (Nlocs) are determined for a fixed moment in time. Using the visibility tool described in section 14.16 the visibility of the

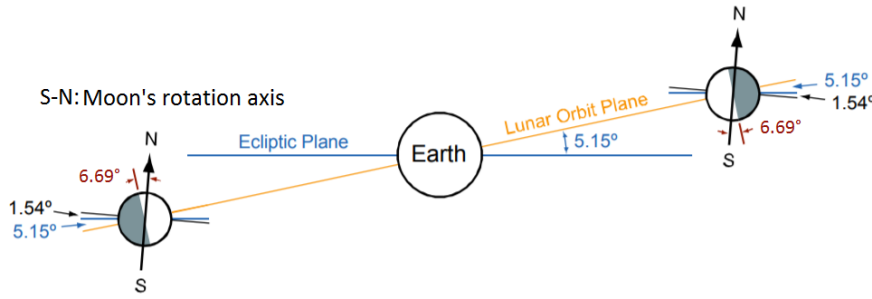


Figure 4.3: Moon Earth plane and orientation assumptions, adjusted from [13, p. 31]

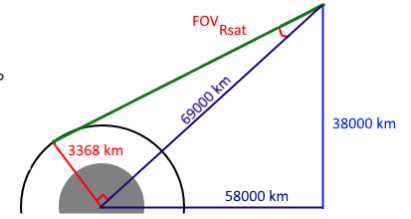


Figure 4.4: Sketch for calculating the required field of view of the Rsat for covering the Moon maximally.

Nsats to the rovers can be determined. The FOV of both the Nsat antenna and rover antenna are chosen as well as the maximum distance between antennas, then the visibility map is inspected for meeting the requirement **IRIS-CON-01** which is met by having at least 2 satellites in view at all times. If this requirement is satisfied, the required FOVs are given to the communication subsystem design group, to check if these FOVs can be achieved and if the link budget can be closed. If, for example, the FOVs required for visibility are too large for the Nsat design, the number of Nsats should be increased and the design should be iterated.

#### 4.1.3. RSAT COVERAGE ANALYSIS

The Rsat coverage analysis is done according to Figure 4.2. The Rsat coverage analysis requires both the Nlocs and Rlocs (Rsat locations) at a fixed moment in time. The Rsat-Nsat FOV and Rsat-Nsat maximum distance are chosen and parameters like total numbers of Nsats in view and number of Nsats per plane in view are calculated.

In Table 4.1 the coverage results for all the configurations during the final phase are shown. Columns 2 to 4 describe the constellation configuration. Column 3 RhxRhb describes the halo orbit, with Rh as the semi-major axis and Rhb the semi-minor axis. For the first set of designs the halo orbit was assumed circular thus Rh and Rhb are equal. For the other orbits, Rh and Rhb were different. Furthermore, these orbits are slanted with respect to the orbital plane of the Moon. Column 5 shows for what percentage of the constellation configurations there are less than 10 Nsats in view, if this is more than zero then the cell is red. Columns 6 to 9 show the amount of Nsats that are visible to the Rsats, it is desired that these amounts are as high as possible such that there are as much Nsats per plane visible as possible. If there are planes where no Nsats are visible then the cell is red. Column 10 and 11 show the time an Nsat is in view of the Rsats expressed in percentage of the Nsats orbital period. The longer the connection time the less frequent the link has to be switched between Nsats, thus resulting in less signal management complexity.

## 4.2. COMMUNICATION FLOW AND ARCHITECTURE

A complete overview of the link design is given in chapter 5. However, as the link design significantly influenced the constellation design, a short overview is given here. The overall idea is that the Nsats will take the signals from the rovers and send it towards the Rsats if they are in view, or otherwise to another Nsats in the same orbital plane. The Rsats send it directly to an Earth based ground station. In case of Nsat failure the Rsats are able to redirect the flow of data however only in the same plane, such that the signal travels through functioning Nsats. A schedule using the rover missions is required to be made for determining which Nsats and Rsats are used at what time. This way orbit maintenance can be planned such that it does not interfere with the missions of the customers. This schedule is uploaded to the Rsats which send the relevant commands to the Nsats. In case of Nsat failure this is detected and this knowledge is sent to Earth such that a redirection of communication flow can happen. This detection is done using simple signals, this way malfunctioning Nsats can be detected even when they are not in use at that moment. This 'alive' signal should be done every couple of minutes to ensure up to date info on the Nsats. More on the operation of the constellation can be seen in Figure A.6 and Figure A.7.

## 4.3. NSAT CONSTELLATION DESIGN

The design of the Nsat constellation is iterated a number of times. An overview of this process is detailed in this section.

### 4.3.1. NSATS ORBIT DESIGN & NUMBER OF NSATS

The Nsats are organised in a Walker delta constellation with notation 50.2:24/6/1. Where the inclination is 50.2°, there are a total of 24 satellites, divided equally among 6 planes which are spread equally around the Moon. The phasing between satellites in adjacent planes is  $15^\circ (= \frac{360}{T_{Nsats} \cdot F_{Nsats}} = \frac{360}{24 \cdot 1})$ . A Walker delta constellation is optimised to prevent satellite collisions. The orbits themselves are circular frozen orbits, which means that the orbital parameters like eccentricity are constant over time. The frozen orbits are taken from [12, p. 61]. Note that in literature it is said that the investigated frozen orbits are close to frozen, so it is expected maintenance will be higher than proper frozen orbits, but lower than traditional lunar orbits. The Nsats have an altitude of 1,629 km. A check is performed to see if the orbit maintenance which is required for these near-frozen orbits fits within the budget. During the midterm it was found that 24 Nsats provide sufficient coverage and assure there are at least two Nsats in view of the rover at all times. While this design satisfies the visibility requirement, it does not guarantee that there are always 10 Nsats in view of the Rsat as seen for option 1 in Table 4.1. On top of that, it is not always guaranteed that each orbital plane has at least one Nsat in view of the Rsats. Since the Nsats are designed to only transmit one rover signal to the Rsats, less than 10 Nsats

in view would mean that less than 10 rovers can be serviced. This results in not meeting the requirement IRIS-06. Furthermore, the largest possible FOV that can be achieved is  $120^\circ$  for phased arrays while the required FOV is  $125^\circ$  with 4 Nsats per plane. While it is only a  $5^\circ$  difference, this means that there is no margin for safety. To guarantee that 10 rovers can be serviced at all time, and to have a margin regarding FOVs, the number of Nsats per plane is increased to six, resulting in 36 Nsats in the network.

#### 4.3.2. NSAT COVERAGE ANALYSIS

In Figure 4.5 the coverage map of the Nsat configuration of the Midterm is shown. To incorporate the increase of the number of Nsats a new coverage analysis is performed. Using the same conditions for the antennas and distances, better performance can be attained. However the maximum required distance and required  $FOV_{Rover}$  can be decreased to reduce the requirements on both the Nsat and Rover, this is shown in Figure 4.6. The main reason for the large required FOV is the fact that the rovers on the poles need to be serviced. Therefore a solution for the rovers is proposed: the type of antenna used is dependant on the latitude of the rover. Below a latitude of  $67^\circ$  antennae are used that have an upwards field of view of  $130^\circ$ , for example Hemi-omni antennae. Above a latitude of  $67^\circ$  a dipole with a FOV to the sides of  $80^\circ$  should be used. This is illustrated in Figure 4.7 and Figure 4.8. Note that a dipole with larger FOV could be used for even better coverage.

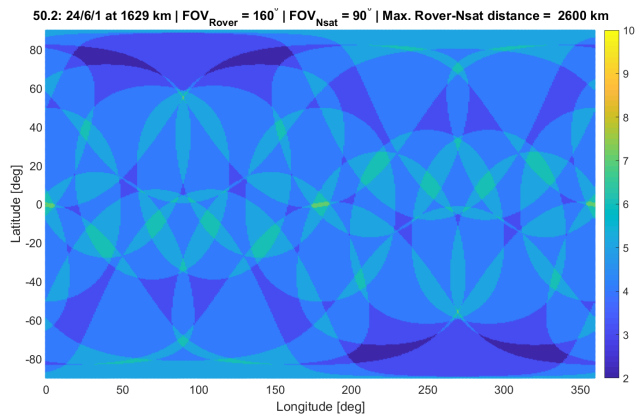


Figure 4.5: 2D visibility map: Midterm configuration

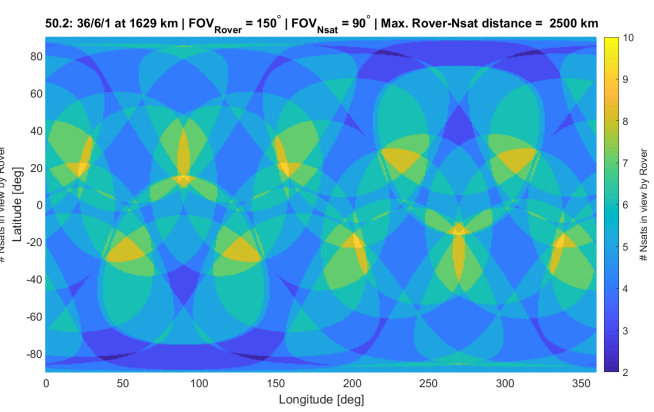


Figure 4.6: 2D visibility map: First iteration

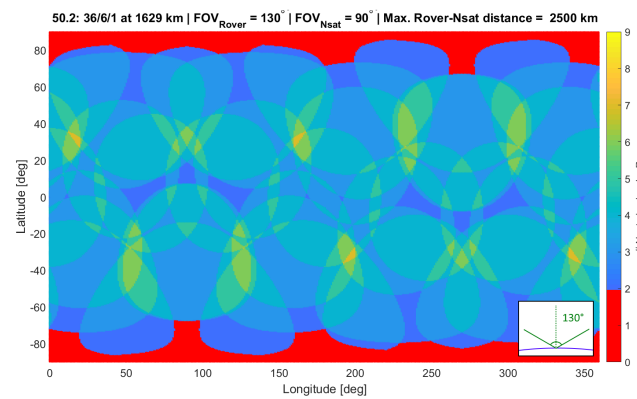


Figure 4.7: 2D visibility map: Second iteration (Hemi-omni)

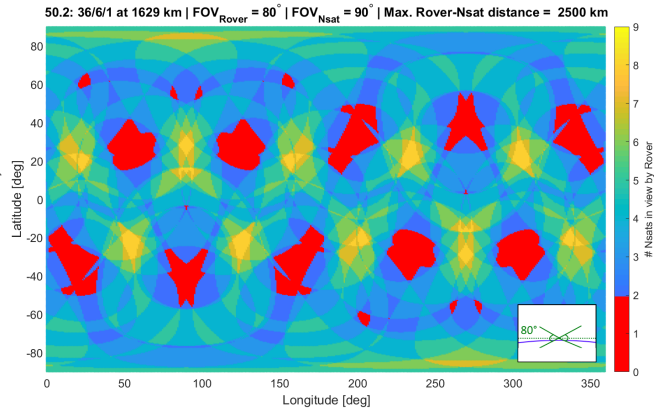


Figure 4.8: 2D visibility map: Second iteration (Di-pole)

#### 4.3.3. NSAT SOLAR ECLIPSE

During eclipses caused by the Earth it is assumed that the IRIS system will not be active, that is, no communication will be performed. This is done as otherwise the Nsat batteries and solar panels would need to be two times bigger, while they are just sparingly used. These Earth eclipses rarely occur and are easily predicted<sup>1</sup>, therefore this downtime can be scheduled. By extension also the Rsats will be non-active. The maximum Earth eclipse is found to be for 80 minutes in 2033 Oct 08.

#### 4.4. RSAT CONSTELLATION DESIGN

The design of the Rsat constellation is iterated a number of times. An overview of this process is detailed in this section.

<sup>1</sup><https://web.archive.org/web/20070305183925/http://sunEarth.gsfc.nasa.gov/eclipse/LEcat/LE2001-2100.html> Accessed on 26.06.2017

#### 4.4.1. RSAT ORBIT DESIGN & NUMBER OF RSATS

From the midterm it was assumed the halo orbit plane is as shown in (1) [Figure 4.9](#). This halo orbit is approximated using a circular orbit around the L1 point. This assumption is used to determine the required field of view of the Nsats and Rsats as well as the distances and the required number of Rsats. It was found that only one Rsat is required for full coverage of the Moon, for this a FOV of the Rsat antenna of  $5.4^\circ$  is required for full Moon coverage according to [Figure 4.4](#). The visibility results for this configuration are shown in [O1 Table 4.1](#). It is seen that there are never more than 10 rovers in view, also the actual contact time of an Nsat to Rsat is only 10 % of the orbit, thus 30 minutes. Therefore the number of required Rsats is increased to 3 and the radius of the halo orbit is increased to 44,000 km, this improvement is found by increasing the number of Rsats and varying the halo orbit radius. Even though there is an improvement in terms of connection time, there is only a 13 % decrease in less than 10 rovers visible as seen in [O2 Table 4.1](#). Since the number of Nsats is also increased to 36, the performance has increased drastically as seen in [O3 Table 4.1](#). Now there are always more than 10 rovers in view, as well that in more than 90 % of the cases there are more than two Nsats per plane in view. It is checked if there could be gone back to only one Rsat however the results show that similar results as [O1](#) are achieved.

Right before the end of the first iteration, it is found that the actual halo orbit is not perpendicular as assumed, but is slanted with respect to the xy plane. Furthermore, the halo orbit is elliptic and not centred around the L1 point as seen in (2) [Figure 4.9](#) and [Figure 3.5](#). Since there is not enough time to verify if the first assumed halo orbit exists, the final halo orbit from trajectory design is used as Rsat orbit. Since this slant is not smaller than  $5^\circ$ , its influence drastically changes the amount of Nsats that are actually visible by the Rsats as seen in [O4 Table 4.1](#). In 50 % of the cases there are less than 10 Nsats in view. The Rsats come much closer to the Moon than was first assumed (as close as 45,000 km compared to 72,000 km) thus due to the limited beam width of the Rsats, not enough Nsats are in view. Since it is not possible to further increase the beam width of the antenna, the choice is made to increase the number of Rsats to six for this orbit. This ensures better performance in terms of coverage as seen in [O5 Table 4.1](#), but does not yet assure a that there are always 10 Nsats in view, which is required for servicing 10 rovers at the same time.

For the second iteration instead of using one Halo orbit around Moon-Earth L1, a second Halo orbit is added which is mirrored with respect to the Earth-Moon plane, the six Rsats are then distributed over these two orbits. The Rsats are equally distributed in each orbit. Thus in each orbit three Rsats are phased  $120^\circ$ , while the phasing between satellites in the two orbits together is 60 degrees. It is found that six Rsats are required to provide the desired coverage. Also, multiple different kinds of phasing are tried but proved to be less effective. These Rsats are equally distributed over two planes, which ensures no collision will occur during the operational lifetime.

#### 4.4.2. RSAT COVERAGE ANALYSIS

The different iterations of the Halo are shown in [Figure 4.9](#), together with the Walker delta constellation. [Table 4.1](#) shows the results for all the different constellations that were considered.

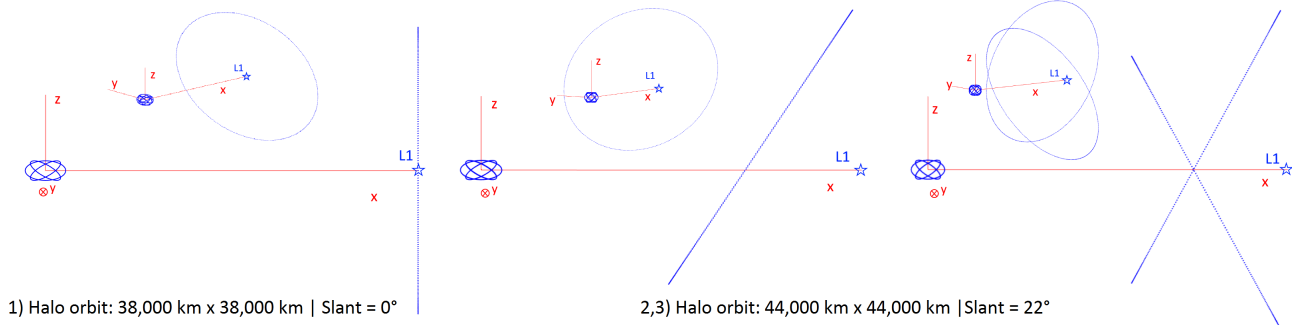


Figure 4.9: Drawings of the 3 main halo orbit configurations that were considered during the design.

Table 4.1: Rsat coverage results for the considered Rsat constellations. Rh = semi-major axis of halo orbit, Rhb = semi-minor axis of halo orbit, P = probability of occurrence,  $t_c$  = connection time.

Option	# Rsats	RhxRhb [1e3 km]	#Nsats	P(<10 Nsat) [%]	P(0 Nsat /plane) [%]	P(1 Nsat /plane) [%]	P(2 Nsat /plane) [%]	P(3 ≥ Nsat /plane) [%]	Mean $t_c$ [%]	Max $t_c$ [%]
O1	1	38x38	24	100.0	46.7	53.3	0.0	0.0	10.2	10.2
O2	3	44x44	24	86.9	0.8	55.9	43.3	0.0	17.5	40.0
O3	3	44x44	36	0.0	0.0	8.6	69.0	22.4	18.5	40.0
O4	3	44x40	36	50.8	3.0	43.1	47.4	6.5	11.3	37.0
O5	6	44x40	36	5.2	0.0	13.8	59.6	26.6	13.7	37.0
O6	6	44x40	36	0.0	0.0	0.2	69.2	30.7	19.3	39.0
O7	6	44x40	24	61.6	0.3	45.8	54.0	0.0	19.3	41.0

#### 4.4.3. RSAT SOLAR ECLIPSE

As discussed earlier, if the Nsats are eclipsed by the Earth, the Rsats will also be not operational. In case an Rsat is eclipsed by the Earth, it is inactive. This occurs maximum twice every month. Using [Figure 4.11](#) the downtime can

be computed, which is the fraction of the orbit of the Rsat that is covered by the Earth:  $\frac{2 \cdot R_E}{2\pi R_h} = \frac{2 \cdot 6378}{2\pi 44,000} = 0.05 \rightarrow T_{eclipse} = 0.05 \cdot 12.25 = 0.6125$  days, however when looking at the time it takes for the orbit to pass by Earth it is  $\frac{2 \cdot R_E}{2\pi d_{Earth-L1}} \cdot \frac{2 \cdot 6378}{2\pi 330,000} = 0.0062 \rightarrow T_{eclipse} = 0.0062 \cdot 29.5 = 0.18$  days. From these calculations it is seen that the maximum eclipse time is 0.18 days, which is given to design the thermal subsystem of the Rsats. Note that Rsats are only in eclipse if within those 0.18 days an Rsat actually passes after the Earth, thus the eclipse occur twice per month at the most, and not necessarily to the same Rsat. The probability of an Earth eclipse occurring for any duration between one second and 0.18 days is equal to  $\frac{0.18}{12.25} \cdot 6$  satellites = 0.0864 = 8.64 % per orbit. These eclipses do not affect the constellation communication performance

## 4.5. FINAL CONSTELLATION DESCRIPTION

The final design of the constellation is described in Figure 4.10.

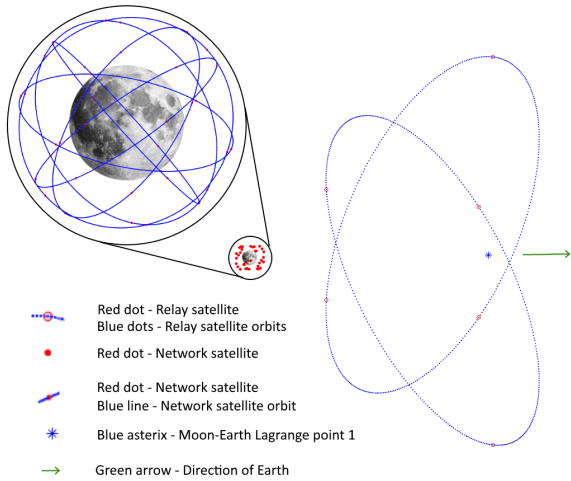


Figure 4.10: The final designed constellation consisting of Nsats in a network and Rsats in 2 halo orbits.

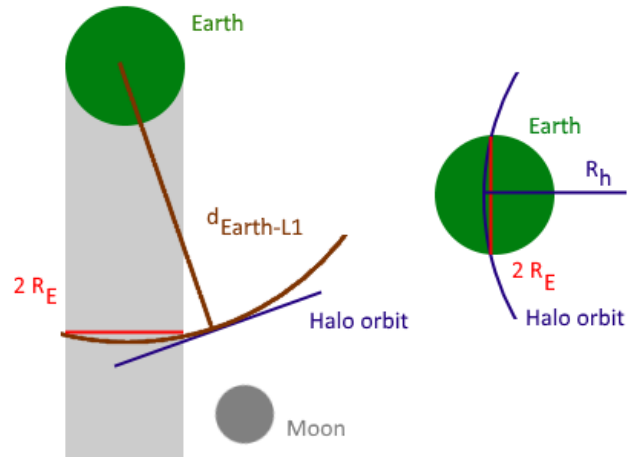


Figure 4.11: Top view of the Earth-Moon plane for eclipse conditions(left), Side view of the Earth-Moon plane for eclipse conditions(right).

### 4.5.1. WALKER DELTA CONSTELLATION

The Nsats are organised in a Walker delta constellation with notation 50.2:36/6/1. Where the inclination is 50.2°, there are a total of 36 satellites, divided equally among 6 planes which are spread equally around the Moon. The phasing between satellites in adjacent planes is 10° ( $= \frac{360}{T_{Nsats} \cdot F_{Nsats}} = \frac{360}{36 \cdot 1}$ ). The orbits themselves are circular frozen orbits, which means that the orbital parameters, for example eccentricity, are approximately constant over time. The Nsats have an altitude of 1,629 km.

The Moon-pointing antenna has a FOV of 90°, this ensures proper coverage of the poles. The Relay-pointing antenna has a FOV of 90°, this ensures that there are 10 Nsats in view of the Rsats at all times.

### 4.5.2. HALO ORBIT AROUND L1

The six Rsats are located in two halo orbits around the Moon-Earth Lagrange point 1. Three Rsats per orbit are equally spaced (120°) within the halo orbit. This halo orbit orientation is seen in (3) Figure 4.9 and the Rsat locations are shown in Figure 4.10. The halo orbits can also be seen in Figure 3.5. The network-pointing antenna has a FOV of 3.57°. The Earth-pointing antennas have a FOV of 120°, this is required to ensure that there is always a Relay-Earth link.

## 4.6. ORBIT MAINTENANCE

Orbit maintenance for the Nsat is estimated using the orbit perturbation (section 14.14) and plane change (section 14.3) tools. The  $\Delta V$  required for maintenance (dependent on time of burn) for a specific orbital plane is estimated by evaluating Kepler elements at each time step of a propagation from the initial orbit conditions. A correction  $\Delta V$  for each time step is estimated by applying the three manoeuvres described in subsection 14.14.2 to change the orbital elements at each step to their nominal values. An example of this estimation for the chosen Walker delta constellation is shown in Figure 4.12. The RAAN change over time can be approximated by a linear function for all planes. This linear trend was assumed as the nominal RAAN. The real RAAN change has a small added periodic component, as seen in Figure 4.13. Other orbital elements are kept the same as the initial conditions.

The correction  $\Delta V$  dependent on correction period (period of time between each correction event) is estimated by dividing the  $\Delta V$  by the time at each time step. Using this estimation, a correction period of 27 days is chosen to minimise  $\Delta V$  required. The total maintenance  $\Delta V$  budget is chosen using the worst case  $\Delta V$  required per correction event. This is the maximum value estimated for any plane for a period spanning from 27 to 32 days (allowing for a five day delay). 22 planes with different RAAN are checked, as shown in Figure 4.15. The rest of the Kepler elements for the initial conditions correspond to that of the chosen Walker constellation. This results in a  $\Delta V$  of 15 ms<sup>-1</sup> per year. The maximum expected  $\Delta V$  per correction manoeuvre is 1.11 ms<sup>-1</sup>. This manoeuvre takes 16.65 s with 1 N thrust, which

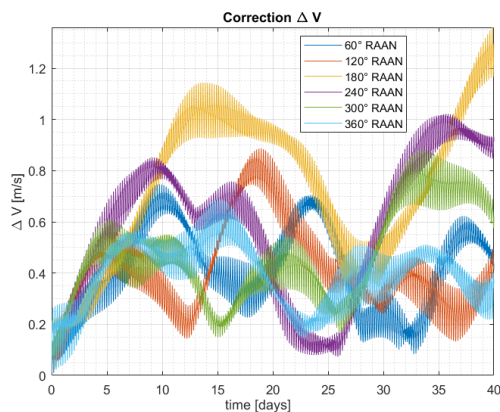


Figure 4.12: Estimated  $\Delta V$  for a single correction event. Each colour corresponds to a different plane of the constellation.

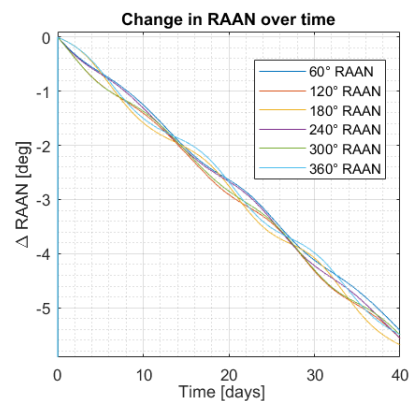


Figure 4.13: Change in RAAN over time, due to perturbations, for each plane of the constellation.

complies with the capabilities of the propulsion subsystem.

For the Rsat, from the midterm a  $\Delta V$  of  $25 \text{ ms}^{-1}$  per year for maintaining the Halo orbit was found. The idea is to perform as little amount of manoeuvres as possible as during manoeuvres the communication link cannot be established either due to less power or reorientation of the Rsat. No link means no service to some of the rovers which means there is some down-time which is to be minimised. Using the trajectory tool the  $\Delta V$  estimated to keep it in its orbit is in the order of  $15 \text{ ms}^{-1}$  per year. After further investigating it is found that this estimate does not contain errors that are made when maintaining the orbit. Thus a more conservative but more realistic value is  $50 \text{ ms}^{-1}$  per year which is taken from [14, s. 15].

#### 4.7. DISPOSAL PROCEDURE

Multiple options for disposing of the Nsats are considered. One option is to insert the Nsat in an orbit which collides with the Moon, however this would cost  $210 \text{ ms}^{-1}$  (more than 50% of the total Nsat  $\Delta V$  budget). Therefore another solution is necessary. In literature it is found that a 1,200 km circular orbit with an inclination of  $55^\circ$  has a lifetime of 14 years [15, p.162]. Since only  $105 \text{ ms}^{-1}$  is available for disposal, the disposal orbit has the aforementioned parameters but only an inclination of  $52.2^\circ$ .

For disposing of the Rsats it is decided to go back to the second Sun-Earth Lagrangian point and from there go in a heliocentric orbit for disposal.  $50 \text{ ms}^{-1}$  is required to come from a L2 Sun-Earth halo orbit into a L1 Moon-Earth orbit. Thus the same amount is required to do the reverse. On top of that for the RDeVe it is found that  $10 \text{ ms}^{-1}$  is required to go from a L2 Sun-Earth halo orbit into a heliocentric orbit. The Rsats have  $100 \text{ ms}^{-1}$  allocated for end-of-life, meaning that there is a certain margin for contingencies.

#### 4.8. SPARES SYSTEM

Since the Nsats are not designed to be redundant, they are prone to failure. To ensure that the constellation provides the required communication, additional spare Nsats are launched with the constellation. These spares are deployed in the Walker delta orbit planes together with the operational satellites. Since these satellites are identical to the operational satellites, they cannot perform orbit plane changes without significantly reducing their operational lifetime. Therefore, these spares are only operational in the orbit plane in which they are deployed and only conduct phasing changes. If an operational satellite malfunctions, it is moved away with phasing manoeuvres or it performs an end-of-life manoeuvre. After this, the spare satellite will conduct a phasing manoeuvre, which can be done within 10 days. Due to this manoeuvre, the satellite will have a reduced lifetime since this manoeuvre requires  $\Delta V$ , which is also required for orbit maintenance.

A certain threshold is determined in section 4.9 for when a new launch from Earth is requested to replenish the amount of spares. When the amount of spares reaches this launch threshold, a new launch is prepared, which will arrive within 183 days with a deployment vehicle capable of delivering satellites to each orbital plane.

The relay satellites are designed to be redundant and it is assumed that they will not fail in five years operation.

#### 4.9. CONSTELLATION RELIABILITY ANALYSIS

To determine the constellation reliability, a reliability analysis is conducted for the network constellation. This is done by simulating the constellation using Monte Carlo simulations. However, before a multi-element reliability analysis can be conducted, first the reliability of a single element has to be investigated. For this, statistical failure data for small satellites (10 kg to 500 kg) is used, which can be seen in Figure 14.22 [16]. A Weibull curve is fitted through this failure data using the Weibull processor described in section 14.8. With this, the failure rate of a single satellite can be obtained at any point in time.

Now that the reliability of a single satellite is known, the system constellation can be analysed. In this case, this

can be done piece-wise without losing accuracy or simplifying the situation. Firstly, the system failure criterion is defined. Since the constellation provides N-1 redundancy, which is proven in subsection 4.1.2, the system does not guarantee 100 % coverage only after two satellites have failed. To have an impact on the constellation coverage, these two satellites have to be next to each other. To prove the reliability of this constellation, the two ways of adjacent satellite are analysed separately: adjacent plane failure and in plane failure of adjacent satellites.

### 4.9.1. ADJACENT PLANE SYSTEM FAILURE ANALYSIS

The out of plane adjacent failure is investigated using the adjacent failure analysis Monte Carlo simulation tool described in section 14.9. For a five year period, the downtime is tracked for satellite failures in adjacent planes. Every time a satellite fails, it is replaced within 10 days. For this analysis it is assumed that infinitely many satellites are present. This can be done since the effect of having limited spares in a plane will be covered in subsection 4.9.2.

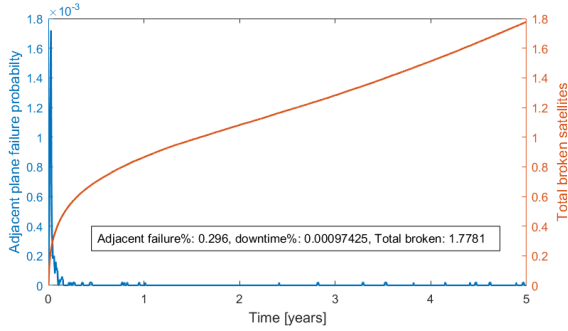


Figure 4.14: Adjacent plane satellite failure analysis results for a Monte Carlo simulation including 6 orbital planes with 6 satellites each, where only out of plane failures are measured (50,000 samples).

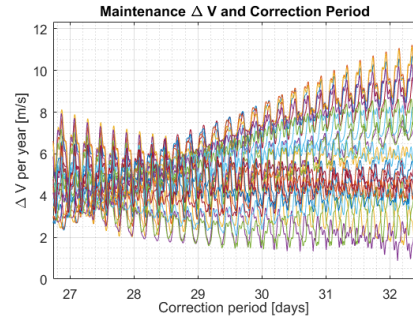


Figure 4.15: Maintenance  $\Delta V$  dependent on correction period, estimated for 22 sample planes. Each colour corresponds to a different plane.

The results of this analysis are displayed in Figure 4.14. The effect of infant failure can be clearly seen in the first months, after which the probability of a failure decreases drastically. At the end of the five years, the beginning effects of wear-out can be seen with the increasing rate of failing satellites. The probability of having an out of plane adjacent failure in the constellation lifetime of five years is only 0.296 % with a negligible downtime and an operational fraction of 99.99903 %. This quantifies the Nsat reliability for adjacent plane failure with a reliability of  $1 - 0.00296 = 99.704 \%$

### 4.9.2. IN-PLANE SYSTEM FAILURE ANALYSIS

For the in-plane system failure analysis, a similar simulation is done. However, the fact that the amount of spares is in fact limited, is taken into account. As discussed before, the spares system operates within one orbital plane. To investigate the amount of spares required and the in-plane reliability, the Monte Carlo analysis is limited to only one plane in the in-plane failure analysis tool from section 14.10.

Before detailed results are generated with the in-plane Monte Carlo simulation, a constellation parameter optimisation is conducted. These parameters are the amount of spare satellites present in an orbit plane at the begin of life of the constellation, the launch threshold and the amount of satellites replenished to an orbital plane at launch arrival. The goal of the optimisation is to reduce the system failure probability, reduce the amount of launches required for the first five years and to reduce the amount of zero satellites present per orbit such that redundancy can be established within 10 days. The optimisation results can be seen in Figure 4.16. Note that the axis scale varies per figure. To achieve minimum reliability and minimum amount of satellites and launches required, the following values are chosen as an optimum. Two initial spares are present in plane, two satellites delivered per launch and a launch threshold of zero spares.

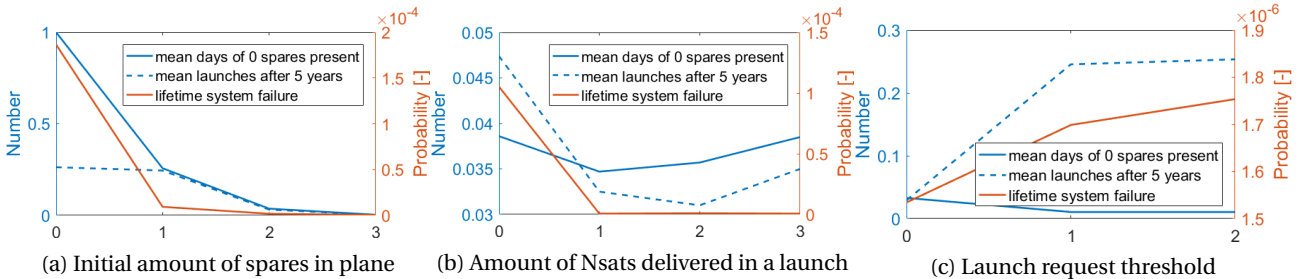


Figure 4.16: Optimisation results of spare parameters analysis.

With these values as input, the final in-plane reliability simulation can be done using the in-plane failure analysis tool described in section 14.10. The results can be seen in Figure 4.17 and Figure 4.18. Figure 4.17 shows the average amount of spares, broken satellites, launches arrived and failure probability over the constellation lifetime. The total probability of having a system failure in the first five years of operation is 0.334 %, so the system reliability is 99.6650 %. A peak in system failure probability of 0.0247 % is observed right after deployment, which resembles the infant failure. After this stage, the probability of system failure drops below 0.01 % after day 40 and is zero for 83.4 % of the time. On average after five years of operation 0.297 satellites have failed, 1.77 spares are present and 0.0313 additional launches

are required.

Figure 4.18 shows histograms for the number of failed satellites and the number of launches required at end of life and the minimum amount of spares present in the plane throughout the lifetime. 74.2% of the time, no satellite failures occur throughout the constellation, 96.9% of the time no additional launches are necessary to maintain the constellation and only 3.58% of the time there is a moment with no spares present in the orbit to restore the system redundancy within 10 days if a failure occurs in that moment.

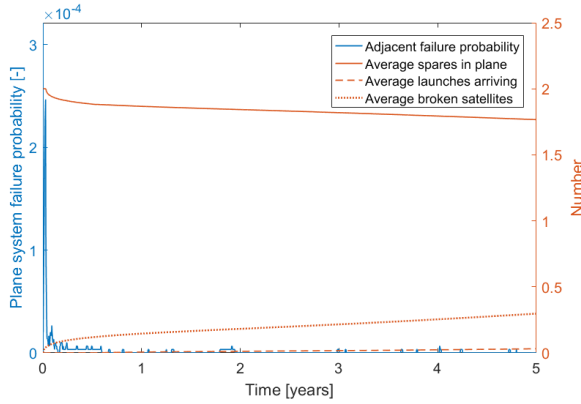


Figure 4.17: Average in-plane failure data over five years (300,000 samples).

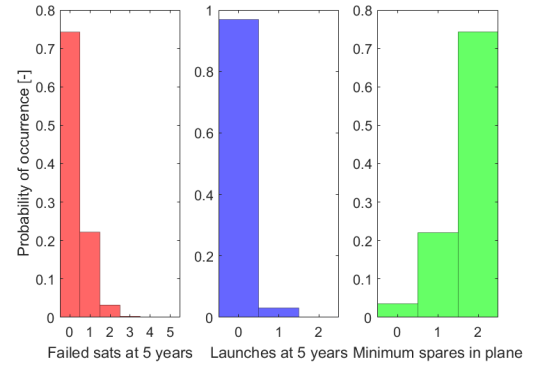


Figure 4.18: Statistical in-plane failure data over five years (300,000 samples).

#### 4.9.3. RELAY RELIABILITY ANALYSIS

A third Monte Carlo simulation is done using the in-plane failure analysis tool. The spares system is disabled and the tool is configured such that a satellite has to fail twice before it is registered as a system failure to simulate the internal redundancy of the Rsats. This is done for one plane of six relay satellites, which results in no system failures after five years for 100,000 samples indicating that no relay satellite failures will occur given that they are fully redundant.

#### 4.9.4. RELIABILITY ANALYSIS CONCLUSION

This reliability analysis has piece-wise quantified the reliability from successful deployment to end of life. For this, an out of plane failure analysis, in-plane failure analysis and relay failure analysis have been done by using Monte Carlo simulations. The total reliability is determined by multiplying the separately calculated reliabilities, as is shown in Equation 4.1. The total constellation reliability is equal to 97.711%, meaning that there is a 2.2892% chance of a system failure in five years. A system failure has a maximum duration of 10 days when a spare is present, which is the case for 96.42% of the time as can be seen in Figure 4.18.

Due to time constraints, the deployment reliability is not investigated. The reliability,  $R$ , of the whole constellation is calculated in Equation 4.1. The computed reliability of 97.7% complies with the required reliability of 97.5% according to IRIS-NCON-01. The remaining 2.5%, a system failure will occur. This will include an adjacent satellite failure which will last up to 10 days and results in a small fraction of maximum 5.56% of the Moon not being covered by the constellation. Furthermore, with a certainty of 96.88%, there are no additional launches required.

$$R = R_{outofplane} \cdot R_{in-plane}^{N_{planes}} \cdot R_{relay} = 0.99704 \cdot 0.99665^6 \cdot 1.00 = 0.97711 \quad (4.1)$$

In this chapter the process of designing the communication link, and its results, are presented.

## 5.1. DESIGN PROCESS

With regards to the communication subsystem, there are four main sources of requirements: customer requirements, requirements flowing down from the constellation design, requirements imposed by other sub-system designs and stakeholder requirements. In addition to the requirements, there are constraints on the system originating from the operational environment.

The link budget as explained in the midterm report is a tool that keeps track of all gains of the system and all the losses [1, p.26]. The derivations of the governing equations used in this tool are presented in SMAD [17, p.519-538]. All assumptions presented in the midterm report are still valid except the assumption regarding the system noise temperature. This assumption is further investigated. It is found that the Moon also radiates energy in the infrared and microwave wavelengths, aside from reflecting sunlight radiation [18]. Furthermore, measurements performed on the Lunar Reconnaissance Orbiter (LRO) indicate a near sinusoidal system noise variation during the course of the LRO's orbit [19]. The minimum system noise temperatures occur when the satellite is close to the edge of the Moon and also when it is furthest away from the lunar surface. At S-Band (2.3 GHz) the LRO experiences a maximum system noise temperature of 138 K, which corresponds to the value used in the midterm extracted from SMAD [17]. However, at X-band (8.4 GHz) the LRO experiences a maximum system noise temperature of 200 K and at K-band (19 GHz) the maximum noise temperature was 240 K.

In reality lower system noise temperatures can be expected. This is due to a number of reasons. The Nsats will be flying at a higher altitude from the Moon, thus experiencing less of the reflected radiation. The Nsats and Rsats are considerably smaller than the LRO (only 0.1% of LRO's volume). This low volume can be translated to short cable lengths reducing the noise coming from the cabling. Lastly, the system noise temperature decreases the further away the satellite is from the centre lunar disk.

An overview of the outputs of interest from the link budget tool is given in Figure 5.1. These outputs give an indication of the link performance, the subsystem components needed and requirements imposed on other subsystems.

Lastly, these outputs of interest are checked if they comply with the requirements. In case of compliance that part of the design is finalised for the current iteration. In case of non compliance a corrective action or a redesign has to be performed depending on the nature of the system non-conformance.

This process is visually represented with a flow chart in Figure 5.1. The rectangular boxes indicate processes, the parallelogram boxes indicate inputs/outputs and the rhomboid blocks indicate decisions. The green arrows indicate compliance and the red ones indicate non compliance

### 5.1.1. MOON-NETWORK LINK

The driving requirement for the constellation is the full coverage requirement IRIS-NCON-01. The constellation group stipulated the value for the required beamwidth and calculated the maximum distance between receiver and transmitter based on the constellation design.

First, to make the connection to the Moon, a parabolic antenna is considered. As explained in the assumptions in the midterm , the estimated power of the rover for communications is calculated to be approximately 40 W [1, p.26]. For the antenna it could use a low-gain omni-directional antenna typically with a gain of 2 dB , resulting in a effective isotropic radiated power (EIRP) of 18 dBW. To close the link, while keeping the 60° beamwidth requirement of the constellation group, the parabolic antenna has to operate in range from 1 GHz to 1.4 GHz. Lower than 1 GHz the diameter of the dish increases to the extent that it clashes with the thrusters and higher than 1.4 GHz the space loss increases more than the gains, thus reducing the margin.

However, according to the International Telecommunication Union's recommendations for frequency usage in the shielded zone of the Moon [20], the operational frequency band of the antenna corresponds to a band of frequencies that are interesting for radio-astronomical observations. Namely, the observation of neutral hydrogen spectral line and continuum observations. Although, these are only recommendations, potential costumers of Project IRIS are parties interested in performing radio-astronomy. Therefore, the operational frequency has to be increased.

As mentioned before, increasing the frequency, while keeping the 60° beamwidth requirement, leads to a reduction of the antenna diameter but also the peak gain of the antenna and an increase in free-space loss. Ultimately resulting in the link not being able to close.

To resolve the issue several possibilities are considered. Horn antennas would be able to provide the gain needed to close the link but the beamwidth would be half of the required beamwidth. Helical antennas can provide the required beamwidth but the gain is not enough to overcome free-space loss.

Another alternative is decreasing the maximum distance between Rx and Tx to minimise space losses. The problem with this solution is the fact that the chosen orbits are so called frozen orbits. Choosing another set of orbits would result in an increase in propellant tank size and mass due to the increased need for orbit maintenance. Furthermore, lowering the orbit height would cause either the number of satellites or the beamwidth to increase. Increasing the

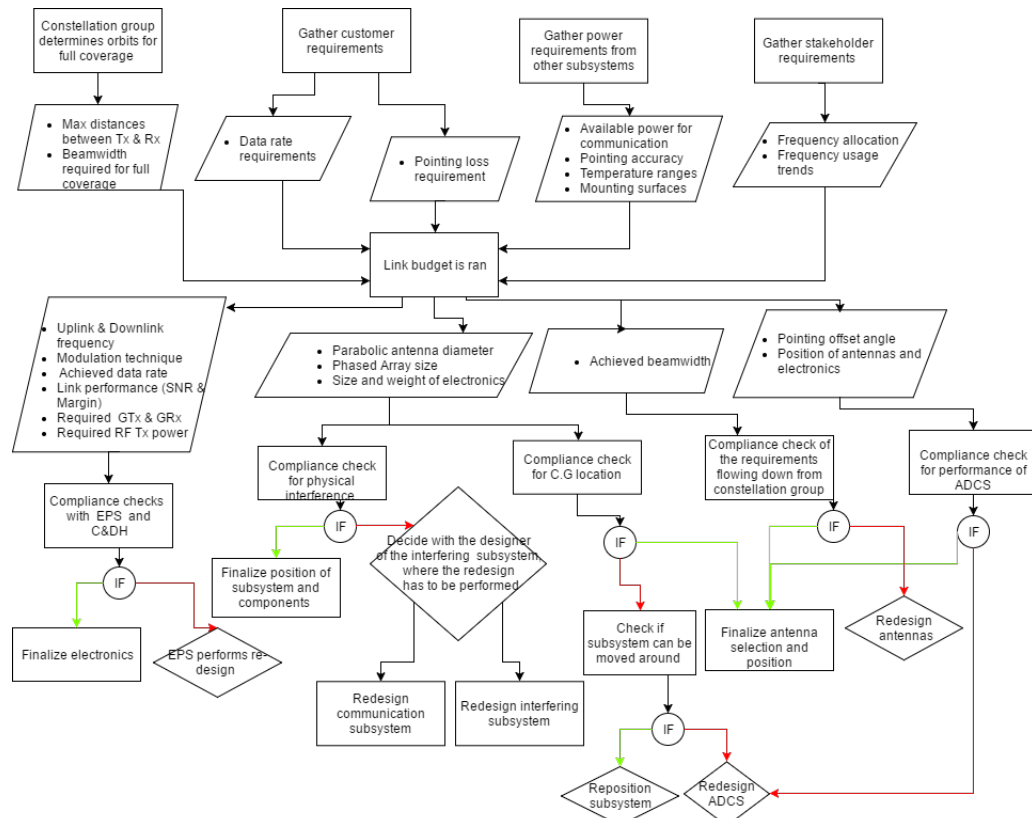


Figure 5.1: Flow diagram of the link design process

number of satellites increases the costs, while increasing the required beamwidth makes it virtually impossible to close the link. Therefore, this option is discarded.

The last option is the use of phased arrays. Phased arrays have been around for a long time, but they were mainly used in radar systems. However, their use in spacecraft is on the rise: they are used in the Messenger and Gaia missions, amongst others. The advantages of such an antenna include the high achievable gains (29 dB for the Messenger spacecraft [21]). Another advantage of this type of antenna is the fact that the beam can be electronically steered by shifting the phase of the individual beams of the elements such that constructive interference occurs in a particular direction. For the Messenger spacecraft the beam could be steered  $\pm 45^\circ$  off centre while still having a gain of 24 dB. This results in lower weight of the spacecraft as there is no need for a gimbal mechanism to point the antenna and eliminates the risk of the mechanism potentially jamming or malfunctioning in space. Furthermore it reduces the required pointing accuracy that the ADCS has to deliver, which can lead to a reduced mass. The biggest disadvantage of this type of antenna is the high power consumption and the increased mass. The Messenger antenna on its own weighed 2.9 kg and the electronics needed for operation consumed 52 W of power [22].

A lot of research has been focused in increasing the data rates in Cubesats while keeping power consumption low. In his Master's Thesis, K. Dang concluded that a phased array the size of a 3U cubesat side could achieve a gain of 14.2 dB, while steered at  $\pm 40^\circ$ , and a peak gain of 17 dB [23]. Theoretically this array can achieve a data rate of 11 Mbps. Klein et al. conclude that a phased array with 16 elements able to fit on the side of a 2U cubesat could provide 11 dB of gain while requiring less than 10 W of power for the transmitter [24].

From the discussion above, it can be concluded that using phased arrays antennas is the superior solution. It scores high in the performance criteria offering excellent power and link performance. Although phased arrays have been around for a long time they have never been flown before on Cubesats, however that is about to change as Kymeta Government Solutions, Inc. plans a mission for flight qualification testing and demonstration of Ka-band phased array antenna on a 3U cubesat with beam steering capabilities and a gain of 24 dB [25].

### 5.1.2. NETWORK-NETWORK LINK

In the case of a rover being on the far side of the Moon, the rover signal will be transmitted to the the Rsat via the Nsats. The driving requirement for this segment of the data transfer is the three second lag time between command and rover response. Two possibilities are considered for achieving this: inter-plane cross-link and intra-plane cross-link. A hybrid between these two is not considered as this would require two extra antennas driving the mass to an unacceptable extent .

The advantage of inter-plane cross-link is that in many cases the rover signal can be transferred to the Rsat via only one cross-link, reducing the lag time. However, the disadvantage is that the Nsats would require either a pointing mechanism for the antenna or require a complicated ADCS to provide pointing. The use of a phase array for this func-

tion is considered risky as the sidelobes of the array could cause interference with the other phased array collecting data from the rover, positioned 90° to it.

In the case of cross-linking only within the planes, the relative attitude between the Nsat that acquires the rover signal and its neighbour is known, therefore the antenna could be mounted in such a position that is always pointing to its neighbour. Clearly the advantage here is the reduced hardware mass and reduced requirements from the ADCS. The disadvantage here is that the rover signal has to be cross-linked at least twice.

To guarantee compliance with the customer specified three second lag requirement, the data rate for this link has to be doubled in order to minimise the cross-link time. The most efficient way to achieve this is to utilise frequencies in the higher K-band and higher. In these frequency bands the available bandwidth allows for data rates in the order of  $\text{Gbits s}^{-1}$ . Furthermore, these frequency bands are steadily becoming the standard for space communication [26, p.71]. Taking into account the doubled data rate for both possible cross-link solutions, it can be concluded that the intra-plane cross-link is the winner due to the reduced hardware required for pointing.

With regards to antenna selection only parabolic antennas are considered as the metal dish minimises interference generated from the side lobes of the phased array. From the link budget tool it is found that a 10 cm dish in diameter operating on 30 GHz can perform the task allowing for transmission at  $1 \text{ Mbits s}^{-1}$ .

### 5.1.3. NETWORK-RELAY LINK

In this segment the design driver is the maximum distance between Rx and Tx. In the best case scenario the maximal distance is calculated to be approximately 70,000 km and in the worst scenario to be 80,000 km. To minimise the risk, this link is sized for the worst case scenario.

In the first iteration of this segment the design is focused on maximising the gains such that the free-space loss can be overcome. For this reason parabolic antennas were selected both on the Nsat and the Rsat. Using the link budget tool it is found that 0.5 m parabolic antennas on both satellites can be used to achieve the connection at the required data rates. However, in case the Nsats would not have an antenna pointing mechanism, usually only one Nsat per plane would be in view of the Rsat. This can lead to an undesirable situation were the user experiences down time.

As with the other segments, the usage of mechanisms is to be limited. For this reason an alternative has to be found. Use of horn or helix antennas not only would not offer any advantage in field of view but the gains are not strong enough compared to the free-space loss. Therefore, the only possible solution is using a phased array. However, using the same phased array as the one that acquires rover signals requires either a parabolic antenna on the Rsat bigger than 2 m in diameter or more than 100 W of RF transmission power, both of which are impossible to achieve.

From research into phased arrays it is found that values as high as 24 dB in gain can be expected in the coming years [27] [28]. Using this value it is calculated that the link can close if the Rsat has a 0.75 m parabolic antenna, which fits in the fairing of the launcher. The pointing of the parabola is done by the ADCS of the Rsat, that will be programmed such that the parabola is always pointing towards the Moon.

### 5.1.4. RELAY-EARTH LINK

The driver in this last segment of the link is the ground-station. In particular, the gains their antennas can achieve and their operational downlink and uplink frequencies. There are several ground-stations around the world with antennas having diameters ranging from a couple of meters up to a couple of hundred meter antennas of the Deep Space Network (DSN). Usage of the DSN for collection of rover data is not feasible due to the fact that the DSN is used actively all year round for the purposes of telemetry and tracking of other missions. It is highly likely that a scientific mission is given priority over a commercial when it comes to the DSN, causing a downtime. Therefore other ground stations are considered. Preliminary research indicated that there are several private or governmental agencies that own ground stations equipped with 10 m diameter dishes<sup>1 2 3 4 5 6</sup>. Due to the abundance of these ground stations it is chosen to use this value as the ground station antenna. The biggest challenge during design of this link is the fact that the attitude of the Rsat has one side pointed to the Moon, meaning that the opposite side, where the Earth-pointing antenna is mounted is not pointing directly to Earth. This is solved by using an equivalent phase array as they are able to point without the use of mechanisms. The link can be closed with no problem while ensuring the required data rates. To summarise the final link design a functional flow of the communications is presented in Figure 5.2.

## 5.2. DATA FLOW

Besides the scientific data that the rover has to transmit back to Earth there is also the housekeeping data generated by the elements of the constellation, that is the rover, the Nsats and the Rsats.

Normally the rover is going to include its housekeeping data along with the scientific data. As mentioned in [subsection 5.1.1](#) the rover will transmit its data to an Nsat. For this link the rover will need to provide an EIRP of 17 dB. This can be achieved by using a low gain, wide pattern omni antenna with a gain of 2 dB and a transmission power of 35W or a higher gain semi-omni-directional antenna with a gain of 4 dB and transmission power of 15 W. In the case of rovers on the poles close consideration of the radiation pattern of the antenna and its position should be done in collaboration with the constellation group. The first satellite that acquires the rover signal will perform a series of processing steps on the signal. The received signal will first be baseband processed, where it will be passed through a low pass filter, a layer of encryption will be applied followed by sampling, quantisation and encoding. After this is

<sup>1</sup>Estrack- [http://www.esa.int/Our\\_Activities/Operations/Estrack/Estrack\\_ground\\_stations](http://www.esa.int/Our_Activities/Operations/Estrack/Estrack_ground_stations) Accessed on 26.06.2017

<sup>2</sup>Near Earth Network- [https://www.nasa.gov/directorates/heo/scan/services/networks/txt\\_nen.html](https://www.nasa.gov/directorates/heo/scan/services/networks/txt_nen.html) Accessed on 26.06.2017

<sup>3</sup>Australian Space Communication- <http://www.spaceacademy.net.au/spacelink/auspacecom.htm> Accessed on 26.06.2017

<sup>4</sup>Orbit-<http://orbit-cs.com/wp-content/uploads/2017/03/Orbit-Gaia200-400-DS-v7.02.pdf> Accessed on 26.06.2017

<sup>5</sup>Kongsberg- <http://www.ksat.no/en/services%20ksat/ground%20network%20services/> Accessed on 26.06.2017

<sup>6</sup>Kratos-ISI <http://www.kratos-isi.com/-/media/kisi/pdf/datasheet-turnkey-earth-stations.pdf?la=en> Accessed on 26.06.2017

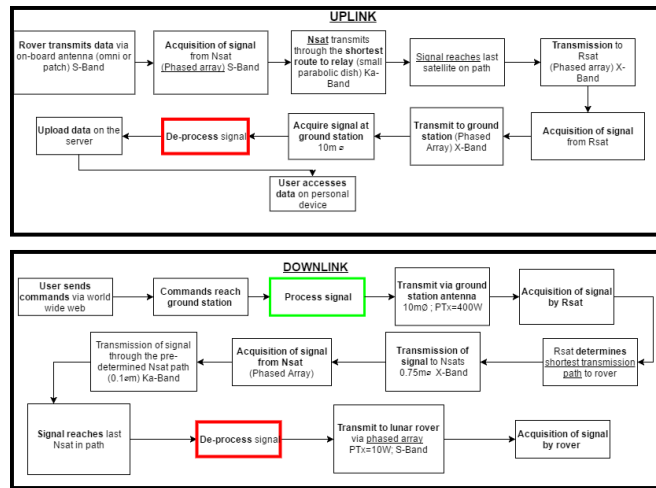


Figure 5.2: Functional flow of the communication

done the signal will be modulated to a Ka-band carrier wave. Lastly, it will be amplified. Most processes done here can be done in the order of  $\mu s$ , the time needed for adding the operations group layer of encryption has to be further investigated.

After the signal has been amplified it will be transmitted to the neighbouring Nsat. From here it will be received from the next Nsat in the transmission path where it will be filtered and amplified again. Then it will be re-transmitted to the next Nsat in the path up until it reaches an Nsat that is in view of the Rsat. Once the Nsat is in view of the Rsat it will transmit to it. This data transmission will be done at the customer specified rate of  $500 \text{ kbit s}^{-1}$ . Once the data arrives at the Rsat it will begin transmission of the data back on Earth at a rate of  $2 \text{ Mbit s}^{-1}$ . Once it reaches Earth the signal will be de-processed, where the inverse of the processing steps, applied on the first Nsat in the transmission path, will be applied to retrieve the data. Then, the data will be distributed to the users, using the ground station optical connections that allow for data rates up to  $500 \text{ Mbit s}^{-1}$ .

The Nsats individually transmit their housekeeping data when they are in view of the Rsat, where it will all be collected and sent back to Earth for analysis. In case an orbital plane is not performing any high data rate uplink from the rover to the Rsat, the housekeeping data can also be cross-linked to the Rsat through the network. This is decided because the customer data take priority over housekeeping.

In order to detect any malfunctioning Nsats, the Nsats will be transmitting a signal to each other. This signal will consist of a message indicating that it is alive and its attitude. This type of message is at most 100 bit in size and can be passed through the network without major disturbance to the flow of scientific data. The life signals after passing through the Nsat will be transferred to the Rsat that will collect it, detect any non-functioning ones and send a report on Earth about the status of the Nsats. In this way the Rsats are aware of the non-functioning satellites and make a selection on the path that the signal has to pass through to avoid the non-functioning Nsat.

Finally, the commands for the rovers and individual Nsat will be collected on the Rsat after they have been transmitted from the ground station. For the rover commands the Rsat is going to know where it is, the user has to specify this, it will select the transmission path and immediately relay the commands so that they reach the rover as fast as possible. The same can be done for the Rsat commands.

The flow of the data and the equipment used to achieve it is visually represented in Figure 5.3. This is the general flow of the data, only two network satellites are indicated in the flow, but in general more than one cross-link will be required before the signal reaches a Nsat in view of a Rsat.

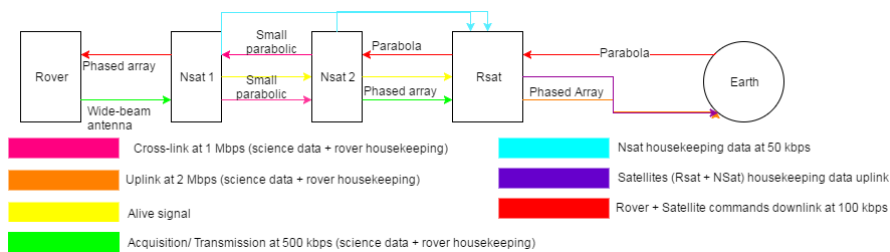


Figure 5.3: General flow diagram of the data including the associated data rate and transmission equipment

### 5.2.1. INVESTIGATION OF THE THREE SECOND LAG TIME

To guarantee compliance with the customer imposed requirement of three second lag time (IRIS-05, a scenario where a 10 kbit command is sent from the ground station to an Rsat, then cross-linked through three Nsats and finally reaches

the rover, after the command has been applied the rover sends back a 10 kbit response. This response is again cross-linked through three Nsats, followed by the Rsat and back to Earth. Two times for each link are calculated: the transit time, which is calculated by dividing the distance by the speed of light and processing time, which is calculated by dividing the command/response time by the data rate of the segment. Note that different data rates are used for uplink and downlink. These data rates can be found in Table 5.1. In Figure 5.4 the investigation process is shown visually. Below each block the processing time is shown and at each arrow the segment max distance is indicated and the associated transit time. The processing and transit times are all added up and the result for total up and down link times are shown. By adding up the up and downlink total time the result is a total round trip time of 3.106 s for the worst case scenario. This scenario uses the distances from Table 5.1.

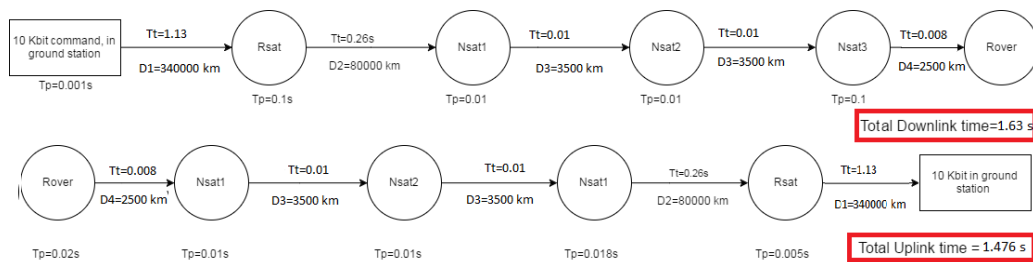


Figure 5.4: Lag time diagram for the worst case scenario, corresponding to the scenario used for sizing the links in Table 5.1

However, during nominal operations the distances between transmitter and receiver are smaller. The nominal distances were calculated from the constellation group to be:  $D_1 = 326,400$  km,  $D_2 = 60,000$  km,  $D_3 = 1,800$  km and  $D_4 = 1,700$  km. While keeping the same data rates as in Table 5.1 and Figure 5.4 the lag time for a 10 kbit command and a 10 kbit response, is calculated to be 2.89 s

### 5.3. LINK PERFORMANCE

In Table 5.1 the results of the link budget tool are shown. As it can be seen all links can be closed with more than 3 dB margin. The system noise temperature used for the calculations corresponds to the system noise temperatures measured on the LRO. As mentioned in the beginning of this chapter this system noise temperature experiences variation through the course of the LRO orbit. The minimum system noise temperature on the LRO was approximately 70 K for S-Band and 60 K for X-Band [19]. These lower temperatures are highly likely to occur in the link segments where the receiving antenna is pointed away from the Moon. That is because one of the biggest contribution in system noise comes from the receiving antenna and the brightness temperature of the body it is pointing at. This occurs during the Earth downlink and crosslink. Therefore the numbers presented in Table 5.1 represent the worst case scenario. In the best case scenario the data rates could be doubled or the transmission power of the satellites could be reduced. The downlink from Earth to the relay (sending commands) has a margin of 19.58 dB, this is due to the power available on the ground station for transmission and the fact that it is transmitting at  $500 \text{ kbit s}^{-1}$ . The ground station power can be reduced at 20 W and the margin would be more than 3 dB. Another option is to increase the data rates at  $20 \text{ Mbit s}^{-1}$  and keep the power at the same level and the link would still be able to close with more than 3 dB

Table 5.1: Results of link budget tool

		Inputs							
Parameter	Unit	Moon-Network		Network-Network		Network-Relay		Relay Earth	
Transmitter power Nsat	W	3		6		25		N/A	
Transmitter power rover	W	15		N/A		N/A		N/A	
Transmitter power Rsat	W	N/A		N/A		5		10	
Transmitter power ground station	W	N/A		N/A		N/A		400	
Loss factor transmitter (Lt) <sup>7</sup>	-	0.8		0.8		0.8		0.8	
Loss factor receiver (Lr) <sup>7</sup>	-	0.8		0.8		0.8		0.8	
Signal uplink frequency	GHz	2.4		31		8.4		8.4	
Signal downlink frequency	GHz	2.28		30		8.2		8.32	
Antenna diameter Nsat	m	N/A		0.1		N/A		N/A	
Antenna diameter ground station	m	N/A		N/A		N/A		10	
Antenna diameter Rsat	m	N/A		N/A		0.75		N/A	
Max distance	km	2500		3500		80000		340000	
Pointing offset angle (spacecraft)	deg	5		1		0.1		0.5	
Boltzman's constant	$dB(KJ^{-1})$					228.6			
		Outputs							
		Uplink	Downlink	Uplink	Downlink	Uplink	Downlink	Uplink	Downlink
Eb/N0 required	dB	6	6	6	6	6	6	6	6
Transmitter power rover	dBW	11.76	N/A	N/A	N/A	N/A	N/A	N/A	N/A
Transmitter power Nsat	dBW	N/A	6.99	7.78	7.78	13.97	N/A	N/A	N/A
Transmitter power Rsat	dBW	N/A	N/A	N/A	N/A	N/A	7	10	N/A
Transmitter power ground station	dBW	N/A	N/A	N/A	N/A	N/A	N/A	N/A	26
Wavelength ( $\lambda$ )	m	0.125	0.132	0.01	0.01	0.036	0.037	0.35	0.36
Transmitting antenna gain (Gt)	dB	4 <sup>8</sup>	13 <sup>11</sup>	26.13 <sup>9</sup>	25.84 <sup>9</sup>	24 <sup>10</sup>	34 <sup>9</sup>	24 <sup>10</sup>	56.3 <sup>9</sup>
Receiving antenna gain (Gr)	dB	13 <sup>11</sup>	4 <sup>8</sup>	26.13 <sup>9</sup>	25.84 <sup>9</sup>	34 <sup>9</sup>	24 <sup>10</sup>	56.3 <sup>9</sup>	24 <sup>10</sup>
Transmission path loss (La)	dB	0	0	0	0	0	0	-0.5 <sup>12</sup>	-0.5 <sup>12</sup>
Space loss (Ls) <sup>13</sup>	dB	-168	-167.56	-193.15	-192.87	-209	-208.8	-221.43	-221.26
Antenna Pointing loss (Lpr) <sup>14</sup>	dB	-0.1	0	-0.26	-0.26	-0.01	-0.01	-0.08	-0.06
Loss factor transmitter	dB	-0.97	-0.97	-0.97	-0.97	-0.97	-0.97	-0.97	-0.97
Loss factor receiver	dB	-0.97	-0.97	-0.97	-0.97	-0.97	-0.97	-0.97	-0.97
Required data rate (R)	$kbits^{-1}$	500	100	1000	1000	500	100	2000	500
System noise temperature (Ts)	$dB(sbit^{-1})$	-57	-50	-60	-60	-57	-50	-61	-57
	K	135	135	240	240	200	200	200	614
	$dBK^{-1}$	-21.3	-21.3	-23.80	-23.8	-23	-23	-23.01	-27.88
Eb/N0	dB	9.04	9.49	9.38	9.19	9.43	9.51	9.20	25.58
Margin	dB	3.04	3.49	3.38	3.19	3.43	3.51	3.20	19.58
Required margin of 3 dB satisfied?	-	Y	Y	Y	Y	Y	Y	Y	Y

<sup>7</sup> Value used in [29, slide 52]<sup>8</sup> <http://www.european-antennas.co.uk/media/2770/ds2063ra.pdf><sup>9</sup> Calculated using equation for parabolic antenna in Table 16-16 in [11, p.484]<sup>10</sup> Assumed from references [27] and [28]<sup>11</sup> From reference [23]<sup>12</sup> From attenuation plot in [17, p.564]<sup>13</sup> Calculated using equation 13-22 in [17, p.556]<sup>14</sup> Calculated using equation 13-21 in [17, p.556]

# 6

## NETWORK SATELLITE DESIGN

The design process of the design of the Nsats, displayed in [Figure 6.1](#), is detailed in this chapter.

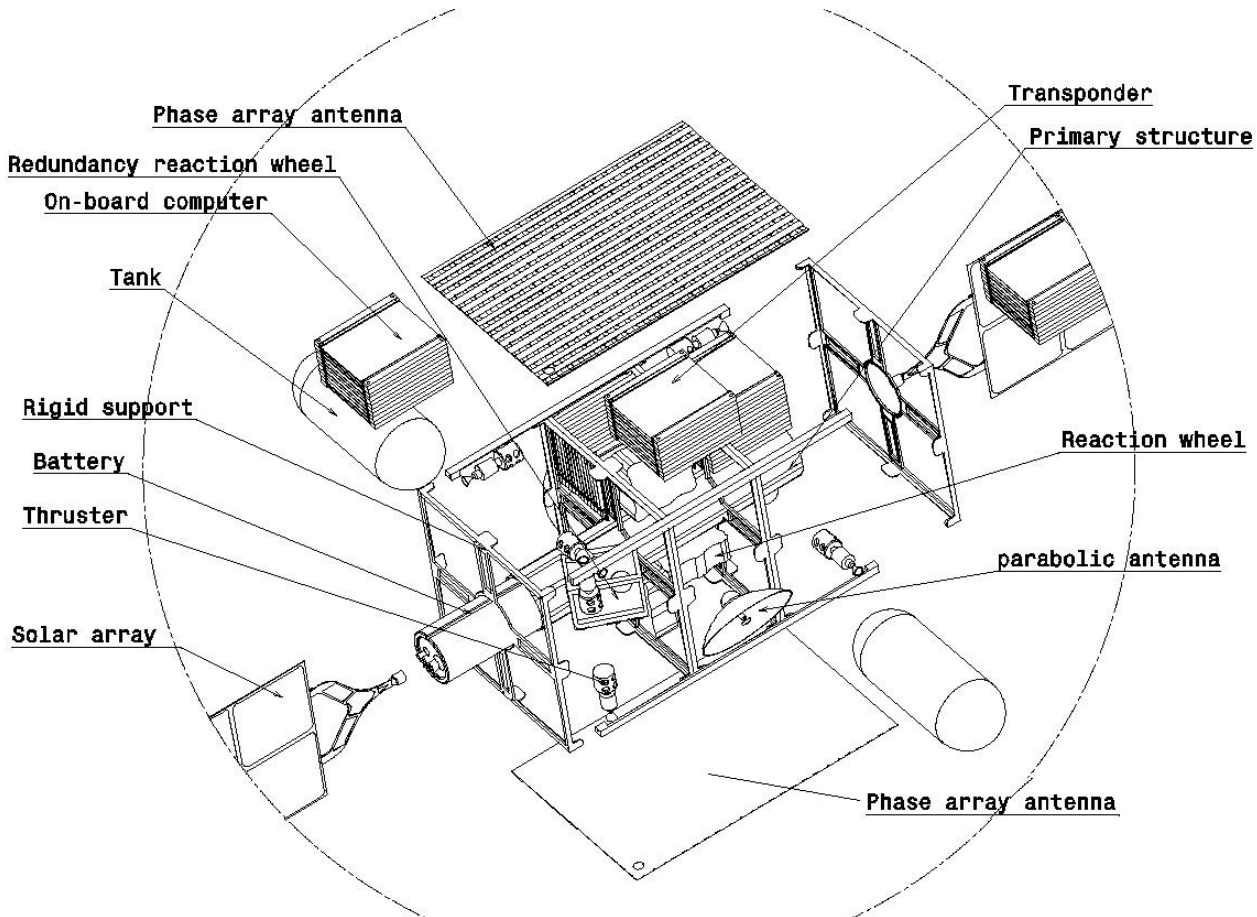


Figure 6.1: Exploded view of the Nsats.

### 6.1. NETWORK SATELLITE LAYOUT

One of the first design choices was where to put the solar panels and antennas. To be able to communicate with the Moon and the relay at the same time, one antenna must face the relay and the other has to face the Moon. This leaves only 4 faces for the solar panels. Since the solar incidence angles are dependant on the position within the orbit and the orientation of the Nsats. If the solar panels can rotate about one axis and are mounted on the other 3x2 face, see [Figure 6.2](#) then the solar incidence angle varies between  $0^\circ$  and  $90^\circ$ . While if mounted on the 2x2 face it varies between  $-52^\circ$  and  $52^\circ$ . Thus the choice is made to mount them on the 2x2 face. The rest of the spacecraft components are also shown in [Figure 6.1](#) and [Figure 6.2](#). The phased array antenna on the bottom of the exploded view, in [Figure 6.1](#) will always be pointed parallel to the Moon's surface. The two parabolic antennas points along the orbit, this is to be able to communicate with the next Nsat within the orbital plane. This is also why the parabolic dishes are angled with respect to the body. The solar panels are now always normal to the orbital plane.

### 6.2. ELECTRICAL POWER SYSTEM

Before designing an electrical power system (EPS), its elements have to be determined. The designed satellite mass will not exceed 50 kg, making it a micro-satellite. Its power requirements are expected to not exceed 1 kW [11, p. 424]. As can be seen in [Figure 6.3](#), for missions longer than 1 month with this power range, either photovoltaics or RTG's are considered most suitable. Since RTG's are not deemed to be sustainable, photovoltaics are selected as the main source of electrical power for this mission. A secondary battery will be included in the electrical power subsystem to

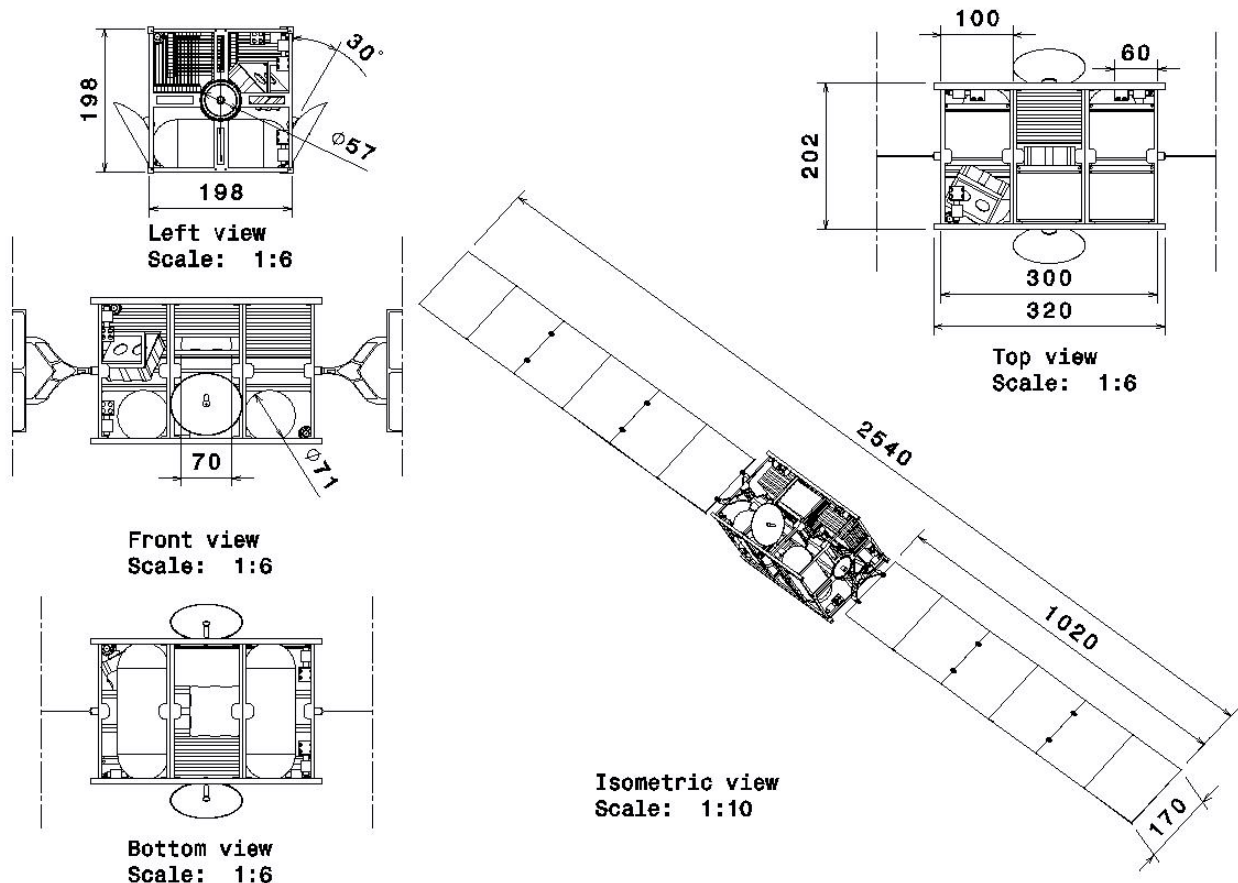


Figure 6.2: Conceptual layout of the Nsat with dimensions in mm.

enable operations during eclipse.

Now that the main components of the electrical power system are known, the type of components and, the components themselves have to be selected.

### 6.2.1. SOLAR ARRAY SELECTION

A solar array consists of solar panels, which are made up of solar cells. Firstly, the solar cell type is chosen by doing a trade-off using general values for each solar cell type. The trade-off table can be seen in Table 6.1 where multi-junction solar cells are chosen. Silicon based and single junction solar cells are considered unsuitable for space applications and not taken into account in this trade-off, since they have generally a higher degradation factor and lower efficiency [31][11, p. 648]. In Table 6.1 it can be seen that flexible copper indium gallium diselenide (CIGS) thin films are cheap and lightweight, but they have a low power density. This causes the required area to increase significantly, resulting in more complicated solar panel deployment mechanisms or even an increase in satellite size. The reflective concentrator has superior power density but requires some degree of active pointing towards the Sun[32]<sup>1</sup>. However, the pointing of the solar array is constrained by the satellite's thrusters. To prevent the thruster plume to partially hit the solar array, the solar array is only allowed to rotate around one axis, making it impossible to actively point towards the Sun using a mechanism. Furthermore, the satellite attitude is constrained by the antenna pointing direction so there is no way to constantly aim the solar array towards the Sun, thus reducing the efficiency of concentrate solar panels significantly.

Table 6.1: Solar cell type trade off table [33]

	Areal power density [W/m <sup>2</sup> ]	Specific mass [kg/m <sup>2</sup> ]	Specific cost [\$/W]	2-axis pointing
Multi-junction	210	3.9	820	Beneficial
CIGS thin film	115	0.90	510	Beneficial
Reflective concentrator	250	4.6	740	Required

<sup>1</sup>[http://www.greenrhinoenergy.com/solar/technologies/pv\\_concentration.php](http://www.greenrhinoenergy.com/solar/technologies/pv_concentration.php) Accessed on 26.06.2017

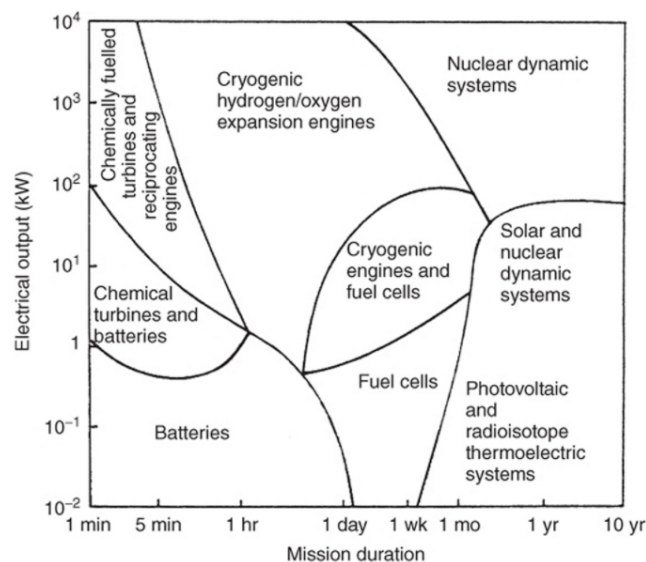


Figure 6.3: The most suitable source of energy for different mission durations and electrical outputs [30].

In Table 6.2 a list of data is given for triple junction solar cells which is used for a trade-off (Azur space<sup>2</sup>, SolAero<sup>3</sup>, Spectrolab<sup>4</sup>, CESI<sup>5</sup>). The Azur Space 3G30C is chosen since it has the highest begin of life efficiency and lowest degradation factor. A downside of the 3G30C is that the solar cell size is relatively large, constraining the flexibility in the final solar panel layout design. If more flexibility is required in a future design iteration, the CESI CTJ30 cell can be chosen with only 8 cm<sup>2</sup> cell area at the cost of a marginal amount of efficiency.

Table 6.2: Triple junction solar cell data for solar cell trade off.

Company	Type	BOL efficiency	Degradation factor ( $1 \times 10^{15}$ MeV)	Voltage temperature gradient [ $\text{mVK}^{-1}$ ]	Current temperature gradient [ $\mu\text{AK}^{-1}$ ]	Solar cell area [ $\text{cm}^2$ ]	mass [ $\text{mg}/\text{cm}^2$ ]
Azur space	3G30C	0.3	0.883	-7.20	4.64	60.36	86
Azur space	3G28C	0.28	0.875	-6.40	9.28	30.18	86
SolAero	ZTJ	0.295	0.85	-7.30	4.07	-	84
Spectrolab	XTJ	0.295	0.85	-6.90	10.6	26.62	84
CESI	CTJ30	0.295	0.84	-6.09	13.2	8	81-89
Spectrolab	ITJ	0.268	0.84	-6.60	17.1	31	84
SolAero	ATJM	0.275	0.85	-6.14	9.50	-	84
SolAero	ATJ	0.275	0.85	-6.14	13.0	-	84

### 6.2.2. SECONDARY BATTERY SELECTION

For the secondary battery, lithium-ion batteries are selected. These batteries have a superior energy density and energy efficiency as can be seen in Table 6.3. Aside from that they also have the capability of having a modular design and no memory effects. For these reasons, Lithium-ion batteries are selected by most of the current space missions and they are also selected for this mission [34, p. 312][11, p. 651][35].

Table 6.3: Secondary battery type general data [11, p. 651].

	Energy density [ $\text{Whkg}^{-1}$ ]	Energy efficiency [%]	Temperature range [ $^{\circ}\text{C}$ ]
Li-ion	125	0.98	10 to 25
Ni-Cd	30	0.72	0 to 40
Ni-H <sub>2</sub>	60	0.70	-20 to 30

Several different Lithium-ion batteries are selected, of which the properties are listed in Table 6.4 (Saft<sup>6</sup>, Quallion<sup>7</sup>,

<sup>2</sup><http://www.azurspace.com/index.php/en/products/products-space/space-solar-cells> Accessed on 26.06.2017

<sup>3</sup><https://solaerotech.com/products/space-solar-cells-coverglass-interconnected-cells-cic/> Accessed on 26.06.2017

<sup>4</sup><http://www.spectrolab.com/dataSheets.htm> Accessed on 26.06.2017

<sup>5</sup>[http://www.cesi.it/services/solar\\_cells/Documents/CTJ30-2015.pdf](http://www.cesi.it/services/solar_cells/Documents/CTJ30-2015.pdf) Accessed on 26.06.2017

<sup>6</sup>[https://www.saftbatteries.com/download\\_file/6X7JMGAnv3Fm6HdmtEv%252B2gt1bZ1bRRVHkjS11M6md92GD2EF7vU%252F30ybbz3W0LG%252BxR8srpA5iCdJ%252FV3IQzTVHQyiTucngZKEg9KkYCLkowAvgaG1hurmcjMAk1k8zAoftL350zXSynM7ama4vPXmbAGs1c5VnvbbrRHY%252BdScNfiS9thiEg%253D%253D/1703\\_Saft-SpaceBrochure\\_Hi-res-final.pdf](https://www.saftbatteries.com/download_file/6X7JMGAnv3Fm6HdmtEv%252B2gt1bZ1bRRVHkjS11M6md92GD2EF7vU%252F30ybbz3W0LG%252BxR8srpA5iCdJ%252FV3IQzTVHQyiTucngZKEg9KkYCLkowAvgaG1hurmcjMAk1k8zAoftL350zXSynM7ama4vPXmbAGs1c5VnvbbrRHY%252BdScNfiS9thiEg%253D%253D/1703_Saft-SpaceBrochure_Hi-res-final.pdf), accessed on 22.06.2017

<sup>7</sup>[http://www.arpae-summit.com/paperclip/exhibitor\\_docs/13AE/Quallion\\_LLC\\_36.pdf](http://www.arpae-summit.com/paperclip/exhibitor_docs/13AE/Quallion_LLC_36.pdf), accessed on 22.06.2017

ABSL<sup>8</sup>). From this trade-off the Saft VL51ES is chosen for its high specific energy. This cell has a cylindrical shape with a diameter of 54 mm and a length of 222 mm. In the case that higher voltages are required in a future design iteration, an array of Saft VES16 could be chosen which are also cylindrical with diameter 33 mm and length 60 mm. These have a lower capacity, which enables a more flexible design at the cost of a lower specific energy. The batteries selected have cell protection, meaning that upon failure, the battery cell will remain in one piece, leaving the rest of the satellite unharmed.

Table 6.4: Lithium-ion secondary battery data for battery trade off.

Company	type	Energy [Wh]	Capacity [Ah]	Voltage [V]	Mass [kg]	Specific energy [Whkg <sup>-1</sup> ]	Volumetric efficiency [Wh/cm <sup>3</sup> ]
Quallion	QL2300A	8.3	2.3	3.6	0.075	110	0.162
Quallion	QL075KA	259	72	3.6	1.820	148	0.328
Quallion	QL015KA	54	15	3.6	0.380	142	0.295
Saft	VL 6P	22	6.6	3.6	0.340	65	0.034
Saft	VL 48E	170	48	3.6	1.130	150	0.074
Saft	VL 51ES	180	51	3.6	1.080	170	0.089
Saft	VES 16	16	4.5	3.6	0.155	155	0.078
Saft	VES 180	180	50	3.6	1.110	165	0.082
Saft	VES 140	140	39	3.6	1.130	126	0.063
ABSL	Modular design	5.4	1.5	3.6	0.052	104	-

### 6.2.3. EPS SIZING

To size the EPS, the power monitoring tool is used, which is described in section 14.13. The final power requirements are obtained from the power budget in chapter 10 and listed in Table 6.5. Here the full activity power is reached if all the subsystems draw the nominal amount of power simultaneously. Since this generally does not happen, a duty cycle is introduced, which is a number between zero and one that represents the fraction of activity per orbit period for each subsystem. This results in an average power requirement, which is a realistic representation of the power that the solar panels have to deliver (excluding battery charging power requirements). The maximum peak power is the power required when all the subsystems consume their peak power. Since this is not expected to happen, separate cases are made which are used for a peak power analysis. For the network satellites, only one significant peak power case is found. This is the momentum dumping case, where during nominal operation, the ADCS and propulsion require their peak power to unload the reaction wheels.

Table 6.5: Nsat general power requirements.

	Power [W]	Time [s]
Full activity	44.82	-
Average power requirement	28.50	continuous
Maximum peak	117.1	-
Momentum dumping case	103	15

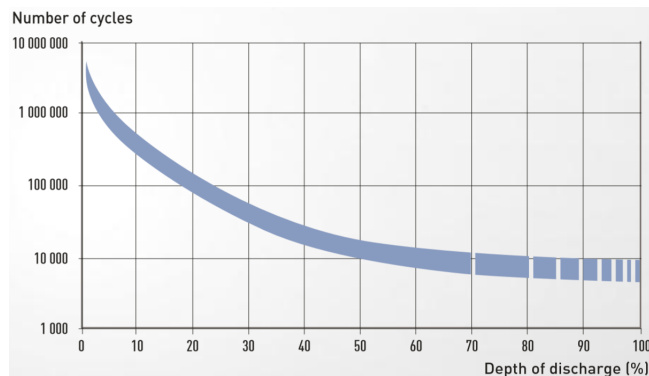


Figure 6.4: Depth of discharge for Saft Lithium-ion batteries at 25 °C for 70 % battery capacity remaining at end of life.<sup>6</sup>

With the average power requirement, the battery and solar array are sized using the power monitoring tool. However, before this is done, the Sun conditions around the Moon are determined.

Since it is not possible to have the solar panels pointing perfectly towards the Sun, an angle of incidence of the panels has to be established. For the chosen satellite design, the worst case would be a beta-angle of 90°. Since the satellite attitude is fully constrained by the communication subsystem, the solar panels would be pointing perpendicular to the Sun, generating no power at all. Since the Walker delta constellation has a non-zero inclination, this scenario will not occur. The Sun angle of incidence for the network orbits can vary between 0° to 51.74° where the maximum angle is determined by summing the orbit inclination of 50.2° and the angle between the Moon's rotational plane and the ecliptic plane, which is 1.54° as can be seen in 4.3. In the EPS sizing, an angle of incidence of 51.74° is used resulting in a factor of  $\cos(51.74) = 0.6192$ .

Furthermore, solar cell degradation is taken into account. For the chosen solar cells, a degradation of 3 % per year can be assumed [36, p. 371], which results in a total degradation factor of  $(1 - 0.03)^5 = 0.8587$  for the lifetime of five years. The solar cell power output depends on its temperature through voltage and current temperature gradients, which is displayed in Table 6.2. From the thermal analysis, the temperature of the solar panel is obtained throughout an orbit period, which varies between -63.9 °C to 23.2 °C. Since the nominal temperature of the solar cell is 28 °C,

<sup>8</sup><http://www.enersys.com/WorkArea/DownloadAsset.aspx?id/D1119&usg=AFQjCNGhpjrSOKHarVv2VU2Dpga0hQiwA&sig2=L5uLdNk1RigRepF1-CVr2Q>, accessed on 22.06.2017

the difference between the nominal cell temperature and the calculated temperature is in the range of  $-91.97^{\circ}\text{C}$  to  $-4.68^{\circ}\text{C}$ . This temperature difference is known for each point in time in the orbit, with which the power output at every time in the orbit is determined. Lastly, the absorptance of the solar cells is  $0.91^2$ .

All these factors together result in the overall solar cell efficiency, which is shown in Figure 6.8 together with the solar array temperature throughout one orbital period. The orbit starts just as it comes out of Lunar eclipse. Then, the solar panels are increasing in temperature to an equilibrium temperature, reducing the efficiency. After 4.03 hours the satellite enters eclipse again, cooling down the solar panels while not being exposed to light. During daytime the satellite energy efficiency is assumed to be 0.85 and during nighttime it drops to 0.65 due to battery usage [17, p. 396]. The last parameter that has to be determined is the depth of discharge of the secondary battery. From Figure 6.4 the depth of discharge can be determined from the fact that the Nsats go through 8,992 cycles in five years for a remaining battery capacity of 70 % at end of life. This results in a depth of discharge of 50 percent. A conservative design is chosen with a depth of discharge of 40 %. This is done since the temperature in the satellite is not equal to  $25^{\circ}\text{C}$  constantly. The satellite experiences thermal cycling where the satellite battery temperature will vary around  $284^{\circ}\text{C}$  to  $294^{\circ}\text{C}$ . This also accounts for unexpected power losses. A depth of discharge of 40 % will ensure that the end of life battery capacity will not be below 70 % of the initial capacity.

#### 6.2.4. EPS DESIGN

The power monitoring tool is used to determine the amount of solar cells and the battery capacity for the network satellite. These parameters are shown in Table 6.6 excluding the thermal data and solar cell parameters. Here the EPS is sized using a 30 % margin on the continuous power requirement from Table 6.6 to take into account unexpected power consumption and losses.

The amount of solar cells to satisfy the continuous power requirement is 43 cells at end of life and the battery capacity is 120.9 Wh for end of life, which means that the beginning of life capacity should be  $120.9/0.7 = 172.7$  Wh. For the battery, one Saft VL51ES Li-ion cell with a capacity of 180 Wh is sufficient for both the continuous and impulse power requirements. To keep the undeployed solar array within the surface constraints of the satellite, the solar cells are distributed over multiple panels of two by two solar cells, which are hinged together such that they can be deployed. In total twelve panels of four solar cells are used (six on both sides on the satellite). One of the two solar arrays is shown in Figure 6.5. One solar cell occupies a square with sides of 85 mm.

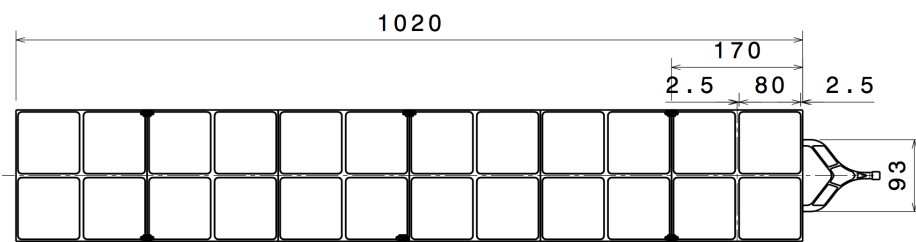


Figure 6.5: Network satellite solar cell layout with dimensions in mm.

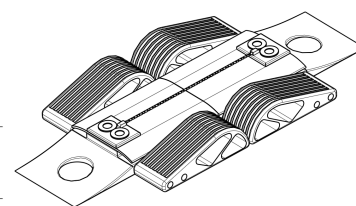


Figure 6.6: Solar array hinge design: tape-spring roll hinges.

With this configuration, the battery state of charge throughout the orbit is determined. This is displayed in Figure 6.7 together with the required power and solar panel output. The difference in required power and solar panel power is caused by power losses in operations. It can be seen that, due to the size of the solar array, the battery state of charge is increased significantly after one orbit rather than being equal at begin and end of the orbit.

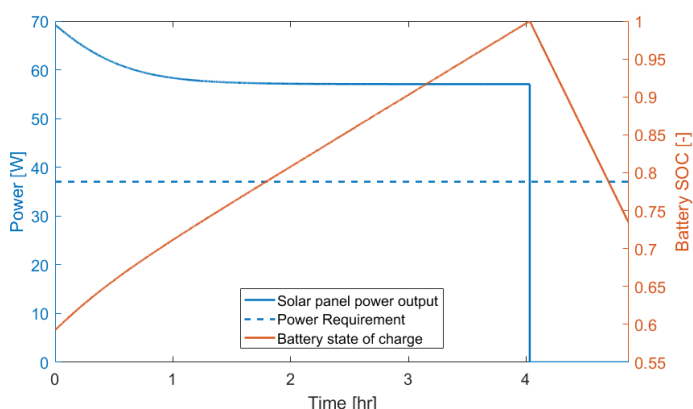


Figure 6.7: Power profile of a network satellite during a single orbit.

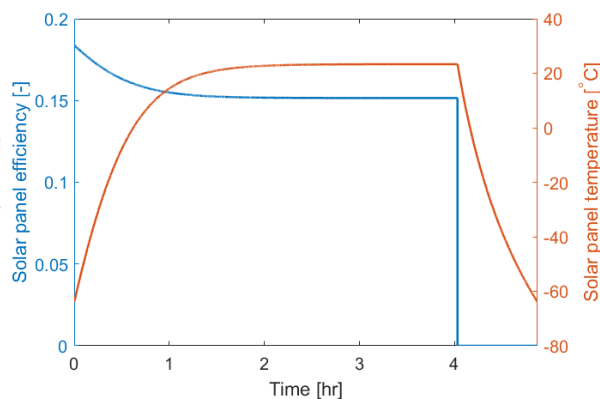


Figure 6.8: Overall solar cell efficiency and solar array temperature throughout one orbit.

Tape-spring roll hinges are used, these automatically lock in deployed position with a minimal amount of moving parts [37]. A tape-spring roll hinge can be seen in Figure 6.6. The total length of this hinge is 16.7 mm with a 13.1 mm distance between the main connection points. The width of this hinge is 8.0 mm and the total mass of a single hinge is 10 g from a CATIA estimate. The rod connecting the solar array with the satellite is estimated to be 200 g from the

CATIA design. The solar array deploys per panel starting with the hinges connecting the first panel to the rod, followed by the rod itself after which the other panels are deployed simultaneously. Lastly, for the cables a 15% margin on the total EPS weight is assumed [11, p. 657].

Table 6.6: Network satellite EPS design input parameters for the calculation tool.

Orbit altitude	1629	km
Average power requirement	28.5	W
Max impulse energy	0.429	Wh
Battery DOD	0.4	-
Degradation	3%	year <sup>-1</sup>
Absorptance	0.91	-
Solar angle of incidence	51.74	degrees
Day efficiency	0.85	-
Night efficiency	0.65	-

Table 6.7: Mass breakdown of the network satellite EPS.

	Amount	Total mass [kg]
Solar cells	0.173 m <sup>2</sup>	0.237 [33]
Solar panel harness	0.173 m <sup>2</sup>	0.102 [33]
Solar panel substrate	0.173 m <sup>2</sup>	0.225 [33]
Hinges	12	0.120
Rod	1	0.200
Rotational mechanism	1	0.250
<b>Solar array mass</b>	<b>2</b>	<b>2.268</b>
VL51ES battery	1	1.08
<b>Subtotal</b>	<b>1</b>	<b>3.368</b>
Cable and component margin	15%	0.505
<b>Total subsystem mass</b>		<b>3.87</b>

### 6.2.5. EPS INTEGRATION

First of all, a number components are included to maximise the efficiency of the EPS. The solar cell power output changes with changing voltage and current. This curve has an optimum operating voltage at which the power generated per cell is maximum called the maximum power point. This point can be tracked using a maximum power point tracker (MPPT) and can be maintained accurately using, for example, an optimised 'perturb and observe' algorithm such as the one presented in [38]. One downside of using an MPPT is that it causes noise in the power flow. However, this can be corrected by using a capacitor. Furthermore, a Sun sensor is present to ensure the orientation of the solar panel is always as optimal as possible, within its one rotational degree of freedom.

Besides optimising the EPS output, the power delivery to each subsystem has to satisfy requirement IRIS-NSAT-EPS-07. In Figure 6.9 the power distribution process is displayed. Power is distributed at a central location to suit the needs of the individual subsystems. Here, for the subsystems, the voltage, average and peak power consumption is given.

For the voltage conversions, it has to be kept in mind that internal voltage should be as close as possible to the voltage required by the components to keep the voltage conversion efficiency as high as possible [11, p. 655]. Since in the design a single lithium-ion battery cell is chosen, the battery voltage is at 2.8 V to 4.2 V[39], which will sometimes need to be converted up to a maximum of 28 V. To reduce the voltage conversion difference for the solar array, it is chosen to wire the solar cells with 3 loops of 8 cells in series per array, resulting in a voltage of 19.5 V to 24.2 V depending on the operating conditions. This is closer to the maximum voltage requirement, reducing the conversion losses. Currently, voltage up and down conversion can be achieved at an efficiency of over 90% within voltage ranges from 2 V to 5 V[39]. It is expected that in the future this conversion becomes more efficient for larger voltage conversions. All the conversion losses and heat generation by EPS components are included in the daytime and nighttime EPS efficiency, which are assumed to be 65% and 85% [11, p. 643].

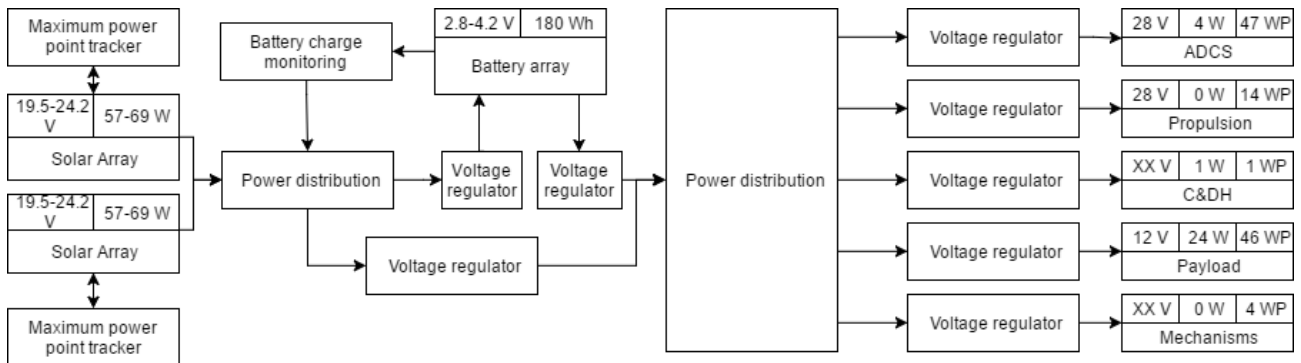


Figure 6.9: Network satellite electrical block diagram showing the power flow between different components.

## 6.3. COMMAND AND DATA HANDLING

The design of the command and data handling involves two major sizing parameters. The first one is the memory size to store on-board data and the second is the speed required by the processor to perform the functions needed.

### 6.3.1. MEMORY SIZE

In order to determine the memory size, all the data that has to be stored on-board is identified. The first type of data is the scientific data the rover is generating on the surface of the Moon and its related rover housekeeping data. As stated in section 5.2, this data has the highest priority to the system and its requirement is to reach Earth in less than 3 seconds. For that reason, this data will not need to be stored on-board the Nsats. Instead it will act only as a channel that this data flow through. The same applies for the Rsat. Once the data reaches it, the Rsat will immediately transmit it to Earth.

The second type of data consists of commands sent from Earth, with as intended receiver either the rover or the satellites of the system, depending from where the commands are originating. The commands intended for the rover have priority over other commands. Therefore they will be transmitted with priority through a predetermined path in the network. After that, the satellite commands will be transmitted either directly (if the intended receiving Nsat is in view of the Rsat) or first they will be transferred to the correct orbital plane, from where they will reach the intended Rsat through cross-links.

The third type of data is the housekeeping data generated from the Rsats and the Nsats. For the Rsat housekeeping data there is no need for the Rsat to store any of it. Since the Rsat will have contact with Earth at all times, it can simply send the data to Earth directly. The Nsat housekeeping data has two possibilities. In case the Nsat is in view of the Rsat, it will send its own housekeeping data to the Rsat, from where it will be transmitted to Earth. The second possibility is the case when the Nsat is on the far-side of the Moon and it does not have any contact with the Rsat. Normally if an orbital plane is not transmitting rover data, the Nsat housekeeping can be cross-linked to the Rsat. However there might be a possibility that a certain plane is constantly acquiring and transmitting rover data. In this case, the Nsat will have to store housekeeping on its memory. The maximum time for an Nsat to come in view of an Rsat is two hours, therefore the data generated during these two hours serves as the worst case scenario for the Nsats in terms of data storage requirement.

To determine the size of the housekeeping data, a list of all the sensors on board the satellite is created. One parameter of importance is the sampling frequency of the sensor data. This sampling frequency is calculated using the Nyquist criteria, which states that the sampling frequency should be at least two times higher than the highest frequency component of the measurement, to mitigate the aliasing of the measurement. Finally, to calculate the data rate of the sensor, the sampling frequency is multiplied by the number of bits that represent it. The data was gathered by consulting the product pages of the leading manufacturers of sensors for space applications. The results of the estimation process can be seen in Table 6.8. It can be seen that during the two hours that the Nsat does not have contact with the Rsat, it will generate less than 55 Mbit of data. For a full day of storage the Nsat will generate less than 0.7 Gbit. Current storage systems have a baseline storage size of 100 Mbit and easily expandable to the Gbit range.

Table 6.8: Estimation of generated housekeeping data for all vehicles.

Sensor type	No. in Nsat	No. in Rsat	No. in Network DeVe	No. in Relay DeVe	Resolution (bits)	Sampling frequency(Hz)	Bit Rate (bps)			
							Nsat	Rsat	N DeVe	R DeVe
Thermal sensors	2	1	1	1	12	1	24	12	12	12
Computer sensors	2	1	1	1	12	1	24	12	12	12
Voltage sensors	13	11	11	11	14	1	182	154	154	154
Current sensors	13	11	11	11	14	1	182	154	154	154
Thruster sensors	7	7	7	7	12	1	84	84	84	84
Sun sensor	7	7	6	8	8	5	280	280	240	320
Star sensor	2	2	N/A	2	8	1	16	16		16
IMU	2	2	N/A	N/A	8	400	6400	6400		
Gyros	N/A	N/A	4	4	8	100			3200	3200
<b>Time to store data (s)</b>	7200	0	0	0	N/A	<b>Total</b>	7192	7112	3856	3952
						<b>Total Data to be stored (bits)</b>	51,782,400	0	0	0

### 6.3.2. CPU SPEED

Sizing the needed CPU speed is more involved. In general, its sizing is based on the number of lines of code and the instructions that need to be performed per second. Since the exact programs that need to be ran in the satellite are not written yet, the design process for this part will be based on statistical data. Using chapter 16.2 in [17], table 16-6 is extracted and from this table the applicable functions that will be performed in the Nsats and Rsats are identified. These functions can be seen in Table 6.9. Table 16-6 indicates the number of instructions per second performed by each function (The K in KIPS does not stand for kilo, it represents  $2^{10} = 1024$ ). Each instruction needs a certain number of clock cycles before it is performed. According to [17, p.607], typical values for clock cycles are about 5 cycles per instruction. For example the Intel386 chip produced in 1985 is used on the ISS, which required approximately 8 clock cycles per instruction. Recent day chips like the RAD750 used on the Lunar Reconnaissance Orbiter need approximately 0.3 clock cycles per instruction<sup>9</sup>.

To account for the functions that have not been identified yet, a safety factor is applied on the number of cycles per instruction, resulting in an estimated 10 cycles per instruction. By summing up all the instructions that need to be performed per second and multiplying that by the number of cycles per instruction, the result is the the number of cycles per second the CPU needs to have. The result of this estimation process can be seen in Table 6.9, here the CPU needs to provide at least 2 MHz of processing speed.

A sensitivity analysis was also performed in Table 6.9, where the number of instructions and the cycles per instructions were increased by 20% and 100%. From the analysis it can be seen that even when the number of instructions doubles, the needed CPU speed is below 8 MHz.

The baseline for current day radiation hardened CPU speed is at 100 MHz and commercially of the shelf (COTS) CPUs with flight heritage can achieve more than 400 MHz of processing speed. As it was also with memory, the choice for CPU and memory in this case is not strictly dictated by the data that need to be handled. This is a result of the advances in electronic components and the ability to have COTS equipment that perform better than required.

<sup>9</sup><http://www.petervis.com/Vintage%20Chips/PowerPC%20750/RAD750.html> Accessed on 26.06.2017

Table 6.9: Estimation of CPU speed for several components

Function	Throughput (KIPS)	Throughput +20% (KIPS)	Throughput +100% (KIPS)
<b>Communication</b>			
Command processing	7	8.4	14
Telemetry processing	3	3.6	6
<b>Attitude sensor processing</b>			
Rate Gyro	9	10.8	18
Sun sensor	1	1.2	2
Star sensor	2	2.4	4
<b>Attitude Determination &amp; Control</b>			
Kinematic integration	15	18	30
Error determination	12	14.4	24
Precession control	30	36	60
Thruster control	1.2	1.44	2.4
Reaction wheel control	5	6	10
<b>Autonomy</b>			
Simple autonomy	1	1.2	2
<b>Fault Detection</b>			
Monitors	15	18	30
Fault correction	5	6	10
<b>Other functions</b>			
Power management	5	6	10
Thermal control	3	3.6	6
Mechanism activation & control	2	2.4	4
<b>Operating system</b>			
Local executive	60	72	120
<b>Total KIPS</b>	176.2	211.44	352.4
<b>No of cycles per instruction</b>	10	12	20
<b>Required CPU frequency (MHz)</b>	1.804288	2.59817472	7.217152

### 6.3.3. RADIATION SHIELDING

The circuit boards which handle all computations are especially sensitive to the harsh radiation environment around the Moon. In order to reduce the amount of single event upsets (e.g. bitflips), build-up of electric charge and chance of short circuits, the computers will be placed inside of a protective layer of material (the radiation vault).

This vault (made from aluminium) should have at least an area density of  $0.5 \text{ g cm}^{-2}$ , which for a density of  $2.8 \text{ g cm}^{-3}$  corresponds to a thickness of approximately 1.7 mm.

A more in depth analysis and/or simulation should be performed to investigate if that amount of shielding is adequate in the lunar radiation environment.

### 6.4. TRACKING AND ORBIT DETERMINATION

An essential part of the mission is knowing where the mission elements are located. This importance arises from many factors such as to guarantee that the launch vehicle is following its pre-determined path, monitoring the deployment process, making sure that the satellites are positioned correctly and have the designed spacing between them.

The driver for the choice of the tracking system, comes from the positioning accuracy needed. From the communications group, the positional accuracy during nominal operations comes from the antenna loss of contact. Visually, this case is represented in Figure 6.10. Line A indicates the accuracy needed, line B indicates the distance between Nsat and Rsat, angle  $\alpha$  represents half of the beamwidth. The required accuracy can be calculated as follows:  $A = \tan(\alpha) \cdot B$ . It can be seen that the value of A will be lowest (higher accuracy) when line B lies on top of line C. The beamwidth can be calculated using equation 13-17 in [17, p.525]. For a 0.75 m diameter dish located on the Rsat transmitting at 8.2 GHz, the beamwidth has a value of approximately  $3.4^\circ$ . Distance C is equal to the distance of the L1 point from the Moon minus the radius of the Moon minus the orbital height, resulting in a distance of approximately 54,000 km. Using the relation above, the required accuracy to mitigate loss of contact results in an accuracy better than 1,600 m. The case of loss of contact with the relay was not considered due two main reasons. First, the phased array that will make contact with the Rsat has a field of view of at least 90 degrees ( $\pm 45^\circ$ ) [40, p.19]. Secondly, the beam width has been tested [28] to be  $5^\circ$ , but also can be expected to be higher than the beam of the parabolic antenna due to the reduced gain of the phased array. Therefore the same accuracy to track the Nsats can be used for the Rsats.

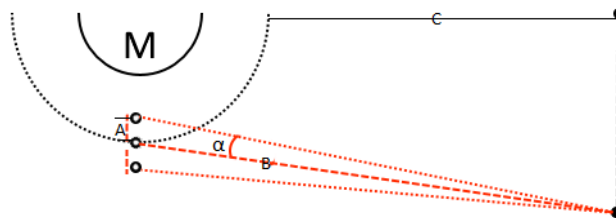


Figure 6.10: Orbital accuracy to ensure no loss of contact

However, this is not the highest accuracy that needs to be provided. During the deployment process as discussed in section 8.9, needs to be better than 150 m in a 10 second measurement time. As a result the choice for the tracking method comes from the accuracy needed during the deployment process.

In order to provide such an accuracy, several possibilities were investigated. The investigated solutions are visualised in the design option tree in Figure 6.10, the options with the red circles indicate options that were discarded. Going from right to left in Figure 6.11, the reasons why the options are rejected will be presented.

#### 6.4.1. OPTICAL METHODS

Starting from the optical based techniques, the visual observation and photography are limited to the brightness of the constellation elements. This creates the risk that the satellite will not be distinguishable for optical observation. A possible mitigation to that risk would be to have sources that emit light on the surface of the satellites, but that would increase the power budget without a significant advantage to the higher level functions of the system. Laser ranging, on the other hand can offer the accuracy required, due to the THz (visible spectrum) that it utilises for measurements. Although the range of the satellite can be measured in cm precision [41], laser ranging does not provide any information about the range-rate. The range-rate represents the velocity in the direction of the tracking station and is an important parameter that together with the model of the gravity field can be used to determine the orbital height of the satellites.

#### 6.4.2. ON-BOARD INSTRUMENTATION

The options related to measurements taken from on-board instrumentation were dismissed for several reasons. Firstly altimeter measurements were considered, the idea originated from the new high resolution maps of the Lunar surface generated from LRO. The basic idea is that the Nsats would perform measurements of the altitude and either transfer the data to Earth for analysis or themselves compare their readings with the LRO maps. The main problem here is the increased mass of the Nsat due to the added altimeter and the space that it occupies in the satellite. Furthermore, if the comparison would be done on board the Nsat, the C&DH subsystem would have to be redesigned such that it can handle the complex operations needed for the analysis. On the other hand, if the readings are sent back on Earth, the system would require higher data rates to guarantee customer satisfaction. Finally, at the orbital altitude the Nsats are flying, the accuracy would considerably decrease. Using the vertical accuracy of the LRO altimeter of 4 m, the decrease in accuracy can be estimated using the fact that the Nsat are at an altitude 32 times higher than the LRO. Therefore, the expected accuracy is  $4 \cdot 32 = 128$  m, which satisfies the required accuracy during deployment.

The use of cameras was discarded because they would generate a lot of data, that would either be analysed on board, straining the command and data handling subsystem, or would lead to higher data rates to transfer them for analysis. Furthermore, the power requirements increase and so does the mass, due to the need of a high resolution camera. Finally the addition of an on-board camera does not contribute to the system level goals.

The use of sensors was discarded due to the heavy computations needed to relate the attitude of the Nsat to the celestial surroundings. Furthermore, even if the data rates would allow the transmission of this data back on Earth, it would take around a minute for the data to be analysed and transferred back to the constellation.

Since all other options for orbit determination through on-board instrumentation have been disregarded, it would not make sense to select a hybrid solution. The added weight does not add functionality to the system and the use of the data rates that nominally will be used for the rover data does not comply with the customer requirement.

#### 6.4.3. RADIOMETRY

The last considered group of tracking techniques considered is radiometric methods. Since all the constellation satellites will be equipped with radios for the purposes of achieving the system goals, this group of techniques has significant advantage over the others. Starting with the very long baseline interferometry, it offers meter accuracy and  $\text{cm s}^{-1}$  [42]. However, it requires performing radio measurements from two stations at the same time, usually stations that have a large separation distance between them. This increases the operational costs, not only due to the fact that two stations have to be hired at the same time but also synchronising these stations together.

The second alternative for this group of tracking methods is radar technology. Two different radar options were considered, ground based radar and radar antennas installed on the Rsats. For the ground based option, it was discovered that radars have limitations when it comes to large distances, due to the required SNR received after the radar signal bounces back. For example the AN/FPS-108 radar used on the United States Space Surveillance Network has a maximum range of 46,000 km<sup>10</sup>. The option of installing a radar system on the relays was rejected due to the high power consumption that radar antennas have. The ASAR instrument on the Envisat consumed 600 W of power on its lowest performance setting and weighed more than 800 kg<sup>11</sup>.

The third alternative considered is the use of the escaping GPS satellites for positioning. Although there are claims about a study performed on the topic by JPL resulting in 100 to 500 meter positioning accuracy from leaking GPS signals on the Moon<sup>12</sup>, such a paper was never found. In 2008 a grant of 1.2 million dollars was awarded for the development of a GPS system around the Moon<sup>13</sup>, but since then the project seems to be discontinued due to allegations regarding the main researcher on the project who is under investigation for trading confidential information<sup>14</sup>.

The fourth option considered was Doppler-ranging. Doppler ranging is a well known technique widely used to perform tracking on satellites. The basic principle consists of comparing the frequency of a received signal to a reference signal. By determining the change of frequency one can determine the velocity of a moving object.

<sup>10</sup><http://www.radartutorial.eu/19.kartei/01.oth/karte003.en.html> Accessed on 26.06.2017

<sup>11</sup> Table-6 in: <https://directory.eoportal.org/web/eoportal/satellite-missions/e/envisat> Accessed on 26.06.2017

<sup>12</sup><http://gpsworld.com/gnss-systemnavigating-moon-12811/> Accessed on 26.06.2017

<sup>13</sup><https://news.osu.edu/news/2008/07/21/lunarnav/> Accessed on 26.06.2017

<sup>14</sup><http://www.businessinsider.com/chinese-ohio-state-professor-rongxing-li-disappeared-2015-9?international=true&r=US&IR=T> Accessed on 26.06.2017

There are two ways Doppler tracking can be achieved. The first one is sequential ranging, where the ground station generates a ranging signal and transmits it to the spacecraft. The spacecraft produces a reference signal in the same band as the uplink, but with an offset in frequency, also known as the turn-around ratio and finally re-transmits this signal back to the ground station. Once this last signal is received on the ground station, the ground station produces a reference signal coherent with it. This final signal is used to demodulate the downlink signal. Once this is done the received range code is compared to the transmitted one and the round trip transit time is determined. Finally, by measuring the change in received reference signal to the station's frequency standard the Doppler shift can be calculated [43, p.10]. New ranging techniques use a sequence of pseudo random noise code (PRN) rather than a sequence of tones [44]. The use of PRN codes ultimately will reduce the power needed for tracking, while allowing the downlink of telemetry as well as an increase in accuracy at greater distances. Two way ranging is considered the most accurate ranging technique, as the measurement error is mostly dependant on the frequency standard of the ground station. For the DSN the Allan standard deviation is  $10^{-5}$  for 60 s averaging time [43, p.16]. Table 3-3 in [43, p.33] indicates the accuracy of 2-way ranging for a single frequency downlink. For downlink at X-Band the DSN can measure a range-rate with an accuracy of  $0.03 \text{ mm s}^{-1}$ .

Another way of performing Doppler tracking, is through one-way ranging. In this method, a single signal is transmitted from the spacecraft and is received on Earth. This ranging method is limited by the frequency standard of the spacecraft produced by an on-board oscillator. Advances in ultra stable oscillators however make it an interesting tracking technique. This is due to the fact that downlink telemetry and tracking can be done simultaneously, while in the two-way technique only tracking or telemetry downlink can be done at a time. Furthermore one-way tracking offers improvements in received SNR, because one way transmissions offer better short term stability and reduce the system noise at the receiver as the antenna is only receiving and not transmitting simultaneously [45]. Using [43, p.15] the following equation is extracted to calculate the range-rate measurement error of one-way Doppler:

$$\Delta \dot{\rho} = c \frac{\Delta f_t}{f_t} \quad (6.1)$$

In Equation 6.1  $c$  is the speed of light,  $f_t$  is the transmission frequency and  $\Delta f_t$  is the shift of frequency due to oscillator instability. The chosen transponders for communication are equipped with temperature controlled crystal oscillator with Allan deviation of  $10^{-9}$ , and output a frequency of 10 MHz. As a result the expected shift in frequency is  $10 \cdot 10^6 \cdot 10^{-9} = 0.01 \text{ Hz}$ , that means that if one wants to transmit at 8.4 GHz in reality the transmission will be done at  $8.4 \cdot 10^9 \pm 0.01 \text{ Hz}$ . Using the values above in Equation 6.1, it is found that the expected Doppler measurement will have an error of  $0.36 \text{ mm s}^{-1}$ . Comparing this value to the one from Table 3-3 in [43, p.33], it can be seen that this value is 10 times higher. In table 3-3 the range error for two-way Doppler is 60 cm, therefore it can be expected that the range error for one-way Doppler will be ten times higher leading to an accuracy of 6 m. This accuracy is more than the needed for deployment.

In conclusion, one-way Doppler tracking method is well suited for the system. It provides more than required accuracy, while at the same time it allows for efficient use of the spacecraft power to perform tracking and telemetry downlink at the same time. As such it will be the chosen method for tracking the Nsats and Rsats. The Rsats will always be able to be tracked because it will always be in view of a ground station. The Nsats will only be tracked when they are on the near side of the Moon and during their transit of the far-side their orbits will be simulated down on Earth.

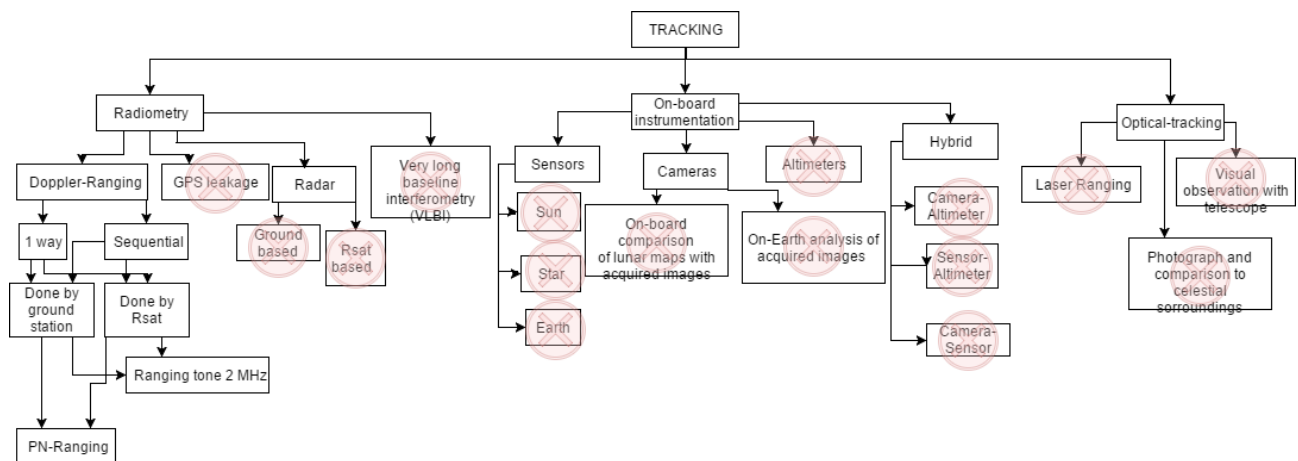


Figure 6.11: Design option tree for tracking and orbit determination

## 6.5. PROPULSION AND TANK SIZING

The propulsion system of the satellite is responsible for the orbit maintenance burns. This is vital for the satellite to maintain the correct orbit. Before the design process starts, the different type of propulsion is discussed and the design process can be seen a small flow chart, this is shown in Figure 6.12. As can be seen, the program needs several inputs, these inputs are put into the propulsion sizing program. This program uses Tsiolkovsky's rocket equa-

tion(Equation 6.2) in combination with equations for the hoop and longitudinal stress to calculate the tank parameters. The program designs a cylindrical tank with spherical end caps, the tank is made of titanium since this is a flight proven tank material and is corrosion resistant. If the thickness of the tank is lower than 1 mm the thickness is set to 1 mm to guarantee manufacturability. The tank is also assumed to be a bladder tank, a tank with a big balloon inside containing the fuel. Outside the balloon there is a pressurising gas, which is assumed to be nitrogen. Also, the required tank volume is increased by 20% to accommodate the pressurant gas. At the end, a safety factor of 1.1 is added. For details see [1, p.20-22]. After the program is run, it is checked if the tank fits in the spacecraft and if the burn time requirement(IRIS-NSAT-PROP-01 in Appendix D) is met. If not, the design is altered by changing some of the input parameters.

$$M_{propellant} = M_{initial} \left( 1 - \frac{1}{e^{\frac{\Delta V}{I_{sp} * 9.81}}} \right) \tag{6.2}$$

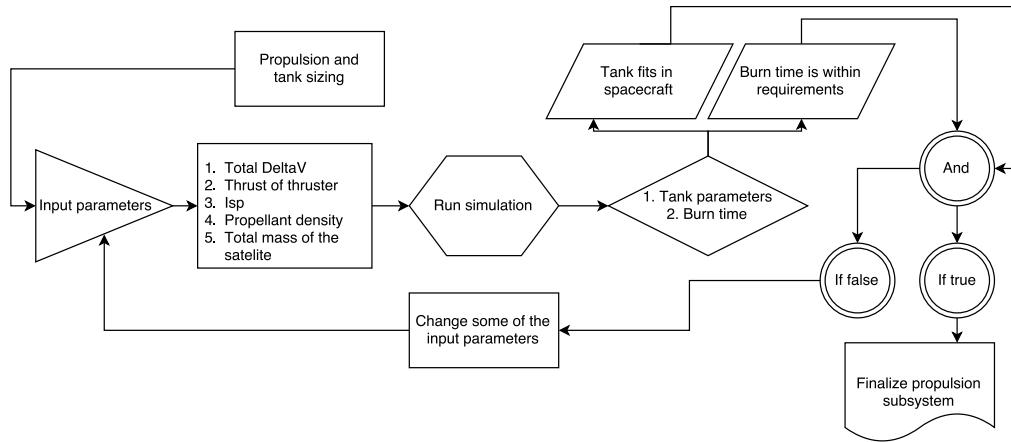


Figure 6.12: Flow chart of the propulsion design process

### 6.5.1. PROPULSION DESIGN

For the Nsat many different systems could be used for propulsion such as chemical propulsion, cold gas and electrical propulsion. Electrical propulsion is excluded due to the limited power generation on the satellites. Cold gas propulsion systems are not that complicated but offer low  $I_{sp}$  (30-80s). This will increase the volume of the propellants, or require gas generators which increases the mass of the system. The last system that can be considered is chemical propulsion. There are many types, but the one suited best for this mission is mono-propellant systems, since they only require one type of propellant and deliver decent  $I_{sp}$  (200-250s).

For the first iteration, a propulsion system is chosen using hydrazine. These are off the shelf systems and there are many choices in thrusters. The following input parameters where put into the calculation program, shown in Table 6.10. The thruster chosen for this was the MR-103M 1 N thruster from Aerojet Rocketdyne.<sup>15</sup> And a worst case scenario  $I_{sp}$  was chosen.

Table 6.10: Input values of propulsion sizing program, the third column is for the second iteration.

Item	Value	Value for second iteration
$\Delta V$	250 $ms^{-1}$	250 $ms^{-1}$
$I_{sp}$	200 s	220 s
Mass satellite	15 kg	15 kg
Propellant density <sup>16</sup>	1.01 $gcm^{-3}$	1.46 $gcm^{-3}$
Manoeuvre $\delta V$	35 $ms^{-1}$	35 $ms^{-1}$

Table 6.11: Output parameters of propulsion sizing program, the third column is for the second iteration.

Item	Value	Value for second iteration
Tank mass	0.53 kg	0.41 kg
Burn time	262.5 s	525 s
Tank height	19.6 cm	19.4 cm
Propellant mass	1.66 kg	1.52 kg
Tank radius	4.6 cm	3.6 cm

The output of the program is shown in Table 6.11. From this it can be seen that the tanks take up already four whole cubes. And nothing else can fit in there together with the tanks. This can be seen in the rough sketch of the satellite in Figure 6.19. From the figure it can be seen that everything is quite cramped and there is no room for thrusters. Therefore it is needed to iterate on the propulsion system. A solution was found, which is using a different fuel. This fuel is a environmentally friendly(green) alternative to hydrazine, which is called AF-M315E [46]. A trade-off was made on the new solution vs the old solution. The trade-off method was the same as the one used in [1, p.7-10].

<sup>15</sup><http://www.rocket.com/files/aerojet/documents/Capabilities/PDFs/Monopropellant%20Data%20Sheets.pdf> Accessed on 25.06.2017

<sup>16</sup>[https://uppsagd.files.wordpress.com/2012/03/advanced\\_monopropellants\\_combustion\\_chambers\\_and\\_monolithic\\_catalyst\\_for\\_small\\_satellite\\_propulsion.pdf](https://uppsagd.files.wordpress.com/2012/03/advanced_monopropellants_combustion_chambers_and_monolithic_catalyst_for_small_satellite_propulsion.pdf) Accessed on 19.06.2017

Table 6.12: Trade off table between AF-M315E and Hydrazine. The  $I_{sp}$  given is the theoretically achievable. <sup>17</sup>

	$I_{sp}$ [s]	Density [ $\text{gcm}^{-3}$ ]	TRL	Sustainability
Hydrazine	233	1.01	9	Highly toxic, hard to handle
AF-M315E	266	1.46	7	Slightly toxic, easy to handle

As seen in Table 6.12 the new green fuel AF-M315E beats hydrazine in every aspect except TRL. This is however a risk that the project is willing to take, since this will solve the space problem and also the new fuel gives better performance. This is illustrated in Table 6.10 and Table 6.11, the values in the third column are values for a system with AF-M315E. The thruster chosen for this fuel was one from Busek. The one in question is BGT-X5 and delivers a thrust of 0.5 N. A layout of the thrusters can be found in Figure 6.1. Since the ADCS and propulsion uses the same thrusters the propulsion system only needs one thruster, this thruster creates a diagonal over the satellite. These two thrusters on the diagonal will be used for the manoeuvres. Since the cg moves during the satellites lifetime these thrusters will induce a torque on the spacecraft. This was analysed in Catia and found that maximum deviation from the thrust diagonal is 5 mm. With a total thrust of 1 N this creates a 0.005 Nm torque, but since the reaction wheels can handle 0.007 Nm<sup>18</sup> the satellite can fire its thrusters without spinning out of control. The decision to move to the new green fuel also benefited the thermal subsystem, this is discussed in section 6.7. This concludes the propulsion sizing of the Nsat.

### 6.5.2. PROPULSION HARDWARE AND SOFTWARE

Since the ADCS and the propulsion subsystem use the same thrusters their computers will be linked. When the thrusters need to fire, the two subsystem computers work together to fire the engines. A small hardware software program is shown in Figure 6.13. As seen in the diagram, when the propulsion computer receives a manoeuvre command it co-ordinates it with the ADCS computer. If the satellites starts deviating of course the ADCS will try to keep it on course, however if not possible the engines are shut down. The propulsion computer will also have detection mechanisms in place in the case one of the two main engines do not fire. Then it will shut down the engines immediately. In the case thruster 1 fails, the spacecraft can still preform a manoeuvre, it will have to fire three other thrusters that cancel out each others moments. This is however inefficient and will lower the lifetime of the satellite. Another possibility is to allow translation, fire the thruster with impulses and correct the attitude with reaction wheels.

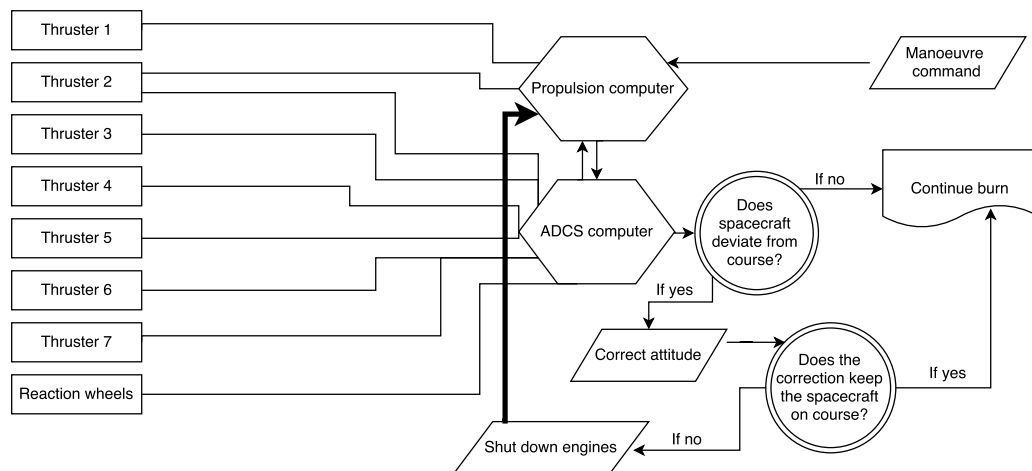


Figure 6.13: Hardware software diagram of the propulsion system. Arrows indicate software decisions and commands. Lines indicate hardware software interaction links

## 6.6. ADCS DESIGN

The attitude determination and control subsystem, as indicated by the name, involves two processes. Attitude determination, which is a process that involves combining a lot of data from different sensors with the prior knowledge of the spacecraft dynamics to provide accurate description of the attitude state. For the sake of clarity, attitude is the three dimensional orientation of the spacecraft's body axis with another reference axis system. While attitude control is the reaction of the spacecraft's rotational dynamics to counter act the disturbances imposed on it by the surrounding environment. These disturbances are often highly predictable and a lot of models and tools have already been established to estimate them. The design process of the ADCS of the Nsat was performed following certain steps that were adapted from [11, p.567]. The steps are summarised in the following list:

<sup>17</sup>[https://uppsagd.files.wordpress.com/2012/03/advanced\\_monopropellants\\_combustion\\_chambers\\_and\\_monolithic\\_catalyst\\_for\\_small\\_satellite\\_propulsion.pdf](https://uppsagd.files.wordpress.com/2012/03/advanced_monopropellants_combustion_chambers_and_monolithic_catalyst_for_small_satellite_propulsion.pdf) accessed on 25.06.2017

<sup>18</sup><http://bluecanyontech.com/rwp100/> accessed on 03.07.2017

1. Determine control modes
2. Define system-level requirements
3. Quantify disturbances environment
4. Select type of spacecraft control
5. Select and size ADCS hardware
6. Define determination and control algorithms
7. Iterate and document

However, the determination and control algorithms will not be determined for this design phase as it is so early to be that detailed. The control modes were chosen such that they are coherent with the mission phases. and then requirements and expectations for the ADCS were defined and documented [Appendix D](#).

#### DISTURBANCE TORQUES

Using the disturbance torques calculator tool developed and described in [section 14.11](#), It was found that the solar radiation pressure induced torque was dominating over the gravity gradient induced torque and therefore it will be used to size the ADCS. This was expected, given the small and symmetric characteristics of the network satellite. The calculated disturbance torque due to solar radiation pressure is  $6.113 \times 10^{-8}$  and the gravity gradient disturbance torque is  $1.711 \times 10^{-10}$ . The solar radiation pressure disturbance torque is then used to calculate the rejection torque after multiplying it with a 1.5 safety factor.

#### REACTION WHEELS AND THRUSTERS

The sizing of the reaction wheel was an iterative process, that made use of the tool developed and described in [section 14.12](#) and the available ADCS components on the market. [Table 6.14](#) gives the specifications of the reaction wheels and the calculated requirements it has to deliver. These results can be regenerated if the tool description is followed together with the inputs in [Table 6.13](#).

Table 6.13: Input variables for ADCS tool

Satellite mass [kg]	13
Satellite dimensions [m x m x m]	0.2x0.2x0.3
Angle $\theta$ between local vertical and all principal axis [deg]	0.1
Reflectivity factor $q$	0.5
Flux [ $W m^{-2}$ ]	1366
Shift of centre of pressure from centre of mass	0.1
Max illuminated area according to the Nsat dimensions	0.0895
Gravitational constant of the Moon [ $m^3/s^2$ ]	$4.9 \times 10^{12}$
Distance from the Moon's centre [km]	3,437.4

Table 6.14: Calculated specification and requirements for the ADCS reaction wheels.

Slew rate [deg/s]	7.5
Disturbance rejection torque [Nm]	9.16E-8
Slew torque reaction wheel [Nm]	0.00615
Momentum storage until next momentum dumping	0.1
Number of orbits till saturation	5

There is no magnetic field at the altitude the Nsat is orbiting at, that and due to the high accuracy required by the communication subsystem, magnetic torquers cannot be used. The only way then to dump the momentum building up in the reaction wheels is by using the thrusters. These thrusters were sized using the tool developed and described in [section 14.12](#). The chosen thruster BGT-X5 is developed by Busek space propulsion and systems. It only weighs 160 grams and is able to supply up to 0.1N of thrust which is sufficient to dump the momentum of the reaction wheels every 5 orbits. The number of thrusters needed is 6 where 2 of those are only for redundancy. Thus there are only 4 active ADCS thrusters during normal operations which means that translation is allowed during momentum dumping. This translation is a price paid for mass reduction purposes. The  $\Delta V$  produced because of this translation is only  $4 \text{ m s}^{-1}$  by the end of the mission life time, thus it can be neglected. The two redundancy thrusters' line of fire is pointing parallel to the solar arrays' longitudinal axis. Should they be needed, the solar panels will have to be rotated 180 degrees during momentum dumping. This is so that they are not affected by the exhaust. The panels can be rotated back after the firing is over.

#### ADCS ARCHITECTURE AND CHOSEN COMPONENTS

After sizing and choosing the sub-components of the ADCS, the architecture illustrated in [Figure 6.14](#) was drawn to show the interactions between the different sub-components. [Table 6.15](#) gives an overview of all the ADCS selected components for Nsat.

Table 6.15: List of the chosen ADCS components

Component	Name	Units	Manufacturer
Reaction wheel	RWP100	4	Blue Canyon Technologies
Thruster	BGT-X5	6	Busek
Star tracker	NST-1 (Nano Star Tracker)	2	TY-Space
Sun sensor	BiSon64	2	Lens R&D

## 6.7. THERMAL DESIGN

For the spacecraft to operate properly there is a desired temperature range. Each subsystem has its own temperature range and the thermal subsystem's job is to keep the subsystems in their desired temperature range. Before the design is done, the different type of thermal control will be discussed. The design process is shortly shown in a flow chart. This can be seen in [Figure 6.15](#). The process starts at the input parameters, then these are inserted into the simulation from which the temperature ranges are output. If the temperature ranges are within the subsystem specifications the thermal design can be finalised. If it does not comply with the subsystem specifications two options are possible, either change the coatings and conductive materials, or select a component that has a different temperature range so that the subsystem can survive the temperature oscillation.

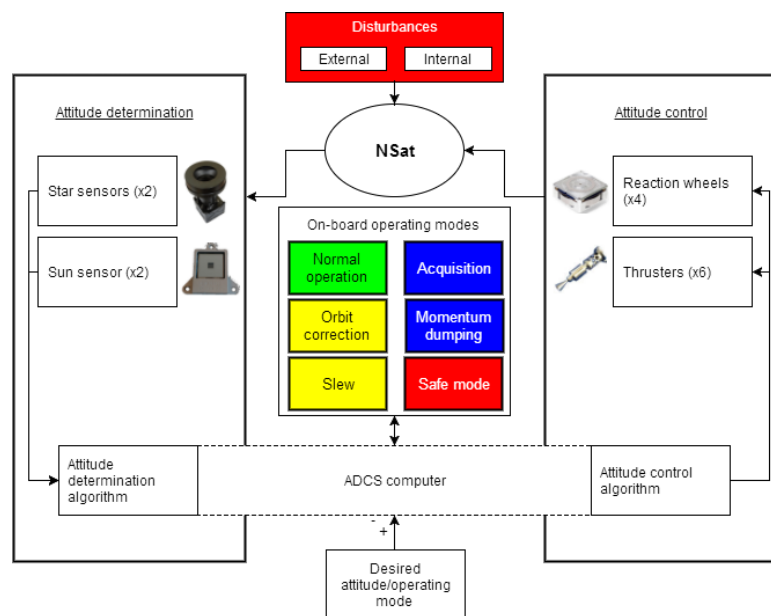


Figure 6.14: ADCS architecture

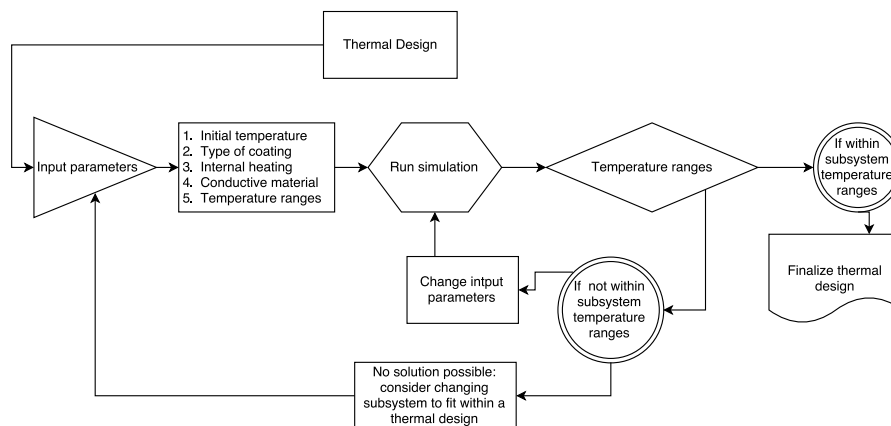


Figure 6.15: Flow chart for the thermal design

### 6.7.1. THERMAL ANALYSIS

There are two main types of thermal control, passive and active. The passive type only uses passive elements, with passive it is meant that it does not have moving parts or parts that require electrical power. This method uses different paints, coatings, radiators and foils to achieve the desired temperature range. The active method can use heaters, coolers and louvres to achieve the desired temperature of the subsystems. Since the Nsat has such a small size and the power system is limited by this, the preferred method will be passive cooling since this requires no power and does not use mechanisms. Now that the preferred method is found, it can be looked the desired temperature ranges for the different subsystems. The temperature ranges are given in [Table 6.16](#)

From [Table 6.16](#) we can see that the most constraining subsystems will be the batteries and the propellant. The thermal tool in, [section 14.15](#), can now be used to analyse the satellite. Note that cable dissipation is neglected due to the cable margin used in the electrical power subsystem, this assumption makes the temperature an underestimation, and the temperature could be a bit higher. The following input numbers were used for the model, they are listed in [Table 6.18](#). The dissipated power values are calculated from the power needed and assuming an efficiency of 70%. Also the orbit period and eclipse time is needed, they are 17.537 s (4.9 h) and 3.028 s (50 min) respectively. These values

<sup>19</sup><http://www.kenkai.jaxa.jp/eng/database/e-gha002.html> accessed on 23.06.2017

<sup>20</sup>[https://uppsagd.files.wordpress.com/2012/03/advanced\\_monopropellants\\_combustion\\_chambers\\_and\\_monolithic\\_catalyst\\_for\\_small\\_satellite\\_propulsion.pdf](https://uppsagd.files.wordpress.com/2012/03/advanced_monopropellants_combustion_chambers_and_monolithic_catalyst_for_small_satellite_propulsion.pdf) accessed on 19.06.2017

<sup>21</sup>[http://batteryuniversity.com/learn/article/charging\\_at\\_high\\_and\\_low\\_temperatures](http://batteryuniversity.com/learn/article/charging_at_high_and_low_temperatures) accessed on 23.06.2017

<sup>22</sup>[http://cdn.intechopen.com/pdfs/22805/InTech-Architectural\\_design\\_criteria\\_for\\_spacecraft\\_solar\\_arrays.pdf](http://cdn.intechopen.com/pdfs/22805/InTech-Architectural_design_criteria_for_spacecraft_solar_arrays.pdf) p.162, Accessed on 23.06.2017

<sup>23</sup>[https://deepspace.jpl.nasa.gov/files/dsn/Brochure\\_IrisV2\\_201507.pdf](https://deepspace.jpl.nasa.gov/files/dsn/Brochure_IrisV2_201507.pdf) accessed on 23.06.2017

<sup>24</sup><https://www.cubesatshop.com/product/cube-computer/> accessed on 23.06.2017

Table 6.16: Table of allowable temperatures

Subsystem	Minimum temperature [°C]	Maximum temperature [°C]
Reaction wheel <sup>19</sup>	-15	55
Propellant <sup>20</sup>	1 (-22 for new propellant)	100
Battery <sup>21</sup>	0	45
Solar cells <sup>22</sup>	-150	120
Antenna System <sup>23</sup>	-20	50
Computer system <sup>24</sup>	-10	70

where calculated with the power system sizing tool in [section 14.13](#)

From the thermal tool an iterative process was used to find the best coating on the outside panels and conductive material between the subsystems. In the following figure the temperature graphs are given, [Figure 6.16](#). Seen in [Figure 6.16](#) on the left is the temperature of the outside panels and the solar panels, where Xp is a 3x2 panel facing in the positive X direction, Xm is a 3x2 panel in negative X direction. Yp and Ym are the same as Xp and Xm only in Y direction. The Zp and Zm are 2x2 panels in the Z-direction. The plot on the right is the temperature of the inside components, only the tank and battery are shown since they are the closest to their limits, the rest is displayed in [Table 6.19](#) with uncertainties included due to simulation errors. The values in brackets are the values for the second design that is discussed later in this section. The last column is for the worst case scenario where the satellites are always in view of the Sun this is only the value for the second design. Seen in [Figure 6.16](#) the temperature fluctuates between day and night time. The big dip in temperature is in the event that the satellite just leaves the eclipse behind the Moon to enter a eclipse behind the Earth, the eclipse time then increases to 8.788 s(2.4 h)<sup>25</sup>. This is considered a worst case scenario and the satellites have to survive this event as well. During this eclipse the antenna system is turned off.

As seen in [Figure 6.16](#) the solar panel fluctuates a lot. This is due to the surface area of the panels is relatively large compared to the mass, hence they change temperature fast. Many different coatings and combination of coatings where tried, see [Table 6.17](#) for the emissivity and absorption values. After many tries the best possible option for this satellite design was made with Ebanol C black-384 ESH UV on X and Y panels, and Goldized kapton on Z panels. The conductive material used is aluminium and when in connection with other material the conductivity is calculated, this done by the method in [section 14.15](#). For aluminium the thermal conductivity is  $204 \text{ Wm}^{-1}\text{K}^{-1}$ <sup>26</sup>. However this solution poses a problem, the propellant tanks get to cold, they are below freezing and their allowable temperature is 1 °C. This can clearly be seen in [Figure 6.16](#). This indicates that the solution has to be altered according to the method in [Figure 6.15](#). The problem is solved by changing the fuel with a lower allowable temperature, in [section 6.5](#) this solution is discussed. However the satellite was redesigned and some subsystems have moved so the thermal design has to be run one more time. The results of the temperatures are given in the brackets in [Table 6.19](#) an the graph is shown in [Figure 6.17](#). From this we see that the second design is the better choice for thermal management since the most critical components are further away from their temperature limits, this design uses the same coatings and insulation as in design number one. From [section 6.5](#) the second solution by changing the fuel is also the superior design. This will be the final design of the thermal control subsystem since it complies with requirement IRIS-NSAT-THRM-01 in [Appendix D](#).

Table 6.17: Emissivity and absorption values [47, p.365].

Coating	Emissivity	Absorption
Aluminium tape	0.21	0.04
Polished aluminium	0.24	0.08
Aluminized kapton (alu outside)	0.14	0.05
Black paint(polyurethane)	0.95	0.90
White paint(silicone)	0.29	0.83
Solar panel(GaAs)	0.88	0.80
Aluminized kapton(alu inside)	0.40	0.63
Goldized kapton (gold outside)	0.25	0.02
Anodized aluminium	0.77	0.84
Ebanol C Black-384 ESH UV <sup>27</sup>	0.97	0.75

Table 6.18: Table of input parameters

Subsystem	Mass [kg]	Dissipated energy [W]
Reaction wheels	1	2
Propellant	1.8	0
Battery	1	3 charging, 8 discharging
Antenna System	2.4	10 transmitting, 3 idle
Computer system	1	6

<sup>25</sup><https://web.archive.org/web/20070305183925/http://sunearth.gsfc.nasa.gov/eclipse/LEcat/LE2001-2100.html> Accessed on 26.06.2017

<sup>26</sup>[http://www.engineeringtoolbox.com/thermal-conductivity-metals-d\\_858.html](http://www.engineeringtoolbox.com/thermal-conductivity-metals-d_858.html) Accessed on 26.06.2017

<sup>27</sup><http://www.solarmirror.com/fom/fom-serve/cache/43.html> accessed on 21.06.2017

Table 6.19: Temperature ranges of the satellite, the numbers in the brackets is the second iteration of the thermal design. All values have a uncertainty of  $\pm 1$  as specified in section 14.15

Subsystem	Minimal temperature normal orbit [°C]	Maximum temperature [°C]	Minimum temperature double eclipse [°C]	Maximum temperature only sunlight [°C]
Reaction wheels	15.6 (18.2)	22.6 (25.7)	0.8 (3.3)	30.0
Propellant tank 1	14.5 (17.2)	21.2 (24.3)	-0.3 (2.3)	28.8
Propellant tank 2	13.9 (16.9)	20.6 (24.1)	-0.9 (2.0)	28.5
Battery	16.5 (19.0)	23.6 (26.5)	1.6 (4.0)	30.9
Antenna System	18.5 (20.9)	25.2 (27.9)	3.7 (6.0)	32.4
Computer system	15.6 (18.5)	24.2 (26.8)	1.1 (3.5)	31.1
Solar panels	-36.1 (-35.5)	55.5 (55.8)	-59.4 (-58.6)	56.4
Outside panel	8.9 (11.2)	19.6 (22.1)	-6.1 (-3.9)	26.0

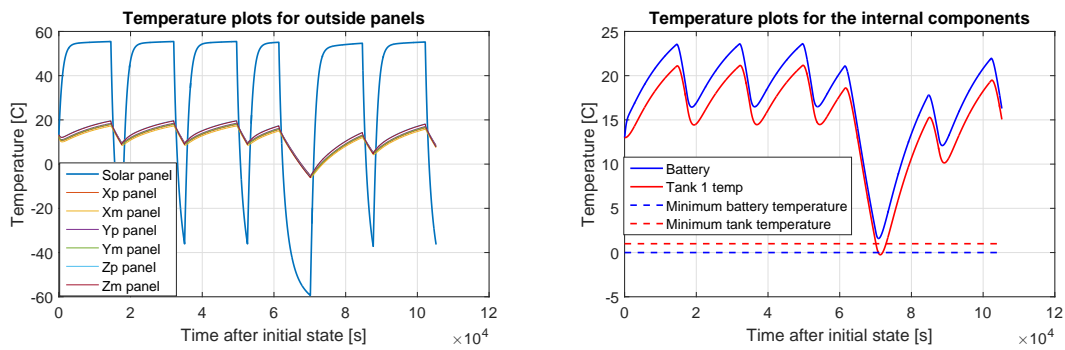


Figure 6.16: On the left, temperature graphs of the outside panels and solar panels. On the right, temperature graphs of the tank and the battery. For the first iteration. Every time the temperature starts decreasing the spacecraft enters eclipse and when it increases the spacecraft exits the eclipse.

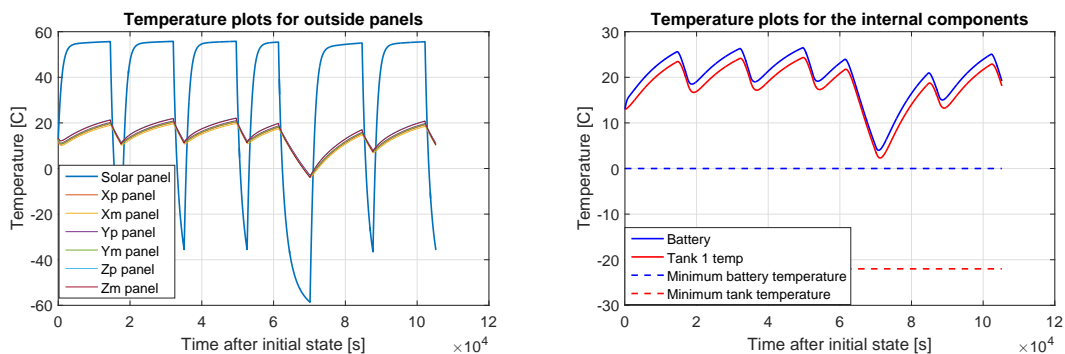


Figure 6.17: On the left, temperature graphs of the outside panels and solar panels. On the right, temperature graphs of the tank and the battery. For the second iteration. Every time the temperature starts decreasing the spacecraft enters eclipse and when it increases the spacecraft exits the eclipse.

### 6.7.2. THERMAL HARDWARE AND SOFTWARE

Since the thermal subsystem is a passive system there will be no mechanisms and heaters. There will however be some thermal sensors on the vital subsystems for monitoring their temperature. If the temperature of these subsystems would go towards their limits, the spacecraft could react by putting the spacecraft in a better attitude for heating or cooling. A small hardware-software diagram is shown in Figure 6.18. Seen in the diagram, the computer is connected to the sensors and if the computer detects that a subsystem is close to its limit it can give the command to the ADCS computer to move to a better attitude for the heat.

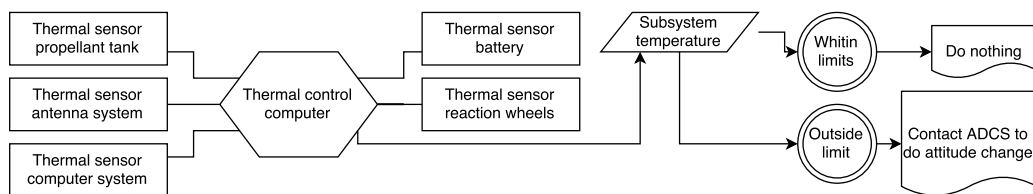


Figure 6.18: Hardware software diagram for thermal control. Arrows indicate software decisions and commands. Lines indicate hardware software interaction links

## 6.8. PRIMARY STRUCTURE DESIGN

This section describes the design of the Nsat's primary structure which is shown in Figure 6.20. The structure is the skeleton of the satellite and should support all the subsystems and protect them. The structure also has to survive the launch loads. The design of the overall structure was done in the steps adapted from [11].

### 6.8.1. STRUCTURAL DESIGN

The starting point of the structure was from the CubeSat standard with 10x10 cm cubes. These cubes are already structurally sized to take launch loads and provide support for the subsystems. However it was quickly found from the preliminary sketch, shown in Figure 6.19 that the propellant tanks were very large, and that the rest of the subsystems were hard to fit within the cube structure. In order to fit every subsystem in the satellite, many of the structural elements needed to be removed. This resulted in a weak structure that could not hold the launch loads. The structure was analysed with the tool developed and described in section 14.7.

The first iteration was quickly discarded. Due to the redesign of the Nsat, the largest difference was in the battery, since the battery became a cylinder with diameter of 54 mm. A central cylinder was constructed around the battery. This can be seen in Figure 6.20, where the cylinder is part number two in the figure. This cylinder will carry the main loads in bending and shear. Structural element number one is the ribs, these ribs are there for mounting subsystems and offer stiffness to the structure and transfer loads from the deployment vehicle to the rest of the structure. Finally structural element number three are the stiffeners. These stiffeners are there to guide the satellite out of the deployment vehicle and provide tensile and compressive resistance to the structure.

The structural sizing tool, in section 14.7, was used to calculate the stresses and moments in the structure and ensure that the cylindrical primary structure does not fail during launch due to the imposed loads in the lateral and longitudinal direction. The main material used for the structure was aluminium. Aluminium has a yield strength of 276 MPa and a density of  $2,830 \text{ kgm}^{-3}$ . The mass of the cylindrical primary structure was calculated to be approximately 0.228 kg while the total mass of all the ribs was estimated to be 0.246 kg and the columns outlining the satellite were estimated to have a mass of 0.104 kg. This results in a total mass of 0.578 kg, however this is only the primary structure.

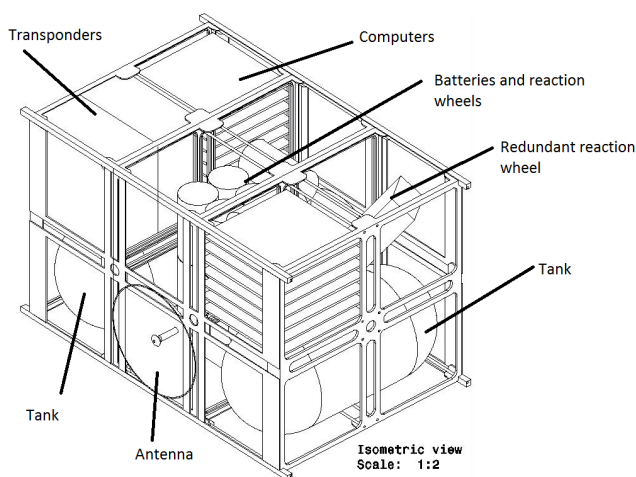


Figure 6.19: Preliminary sketch of the satellite

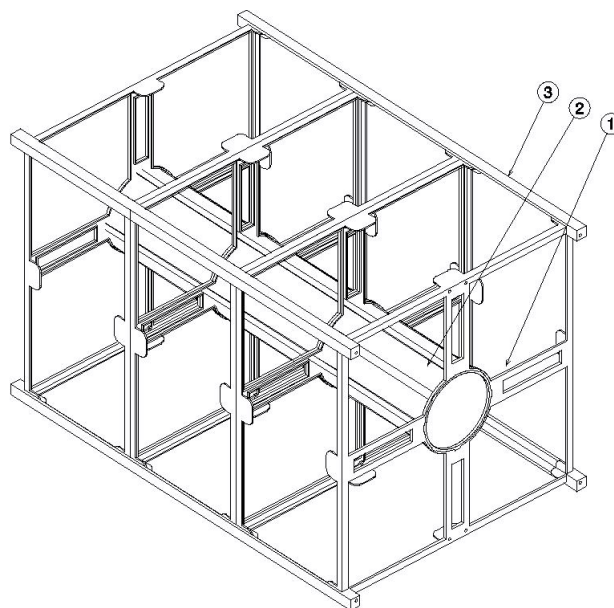


Figure 6.20: Isometric view of the primary structure

### 6.8.2. CENTRE OF MASS

After the preliminary Catia model was developed, it was used to estimate the location of the centre of gravity. Using the inertial measuring tool. The centre of gravity was found to be deviating 0.011 m away from the geometric centre of the satellite when the propellant tanks are full. When the tanks are empty this deviation is 0.018 m



This chapter details the process of designing the relay satellites.

### 7.1. RELAY SATELLITE LAYOUT

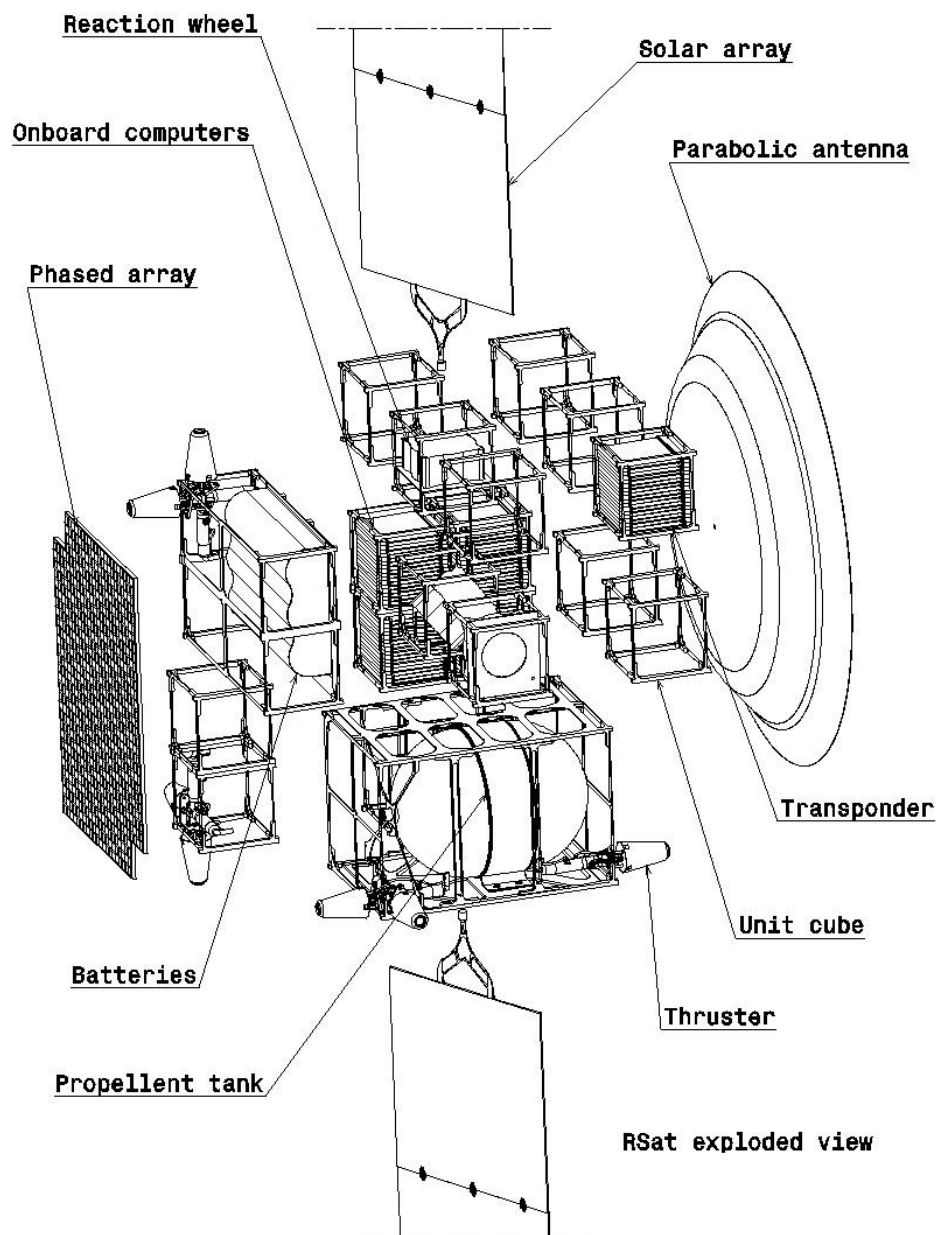


Figure 7.1: Exploded view of the Relay satellite (Rsat).

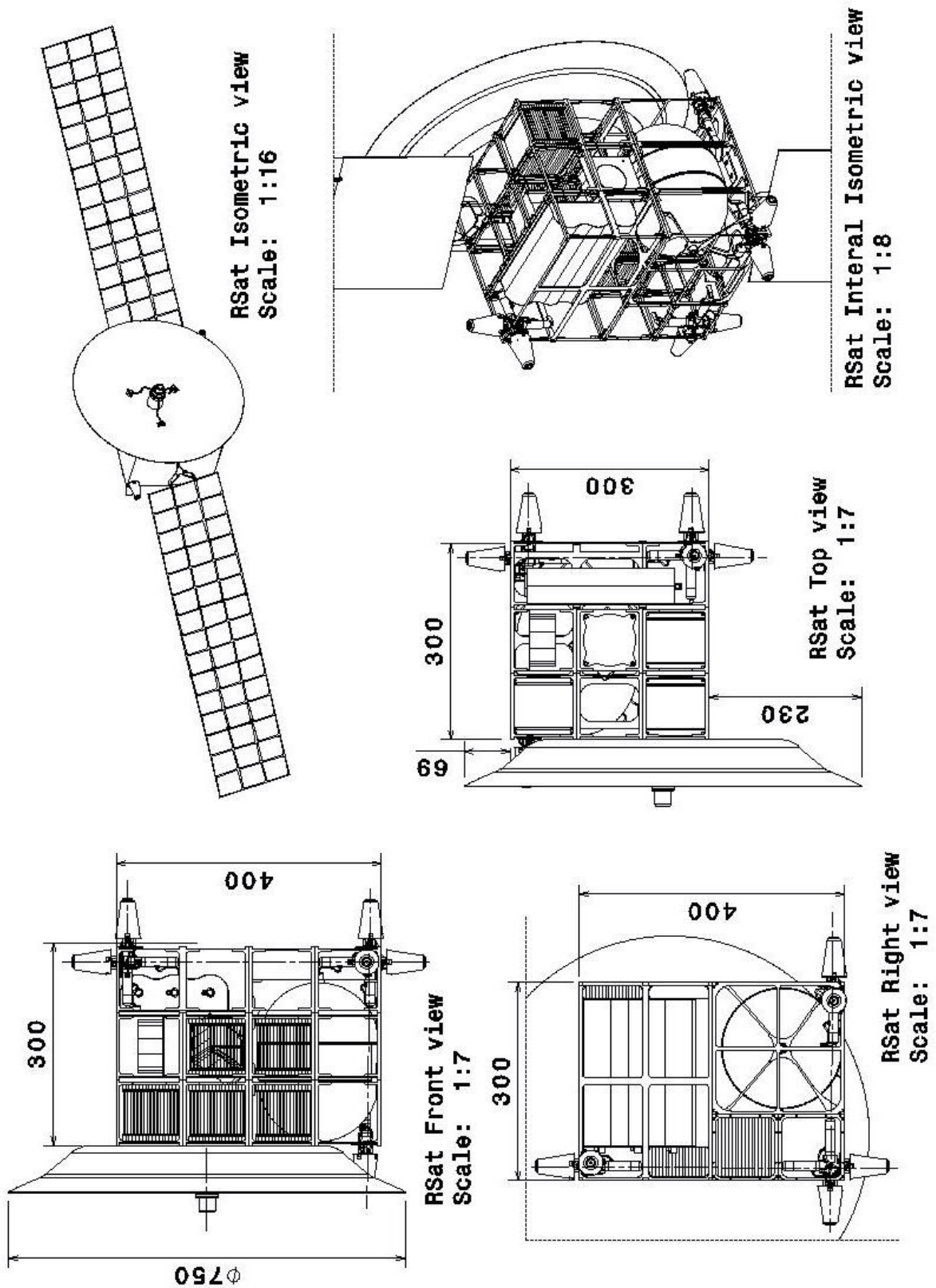


Figure 7.2: Conceptual layout of the Relay satellite (Rsat) with dimensions in mm.

The first design choice which is considered is the placement of the solar panels and antennas. To be able to communicate with the Moon and the Earth at the same time, one antenna must face the Earth and the other has to face the Moon. This leaves only 4 faces for the solar panels. Since the solar incidence angles are dependant on the position within the halo orbit and the orientation of the Rsats. If the solar panels can rotate about one axis and are mounted on the other 3x4 face, see [Figure 7.2](#), the solar incidence angle varies between  $0^\circ$  and  $90^\circ$ . While if mounted on the 3x3 face it varies between  $-46^\circ$  and  $46^\circ$ , such a variation is shown in [Figure 7.3](#). Thus the choice is made to mount them on the 3x3 face. The rest of the spacecraft components are also shown in [Figure 7.1](#) and [Figure 7.2](#).

## 7.2. ELECTRICAL POWER SYSTEM

The electrical power subsystem of the Rsat is designed using a similar process as for the Nsats, described in [section 6.2](#). Using an identical reasoning, photovoltaics with a secondary battery are chosen. To determine the type of solar cells, [Table 6.1](#) is used. Again multi-junction solar cells are chosen since active two-axis pointing is not available and it has a significantly higher areal power density compared to thin film solar cells. The chosen solar cell is the Azur space 3G30C and the selected battery is the Saft VL51ES, similarly to the Nsat.

From the power budget, power requirements are obtained, which can be seen in [Table 7.1](#) where the meaning of the different power requirements is explained in [section 6.2](#). For the relay satellites, one relevant peak power case is found, which is during the reaction wheel momentum dumping where the reaction wheel and thruster are using maximum power.

Table 7.1: Rsat general power requirements.

	Power [W]	Time [s]
Full activity	102.8	-
Average power requirement	94.00	Continuous
Maximum peak	145.1	-
Momentum dumping case	141.0	22

Table 7.2: Relay satellite EPS design input parameters for the calculation tool.

Average power requirement	94.0	W
Max impulse energy	0.862	Wh
Battery DOD	0.9	-
Degradation	3%	year <sup>-1</sup>
Absorptance	0.91	-
Temperature	320	K
Day efficiency	0.85	-
Night efficiency	0.65	-

The environment of the relay satellites is different from the network satellites. They always receive sunlight and thus do not require battery sizing based on eclipse time. The EPS is not sized for the Earth eclipse as it will occur to maximum 1.5 % of the halo orbit twice per month. Furthermore, due to the slanted halo orbits, the solar angle of incidence varies throughout the orbit time. This is shown in [Figure 7.3](#) for each halo satellite. It can be seen that the cycle does not perfectly repeat after 12.25 days. This is because the halo orbit period and the orbit of the Moon around the Earth do not line up. This causes each period to be slightly shifted. From these satellites, the satellite with the worst angle of incidence is selected, which is highlighted in the figure. The effect of this on the solar cell efficiency is shown in [Figure 7.4](#), which is calculated by taking the cosine of the solar angle of incidence.

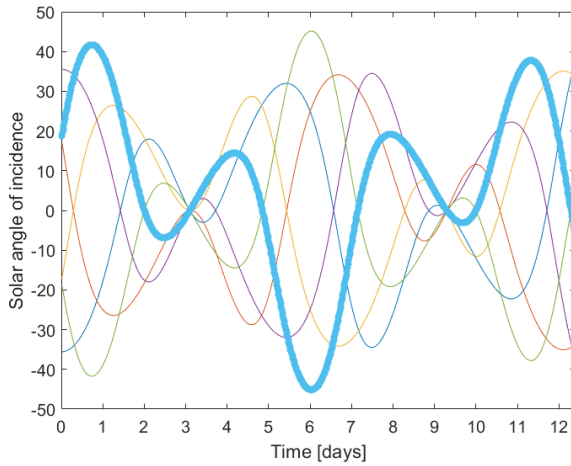


Figure 7.3: Varying solar angle of incidence for the relay satellites throughout the orbit.

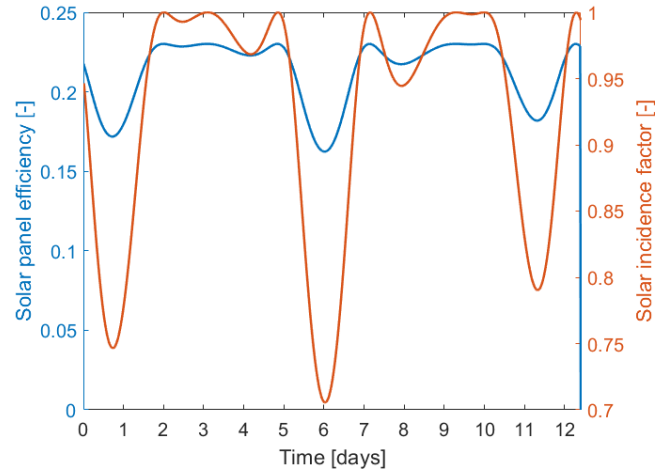


Figure 7.4: Solar panel efficiency throughout the halo orbit due to changes in the solar incidence angle.

Since the orbital period of the relay satellites takes 12.25 days, the battery goes through roughly 150 cycles. This means that battery degradation due to the number of discharge cycles is negligible, even with a 100 % depth of discharge. Since some power reserve always has to be present, a depth of discharge of 90 % is chosen. All the input parameters are shown in [Table 7.2](#) excluding the angle of incidence and solar cell parameters. The degradation and absorptance are the same as in the Nsat case since the same type of solar cells are used.

With these parameters, the EPS can be sized using the power monitoring tool. This results in a required amount of solar cells of 79 and a battery capacity of 468 Wh. The solar panels themselves are designed similarly to the Nsat solar panels. They consist of separate panels connected with the same hinges used in the network satellite, as is shown in [Figure 7.5](#). Each panel consists of 9 solar cells and with five panels on both sides of the relay satellite, a total of 90 solar cells are present. Having a total of 81 solar cells would have been possible as well, but since the design philosophy of the Rsat is to have more redundancy, 90 cells are chosen. The solar cell layout can be seen in [Figure 7.5](#). These solar

cells are wired in five loops of nine solar cells, which results in an operational voltage of around 20.6 V. The solar arrays are connected to the satellite with a titanium rod and contains a rotational mechanism which allows rotation around its longitudinal axis. With the increased amount of solar cells, the required battery capacity drops down to 298 Wh for a depth of discharge of 90 %. Due to this, two Saft VL51ES cells are sufficient. For redundancy one cell is added which results in a total capacity of 540 Wh. These battery cells will be linked in series, totalling an operational voltage of 8.4 V to 12.6 V.

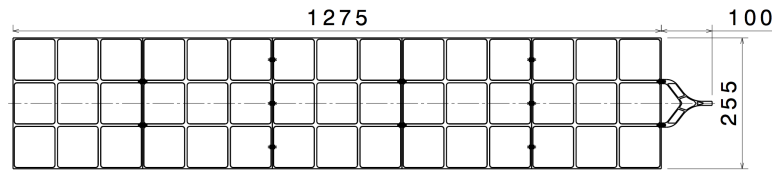


Figure 7.5: Relay satellite solar cell layout with dimensions in mm.

With the chosen configuration, the power profile of one halo orbit is calculated, which can be seen in Figure 7.6. Mostly, the battery is fully charged with the exception of two points, where the generated power drops due to the solar angle of incidence fluctuation. The battery charge remains above 50 %. With including redundant wiring and components, the Rsat EPS is fully redundant.

Lastly, the electrical block diagram for the relay satellites is shown in Figure 7.7 and the mass breakdown can be found in Table 7.3.

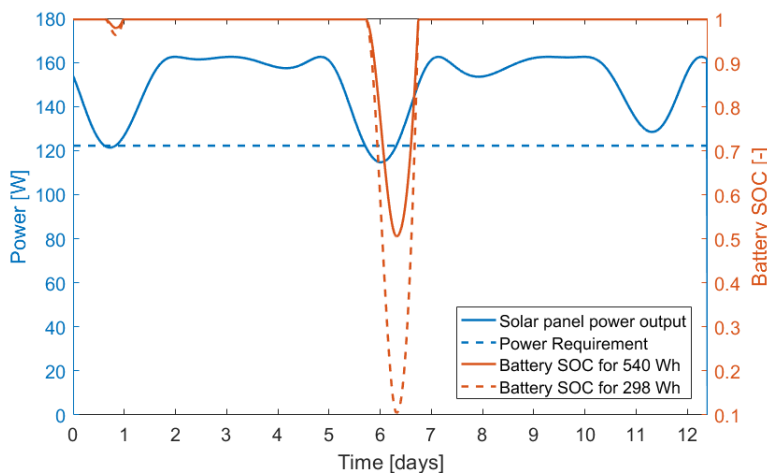


Table 7.3: Mass breakdown of the relay satellite EPS

	Amount	Total mass [kg]
Solar cell blanket	0.325 m <sup>2</sup>	0.445 [33]
Solar panel harness	0.325 m <sup>2</sup>	0.192 [33]
Solar panel substrate	0.325 m <sup>2</sup>	0.423 [33]
Hinges	12	0.120
Rod	1	0.300
Rotational mechanism	1	0.250
Solar array mass	2	3.46
VL51ES battery	3	1.08
Subtotal	1	6.70
Cable and component margin	15%	1.005
<b>Total subsystem mass</b>		<b>7.705</b>

Figure 7.6: Power profile of the halo satellite.

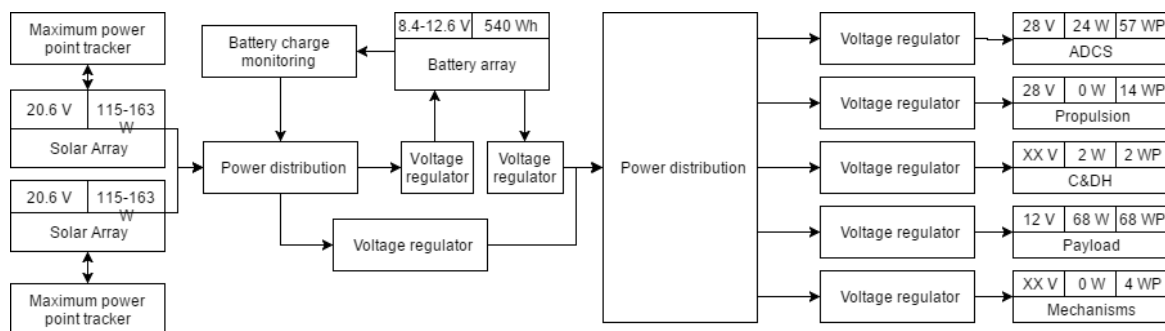


Figure 7.7: Relay satellite electrical block diagram

### 7.3. COMMAND AND DATA HANDLING

The sizing method for the C&DH subsystem is discussed in section 6.3. The Rsat will need to be equipped with faster processors than the Nsats. The reason for that is the fact that except for the nominal functions that the Nsats will perform, they will have to do more complex operations. Such operations include keeping track of all functioning and non-functioning Nsats and determining the shortest transmission path to the rover. The Rsats can be considered as the head of the system, all information passes through them, it's transmitted through them and delegated accordingly to the Nsats. The last ones can be thought of as the limbs of the system, through which the end goal is achieved.

As discussed in section 6.3, the housekeeping data generated on board the Rsat will always be transmitted back to Earth as the Rsats will always be in view of the ground stations. However due to the fact that it will be the collector of all information it will also need to have bigger storage capacity. The estimated capacity, is based on a scenario where for some unexpected reason, a link with a ground station can not be established for at most 24 hours. Using the results

of Table 6.8, both a Nsat and Rsat generate around 0.6 Gbit of house keeping data. Assuming that each Nsat plane will correspond to one Rsat, then the Rsat will need to store the housekeeping of 6 Nsats and its own housekeeping. Resulting in 4.2 Gbit of storage needed. For uncertainty purposes and to account for the rover housekeeping the final storage size shall be no less than 5 Gbit. Furthermore, the circuit boards will be placed within a layer of protective material to shield against radiation, similar to the Nsat.

## 7.4. TRACKING AND ORBIT DETERMINATION

Tracking of the satellites will be done using one-way Doppler. The reason for using this method is explained in section 6.4.

## 7.5. PROPULSION AND TANK SIZING

The propulsion system of the Rsat is similar to the one on the Nsat, section 6.5. The same design flow is used which can be seen in Figure 6.12.

### 7.5.1. PROPULSION DESIGN

The Rsat went through the same two iteration cycles for the propulsion design as the Nsat design. However, since the Rsat is much larger the change in terms of space is less severe. However, the tank decreased in size and the overall mass of the system went down as well. A summary of the values are given in Table 7.4 where the inputs of the program are given. In Table 7.5 the outputs of the program are shown. As seen in both tables the option with the green fuel AF-M315E is the better option for the Rsat as well. For the calculations the same thrusters were used as for the Nsat in section 6.5

Table 7.4: Input values of propulsion sizing program, the third column is for the second iteration

Item	First iteration	Second iteration
$\Delta V$	400 ms <sup>-1</sup>	400 ms <sup>-1</sup>
$I_{sp}$	200 s	220 s
Mass satellite	32 kg	32 kg
Propellant density <sup>1</sup>	1.01 gcm <sup>-3</sup>	1.46 gcm <sup>-3</sup>
Manoeuvre $\Delta V$	20 ms <sup>-1</sup>	20 ms <sup>-1</sup>

Table 7.5: Output parameters of propulsion sizing program, the third column is for the second iteration

Item	First iteration	Second iteration
Tank mass	0.95 kg	0.66 kg
Burn time	320 s	640 s
Tank height	36.3 cm	25.2 cm
Propellant mass	5.9 kg	5.4 kg
Tank radius	9 cm	9 cm

### 7.5.2. PROPULSION HARDWARE AND SOFTWARE

The Rsat will use the same architecture for controlling the main engines as the Nsat, this is shown in Figure 6.13. Also the Rsat will use the same engines as the Nsat, since the manoeuvres the Rsat makes are with low  $\Delta V$  (max 25 ms<sup>-1</sup>). The layout of the thrusters is shown in Figure 7.1 and Figure 7.2. The engines of the Rsat will also use a diagonal thrust line. It was analysed in Catia that the maximum deviation of the cg from the diagonal was 2.5 mm this accounts for 0.0025 Nm with a thrust level of 1 N. The reaction wheels can deliver 0.025 N m<sup>2</sup> hence the satellite will not spin out of control.

## 7.6. ADCS DESIGN

The sizing method and steps taken to realise the attitude determination and control subsystem of the relay satellite are exactly the same as of the network satellite which was described in section 6.6. The only difference of course is the final calculated requirements and expectations the ADCS needs to fulfil to realise the desired attitude control. In this section the main differences between the ADCS of network and the relay satellites are explained.

Firstly, the relay satellite only experiences disturbance torques that are induced from the solar radiation pressure. It was calculated that at a maximum illuminated area of 0.187 m<sup>2</sup> perpendicular to the Sun's radiation, reflectivity factor of 0.5 and a 0.1 m shift between the centre of mass and centre of pressure, the solar radiation pressure disturbance torques acting on the Rsat is  $1.28 \times 10^{-7}$  Nm. To counter that torque the reaction wheels and thrusters are sized and the results in Table 7.8 are achieved. These calculations can be reproduced if the parameters in Table 7.7 are input in the reaction wheel and thruster sizing tool described in section 14.12. It should be noted that the disturbance rejection torque is calculated by multiplying the disturbance torque with a safety margin of 1.5. Moreover, Table 7.6 gives an overview of the selected ADCS components and their manufacturers. In addition, when the thrusters fire to dump the momentum they will first fire in one direction after which the spacecraft turns 180° and fires a second time to cancel out the  $\Delta V$  created from the first burn.

Table 7.6: List of the chosen ADCS components for the Rsat

Component	Name	Units	Manufacturer
Reaction wheel	RWP100	4	Blue Canyon Technologies
Thruster	BGT-X5	6	Busek
Star tracker	NST-1 (Nano Star Tracker)	2	TY-Space
Sun sensor	BiSon64	2	Lens R&D

<sup>1</sup>[https://uppsagd.files.wordpress.com/2012/03/advanced\\_monopropellants\\_combustion\\_chambers\\_and\\_monolithic\\_catalyst\\_for\\_small\\_satellite\\_propulsion.pdf](https://uppsagd.files.wordpress.com/2012/03/advanced_monopropellants_combustion_chambers_and_monolithic_catalyst_for_small_satellite_propulsion.pdf) Accessed on 19.06.2017

<sup>2</sup><http://bluecanyontech.com/rwp500/> accessed on 03.07.2017

Table 7.7: Input variables used to size the reaction wheels and momentum dumping thrusters.

Satellite mass [kg]	30
Satellite dimensions [m x m x m]	0.3x0.3x0.4
Reflectivity factor $\rho$	0.5
Flux [ $\text{Wm}^{-2}$ ]	1366
Shift between centre of pressure and mass [m]	0.1
Max illuminated area according to dimensions [ $\text{m}^2$ ]	0.187

Table 7.8: Calculated specification and requirements that the chosen reaction wheel has to achieve

Slew rate [deg/s]	6
Disturbance rejection torque [Nm]	1.92E-7
Slew torque reaction wheel [Nm]	0.02
Momentum storage until next momentum dumping	0.5
Number of orbits till saturation	135

### 7.6.1. CENTRE OF GRAVITY

After most of the subsystems of the relay satellite were sized the centre of gravity position was determined. The method used to determine the centre of gravity required the use of Catia's inertial measure tool. The final centre of gravity was found to be deviating 0.0982 m from the geometric centre, this is the case when the main propellant tank is full. It was also found that when the tanks are empty the centre of gravity deviates 0.110 m.

## 7.7. THERMAL DESIGN

The thermal design of the Rsat is done in the same way as the Nsat. See Figure 6.15 for the design flow. The Rsat has a quite different environment than the Nsat. Since the Rsat is more or less constantly in view of the Sun. Except for the special case when it goes into eclipse behind the Earth.

The thermal control of the Rsat is designed to be passive just as the Nsat, for the same reasons. The power needed to heat or cool the spacecraft would make the EPS too large. Hence the same inputs to the thermal tool are given, but they have a different value. The values are given in Table 7.9. The layout of the subsystems are given in Figure 7.1 and Figure 7.2.

Table 7.9: Table of input parameters

Subsystem	Mass [kg]	Dissipated energy [W]
Reaction wheels	1	6
Propellant	1.8	0
Battery	1	9 charging, 24 discharging, 3 idle
Antenna System	2.4	10 transmitting, 3 idle
Computer system	1	12

Table 7.10: Table of maximum and minimum temperatures

Subsystem	Maximum temperature [ $^{\circ}\text{C}$ ]	Minimum temperature eclipse [ $^{\circ}\text{C}$ ]
Reaction wheels	29.3	-6.4
Propellant tank	27.4	2.3
Battery	36.1	1.5
Antenna system	29.6	-6.0
Computer system	31.4	-6.9
Solar panels	52.1	-104.0
Outside panel	20.0	-27.2

The design is iterated for different potential coatings, the same as for the Nsat, which are shown in Table 6.17. Since the Rsat uses the same type of components as the Nsat the same allowed temperature ranges can be used. They are shown in Table 6.16. Aluminized kapton is used as a solution with aluminium facing the satellite body. The spacecraft is able to stay inside the defined temperature ranges with this design. The satellite also survives the long eclipse of 12,960 s (3.6h), when it is behind the Earth, this eclipse time comes from the calculations done in subsection 4.4.3. The antennas will be turned off during the eclipse. All the surfaces of the spacecraft use this coating. The conductive material is the same as for the Nsat. The battery however needs some insulation to retain its temperature during the eclipse. The insulation used is Polytetrafluoroethylene (PTFE). It needs a 2cm layer of insulation to be able to stay warm enough. The thermal conductivity of PTFE is 0.25<sup>3</sup>. The thermal conductivity is then  $123 \text{ Wm}^{-1}\text{K}^{-1}$  for the conduction paths towards the battery. The temperature graph and table of the temperatures are given in Figure 7.8 and Table 7.10 respectively. The change of the propellant in section 7.5 did not affect the thermal design of the Rsat in a huge way as the satellite did not require a redesign (only the propellant tank got smaller). The temperature of this design complies with the requirement IRIS-RSAT-THRM-01 in Appendix D

The Rsat uses the same method as the Nsat to control its temperature in case of an emergency see Figure 6.18 for the hardware-software diagram.

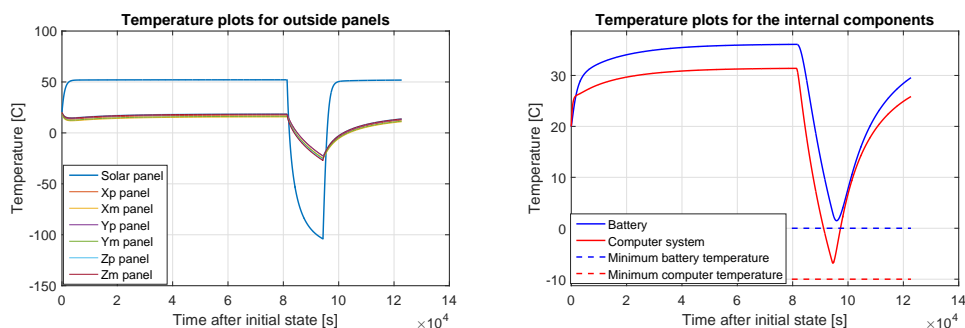


Figure 7.8: On the left, temperature graph of the outside panels and solar panels. On the right the internal temperatures of the computer system and the batteries. When the temperature starts decreasing the spacecraft enters eclipse and when it increases the spacecraft exits the eclipse.

<sup>3</sup>[http://www.engineeringtoolbox.com/thermal-conductivity-d\\_429.html](http://www.engineeringtoolbox.com/thermal-conductivity-d_429.html) Accessed on 26.06.2017

## NETWORK DEPLOYMENT VEHICLE DESIGN

The design of the NDeVe is described in this chapter.

### 8.1. NETWORK DEPLOYMENT VEHICLE LAYOUT

**Overview** The network deployment vehicle consists of an octagonal prism, shown in Figure 8.1. In the figure, the x-axis is defined as being in the direction of the thrust vector, the z-axis is in the direction of the parabolic antenna (receiving) and the y axis is chosen to complete a right handed system. In the upper part, the Nsats are mounted to a hollow central column inside of which the pressurant tank, the on board computer and a reaction wheel are placed. The lower part is filled with 3 remaining reaction wheels, placed at the outer edges. Together with the wheel in the top, they form a pyramid configuration. Furthermore, the lower part is filled with the propellant tank and the main propulsion unit, including pressure pumps and leads.

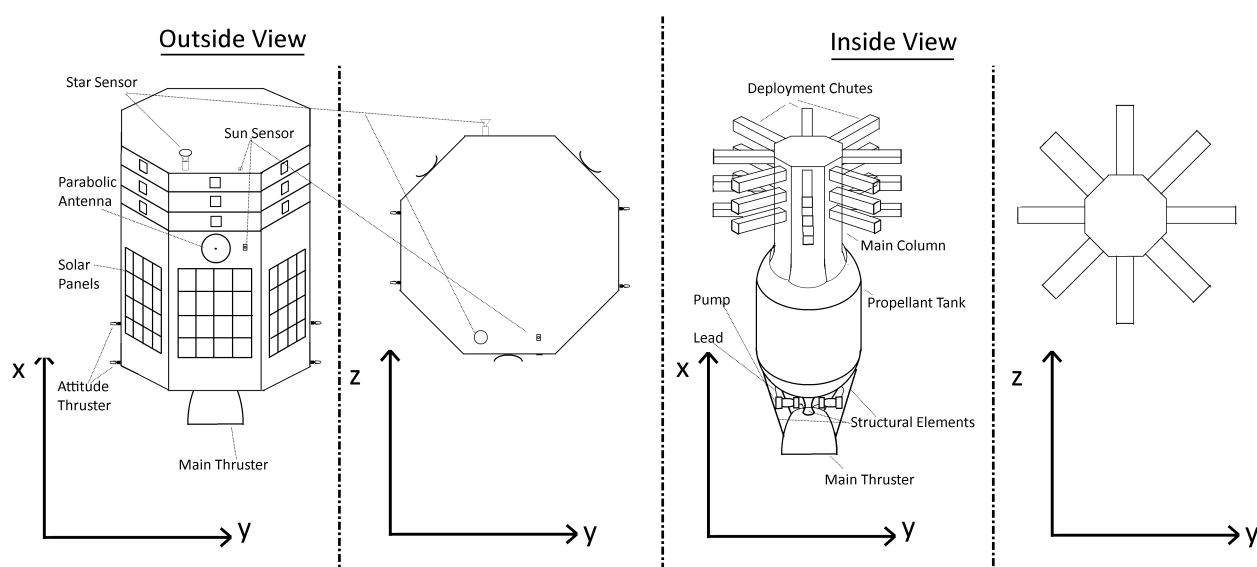


Figure 8.1: A sketch of the outside and inside of the deployment vehicle.

**Major Design Decisions** One of the first design decisions on the deployment vehicle was the total number of separate vehicles. Due to the increase in network satellites from 24 to 48 and an increase in the  $\Delta V$  of the RAAN change manoeuvre, the mass of the DeVe increased by almost a factor of 3 from the initial estimate. This mass could be decreased again by adding a second deployment vehicle. The advantages of this are the decreased payload mass and the decreased number of burns.

Due to their increased number, the number of burns that have to be performed need to be assigned. The first option in this trade off is keeping the old configuration with a single vehicle and it performs all five burns to get the satellites into the six desired orbits. Two more options are available in case the number of vehicles is increased. The first of the latter is having one vehicle perform two burns and another performing three burns. The second is having both vehicles perform a small burn followed by two larger ones. In Figure 8.2, the paths taken by these three concepts are illustrated.

Table 8.1: Trade off deployment vehicle number and burn procedure

	1 Vehicle with 5 burns	2 Vehicle with 2+3 burns	2 Vehicles with 2.5+2.5 burns
Mass Vehicle 1 [kg]	5,722	1,970	2,274
Mass Vehicle 2 [kg]	N/A	2,885	2,274
<b>Overall Mass[kg]</b>	5,722	4,957	4,548

Table 8.1 shows the total masses computed at an early stage of the final design for the three concepts mentioned above. As it can be seen in Table 8.1, the overall mass is highest in the first option and smallest in the third. In addition

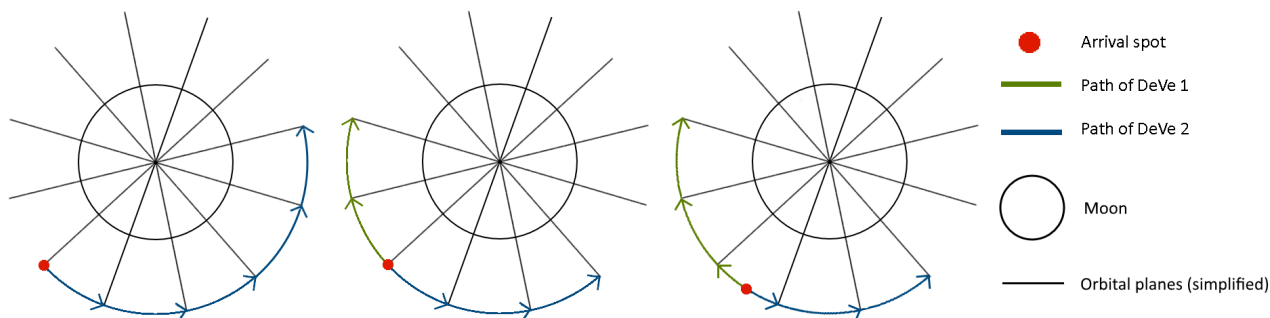


Figure 8.2: An illustration showing the differences in the burns performed by the three deployment vehicle concepts

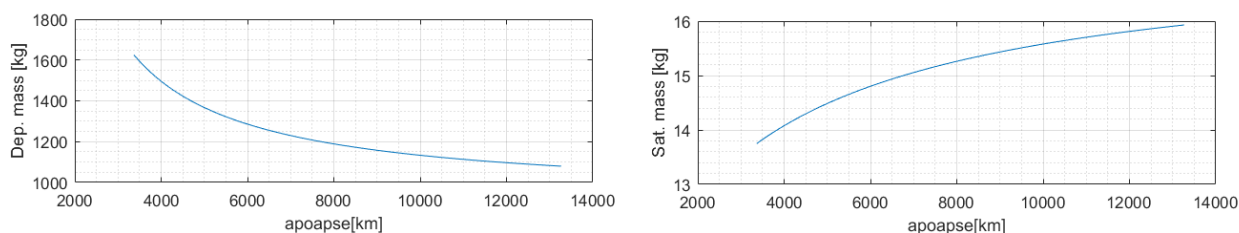


Figure 8.3: A figure illustrating the effect of increasing the apoapsis of the deployment orbit on both DeVe mass and Nsat mass

to a lower mass, the risk of losing a large number of satellites (e.g. due to engine failure of the DeVe) is lower. For these reasons, the third concept was chosen.

An additional decision that was made in the design process was the eccentricity of the deployment orbit. A higher eccentricity decreases the  $\Delta V$  of the RAAN change manoeuvre, however an additional manoeuvre has to be performed by the satellites in order to circularise the orbit. This will have two effects on the deployment vehicle. On the one hand, the propellant mass of the DeVe is decreased but the payload mass increases. The overall effect can be seen in Figure 8.3. The graph on the left shows the total weight of the deployment vehicle (including the propellant and payload) as a function of the apoapsis altitude of the deployment orbit. It can be seen that the mass decreases quite drastically for low altitudes and then flattens out for higher values.

On the right hand side of Figure 8.3, the corresponding satellite mass can be seen. However, there are multiple other factors to consider apart from the mass. The addition of a circularisation manoeuvre increases the complexity of the mission and requirements on the satellite. Furthermore, the available space is highly limited. Increasing the propellant mass of the satellite by 1 kg will also increase the volume of the propellant tank by approximately 1 litre or 1u of a cubesat. This is deemed not acceptable as a large space is already taken up by the antennas and the fuel for orbit maintenance.

## 8.2. ELECTRICAL POWER SYSTEM

The Nsat deployment vehicle has a mission duration in the order of 10 days, Figure 6.3 has to be visited again to determine which types of EPS types are relevant for this vehicle design. With a power requirement below 1 kW and the short mission duration, primary batteries, fuel cells and a photovoltaic system with secondary battery are considered. Due to their non-sustainable nature, RTG's are not considered. From the average power requirement from Table 8.3, the energy required can be calculated for 10 days as follows:  $E = P \cdot t = 79.13 \cdot (10 \cdot 24) = 1.90 \times 10^4$  Wh. Multiplying the energy and power requirements with the specific energy and power, the EPS mass can be estimated. Since the solar panels generate energy throughout the 10 days, the battery is sized on the maximum peak power requirement for one hour, which is equal to 602 Wh. It can be clearly seen that the solar photovoltaic option has the least mass by far making it the chosen EPS type.

Table 8.2: Network deployment vehicle EPS type trade-off.

	W/kg	Wh/kg	EPS mass [kg]
Primary battery	0	800	23.7
Fuel cell	275	2.78	6,837
Solar photovoltaic	100	125	5.61

Table 8.3: Nsat deployment vehicle power requirements.

	Power [W]	Time [s]
Full activity	148.3	-
Average power requirement	79.13	continuous
Maximum peak	602	-
180° slew manoeuvre case	532	222
Deployment case	218.3	80

With the power requirements and the EPS type known, the solar panel and secondary battery can be sized. The area

per side available is  $1.60 \cdot 0.83 = 1.328\text{m}^2$ . Due to the large area available, CIGS thin film from Table 6.1 is chosen as solar cell type for its low specific mass.

The network deployment vehicle is assumed to always be in sunlight. The inclination is assumed to be on average  $40^\circ$  since the vehicle attitude is constrained by the communication subsystem. Solar panel degradation is not considered due to the short lifetime (a degradation in the order of 0.01 % can be expected). In Table 8.4 the EPS parameters can be seen. The average power requirement has increased with 4.67 W, which is based on a battery recharge after the  $180^\circ$  slew manoeuvre within 12 hours with an overall efficiency of 65 % [11, p. 643]. Due to the constant exposure to sunlight, the temperature is assumed to be 320 K on average for the solar panels.

Table 8.4: Network satellite EPS design input parameters for the calculation tool.

Average power requirement	83.8	W
Max impulse energy	32.8	Wh
Battery DOD	0.9	-
Absorptance	0.90	-
Temperature	320	K
Solar angle of incidence	40	degrees
Average efficiency	0.85	-

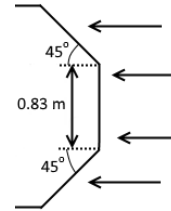


Figure 8.4: Network deployment vehicle solar incidence in worst-case.

The resulting solar panels have to generate 185.9 W, which translates in an area of  $1.609\text{m}^2$ . Due to the octagonal configuration, the minimum area that receives sunlight, is calculated as follows:  $A_{sol} = (1 + 2 \cdot \cos(45)) \cdot (0.83 \cdot 1.60) = 3.21\text{m}^2$  as can be seen in Figure 8.4. Each side of the octagon will contain  $0.805\text{m}^2$  to satisfy the power requirement, which comes down to a total area of  $6.44\text{m}^2$ .

The battery capacity is determined to be 36.4 Wh with a maximum depth of discharge of 90 %. From Table 6.4 the Saft VL 6P is chosen, which is designed for high discharging currents occurring during the peak power cases<sup>6</sup>. Only two battery cells are required, however it is decided to go with three cells for redundancy. This also reduces the discharge current from 73.9 A to 49.3 A since the cells are connected in series, resulting in a higher voltage and a lower current for the same power delivery. Using three cells, the total battery capacity is 66 Wh.

Lastly, a margin for cables and components is added. This margin is higher than for the satellites due to the fact that wire mass increases with increasing current. For 50 A this is about  $200\text{gm}^{-1}$  [11, p. 658]. Therefore the margin has doubled with respect to the satellite design to 30 % of the EPS mass. The mass breakdown of the final EPS is displayed in Table 8.5. The EPS block diagram can be found in Figure 8.5

Table 8.5: Mass breakdown of the network deployment vehicle EPS.

	Amount	Total mass [kg]
Solar panels	$6.44\text{m}^2$	5.80 [33]
VL 6P battery	3	1.02
	Subtotal	6.82
Cable and component margin	30%	2.05
	<b>Total subsystem mass</b>	<b>8.86</b>

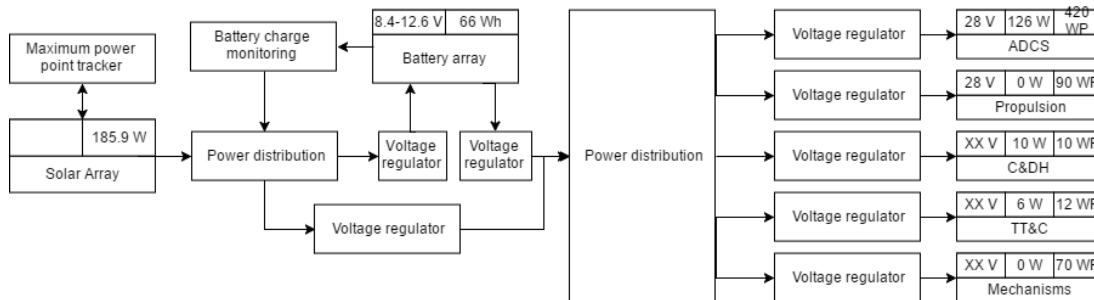


Figure 8.5: Network deployment vehicle electrical block diagram showing the power flow between different components.

### 8.3. COMMAND AND DATA HANDLING

In Table 6.8, the number of sensors of the network deployment vehicle are given and their generated data rate is calculated. The output of this is that the deployment vehicle is going to generate housekeeping data at  $3,856\text{bits}^{-1}$ . Again using as the worst case scenario 24 hours of storage time the resulting storage capacity is less than 400 Mbit. In terms of processing speed the deployment vehicle can use the same CPU that will be chosen for the Nsat. This is because the number and the nature of functions on the Nsat and the deployment vehicle are comparable.

### 8.4. TRACKING AND ORBIT DETERMINATION

The communication between the ground station and the deployment vehicles only consists of housekeeping data and commands. This was assumed to require a data rate of  $100\text{kbits}^{-1}$ . The link budget tool described in the Midterm

report was used to size the antenna system necessary to send this data rate down to ground stations on Earth [1, p.26]. The chosen tracking method will be one-way Doppler as it can provide the required accuracy with no need for extra equipment, as explained in section 6.4. It was found that using a 20 cm parabolic dish and 12 W of power, the link can be closed with a minimum margin of 3 dB.

## 8.5. PROPULSION

The engine of the network deployment vehicle needs to perform five burns of varying  $\Delta V$  requirements. The first burn (insertion into an inclined lunar orbit) is the largest with a velocity increment of  $1,358 \text{ ms}^{-1}$ . As the assumption was made that the burn is impulsive, the burn time should be small compared to the orbital period.

As a high thrust is required for a small burn time, the options of electrical propulsion (well below 1 N) as well as cold gas (from 0.05 N to 200 N) are not feasible [17, p.644]. The remaining options which have a high thrust are solid propellant, mono-propellant engines and bi-propellant engines. Additionally, the specific impulse should be high to reduce the amount of propellant. Solid rocket engines were not considered due to their inability to fire the engine multiple times and the difficulty in controlling the reaction. Of the two remaining options, bi-propellant engines generally have a higher specific impulse ( $\sim 300 \text{ s}$ ) than solid propellants ( $\sim 230 \text{ s}$ ) and as such were chosen for this design.

A multitude of options are available for the choice of fuel and oxidiser, however, many combinations require cryogenic cooling of the oxidiser and the fuel. Keeping more than a ton of fuel at cryogenic temperatures ( $\sim 90 \text{ K}$ ) for multiple days is not feasible due to the increase in system complexity. Therefore, all cryogenic propellants were excluded. A common fuel for bi-propellant engines is hydrazine and its derivatives with nitrogen tetroxide as oxidiser.

In order to find a suitable engine for the main propulsion units, bi-propellant engines produced by Aerojet Rocket-dyne<sup>1</sup> were considered.

The R-40B rocket engine<sup>1</sup> can produce a thrust of 4 kN with a specific impulse of 293 s and a mass of 6.8 kg. Due to its high thrust capability, flight proven design and high  $I_{sp}$  for a MMH based engine, this product is chosen for the main propulsion system of the network deployment vehicle. The pumps and leads necessary to complete the propulsion system are assumed to be just as heavy as engine itself, leading to a mass of the propulsion system of 20.4 kg. The amount of propellant was determined using the tool described in the Midterm report [1, p.31]. For the burns shown in Table 8.6, the amount of propellant necessary is 1,130.2 kg.

Table 8.6:  $\Delta V$  of burns to be performed by both network deployment vehicles (in  $\text{ms}^{-1}$ )

Insertion Burn	30° RAAN Change	60° RAAN Change (x2)	EOL Burn
1358.43	472.88	927.44	116

## 8.6. ADCS DESIGN

Table 8.7: Trade off between insertion burn stabilisation methods

	Performance	Dry Mass	Wet Mass	Power	Risk
Control Moment Gyroscopes	Very precise torque control. Can also be used for performing attitude control	2 · 40 kg	0 kg	80 W	Low
Control thrusters	Control thrusters are otherwise not necessary	8 · 1 kg + 2kg	40 kg	70 W	Medium
Thrust vector control	Alleviates build up of angular momentum Precise orbit insertion possible. Requires high frequency attitude determination	7 kg	0 kg	20-40 W	Medium

The main driver for the ADCS of the deployment vehicle is keeping the vehicle stable during the insertion burn. This is due to the fact that the vehicle only spends approximately 200 hours in space (and therefore disturbance torques have only little time to build up). Most of that time is spent far away from both the Earth, its atmosphere and magnetic field, and the Moon. The biggest disturbing force is then the solar radiation pressure, which can be computed using Equation 8.1 [11, p.571].

$$T_s = \frac{\Phi}{c} A_s (1 + q) (cp_s - cm) \cos(\varphi) \quad (8.1)$$

Where  $T_s$  is the solar radiation pressure torque in Nm,  $\Phi$  is the solar constant adjusted for the distance in  $\text{Wm}^{-2}$ ,  $c$  is the speed of light in  $\text{ms}^{-1}$ ,  $A_s$  is the sunlit surface area in  $\text{m}^2$ ,  $q$  is the unit-less reflectance factor,  $\varphi$  is the solar incidence angle from the Sun in  $^\circ$ , and  $cp_s$  and  $cm$  are the centre of pressure and mass in meter, respectively.

Assuming that the average received radiation pressure is  $1,366 \text{ Wm}^{-2}$  (value in LEO), the illuminated area is the diameter times height ( $2.17 \cdot 2.5 = 5.425 \text{ m}^2$ ), the reflectance is 0.07 (averaged between black paint and solar panels), the moment arm is 0.5 m, a solar incidence angle of  $0^\circ$  the resulting solar radiation pressure torque is equal to  $1.32 \times 10^{-5} \text{ Nm}$ . Over the entire duration of approximately 200 hours, this will build up to a total of  $1.32 \cdot 10^{-5} \cdot 200 \cdot 3600 = 9.52 \text{ Nms}$ . Assuming a safety margin of 50 %, the necessary amount of momentum storage is  $14.28 \text{ Nms}$ . This value is achievable by reaction wheels such as the HR-14 produced by Honeywell, which can store up to  $75 \text{ Nms}$ .<sup>2</sup> Therefore, no momentum dumping is necessary.

<sup>1</sup><http://www.rocket.com/propulsion-systems/bipropellant-rockets> Accessed on 26.06.2017

<sup>2</sup>[ftp://apollo.ssl.berkeley.edu/pub/Pointing\\_Studies/Hardware/Honeywell%20Reaction%20Wheels.pdf](ftp://apollo.ssl.berkeley.edu/pub/Pointing_Studies/Hardware/Honeywell%20Reaction%20Wheels.pdf) Accessed on 22.06.17

Four of the HR-14 reaction wheels are chosen in a pyramid configuration to achieve a redundant attitude control system.

To estimate the disturbing torque from the main engine, the known thrust of the engine is applied at a certain offset from the centre of mass. This offset can be caused by an uncertainty in the position of the c.g. or an angle offset of the thrust vector. A centre of gravity offset of 1 cm is assumed together and an angle offset of  $\theta = 0.5^\circ$ . This leads to an additional  $h/2 \cdot \sin(\theta) \approx 0.01m$  offset from the centre of gravity. Therefore, the effective moment arm is 2 cm for this analysis [11, p.574]. The thrust of the engine is known to be 4 kN, causing a torque of 80 Nm over the entire burn duration of approximately 480 s, resulting in the build up of 38,400 Nms of angular momentum. In order to keep the vehicle stable during that time, both the torque created by the thruster needs to be countered or eliminated and the resulting angular momentum needs to be dumped. Four options are considered to solve this problem, shown in Table 8.7.

- **Spin stabilisation:** To keep the body stable, the gyroscopic effect can be utilised to keep the maximum angular deviation within an acceptable region.
- **Control Moment Gyroscopes:** The only actuator (except for thrusters) to be able to counter the resulting torque from the main engine are control moment gyroscopes.
- **Control Thrusters:** The other actuation method is using thrusters to counter the resulting torque of the main engine. These thrusters need to provide a minimum thrust of  $80Nm/2.5m = 32N$  in the best case.
- **Thrust vector control:** If the thrust vector can be pointed, the torque and build up of angular momentum can be avoided all together.

These options were traded off based on their general performance, the dry mass and wet mass that is added to the vehicle, the required power and their risk.

Pure spin stabilisation was considered but deemed unfeasible due to the high burn time ( $\sim 480$  s) and the high torque generated by the engine (80 Nm). This would lead to unreasonably high rotation rates required to keep the precession within a few degrees from the axis of rotation. Control moment gyroscopes would be able to counter the torque created by the thruster, however they do not have enough momentum storage for the entire burn. Therefore they could only be used together with thrusters. Furthermore, they need the largest amount of power to perform their function.

The thrusters themselves lose out in terms of performance, as eight thrusters to counter those torques may not be necessary at all, as the build up of disturbance torque momentum can be stored in the reaction wheels.

It can be seen that the thrust vector control wins in terms of mass. Additionally, it virtually eliminates any build up of angular momentum and allows for precise orbit insertion. Thrust vector control is chosen due to its good performance, its small mass and low power.

During the deployment of one layer of satellites, the deployment vehicle is expected to rotate at  $45^\circ s^{-1}$ . The reaction wheels are not sufficient to accelerate it to that speed, as the angular momentum storage required is equal to  $I \cdot \omega$ , where  $I$  is the mass moment of inertia and  $\omega$  is the rotational speed. The mass moment of inertia can be estimated as  $I = m \cdot r_{gyro}$ , where  $m$  is the total mass of the vehicle in kg and  $r_{gyro}$  is the radius of gyration in m. Assuming a radius of gyration that is 90% of half the diameter (which is a conservative estimate given that most mass is concentrated in the centre), the mass moment of inertia can be estimated to be  $1827.28 \cdot 0.9765^2 = 1,742.4 \text{ kgm}^2$ .

With the given rotational speed, the necessary angular momentum is  $1742.4 \cdot \pi/4 = 1,368.4 \text{ Nms}$ . This is beyond the capabilities of reaction wheels. Therefore, thrusters are necessary to speed up and slow down.

A set of 4 thrusters is installed to perform this acceleration. As time is not a constraining factor, the thrust of each can be small and therefore the 4 N monopropellant thruster MR-111C, produced by Aerojet Rocketdyne, is selected. With this thruster, the burntime is equal to  $t_b = I \cdot \omega / F_t / d$ , where  $F_t$  is the thrust in N and  $d$  is the distance between a thruster pair in m. When the thrusters are placed on the outside skin, this leads to a burn time of  $t_b = 157.6$  s. For the selected thruster, which has a mass flow  $\dot{m} = 1.5 \text{ gs}^{-1}$ , the required fuel to perform this manoeuvre three times with consequent braking is  $m_f = 6 \cdot t_b \cdot 2\dot{m} = 2.84 \text{ kg}$

To be able to send to Earth from the Moon, a pointing accuracy of the ADCS needs to be at least equal to the angular resolution of the Earth as seen from the Moon. This is expressed as  $\arctan(R_E/a_M)$ , where  $R_E$  is the Earth radius and  $a_M$  is the semi major axis of the lunar orbit. This angular size is equal to  $0.94^\circ$ . The sensor accuracy needs to be better than this value. Additionally, the attitude needs to be updated often during the burn manoeuvres, as the thrust vector control requires almost constant knowledge of the attitude ( $\sim 40 \text{ Hz}$ ) [48, p.17].

For these reasons, the selected sensors are 3 star trackers, 6 Sun sensors and 4 gyroscopes. The star and Sun sensors provide redundant 3 axis determination and the gyroscopes are used to acquire the attitude in between the other sensor measurements. The components of the ADCS can be seen in Table 8.8.

Table 8.8: ADCS Components of the Network Deployment Vehicle

Type	Company	Amount	Mass	Power	Accuracy	Control Force/Torque
Sun Sensor	New Space Systems <sup>3</sup>	6	35 g	0.0375 W	0.1°	-
Star Sensor	TY-Space <sup>4</sup>	3	0.245 kg	1 W	7 arcsec	-
Ring Laser Gyroscope	Optolink <sup>5</sup>	4	0.9 kg	6 W	0.01 °h <sup>-1</sup>	-
Reaction wheels	Honeywell <sup>6</sup>	4	7.5 kg	22 W to 105 W	-	4 Nm
Attitude thrusters	Aerojet Rocketdyne <sup>7</sup>	4	0.33 kg	8.25 W	-	4 N

## 8.7. THERMAL DESIGN

The thermal behaviour of the deployment vehicle was investigated using the thermal tool described in the midterm report [1, p.22]. Due to time constraints, a more in depth analysis was not possible.

The outside of the deployment vehicle is covered to a large extent with solar panels with an absorptance of 0.90 and an emittance of 0.80. The remaining outside skin will be covered with anodised aluminium which has an absorptance and emittance of 0.77 and 0.84, respectively (see subsection 6.7.1). As the calculation tool used is greatly simplified, the side panels need to have a uniform absorptance and emittance. Therefore, the values for solar panels and aluminium are averaged based on their areas, according to Equation 8.2.

$$\bar{x} = \frac{A_2 x_1 + A_1 x_2}{A_1 + A_2} \quad (8.2)$$

Where  $x$  is the value of interest (in this case either absorptance or emittance),  $A_1$  is the area occupied by the first material and  $x_1$  the value of interest of the material (the same goes for  $A_2$  and  $x_2$ ).

As the solar panels take up an area of  $0.805 \text{ m}^2$  of one side panel (with an area of  $3.21 \text{ m}^2$ ), the resulting absorptance value of the side panels is 0.8026 and the corresponding emittance is 0.8300.

Furthermore, the octagonal shape of the vehicle is approximated by a cuboid, where the top face has the area of the octagon and the side faces have the minimum and maximum projected area of the octagonal prism sides.

This analysis results in the graphs seen in Figure 8.6. The left side shows the temperature in the hottest possible case

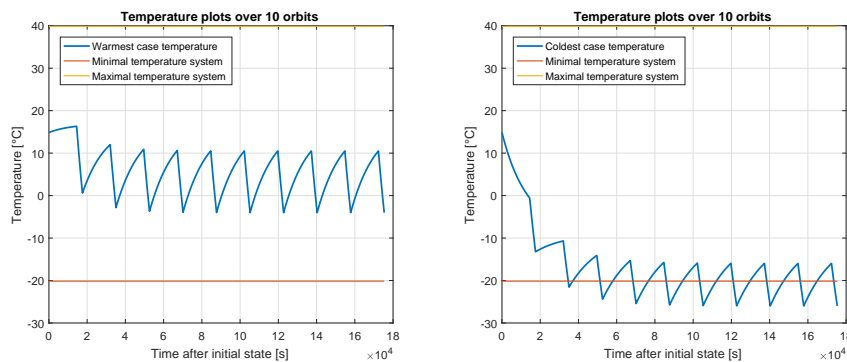


Figure 8.6: The temperatures of the deployment vehicle when in orbit around the Moon. The left side shows the hottest case, the right side the coldest case. The vehicle faces are covered with anodised aluminium and solar panels.

(i.e. the greatest area is illuminated by all incoming radiation sources). The right hand side shows the coldest case, which is defined as the solar radiation hitting only the large side of the vehicle and the remaining radiation (from the Moon and Earth) hitting the smallest side.

As can be seen in the graph, these situations lead to unacceptable temperatures in the spacecraft. To remedy this, the coatings of the vehicle were iterated to find a good solution. The best one (with the coatings specified in Table 6.17) is a black coating on the sides with the solar panels (leading to absorptance and emittance values of 0.9375 and 0.80000) and anodised aluminium on the top and bottom faces. This combination leads to the graphs seen in Figure 8.7. The temperatures are now within the temperature bounds specified in requirement IRIS-NDEVE-THRM-01. Nonetheless, a more in depth simulation of the internal temperature distribution should be performed.

## 8.8. STRUCTURES DESIGN

In this section, the structural sizing is presented followed by the calculation of the centre of gravity for the preliminary placement of subsystems.

### 8.8.1. STRUCTURAL SIZING

The outside structure has an octagonal shape. This is due to the number of satellites which need to be deployed into a single orbital plane. To minimise the risk of collision, the satellites should be launched away from a single point. This will give rise to a structure which is not very compact, however, the payload bay of the falcon 9 launcher is more than large enough to contain two of the current deployment vehicles which have outer dimensions of 2.5 m height by 2.17 m width along the diagonal. The usable payload bay of the Falcon 9 is 4.6 m in diameter and 6.7 m in height (before the structure tapers towards the top) [8]

The structure of the deployment vehicle consists of four main elements: the fuel tanks, the main column to which the satellites are mounted, the outer skin and additional supporting structure. The main column was sized with the tool described in the mid term report [1, p.29]. Additionally, the guiding rails holding the satellites were sized using the updated tool (see section 14.5).

<sup>3</sup>[www.cubesatshop.com/wp-content/uploads/2016/06/NewSpace-Sun-Sensor.pdf](http://www.cubesatshop.com/wp-content/uploads/2016/06/NewSpace-Sun-Sensor.pdf) Accessed 03.07.17

<sup>4</sup>[www.ty-space.com/en/uploadfile/files/201611/201611041520381229.pdf](http://www.ty-space.com/en/uploadfile/files/201611/201611041520381229.pdf) Accessed 03.07.17

<sup>5</sup>[www.optolink.ru/ftpgetfile.php?id=74](http://www.optolink.ru/ftpgetfile.php?id=74) Accessed 03.07.17

<sup>6</sup><https://www.honeywell.com/industries/aerospace-and-defense> Accessed 03.07.17

<sup>7</sup>[www.rocket.com/files/aerocket/documents/Capabilities/PDFs/Monopropellant%20Data%20Sheets.pdf](http://www.rocket.com/files/aerocket/documents/Capabilities/PDFs/Monopropellant%20Data%20Sheets.pdf) Accessed 03.07.17

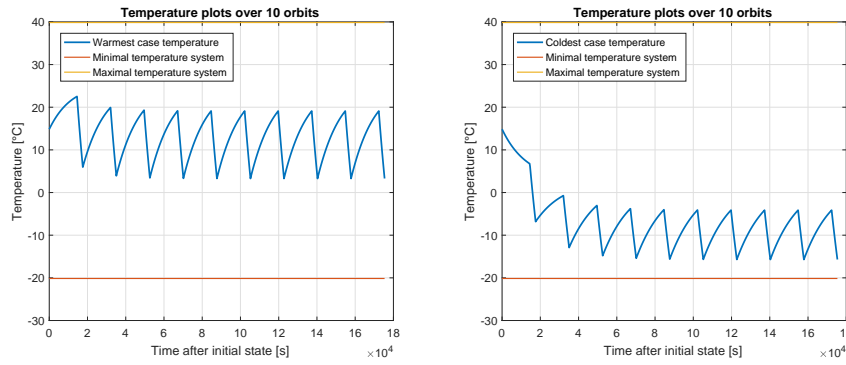


Figure 8.7: The temperatures of the deployment vehicle when in orbit around the Moon. The left side shows the hottest case, the right side the coldest case. The vehicle faces are covered with black paint, anodised aluminium and solar panels.

Given the loading conditions of the Falcon 9 launcher (6g in longitudinal direction and 2 g in lateral direction as specified in the "User's Guide") the dimensions were found for the main column and the guiding rails, shown in Table 8.9 and Table 8.10, respectively.

Table 8.9: Deployment Vehicle main column parameters

Diameter	Height	Thickness	Max. occurring Von Mises Stress	Nat. Freq.
0.76 m	0.9 m	1 mm	217.3 MPa	48 Hz long., 77 Hz lat.

Table 8.10: Deployment Vehicle guiding rails parameters

Length	Width / Height	Thickness	Max. occurring Von Mises Stress	Ratio Max. compressive load/ buckling load
0.5 m	3 cm	1 mm	18.7 MPa	0.898

The fuel tank was sized using the tank sizing tool described in the midterm report, based on the amount of propellant necessary (1,130.2 kg) [1, p.20]. As a bi-propellant engine was selected, a tank for the oxidiser, fuel as well as pressurant is needed. First, these three separate tanks were considered. However, it proved to be difficult to connect them to the remaining structure due to their size. Instead, a decision was made to integrate the oxidiser and fuel into a combined tank, while keeping the pressurant separate. This large tank is integrated into the rest of the main structure and has a direct connection to the column in the upper part. It was sized using the propellant tank tool [1, p.21]. The resulting mass of the tank mass is equal to 57.18 kg. This is very close to the weight of a commercially available combined fuel and oxidiser tank for MMH/MON-3 with a similar total propellant volume (52 kg for 1,200 L)<sup>8</sup>. The skin contributes to the overall weight, but carries no significant loads. A skin thickness of 0.5 mm was assumed to be enough to withstand the launch loads under their own weight and the subsystems mounted to the outside skin. For an octagonal outside skin with length along the diagonal of 2.17 m and height of 2.5 m, made from aluminium 7075-T6, the skin weight is equal to 19.8 kg. The remaining structural members (e.g. to connect skin and main column) were not sized due to time constraints. It is assumed that their weight is equal to the weight of the skin itself.

### 8.8.2. CENTRE OF GRAVITY CALCULATION

The vehicle is mostly symmetric about the longitudinal axis passing through the centre of the octagon. The offset on the vertical axis however can be significant. Equation 8.3 is used to calculate the centre of gravity position

$$\bar{x} = \frac{\sum_{i=0}^N x_i \cdot m_i}{\sum_{i=0}^N m_i} \tag{8.3}$$

Where  $\bar{x}$  is the location of the cg in m,  $N$  is the total number of separate elements, and  $x_i$  and  $m_i$  are the cg and mass of one element in m and kg, respectively. In this case, the elements considered were the payload, the propellant plus tank, the structure, the outer skin and all remaining subsystems. It is assumed that both the payload, the column and the subsystems located inside the column all have their cg in the geometric centre of the column itself. Furthermore, it is assumed that cg of the skin and supporting structure is located in the geometric centre of the octagon.

Two cases are considered: the first is a fully loaded deployment vehicle and the second is a completely empty vehicle (no propellant or payload). In the first case, the the cg can be found to be at 1.15 m from the bottom of the vehicle. In the second case, the location is found at 1.66 m from the bottom. These differences will not have an effect on the stability of the spacecraft, as the main thruster is capable of thrust vector control and the performance of the reaction wheels is sufficient to turn the vehicle (with only slightly longer time to turn).

<sup>8</sup>[www.space-propulsion.com/brochures/propellant-tanks/1207lt-mon-mmh-tank-ost-24-0.pdf](http://www.space-propulsion.com/brochures/propellant-tanks/1207lt-mon-mmh-tank-ost-24-0.pdf) Accessed on 22.06.2017

### 8.9. DEPLOYMENT PROCEDURE DESIGN

The main objective of the deployment procedure is to avoid collisions of the satellites after deployment as well as keeping the velocity increment that is delivered to each satellite small.

Three measures have been taken to reduce the change of collision to a minimum: The satellites are deployed away from a central point instead of next to each other; The DeVe is rotating during the deployment to introduce asymmetry in the direction of the  $\Delta V$ 's delivered to the satellites; There is a time delay between successive deployments. Furthermore, the plane in which the satellites are deployed is a key factor.

Figures 8.8a to 8.8d, show the relative distances of the satellites to one another over one orbital period. In Figure 8.8a, neither a rotation rate nor a delay time in the deployment were used. It can be seen that although the maximum distance is relatively large, the distances are almost perfectly symmetric around the time  $t = 2.4$  hours, which is half an orbital period. This indicates that the satellites will come very close to each other again after one orbital period. The minimum distance the satellites encounter is only 15 m.

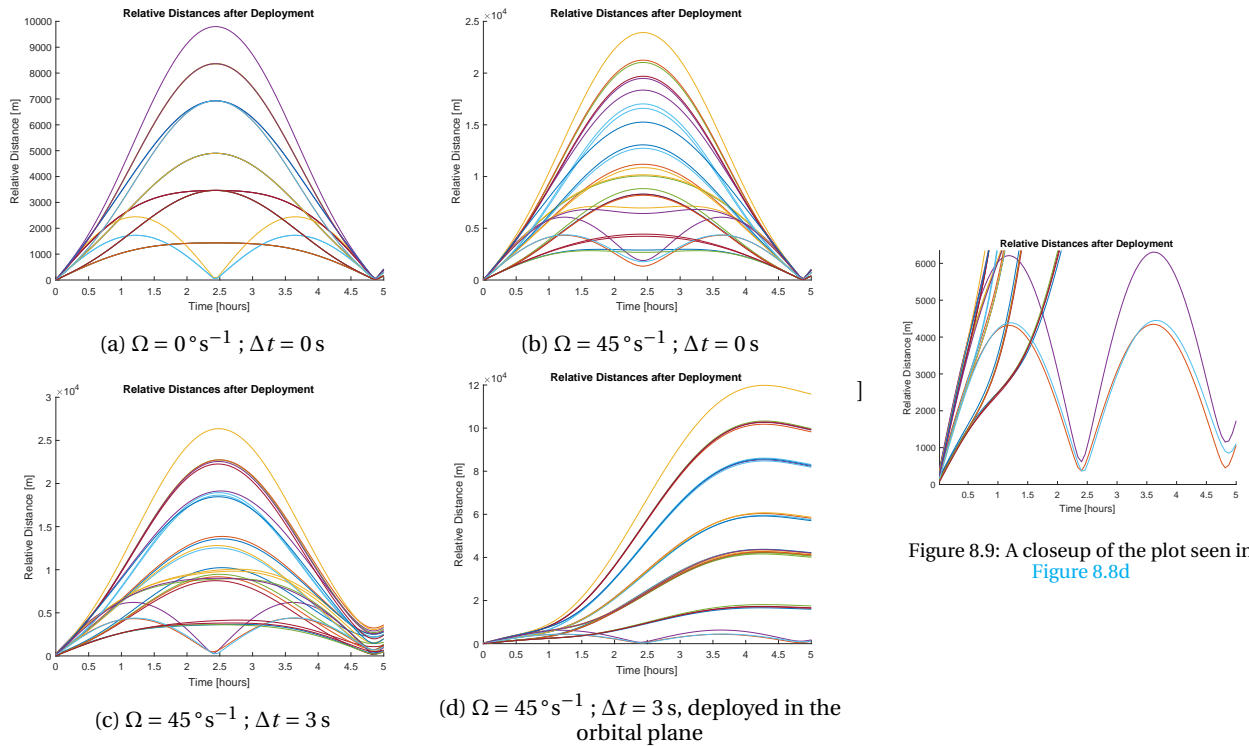


Figure 8.8: Relative distances of all satellites to each other, plotted over one orbital period.  $\Omega$  is the rotational speed,  $\Delta t$  is the timing offset

In Figure 8.8b, the deployment vehicles was given an initial rotation rate of  $\Omega = 45^\circ \text{s}^{-1}$ , but all satellites are deployed at once. As expected, the satellite distances are no longer perfectly symmetric. It is notable, that now the minimum distance after half an orbital period ( $\sim 1,100 \text{ m}$ ) is much higher than before. However, they come very close again after half and one orbital period. The minimum distance encountered with these settings increases to 27 m which is still very small.

Introducing a delay time in the deployment sequence results in the graph of Figure 8.8c. The minimum distance after half an orbital period increased again to approximately 300 m. This can be explained by the fact, that the initial increase in distance came from slight differences in the orbital period of the individual satellite orbits. With an unfortunate delay sequence, this advantage is reduced again. Additionally, the satellites are spaced much further apart in this case, as can be seen in the high range of distances after one orbital period. In the previous plots, the relative distances approach a common value, whereas in this case, the range of values are much larger. The minimum distance in this case is  $\sim 150 \text{ m}$ .

The distances could even be increased more by deploying the satellites such that their individual orbital periods have the highest difference for a given  $\Delta V$ . This can be achieved by deploying the satellites within the orbital as opposed to in a perpendicular plane. This change resulted in Figure 8.8d. The distances are much higher than in the previous conditions. The satellites also do not converge again to a single location after one orbital period. In Figure 8.9, a closeup of Figure 8.8d can be seen. Now, the minimum distance is in fact after after half an orbital period as opposed to a full orbit. In this case, the value of the distance at the closest point is  $\sim 360 \text{ m}$ .

Due to the fact that the fourth strategy shows the best behaviour overall and the highest minimum distance, it will be used to deploy the satellites. Additionally, it should be investigated, whether the deployment sequence can be used to get the satellites into the correct phasing and thereby reducing the amount of  $\Delta V$  required.

Figure 8.9: A closeup of the plot seen in Figure 8.8d

## RELAY DEPLOYMENT VEHICLE DESIGN

The RDeVe is designed in this chapter.

### 9.1. RELAY DEPLOYMENT VEHICLE LAYOUT

The relay deployment vehicle consists of an adaptor ring which acts as the main structural element to which the remaining subsystems are mounted. The configuration can be seen in Figure 9.1. In the figure, the x-axis is defined in the direction of the movement, y defined along the axis of the solar panels and z is going into the plane to complete a right handed system.

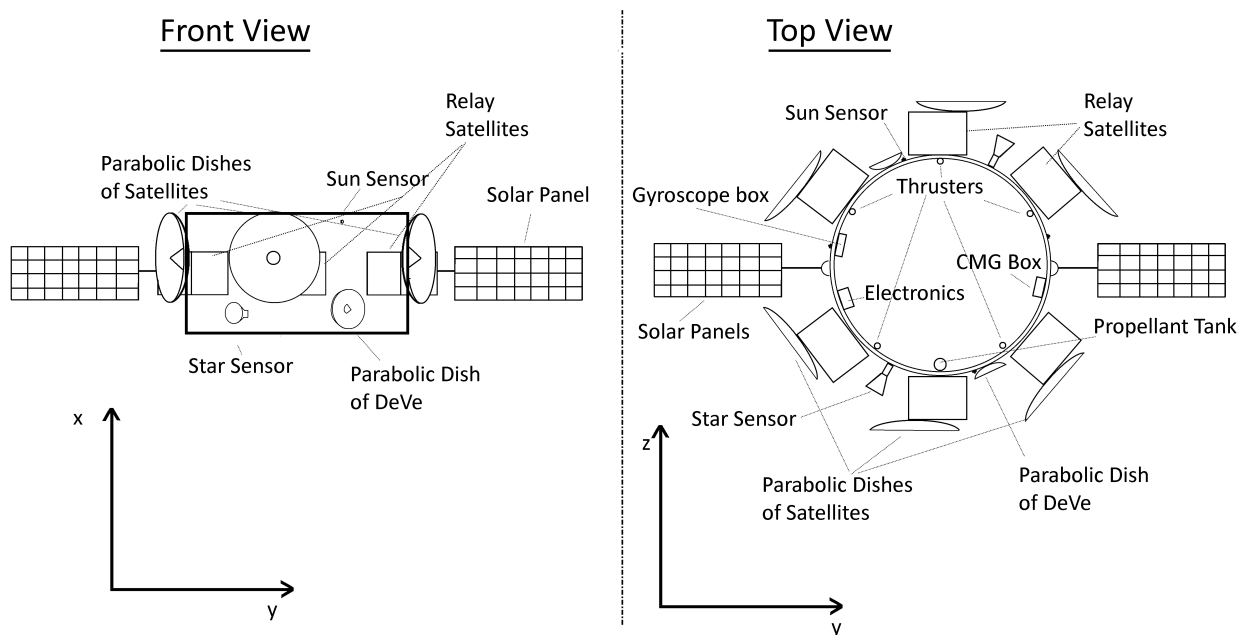


Figure 9.1: Sketch of the Relay Deployment Vehicle Layout.

### 9.2. ELECTRICAL POWER SYSTEM

The Rsat deployment vehicle is active for about 200 days with a power requirement below 1 kW. From Figure 6.3 it is chosen to use solar cells with a secondary battery for peak loads. In Figure 9.1 it can be seen that dedicated outward pointing solar arrays are necessary due to a lack of space on the vehicle itself. Since this panel has to be deployed, its area is minimised and as such, the Azur space 3G30C triple junction solar cell is used from Table 6.2 due to its high efficiency.

The power requirements are shown in Table 9.1

Table 9.1: Rsat deployment vehicle general power requirements.

	Power [W]	Time [s]
Full activity	80.12	-
Average power requirement	76.30	continuous
Maximum peak	210.6	-
Momentum dumping case	95.50	60
Trust manoeuvre case	126	500

Table 9.2: Rsat deployment vehicle EPS design input parameters for the calculation tool.

Average power requirement	80.23	W
Max impulse energy	17.5	Wh
Battery DOD	0.9	-
Degradation	3%	year <sup>-1</sup>
Absorptance	0.91	-
Temperature	320	K
Solar angle of incidence	0	degrees
Average efficiency	0.85	-

The maximum impulse energy is determined from the thrust manoeuvre. Since after this manoeuvre no large power consuming activities are planned, the recovery time is set to 10 days. This increases the average power requirement

by 0.11 W. Since the relay deployment vehicle is assumed to be in sunlight constantly, the temperature reaches an equilibrium and will remain constant at 320 K. The solar panels can have a solar angle of incidence of  $0^\circ$  since the attitude of the satellite is not completely constrained. The rear of the relay deployment vehicle has to point towards Earth for communication, which means that rotation around one axis is possible. Furthermore, the solar panels have one rotational degree of freedom around their longitudinal axis with a rotation mechanism.

These inputs result in a solar array consisting of 51 solar cells. The final configuration has 54 solar cells divided over two solar arrays with a total area of  $0.390 \text{ m}^2$ . Both solar arrays consists of three panels of nine solar cells each. A similar hinging system is used as for the satellites and a rod is present to connect the solar array to the vehicle. The mass of this rod is estimated using CATIA to be 200 g.

The battery capacity requirement for a depth of discharge of 90 % is 19.4 Wh. Identical to the situation of the Nsat deployment vehicle, Saft VL 6P batteries are chosen to ensure no battery damage due to high discharge amperage. For redundancy, two Saft VL 6P cells are chosen with each a capacity of 22 Wh. They are connected in series, which results in a maximum discharge current of 17.5 A and a maximum cable mass of  $50 \text{ gm}^{-1}$ . To include this, a cable margin of 20 % is included. The mass breakdown and electrical block diagram of the relay deployment vehicle can be seen in Table 9.3 and Figure 9.2 respectively.

Table 9.3: Mass breakdown of the relay deployment vehicle EPS

	Amount	Total mass [kg]
Solar panel	0.195 $\text{m}^2$	0.76 [33]
Hinges	7	0.07
Rod	1	0.200
Rotational mechanism	1	0.250
Solar array mass	2	2.56
VL 6P battery	2	0.68
<b>Subtotal</b>	<b>1</b>	<b>3.24</b>
Cable and component margin	20%	0.65
<b>Total subsystem mass</b>		<b>3.89</b>

Table 9.4: Structural dimensions of deployment ring.

Entity	Value
Outer radius	0.6 m
Height	1.0 m
Thickness	5 mm
Mass	52.7 kg

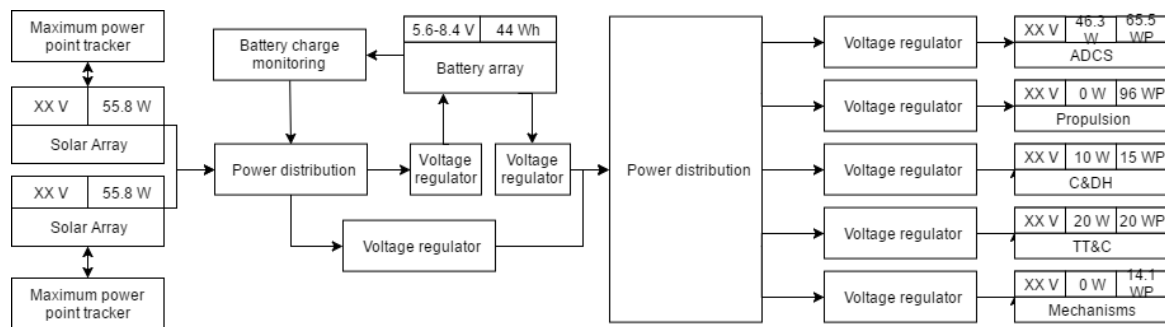


Figure 9.2: Relay deployment vehicle electrical block diagram showing the power flow between different components.

### 9.3. COMMAND AND DATA HANDLING

Using Table 6.8 and the assumption used in sizing the storage capacity of the network deployment vehicle, the relay deployment vehicle will need an estimated capacity of less than 400 Mbit. For the CPU it can use the same one that will be used in the NDeVe as similar functions will be performed.

### 9.4. TRACKING AND ORBIT DETERMINATION

Similar to the NDeVe, the communication for the RDeVe consists only of housekeeping data and commands. Again, a 20 cm parabolic antenna is selected. However, due to the greater distance to the Lagrange point, the power requirement for communication is 20 W in this case. With these parameters, the link closes with a 3 dB margin. Tracking will be performed using one-way Doppler as explained in section 6.4.

For redundancy, two dishes will be mounted on the ring.

### 9.5. PROPULSION DESIGN

The propulsion system in this case only needs to perform two burns. The first ( $\Delta V = 146.82 \text{ m s}^{-1}$ ) inserts the vehicle into a halo orbit around the Sun-Earth Lagrange point, where the ring will deploy the satellites. The second burn ( $\Delta V \approx 10 \text{ m s}^{-1}$ ) then takes the RDeVe out of the halo orbit and into a heliocentric orbit. Although the first manoeuvre is comparatively small in terms of the  $\Delta V$  requirement, it needs to be precise, as already a small deviation causes the vehicle to leave the intended halo orbit. Due to this, a set of multiple thrusters with throttling capability have been selected. They can be mounted on the inside of the the ring and therefore not interfere with the remaining subsystems. A minimum of three is required to be able to account for an uncertainty in the centre of gravity. For redundancy, four thrusters will be used to reduce the risk of engine failure.

Mono-propellant engines are selected in this case for two reasons: First, the increased propellant mass is not an issue as the burn is very small. Even a factor of two increase in the propellant mass would only be a few kilograms of

additional weight. Second, a mono-propellant engine is simpler and therefore more reliable. As the overall risk of the trajectory is quite high, choosing a simpler system that reduces the chance of failure is considered a priority. In order to perform the insertion burn even when a thruster unit fails, a certain minimum number of engines is required. Five is the smallest number, where even if any of the thrusters fails, there is still a region in which the centre of gravity can be positioned (see Figure 9.3) and the vehicle remain stable. This is obviously not the case for only three thrusters (if one of them fails, the centre of gravity has to be on the line between the thrusters). This can be remedied by using four thrusters. Now, if one specific thruster fails, the centre of gravity can still be located in the triangle formed by the three remaining thrusters. However, since it can not be known, which specific thruster might fail, the c.g. needs to be at the intersection area of the 4 possible failure regions. However, this region consists only of a single point, the centre of the original rectangle, shown in black in Figure 9.3. Since the c.g. can only be placed at this single point and still remain stable if any thruster fails, four thrusters are not sufficient to ensure stability during the insertion.

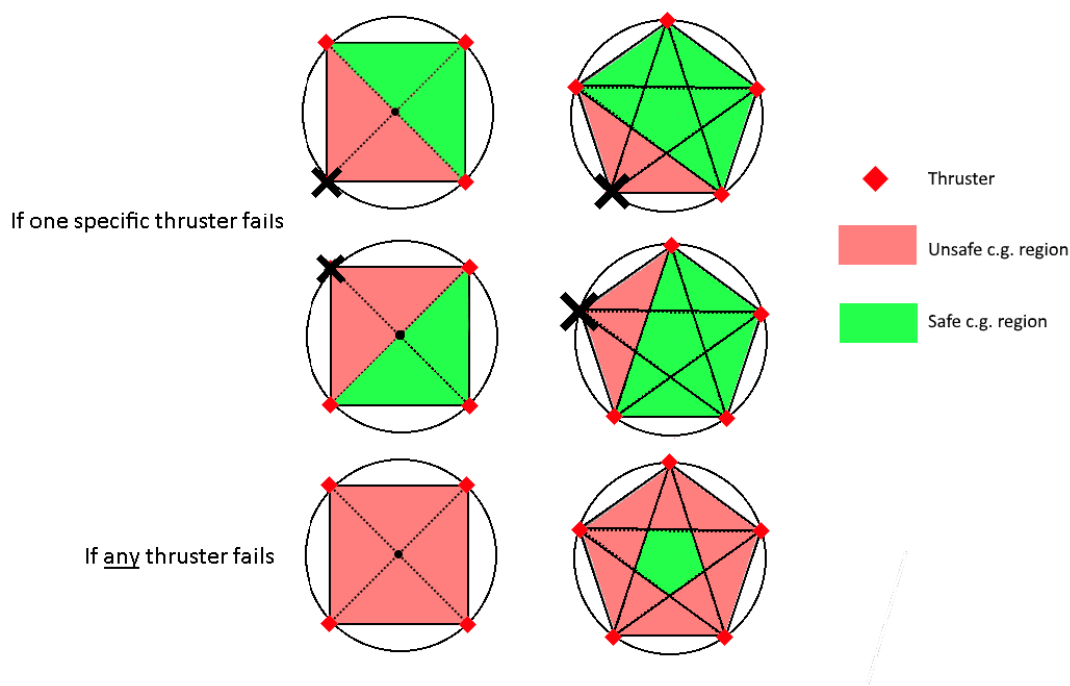


Figure 9.3: An illustration showing the stable c.g. regions with a 4 and 5 thruster configuration.

For five thrusters, the situation is different. All areas of stability in case of thruster failure overlap in the green region in the centre. For this reasons, five thrusters are chosen. Five engines of the type MR-106L, produced by Aerojet Rocketdyne<sup>1</sup> were chosen for the propulsion system. They produce a nominal thrust of 22 N with a maximum and minimum of 34 N and 10 N, respectively

Using these thrusters, the amount of propellant needed can be calculated. Since the trajectory needs to be precise, a certain margin is taken on the  $\Delta V$  that the engines have to deliver. It is assumed that the actual burn (due to corrections, etc) will take 50 % more  $\Delta V$  than initially assumed. The engines therefore need to give a  $220.23 \text{ m s}^{-1}$  velocity increment. Using the previously developed tool, the amount of propellant was determined to be 20.8 kg.

## 9.6. ADCS DESIGN

The ADCS of the RDeVe is mainly constrained by the pointing requirement of the communication subsystem. Furthermore, a precise attitude determination is necessary to minimise the error in the insertion burn. Due to the choice of having multiple thrusters, no additional attitude control during the insertion burn is necessary.

To meet the requirement of  $0.24^\circ$  pointing accuracy, two star sensors were selected. Furthermore, six Sun sensors are chosen to be able to see the Sun in any attitude. In case the star sensors are not able to determine the attitude (e.g. if bright object is in their view), the sun sensors are not sufficient to determine the attitude. Therefore, a redundant set of 4 ring laser gyroscopes is selected to compliment them. The components and their specifications can be found in Table 9.5.

Adding all powers and masses together, the total power consumed is 46.3 W and the total mass is 11.1 kg.

<sup>1</sup>[www.rocket.com/files/aerojet/documents/Capabilities/PDFs/Monopropellant/20Data/20Sheets.pdf](http://www.rocket.com/files/aerojet/documents/Capabilities/PDFs/Monopropellant/20Data/20Sheets.pdf) Accessed on 24.06.17

<sup>2</sup>[www.cubesatshop.com/wp-content/uploads/2016/06/NewSpace-Sun-Sensor.pdf](http://www.cubesatshop.com/wp-content/uploads/2016/06/NewSpace-Sun-Sensor.pdf) Accessed 03.07.17

<sup>3</sup>[https://www.sst-us.com/downloads/datasheets/rigel--star-tracker-datasheet\\_v112](https://www.sst-us.com/downloads/datasheets/rigel--star-tracker-datasheet_v112) Accessed 03.07.17

<sup>4</sup>[www.optolink.ru/ftpgetfile.php?id=74](http://www.optolink.ru/ftpgetfile.php?id=74) Accessed 03.07.17

<sup>5</sup><https://www.honeybeerobotics.com/wp-content/uploads/2014/03/Honeybee-Robotics-Microsat-CMGs.pdf> Accessed 03.07.17

<sup>6</sup>[www.rocket.com/files/aerojet/documents/Capabilities/PDFs/Monopropellant/20Data/20Sheets.pdf](http://www.rocket.com/files/aerojet/documents/Capabilities/PDFs/Monopropellant/20Data/20Sheets.pdf) Accessed 03.07.17

Table 9.5: ACDS components of the Relay Deployment Vehicle

Type	Company	Amount	Mass	Power	Accuracy	Control Force/Torque
Sun Sensor	New Space Systems <sup>2</sup>	6	35 g	0.0375 W	0.1°	-
Star Sensor	Surrey Satellite Technology <sup>3</sup>	2	2.6 kg	7 W	3 arcsec	-
Ring Laser Gyroscope	Optolink <sup>4</sup>	4	0.9 kg	6 W	0.01 °h <sup>-1</sup>	-
Control Moment Gyroscope	Honeybee <sup>5</sup>	4	0.775 kg	1.5 W to 2 W	-	0.112 N m
Attitude thrusters	Aerojet Rocketdyne <sup>6</sup>	12	0.33 kg	8.25 W	-	4 N

## 9.7. THERMAL DESIGN

Due to time constraints, no thermal analysis of the deployment ring was performed.

## 9.8. STRUCTURE DESIGN

In this section, both the structural sizing as well as the centre of gravity calculation are considered.

### 9.8.1. STRUCTURAL SIZING

The relay satellites are delivered into their halo orbit by means of a low-energy transfer. However, since only six Rsats are required, there is no need for a sophisticated deployment vehicle, contrary to that which carries the network satellites. Deployment rings have shown to be an effective solution to carry multiple payloads in one launcher and will be employed to transport the Rsats. A ring-design is evaluated in the structural analysis for the deployment using section 14.6. Boundaries are applied such that its minimal height is 0.40 m which corresponds to the height of the mounted Rsat, and its maximum height is bound to 3.0 m corresponding to the maximum allowable payload height of the chosen launcher (PSLV) [9, p. 4]. In a similar fashion, the outer diameter is capped off at 2.0 m [9, p. 4] to consider the dimensions of the PSLV's fairing. Furthermore, the thickness has a minimum bound of 1.0 mm to take into account manufacturing limitations and 100 mm to prevent the mass from exceeding the payload capacity of the launcher. The specified launch loads of the PSLV are 1.1 g in the lateral direction and 6.5 g in the longitudinal one [9, p. 6]. The vibrations the payload will experience by the launcher are directly taken from [9, p. 6]. The mass of the relay satellites is rounded up to 32.0 kg to consider a conservative case. The material selection is Aluminium 6061-T6<sup>7</sup>. Finally, for all calculations a safety margin of 1.5 is applied.

The ring proves to be extremely resilient due to its short and stubby nature. So much so that it can easily be altered to accommodate the dimensions of the relay satellites and other subsystems. Hence the overall dimensions of the ring are dependent on the size of the relay satellites and their subsystems, and the subsystems of the deployment vehicle. This is concurrently updated with the design of the Rsats and the final structural dimensions of the ring are shown in Table 9.4. Variable thickness is not needed to accommodate the additional loads from the Rsats.

The relay satellites will be deployed instantly using explosive bolts. Therefore, no tailored mechanism is needed. This release from the interface ring typically gives very high but short shock-loads and do not drive the structural design, especially when considering relatively small satellites (from discussion with Jasper Bouwmeester).

### 9.8.2. CENTRE OF GRAVITY CALCULATION

Many parts of the vehicle have a symmetry around the centre of the ring (e.g. the ring itself, the solar panels, the satellites mounted to the ring, etc). The only parts which change the cg away from the ring centre are: the propellant tank, control moment gyroscopes, electronics and sensor gyroscopes. The combined weight of those systems is 37.66 kg and consists of the 6.7 kg for the sensor and control moment gyroscopes, 32.85 kg for the propellant tank including content, and 5.85 kg for the electronics and computers. To minimise their impact, they are placed on opposite sides, which leaves a surplus of 20.3 kg on the side of the propellant tank. Therefore, the offset from the centre is equal to  $\bar{x} = r \cdot m/m_{total} = 0.6 \cdot 20.3/315.77 = 0.0385$  m.

The other case worth considering is after the satellites have been deployed and the most of the propellant has been expelled. This leads to a surplus of 12.55 kg on the side of electronics and gyroscopes. Using the same relation as above, the offset from the centre is now  $\bar{x} = 0.6 \cdot 12.55/97.79 = 0.077$  m. This is well within the range given by the thruster configuration to stay stable during the burns. In terms of vertical distance, is it assumed that this does not affect the stability of the vehicle.

<sup>7</sup><http://asm.matweb.com/search/SpecificMaterial.asp?bassnum=ma6061t6> Accessed on 26.06.17

## TECHNICAL BUDGET MANAGEMENT

This chapter gives an overview of the development of the technical budgets over time.

### 10.1. CONCURRENT ENGINEERING STRATEGY

For managing the technical budgets, a shared spreadsheet is used that is accessible to everyone within Project IRIS and is updated real-time. The midterm technical budget is used as a basis which is expanded to the final budgeting tool [1, p. 46]. For each budget a breakdown is made including all the relevant components for that particular budget. This budget tool has been a great help in allowing concurrent engineering between the different groups (constellation, trajectory, deployment and satellite) and also within the groups between different disciplines. Any time someone needs a value, it is present in the budget tool. If this value later turns out to be outdated, the new value can be found in the budget overview, which can be used for the following iteration. This process prevents anyone from having to wait on others for new values while concurrently improving the design.

### 10.2. ENGINEERING BUDGETS

In this section a budget overview is given of the budgets that have been actively used in the design process for multiple iterations. Each of the budgets contains a graph which shows the progression of the budget towards the final value. The total value of each iteration has been normalised to the value of the final iteration for easier comparison. Even though it is more conventional to normalise towards the initial value to see the deviation from the initial budget, here the opposite is done. The reason for this is the fact that not every vehicle has the same amount of iterations and some vehicles have been re-purposed multiple times throughout the design process, making the earlier estimation no longer relevant to the vehicle design. Note that only the initial, midterm and final iteration of the budgets have been locked simultaneously, the other iterations might have been completed at different times and are not comparable across budgets (e.g. iteration 2 of the mass budget and power budget could be in a different design phase between midterm and final).

#### 10.2.1. MASS BUDGET

Throughout the design process, the mass budget has been the most important engineering budget and has seen the most iterations. The initial mass budget was obtained from statistics from SME [11, p. 422]. In the midterm these estimates have been mostly replaced with values calculated by preliminary tools, after which the calculations are improved in detail and finalised in the final. Throughout the project, the initial budget is used as a means to check which subsystems are over budget. For this, a contingency factor of 0.85 is used as is determined in previous reports [5, p. 29]. This means that the budget available for each subsystem is reduced with 15 % to increase the likelihood of staying within budget. The mass progression throughout the project can be seen in [Figure 10.1](#) and the final mass breakdown for each vehicle is shown in [Table 10.1](#).

The initial mass of the Nsat was based on CubeSat statistics for an eight unit CubeSat with 1.33 kg/unit dry mass and was estimated to be 10.64 kg or 13.51 kg including wet mass [49] where one unit is a cube with 10 cm sides. The Nsat final mass of 15.04 kg has increased with 9 % with respect to the midterm budget mostly due to the increasing power requirements on the satellite.

For the NDeVe, statistics are (partially) used up to the first iteration, after which an increase in mass can be seen after the initial mass calculations are done. These calculations have been optimised, which resulted in a gradual reduction of the vehicle mass with a final mass of 1,393 kg, which is only 83.5 % of the midterm budget.

The Rsat was initially assumed to be a 30 unit satellite, which appeared to be oversized in the midterm leading to significant mass reduction. The mass reduction in the first iteration has been caused by a design change of no longer using a single relay satellite but three and finally six Rsats to ensure connection between Rsat and Nsat, reducing communication requirements.

The RDeVe went through quite some drastic changes. In the midterm, it was thought to be a 2,400 kg vehicle, which for the first iteration got reduced to only a structural ring to keep the Rsats together. This was deemed insufficient when the number of Rsats increased from one and a spare to six active satellites. In the second iteration, the RDeVe was a deployment vehicle with all the subsystems in place. These values have been optimised in the following iterations, reducing the mass to its final value, 129.0 kg.

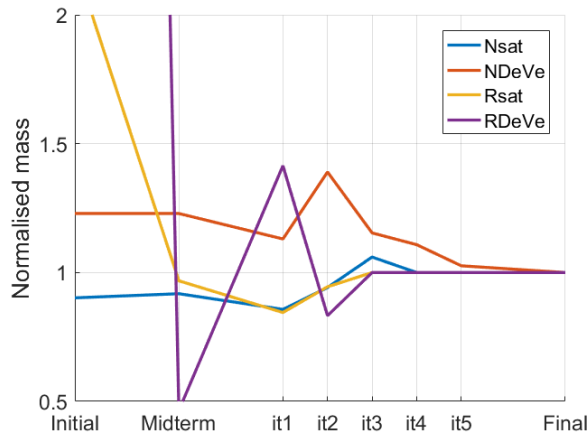


Figure 10.1: Mass budget progression of the different vehicles throughout the project phases.

### 10.2.2. POWER BUDGET

The setup of the power budget is identical to the mass budget. An initial budget was set up using SMAD statistics [17, p.424]. These values are replaced by initial calculated values in the midterm which are optimised in the final. For each power budget a margin of 1.3 is used in the EPS design. This is done to ensure enough power is available, even when power requirements, degradation or power losses are higher than expected. The power budget flow is shown in Figure 10.2 and the power breakdown per vehicle with the duty cycles (dc) is given in Table 10.2 for each subsystem. The power subsystem is not included in this table since its power consumption is processed in the EPS efficiency and not included in the budget. Note that the values given in Table 10.2 are the power requirements under normal operations, which does not include peak power requirements. Since some elements only consume power in certain situations, they use on average 0 W. The peak power consumption can be found in the electrical block diagrams for each vehicle.

The Nsat power fluctuations have been quite large from 15 W to 95 W. This is caused by the communication subsystem which takes up most of the power budget.

The NDeVe and RDeVe power requirement has first been determined at the first iteration, after which only the ADCS power increased, which takes up 80 % of the total power budget.

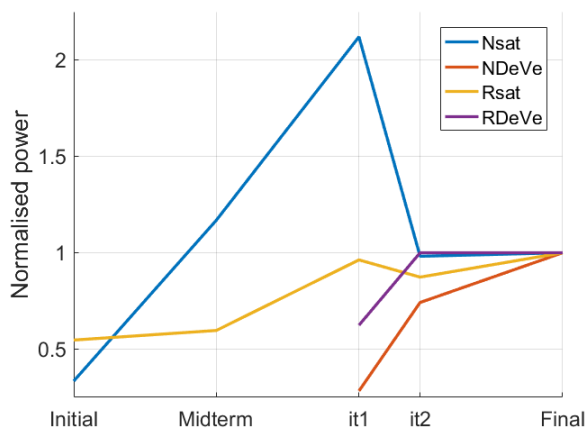


Figure 10.2: Power budget progression of the different vehicles throughout the project phases.

### 10.2.3. $\Delta V$ BUDGET

For the  $\Delta V$  budget, no initial budget was created since this was considered too mission specific. The  $\Delta V$  budget progression is shown in Figure 10.3 and the values are displayed in Table 10.3.

The Nsat and Rsat  $\Delta V$  is mainly influenced by recalculating the required orbit maintenance  $\Delta V$  with increasing detail and optimising the end of life manoeuvre. Note that for the Nsat tank sizing an additional  $15 \text{ m s}^{-1}$   $\Delta V$  as a margin. For the Rsat, insertion in the final halo orbit is done by the satellite in the first and final iteration, in the second iteration, this was taken care of by the Rsat deployment vehicle, causing a large difference between the iterations. The NDeVe  $\Delta V$  increased during the first iteration due to an ascending node change recalculation. This, together with the orbit injection is optimised to reduce the  $\Delta V$  again. The RDeVe was only a structural ring during the midterm which did not provide any  $\Delta V$ . In the first iteration the required orbit injection and end of life manoeuvre  $\Delta V$  are calculated, after which the orbit injection is recalculated and optimised.

Table 10.1: Mass budget overview of the designed vehicles [kg].

	Nsat	NDeVe	Rsat	RDeVe
Electrical Power	3.87	8.86	7.71	3.89
Structure	2	95.87	5.62	52.7
ADCS	2.89	35.54	4	11.08
Propulsion	0.66	85.72	1.18	7.7
Thermal	0.1	22.28	1	12.67
Payload (TT&C)	3.1	6	4.5	3.9
C&DH	1	9.02	2	5.85
<b>Dry mass</b>	<b>13.63</b>	<b>263.3</b>	<b>26.01</b>	<b>66.16</b>
Propellant	1.42	1130	5.12	31.2
<b>Total mass</b>	<b>14.97</b>	<b>1393</b>	<b>31.13</b>	<b>129.0</b>
Midterm budget	13.74	1669	30.13	2400
<b>Final/midterm</b>	<b>109%</b>	<b>83.5%</b>	<b>103%</b>	<b>5.38%</b>

Table 10.2: Power budget overview of the designed vehicles [W]

	Nsat		NDeVe		Rsat		RDeVe	
	P	dc	P	dc	P	dc	P	dc
ADCS	4	1	126	0.5	24	1	46.3	1
Propulsion	0	-	0	-	0	-	0	-
Thermal	0	-	0	-	5	-	0	-
C&DH	1	1	10	1	2	1	10	1
TT&C	36	0.65	12	0.5	68	1	20	1
Solar panel mechanism	3.82	0	0	0	3.82	0	3.82	0
Total	44.8	0.636	148	0.534	103	0.914	80.1	0.952
<b>Average</b>	<b>28.5</b>		<b>79.1</b>		<b>94.0</b>		<b>76.3</b>	

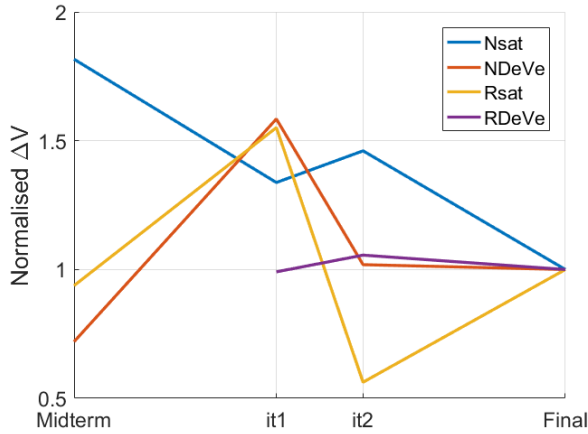


Figure 10.3:  $\Delta V$  budget progression for the different vehicles throughout the project phases.

Table 10.3:  $\Delta V$  budget overview of the designed vehicles [ $\text{ms}^{-1}$ ].

	Nsat	NDeVe	Rsat	RDeVe
Injection	0	1358	50	146.8
Inclination change	-	0	-	-
RAAN change	-	2328	-	-
Phasing	35.01	-	-	-
Maintenance	75	-	250	0
End of life	105	116	100	10
<b>Total</b>	<b>215.0</b>	<b>3802</b>	<b>400</b>	<b>156.82</b>

	Network transfer vehicle	Relay transfer vehicle
Lift off	9616	9616
First burn	3060	3185
Second burn	done by NDeVe	done by RDeVe
<b>Total</b>	<b>12676</b>	<b>12801</b>

### 10.3. ADMINISTRATIVE BUDGETS

The administrative budgets are set up to give an overview of certain values at an easily accessible, central location. From these budgets, requirements for subsystems can be obtained to ensure that the final design can be validated against these requirements. In Table 10.4, Table 10.5 and Table 10.6 an overview of the volume, thermal and datarate budgets are given respectively. The volume budget consists of the volumes assigned to each subsystem within the satellite and therefore consists of preliminary numbers. Each subsystem has to remain within this volume. From the volume budget overview it can be seen that the Nsat internal volume is completely distributed over the subsystems, whereas for the Rsat, only 47 % of the volume is used. This means that this satellite could be decreased in size, which corresponds with the fact that the initial mass estimate of this satellite based on its volume, is also too high. However, this is not considered with the current design due to the fact that the external surface area is completely in use. From the thermal budget it can be seen that the most significant external influence is, as expected, the Sun radiation. Furthermore, the EPS and payload dissipate a variable amount of power as heat under different circumstances. An overview of the thermal budget for the Rsat can be found in section 7.7. The data rate budget shows an overview of the up and downlink between the vehicles and Earth.

Table 10.4: Volume budget overview for the satellites [ $\text{cm}^3$ ].

	Nsat	Rsat
Power	1500	1500
Structure	1000	2000
ADCS	1000	1000
Propulsion	1000	1000
Thermal	500	500
Payload	2000	3000
C&DH	1000	2000
Propellant	4000	6000
<b>Total</b>	<b>12000</b>	<b>17000</b>
Available	12000	36000

Table 10.5: Thermal budget overview for the two satellites.

	Temperature range for both sats [ $^{\circ}\text{C}$ ]	Received power Nsat [W]	Received power Rsat [W]
Power	0/45	3-8	9-24
ADCS	-15/55	2	6
Propulsion	-	0	0
Thermal	-	0	0
Payload	-20/50	10	10
C&DH	-55/125	6	6
Propellant	-22/100	0	0
Sun radiation	-	122.4	243.2
Moon infra-red	-	7.26	0.094
Earth infra-red	-	0.006	0.014
<b>Total</b>		<b>150.7-155.7</b>	<b>274.3-289.3</b>

The reliability, pointing accuracy and surface budgets are not used while they have been present in the budget tool. The reliability budget requires a lot of details of the final design to be known and even then statistical data has to be found or generated on products used to complete the budget. For this project, this is considered too in depth and general satellite failure statistics are used. The pointing accuracy budget also requires a lot of details about the final satellite assembly. It includes various sources of pointing errors such as attitude determination errors, uncertainties in target location. Without using the budget, the ADCS is designed to have an accuracy that fulfils the requirements is deemed sufficient at this stage of the design. The surface budget turned out to be obsolete since an external satellite layout has been designed without too many conflicts and without usage of this budget. Lastly, in Table 10.7 the total launch masses are shown for the network and relay launch.

Table 10.6: Datarate budget throughout constellation [ $\text{kbits}^{-1}$ ].

Moon-Nsat	Uplink	500
	Downlink	100
Nsat-Nsat	Uplink	1000
	Downlink	1000
Nsat-Rsat	Uplink	500
	Downlink	100
Rsat-Earth	Uplink	2000
	Downlink	500

Table 10.7: Total mass overview for both launches.

	Individual mass	Amount	Total mass [kg]
Nsat	14.97	48	719
NDeVe	1393	2	2787
Network launch mass			3506
Maximum launch mass (TMI)			4020
Rsat	31.13	6	187
RDeVe	86.89	1	86.9
Relay launch mass			274
Maximum launch mass (TMI)			1350



To test the robustness of the design, a sensitivity analysis is performed. This is done by varying certain system parameters and the influence of these changes on the design within the different design disciplines. Since the project contains a lot of elements focus is on the main system elements. The effect of changes to the design of only some subsystems is discussed.

### 11.1. CHANGING NETWORK ORBITAL ALTITUDE

The orbital altitude is increased and decreased to analyse the impact on the existing design.

#### 11.1.1. TRAJECTORY DESIGN

The design of the direct transfer trajectory is mainly dependent on the required orbital height of the Nsats. A change in this orbital height causes a change in optimal trajectory. This change can be best quantified in the required  $\Delta V_{22}$  to insert in the orbit. This  $\Delta V_{22}$  is optimised for each orbital height using the method described in section 3.2. The results are displayed in Figure 11.1. It is concluded that with decreasing orbital altitude, the required  $\Delta V_{22}$  increases due to the fact that the orbital velocity is higher for a lower orbital radius.

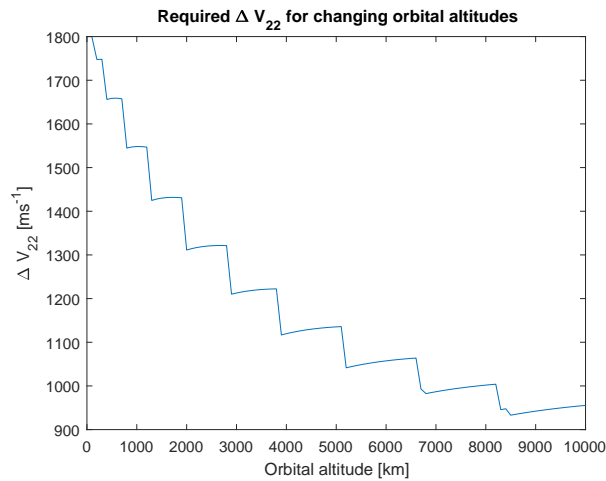


Figure 11.1: Change of required  $\Delta V_{22}$  for orbit insertion with changing orbital altitude.

### 11.1.2. CONSTELLATION DESIGN

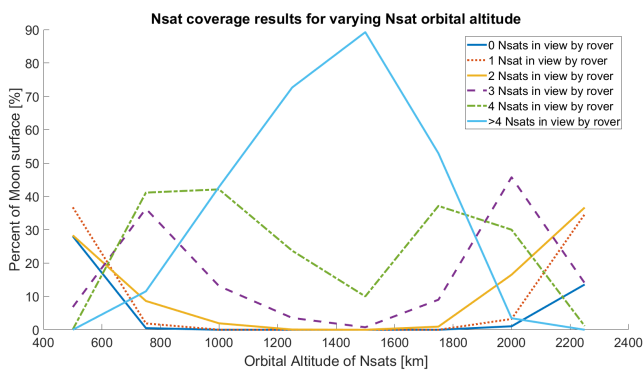


Figure 11.2: Nsat coverage results for altitudes between 500 km and 2,250 km

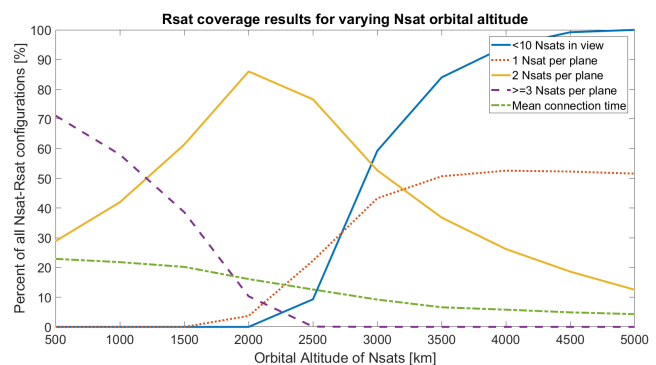


Figure 11.3: Rsat coverage results for altitudes between 500 km and 5,000 km

In Figure 11.2 the coverage results for Nsats are given for the varying orbital altitude. It is seen that the orbital altitude used in the design 1,629 km is close to the optimum, which is around 1,500 km. At the optimum, most of

the time most of the Nsats are in view. This graph also shows that the orbital altitude can be varied from 1,000 km to 1,750 km without influencing the Nsat design in terms of the communication subsystem, as within this range there are always at least two Nsats in view or even more. The lower bound for the orbital altitude is determined by the Nsat antenna field of view angles, which need to become bigger with decreasing altitude. While for altitudes above the design altitude the antenna field of view angles can become smaller, but in order to close the link budget the power for transmission needs to be increased.

In Figure 11.3 the coverage results of the Nsats by the Rsats are given for the varying orbital altitude. For Rsat coverage it is seen that for orbital altitudes from 500 km to 2,000 km, the Rsat communications subsystem does not need to change since there are still 10 Nsats in view meaning that 10 rovers can be serviced. However it is seen that above 1,500 km the chance that there is a plane with only one Nsat in view becomes bigger. Thus the communication design should change if higher orbital altitudes are chosen. The mean connection time between an Nsat and the Rsats decreases with increasing Nsat altitude.

The chosen orbits are frozen orbits, this means that deviating from the current design results in more  $\Delta V$  required for orbit maintenance. However in general it can be said that the best orbital lifetimes for lunar orbits are around 1,500 km [15, p. 163] and deviating from this results in more required orbit maintenance.

### 11.1.3. SATELLITE DESIGN

From constellation design, it is seen that the current design does not need major changes between an orbital altitude of 500 km and 2,000 km. For altitudes below the bounds, the Antenna FOV needs to become bigger. However the maximum FOV of the currently selected phased arrays is  $120^\circ$  which is not sufficient, making the current design unfeasible. On top of that, for lower altitudes the eclipse over Sun ratio would increase, which could lead to bigger solar panels and batteries and thus a heavier Nsat. It could also be that due to the lower altitudes, the communication distance is smaller, decreasing the space loss, which leads to less power required for closing the link budget. For higher altitudes, the power needed to close the link budget would need to become bigger, again increasing the mass of the solar panels and batteries. For different altitudes, the required  $\Delta V$  for orbit maintenance increases, along with the amount of required propellant. This would lead to heavier and larger Nsats.

It can be said that the Nsat design is dependent on its orbital altitude according to the reasons mentioned above. It is seen that these relations are very intertwined so it is not possible, with the remaining resources, to properly quantify the effect of these changes on the actual satellite design.

### 11.1.4. DEPLOYMENT VEHICLE DESIGN

The RDeVe is entirely unaffected by this design change as the number of Rsats is the same as it already disconnects from the satellites at the Sun-Earth Lagrange point.

The NDeVe, on the other hand, is more strongly affected as a change in the number of satellites could cause an entire redesign of the structure of the deployment vehicle. Changes in the mass of the satellites would also increase the structural weight of the deployment vehicle, albeit only a small increase. Furthermore, a change in the altitude changes the  $\Delta V$  required to perform RAAN changes. The higher the altitude, the less propellant required. A smaller propellant tank can be taken or the existing one filled to a lesser extent. On the other hand, for lower altitude the propellant increases. At 500 km orbital altitude, this mass increase is equal to 263.71 kg, a percentual increase of 23.3%. This does not prompt a redesign of the tank, which can handle an additional 32% propellant. Furthermore, the total launch mass for such an altitude is 4,032.96 kg which is slightly higher than the launch capabilities of the Falcon 9 to Mars. It can be assumed that the transfer to the Moon is still possible, even with the increased mass.

### 11.1.5. CONCLUSION

For the trajectory, higher altitudes result in lower required  $\Delta V$ , while for constellation this results in worse Nsat-Rsat visibility. It is also seen that for altitude variation between 1,000 km and 1,750 km, the Nsat design does not need to be altered except for the propellant tanks which will need to become bigger.

## 11.2. CHANGING THE NUMBER OF ROVERS TO BE SERVICED

Increasing the amount of rovers could be interesting for future development of the constellation. Here the impact on the system of changing the number of rovers is analysed.

### 11.2.1. TRAJECTORY DESIGN

The designs of both the direct transfer and the low-energy transfer is not significantly influenced by the number of rovers to be serviced. The only thing which can be influenced is a changing orbital altitude, of which the effect has already been described. Furthermore, if the mass is increased significantly another launcher might be needed. However, this does not significantly change the design of the trajectories themselves, as long as the thrusters of the launcher, deployment vehicles and satellites are capable of performing the designed manoeuvres.

### 11.2.2. CONSTELLATION DESIGN

In Figure 11.4 the Rsat coverage results for varying number of rovers is shown. Note that the system can of course handle less than ten rovers. It can be seen that the current constellation can even handle 11 rovers simultaneously, but when the number of rovers is increased, an increasing percent of the time there are less Nsats in view of the Rsat than there are rovers. To cope with more rovers, there are multiple ways in which the design would need to change. (1) By increasing the number of Nsats per orbit, there are more Nsats in view of the Rsats. (2) By letting the Nsats be able to send two rover signals at the same time.

Each Rsat can handle three Nsat signals at the same time. As there are six Nsats, the Rsats can sustain 18 signals at the same time. Thus, by trading redundancy in Rsat data rates, the available data rates for rovers can be increased.

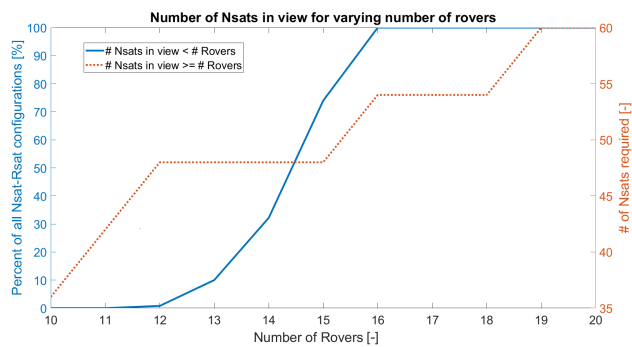


Figure 11.4: Rsat coverage results for number of rovers between 10 and 20

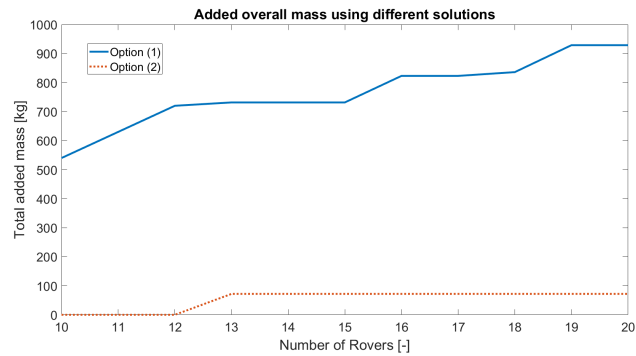


Figure 11.5: Added overall mass of Nsats for number of rovers between 10 and 20

### 11.2.3. SATELLITE DESIGN

First, the impact on the Nsat is analysed for the different proposed options.

(1) This means that the Nsats will need to be able to handle higher data-rates through the inter-Nsat network. Per extra signal, a maximum of 3 watt is required. Per Watt that is required extra, the extra mass required by the solar panels and batteries is roughly  $80 \text{ gW}^{-1}$ . Thus, for 3 W extra, 240 g per Nsat is required.

(2) This means that the Nsats will need to handle larger data-rates in the inter-Nsat link as well as the Nsat-Rsat link. The power required to send one signal of 500 kbit is 25 watt, thus, this is required for every extra signal. The weight increase in EPS for one extra signal is 2 kg. This means that since at least 2 Nsats are always in view, instead of guaranteed 12 rover serviced, 24 rovers can now be serviced (or double the data rate per rover). Such a drastic increase in EPS mass will also require to re/design the ADCS to able to rotate the Nsat since the solar panels add a lot of mass outwards, thus increase the moment of inertia. Due to the increase in battery size there should also be a need to investigate the thermal design again.

In Figure 11.5 The two options are compared, it can be clearly seen that adding 2 kg results in less overall mass than by increasing the total number of Nsats. However the 2 kg results in more redesign of the Nsat especially the EPS, ADCS and C&DH.

Both options above require also an increase in either number of Rsats or the data-rates they can handle if the number of rovers is above 18. Either the number of Rsats could be increased or the data rates they can handle is increased.

A data rate increase leads to 3 watt required for every 500 kbit signal extra. Every added Watt of power means 27 g extra in solar panels and batteries. Thus for 3 watt, 80 g is required. In terms of overall weight it is better to increase the data-rates than to add extra Rsats. Extra Rsats also require redesign of the deployment vehicle and re-choosing the launcher.

### 11.2.4. DEPLOYMENT VEHICLE DESIGN

An increase in weight of 80 g for each RSat does not change the structural sizing of the relay deployment vehicle.

For the NDeVe however, the increase in mass of the Nsat EPS is substantial. Assuming that the 2 kg increase in mass causes an additional 1 kg increase in structural weight and ADCS mass, this will cause an overall increase of 12.6 kg. Furthermore, due to the increased payload mass, the amount of propellant increases by 54 kg. Again, no redesign in the propellant tank is required due to this change. The increase in mass is also not so substantial and does not increase the total launch mass (increased to 3,781 kg) beyond the capabilities of the Falcon 9.

### 11.2.5. CONCLUSION

The current design can support up to 11 rovers. For an increase in rovers, the Nsats and NDeVe will have to change the most. Two options were investigated. By increasing the number of Nsats its EPS will have to be increased in weight by only 80 g and the NDeVe will have to change significantly. By increasing the data rates, the Nsats will become 2 kg heavier. This has a negligible effect on the NDeVe.



## OPERATIONS AND MISSION PLANNING

In this chapter the operations and planning of the mission are discussed.

### 12.1. OPERATIONS

Executing a successful project in terms of efficiency - i.e. realising a project within the schedule, budget and scope - is assured by a systematic implementation of standardised practises in the field of space projects, by regular planning updates and design compatibility checks. These contribute to the assurance of customer satisfaction by ensuring that the design meets the customers requirements. The latter is important, but not necessarily enough to match their expectations. The system should also have a defined operational structure and detailed processes to guarantee full functionality. Furthermore, a detailed operation progression is a good indicator of the operational costs and can serve as an attraction point for new costumers. Initially there is a pre-launch and launch phase, followed by the trajectory that will take the system to the desired location. The next step is the deployment of the satellites, and finally continuous operation of the constellation. Additionally, the system will have to send and receive information via a ground station serving as a collection point. Several ground stations may be needed to provide a 24/7 link, their number and locations will be determined in later stages of the project. The main selection criteria for a ground station will be its cost and reliability. Possible ground stations are presented in the footnotes of [subsection 5.1.4](#).

#### 12.1.1. LAUNCH AND PRE-LAUNCH ACTIVITIES

In this project the design of the launcher is out of scope and the group will only select appropriate ones for their mission. The selected launchers are SpaceX's Falcon 9 for the direct transfer and ISRO's PSLV-XL used for the low-energy transfer to deliver the relay satellites. As such, the launch provider will serve as a contractor to the project with the main responsibilities being: supplying the launcher and handling all pre-launch and launch activities.

#### 12.1.2. TRAJECTORY ACTIVITIES

During the trajectory phase, it will be necessary to analyse telemetry data in order to determine if the trip is going as planned. In case it is not, corrective actions (e.g firing a thruster to correct for disturbances) should be performed. However, the effectiveness of the correction is limited by the time within which the deviation is detected and hence, the vehicle needs to be closely monitored. This can be achieved utilising two ground station (one on the day side and one on the night side of Earth). The telemetry data will be forwarded from the ground station to the operations group for analysis and in case of a mishap, they will make a decision on how the disturbance will be counteracted. This cuts down operational cost as there is no need for an external party to be hired.

#### 12.1.3. DEPLOYMENT ACTIVITIES

After the desired location is reached, the deployment phase commences. During this phase at least three ground stations will be required for continuous contact as fault is the deployment process has the potential to cause a system failure. A loss of communication is hence unacceptable. Furthermore this process will generate telemetry data from the individual satellites that will be again forwarded from the ground station to the operations group for analysis.

#### 12.1.4. CONSTELLATION ACTIVITIES

After the constellation has been established, nominal operations can begin. This phase will most likely utilise the same ground stations used to monitor the deployment as it is a costumer requirement to maintain a 24/7 link with Earth. A representative flow of this process can be found in [Figure 5.2](#). The required man-power for operations can be minimal as the overall process can be automated.

### 12.2. MISSION PLANNING

This section describes a preliminary planning of the execution of the mission. An overview of this planning is included in [Figure 2.1](#).

#### 12.2.1. DIRECT TRANSFER

Once the relay satellites are in orbit, a direct transfer is performed. The first burn  $\Delta V_{21}$  is performed with the Moon at its apogee. In order to have some buffer time, it is chosen to perform this burn when the Moon approaches its apogee at 21:41 on the 25th of September 2029 (UTC+02).<sup>1</sup> To allow for a temporal margin between launch and the first burn, it is decided that the launch shall take place around the 20th of September 2029. After the first burn it takes 107.9 hours to reach the required orbit around the Moon. Plane changes are then performed which take another 33.95 hours. Lastly, the phasing manoeuvre takes 46.65 hours to complete. This means all the satellites will be in place on the 3rd of October 2029 (UTC+02).

If the timing of  $\Delta V_{21}$  is off, the desired orbit can still be reached. However, this does come at a cost of additional  $\Delta V$ . For example, if the burn is performed a minute late,  $\Delta V_{21}$  needs to be increased by  $5.0 \text{ m s}^{-1}$  and  $\Delta V_{22}$  has to be

<sup>1</sup><https://www.timeanddate.com/astronomy/moon/distance.html?year=2029&n=338> Accessed on 26.06.2017

increased by  $250.5 \text{ ms}^{-1}$ . These values are computed for the case where  $\Delta V_{21}$  is applied in the retrograde direction. The amount of additional  $\Delta V$  needed if the burn is mistimed should be optimised by investigating the application of  $\Delta V_{21}$  in different directions than the velocity in the future.

Another option if the burn window is missed, is to wait another month until the Moon is at its apogee again at 08:58 on the 10th of May 2029. However, if the deployment vehicle is already in LEO, this is not the best option. This means that the vehicle would need to spend another month in space which poses risks in term of radiation and operational viability.

### 12.2.2. LOW-ENERGY TRAJECTORY

To make sure the direct transfer can launch on the 20th of September 2029, the Rsats have to already be in place. To have sufficient buffer time, it is chosen that the Rsats have to be in the halo orbit a month before the scheduled launch of the Nsats, on the 20th of August 2029. The total trajectory takes 347 days, therefore  $\Delta V_{11}$  has to be performed on the 7th of September 2028. Therefore, the launch should take place in the beginning of September 2028. This means  $\Delta V_{12}$  is applied on the 1st of January 2029.  $\Delta V_{13}$  is performed on the 24th of February 2029, and  $\Delta V_{14}$  is applied on the 26th of June 2029.

However, for the low-energy transfer the dates should be checked to match with the designed relative positions of the Sun, Earth and Moon using an advanced ephemeris tool. The consequences of missing the burn window are larger for the low-energy transfer than for the direct transfer as this trajectory is chaotic. Therefore, if the window is missed, it could be that a new trajectory has to be designed.

## 12.3. STRATEGY FOR EXTENDING MISSION DURATION

If cost allocation is positive, it is possible that the customer desires a mission extension up to 15 years. One option would be to relaunch the entire constellation every five years and so they remain in their design frame. However, this might be more costly than necessary. To investigate the option of maintaining the constellation for up to 15 years, the satellite reliability, available power and  $\Delta V$  are investigated.

### 12.3.1. RELIABILITY ASPECT

From the reliability curve used for the reliability analysis shown in [Figure 14.22](#), an initial trace of a wear-out stage can be seen. From [16, p. 7] it is taken that this model is valid up to 15 years and that the probability of an individual satellite failure is 0.091525. This means that after 15 years on average 9.15 % of the network satellites have failed. This results in an average satellite failure of 0.548 satellite failures per plane in 15 years from a Monte Carlo simulation. As long as the relay satellites do not fail, the constellation can be maintained with the existing strategy.

### 12.3.2. POWER ASPECT

Over time, the solar cells degrade with 3 % per year. After 15 years, the solar array produces only 63.3 % of the begin-of-life power. The EPS design is very conservative due to a contingency factor of 1.3. Therefore both the Rsat and Nsat still produce enough energy. Concerning the battery degradation, the Nsat would perform about 27,000 cycles with a depth of discharge of 40 %. From [Figure 6.4](#) it can be seen that this still falls in the acceptable zone, but a battery capacity degradation of more than 70 % should be expected. Due to the low peak loads this does not pose a direct problem. The Rsats only have about 450 cycles after 15 years, which does not affect the battery degradation.

### 12.3.3. $\Delta V$ ASPECT

Extending the mission with 15 years, means that each satellite has to perform three times as much orbit maintenance. Since each satellite only has a limited amount of  $\Delta V$  available, this could become problematic. Currently, the amount of  $\Delta V$  on the network satellites assumes a worst case of  $15 \text{ ms}^{-1}$  per year which comes down to a total of  $75 \text{ ms}^{-1}$ . In a positive scenario, the  $\Delta V$  margin could be used for orbit maintenance as well, which increases the amount of  $\Delta V$  up to a maximum of  $110 \text{ ms}^{-1}$ . From [Figure 4.12](#) it can be seen that a minimum orbit  $\Delta V$  of  $7 \text{ m/year}^{-1}$  can be achieved with corrections about every 28 days. This would enable the network satellites to operate for 15.7 years. A more detailed analysis has to be done in order to confirm this and optimise it to increase the Nsat lifetime even further. It also has to be realised that this scenario is a very positive scenario, which might not be realistic.

For the Rsats, the orbit maintenance is taken from literature. To determine its accuracy, a studie has to be performed which would potentially lead to a  $\Delta V$  reduction for orbit maintenance, increasing its lifetime.

### 12.3.4. CONCLUSION

Using the current EPS design, amount of propellant and reliability model, extension up to 15 years can be done without redeploying the entire constellation. Using the proposed Nsat spares approach proposed in [section 4.7](#), the constellation can be continued for 15 years.

For the Rsats, power and reliability is not a problem for mission extension either. However, the amount of orbit maintenance has a high level of uncertainty. It has to be kept in mind that replacing an Rsat takes about a year. To ensure constellation uptime, it can be considered to launch Rsats after five years even if no failures have occurred as a pre-emptive measure.

Before a mission extension could be proposed after the initial five years, an in-depth radiation analysis has to be done, the reliability model has to be updated with actual failure data and the  $\Delta V$  allocation for orbit maintenance should be investigated.

## MANUFACTURING, ASSEMBLY AND INTEGRATION PLAN

The manufacturing, assembly and integration of the vehicles is discussed in this chapter. The standards as set by the European Cooperation for Space Standardization (ECSS) are used throughout this phase of the mission.<sup>1</sup> As described in chapter 12 the Nsats are launched only after the Rsats are in place. Therefore, the Rsats and RDeVe are given priority in the manufacturing, assembly and integration of the vehicles. Aside from this requirement, it is also paramount that there is enough time in the planning for the testing of the sub-components as well as the subsystems as a whole. The entire manufacturing, assembly and integration process is displayed in Figure 13.1.

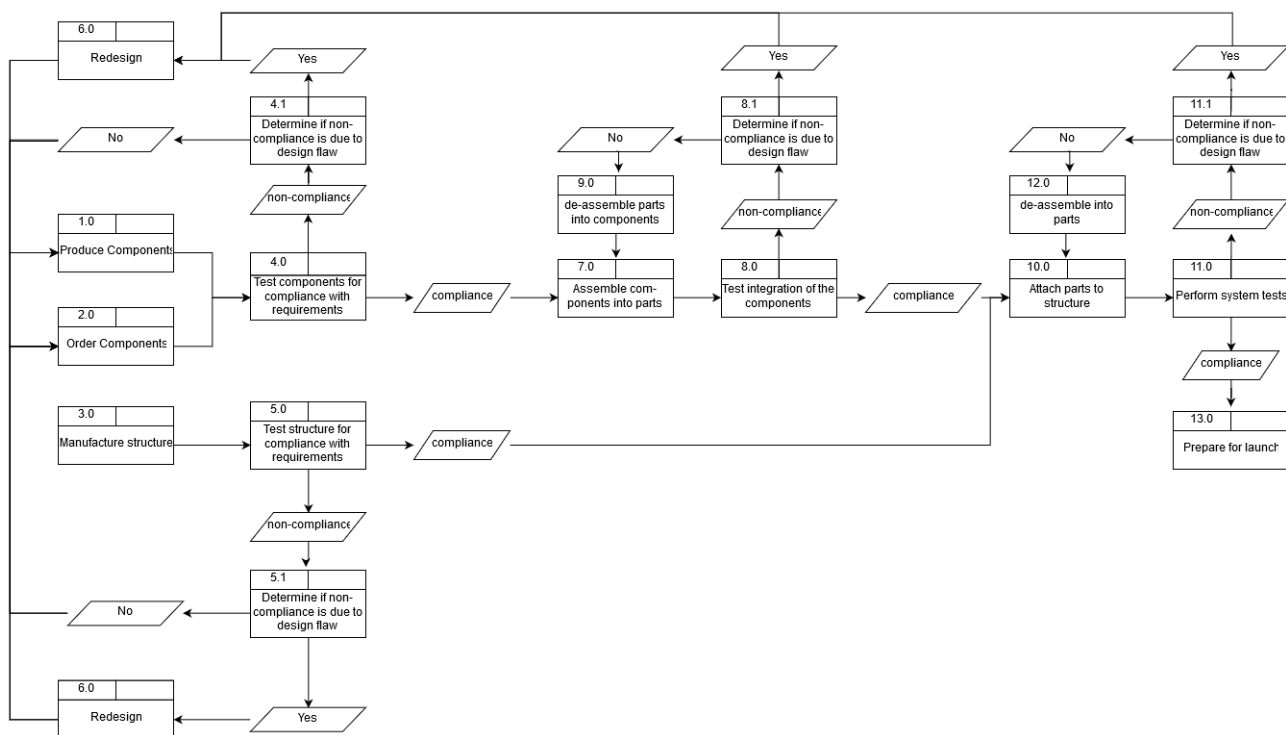


Figure 13.1: Flow of the manufacturing, assembly and integration

The manufacturing of the vehicles starts with the production of components. Difference is made between components which are bought of the shelf and components which are specially designed by Project IRIS. These specially designed components will be outsourced to companies such as ISISpace<sup>2</sup> on a contractual basis. Products produced by Project IRIS should be tested if they comply with the requirements, as external companies perform these tests themselves. However, some testing should be performed to ensure that these companies deliver quality components. If the requirements are not met, it is determined whether the non-compliance is caused by design flaws or by manufacturing mistakes. After that, the components are re-manufactured with or without re-design. This process is repeated for the assembly of the components into parts, and for attaching said parts to the structure. When everything is manufactured and assembled, and all the tests are passed, the vehicle is made ready for launch. This phase involves attaching satellites to their respective deployment vehicles, and deployment vehicles to the launcher.

The number of Nsats to be produced is large (around 48). This introduces a learning curve as the manufacturing staff establishes routine. Furthermore, as a lot of these satellites have to be produced it is more profitable to create specialised tools, rigs and assembly lines for this vehicle than for the deployment vehicles. This can decrease the production time, justifying the increased costs for creating this tooling.

<sup>1</sup><http://ecss.nl/standards/ecss-standards-on-line/active-standards/product-assurance/> Accessed on 03.07.2016

<sup>2</sup><https://www.isispace.nl/> Accessed on 26.06.2017



To create the final design of the system, multiple tools are used. This chapter describes the different tools which are also verified and validated.

### 14.1. TRAJECTORY SIMULATION TOOL

The trajectory simulation tool is used to simulate trajectories in two different systems: in the Earth-Moon system and in the Sun-Earth system. The underlying principles for these tools are the same, although different systems are modelled.

#### 14.1.1. ASSUMPTIONS

For both the trajectory models (Earth-Moon and Sun-Earth) assumptions are made, which are discussed below in this section. Assumption which are applicable to only one the models will be discussed in their respective sections. simulation.

**Negligible mass of the spacecraft** It is assumed that the mass of the spacecraft is zero, and that it does not influence the motion of the Moon, Earth or the Sun. In reality the mass of the spacecraft (Nsats with DeVe or Rsats with DeVe) is in the order of tens of kilograms. The mass of the Moon, Earth and Sun are  $0.07346 \times 10^{24}$  kg and  $5.9723 \times 10^{24}$  kg and  $1,988,500 \times 10^{24}$  kg respectively. Therefore, the assumption that the mass of the spacecraft is negligible compared to the masses of the planets is accurate and will not have a noticeable influence on the simulation.

**Impulsive manoeuvres** Manoeuvres calculated for high-thrust options are modelled to be instantaneous. In reality, the manoeuvres take in the order of tens of seconds to perform. Compared to a transfer time in the order of days (direct) or months (low-energy) it is negligible. Therefore, there is only a negligible effect on the simulations.

**Approximation of Sun, Earth and Moon as point masses** The Sun, Moon and Earth are modelled as point masses. In reality, the irregular mass distributions of these bodies will perturb the trajectory of the satellite. The most significant component of this perturbation near the Earth is the J2 effect. This is the the perturbation due to the equatorial bulge of the Earth. The analytic relation for the rate of change of the orbital parameters due to the J2 perturbation is given in equation Equation 14.1 [11, p.212].

$$\Omega_{J2} = -1.5nJ_2\left(\frac{R_E}{a}\right)^2(\cos(i))(1-e^2)^{-2} \quad \omega_{J2} = 0.75nJ_2\left(\frac{R_E}{a}\right)^2(4-5\sin^2(i))(1-e^2)^{-2} \quad (14.1)$$

With an inclination of  $29^\circ$  with respect to the equator, after a day, the argument of ascending node of the transfer orbit changes by  $3.8 \times 10^{-13}^\circ$ , and the argument of periapse changes by  $8.0 \times 10^{-13}^\circ$ . This is small enough that it can be neglected for the design of the transfer.

**Solar radiation pressure** The models do not incorporate perturbations due to the Solar radiation pressure. The Solar radiation at the distance from the Sun to Earth and to the Moon is approximately  $4.6 \times 10^{-6} \text{ Nm}^{-2}$  [50, p. 4]. The gravitational force of Earth at L1 of the Earth-Moon system is  $3.7 \times 10^{-2} \text{ Nm}^{-2}$  for a satellite of 10 kg, according to Newton's Law of Universal Gravitation [11, p. 198]. This is more than 8000 times higher compared to the solar radiation pressure. Therefore, this assumption will not introduce sizeable errors.

**Aerodynamic drag** Satellites in LEO endure a sizeable aerodynamic drag which causes a reduction of the semi-major axis over time. This aerodynamic drag is not incorporated in the simulation of the transfer trajectory. For the design purposes this is a valid approximation as the effect of the aerodynamic drag is only significant over longer periods of time and will be counteracted by orbit maintenance.

**Adams-Bashforth-Moulton PECE solver** The equations of motion generated from the circular restricted 3-body problems are solved using the ode113 functionality of MATLAB. This functionality employs the Adams-Bashforth-Moulton PECE scheme to solve the non-linear differential equations. To check the error of the solver, a 500 km LEO orbit is propagated for 1000 periods, which equals 65.6 days. The Relative Tolerance is set to its maximum of  $2.22045 \times 10^{-14}$ .

The errors introduced due to the Adams-Bashforth-Moulton scheme are presented in Table 14.1.

Table 14.1: Error introduced due to Adams-Bashforth-Moulton propagation

	Radius[m]	Velocity [m/s]
Initial	6,871,000	7,616.312
After 1,000 periods	6,870,857.1	7,616.470
Error %	-0.00208	0.00208

### 3-BODY EARTH-MOON MODEL ASSUMPTIONS

**Circular Moon orbit** In the direct transfer this assumption is not made: the eccentricity of the orbit of the Moon is incorporated in the model. For the low-energy transfer this is not incorporated. The eccentricity of the orbit of the Moon is 0.0554. Therefore, this assumption significantly influences the simulation. The transfer time is overestimated and the insertion burn is over- or underestimated. However, as a first approximation for the design of the complex low-energy transfer this assumption is valid.

**Planar motion Earth-Moon** The inclination of the orbit of the Moon around the Earth is assumed to be zero in the model. However, the inclination in reality is 5.145°. This does influence the simulation of the transfer trajectory as it changes the inclination at which satellites arrive at the Moon. By not taking this into account, the computed  $\Delta V_{22}$  required for orbit insertion and inclination change can slightly vary from reality. The computed value of  $\Delta V_{22}$  to insert into a 46.0° inclined lunar orbit for the assumed arrival inclination of 0° is 1,358.4 m s<sup>-1</sup>. The maximum inclination with respect to the rotational axis at which the satellite arrives at the Moon is 6.69°. In this case, the computed value for  $\Delta V_{22}$  is 1,219.5 m s<sup>-1</sup>. Therefore, this significant difference should be taken into account in future detailed iterations of the trajectory design or sufficient reserve fuel should be taken to the Moon.

**Stationary Earth** The Earth is modelled as being stationary in the inertial frame. In reality Earth is orbiting the Sun at high velocities. However, only velocities relative to the Moon and the Earth are of concern for this aspect of the trajectory design. Therefore, this is an accurate choice of reference frame.

**Perturbations from the Sun's gravity** The Sun's gravity is not the same for the Moon and Earth as they are at different positions relative to the Sun. This results in a disturbing force in the Earth-fixed inertial reference frame. This force is neglected in the simulation of the transfer orbit. The perturbation of a satellite at the orbit of the Moon is 1.519 × 10<sup>-5</sup> m s<sup>-2</sup> in the worst case scenario. This is computed using Newton's Law of Universal Gravitation [11, p. 198]. The acceleration due to the Earth's gravity is 2.698 × 10<sup>-3</sup> m s<sup>-2</sup>. Therefore, the relative perturbation is 0.56 % with respect to the Earth's gravitational acceleration and can be neglected and the effect on the results is negligible.

### 3-BODY SUN-EARTH MODEL ASSUMPTIONS

**Circular Earth orbit** The Earth is modelled in a circular orbit around the Sun with a radius of 149.6 × 10<sup>6</sup> km. While in fact the Earth's orbital eccentricity is 0.0167, which causes the perihelion to be 147.09 × 10<sup>6</sup> km and aphelion 152.10 × 10<sup>6</sup> km. Using Newton's Law of Universal Gravitation it was found that the gravity force differs in the perihelion by 3.44 % and in the aphelion 3.26 % compared to the model [11, p. 198]. This does not influence the design of transfer from the Earth to the Moon.

**Stationary Sun** The Sun is modelled as being stationary in the inertial frame. In reality the Sun is moving through space at very high velocities (250 km s<sup>-1</sup>). However, only velocities relative to the Sun and Earth are of concern for this aspect of the trajectory design. Therefore, this is an accurate choice of reference frame.

#### 14.1.2. TOOL DESCRIPTION

The trajectory simulation tools, which simulate trajectories in the Sun-Earth system and Earth-Moon system, are created in MATLAB. They are both numerical approximations of circular restricted 3-body problems. In this circular restricted 3-body problem all accelerations are determined by Newton's Law of Universal Gravitation [11, p. 198]. The tool makes use of MATLAB's "ode113" differential equation solver [51, p.1-22]. This function takes as input: a function defining the accelerations, the time-span to be simulated, the initial conditions and options, such as tolerance and possible events. The functions used to define the accelerations make use of Equation 14.4, which combines Newton's Law of Universal Gravitation (Equation 14.2) and Newton's Second Law (Equation 14.3) [11, p.198]. In which  $\mathbf{F}$  is the force vector in N,  $G$  is the universal gravitational constant of 6.6740 × 10<sup>-11</sup> m<sup>3</sup>kg<sup>-1</sup>s<sup>-2</sup>,  $M$  is the mass of the main attracting body in kg,  $m$  is the mass of the satellite in kg,  $\mathbf{r}$  is the position vector in m,  $\mathbf{a}$  is the acceleration vector in m s<sup>-2</sup> and  $\mu$  is the standard gravitational parameter of the main attracting body in m<sup>3</sup>s<sup>-2</sup>.

$$\mathbf{F} = \frac{-G(Mm)}{r^3} \mathbf{r} \quad (14.2) \quad \mathbf{F} = m\mathbf{a} = m\ddot{\mathbf{r}} \quad (14.3) \quad \ddot{\mathbf{r}} = \frac{-(GM)}{r^3} \mathbf{r} = \frac{-\mu}{r^3} \mathbf{r} \quad (14.4)$$

The initial conditions of the Sun, Earth and Moon are determined using Kepler's laws. [11, p.198]. The  $\Delta V$ 's applied to the satellites are modelled by adding this increase in the velocity to the initial conditions of the simulation.

#### 14.1.3. VERIFICATION

##### UNIT TESTS

The first unit test is propagating a 500 km altitude LEO for 1,000 periods. As seen in Table 14.1 the accumulated error with respect to the simplified model is -0.00208 % for the position and 0.00208 % for the velocity. This verifies that the tool accurately simulates the simplified model.

The next unit test which is conducted involves the orbit of the Moon in the Earth-Moon system. This orbit is simulated until it reaches the starting point, so exactly one orbit. According to the Kepler equations the period of a circularised Moon orbit should be equal to Equation 14.5 [11, p.199]. In which  $T$  is the period of one orbit in s,  $r$  is the radius of the circular orbit in m and  $m$  is the mass in kg.

$$T_{Moon} = 2\pi \sqrt{\frac{r_{Moon}^3}{G(m_{Moon} + m_{Earth})}} = 2,362,916.985 \text{ s} \quad T_{Earth} = 2\pi \sqrt{\frac{r_{Earth}^3}{G(m_{Sun} + m_{Earth})}} = 31,560,301.6 \text{ s} \quad (14.6)$$

According to the simulation the period is 2,362,916.985 s. Therefore the simulated Moon orbit accurately represents the simplified Moon orbit.

The same unit test is conducted for Earth's orbit in the Sun-Earth system. According to the Kepler equations the period of a circularised Earth orbit should be equal to Equation 14.6 [11, p.199]. According to the simulation the period of Earth's orbit is 31,558,874.7 s. This deviates by  $-0.00452\%$ . Therefore, the transfer simulation tool accurately simulates the simplified orbit of the Earth.

### SYSTEM TEST

The last verification step is performing a system test. This system test is performed by modelling a simple Hohmann transfer from a 500 km altitude LEO to an orbit with an altitude of 10,000 km above the Earth's surface. According to the Kepler equations the  $\Delta V$ 's needed for this transfer manoeuvre are equal to Equation 14.7 and Equation 14.8 [17, p.131].

$$\Delta V_1 = \sqrt{\frac{2\mu_{Earth}}{r_1} - \frac{2\mu_{Earth}}{r_1 + r_2}} - \sqrt{\frac{\mu_{Earth}}{r_1}} = 1,423.5 \text{ ms}^{-1} \quad \Delta V_2 = \sqrt{\frac{\mu_{Earth}}{r_2}} - \sqrt{\frac{2\mu_{Earth}}{r_2} - \frac{2\mu_{Earth}}{r_1 + r_2}} = 1,140.1 \text{ ms}^{-1} \quad (14.7) \quad (14.8)$$

This transfer is simulated by applying these  $\Delta V$ 's to a satellite which is in the specified starting orbit with an altitude of 500 km above the Earth's surface. The results of this simulation are displayed in Figure 14.1. In Figure 14.1 the black triangles indicate the locations where the burns are applied. In Figure 14.2 the development of the radius and the velocity of the satellite during the transfer is displayed.

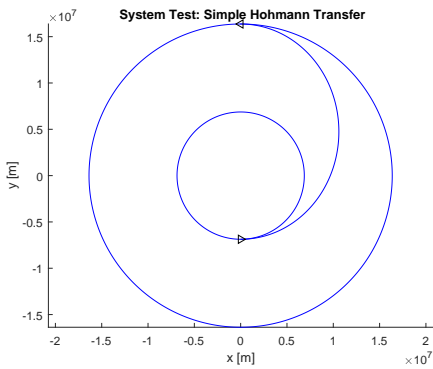


Figure 14.1: Simulation of a simple Hohmann Transfer.

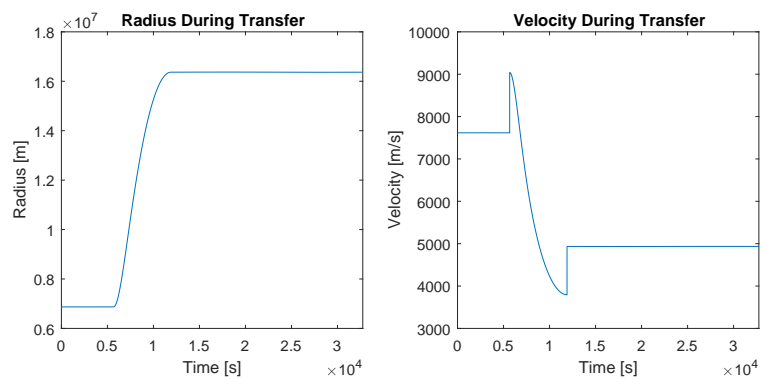


Figure 14.2: Change of radius and velocity during a simple Hohmann transfer.

The resulting figure as well as the graphs show that the tool accurately simulates the model. The calculated  $\Delta V$ 's cause a change of orbit from 6,871 km radius (500 km altitude) to 16,871 km radius (10,000 km altitude). This can be seen in Figure 14.1. Also, the final radius and velocity is constant, a characteristic of a circular orbit. This verifies the transfer simulation tool.

#### 14.1.4. VALIDATION

The validation of the trajectory simulation tool is done by computing, and simulating, a transfer trajectory. This is then compared to the available literature. For this validating purpose, the design of the direct transfer is used. An explanation of this trajectory and its design is given in section 3.2. This trajectory, requires a  $\Delta V_{21} = 3,059.9 \text{ ms}^{-1}$  and a  $\Delta V_{22} = 1,358.43 \text{ ms}^{-1}$ . This accumulates to a  $\Delta V_{total} = 4,418.4 \text{ ms}^{-1}$  for the transfer. According to [52, p. 282] an optimal direct transfer from a 167 km altitude LEO to a 100 km altitude LLO requires a minimum  $\Delta V_{total} = 3,947.0 \text{ ms}^{-1}$ . This is a difference of 11.94%. This can be explained by the fact that the starting and final orbit of the reference literature and the direct transfer are different. Also, the transfer trajectory computed with the tool also includes an inclination change. These reasons cause the results achieved using the tool to deviate from the results achieved in [52, p. 282]. This deviation of 11.94% is reasonable. Therefore, it can be concluded that the tool is valid.

## 14.2. ROTATING FRAME TOOL

In order to be able to convert positions and velocities between different reference frames, a rotating frame tool is created. This tool specifies a rotating frame which rotates with either the Moon or the Earth, depending on which system is simulated.

### 14.2.1. ASSUMPTIONS

**Constant rotation rate** The rotating tool assumes that the rotating frame rotates with constant angular velocity with respect to the inertial reference frame. As the rotating frame with the Earth or the Moon, this implies that the orbits of the Earth and the Moon are assumed to be circular. As this assumption is made for the low-energy trajectory design, it does not introduce any errors. This rotation tool cannot be used to convert velocities to the rotating frame as for that transfer the elliptic orbit of the Moon is used.

### 14.2.2. TOOL DESCRIPTION

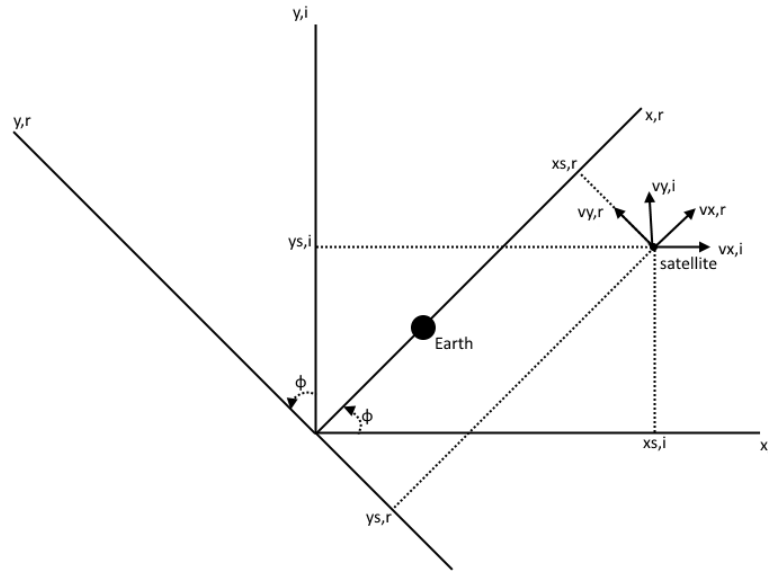


Figure 14.3: Schematic representation of the rotating frame.

This tool rotates over the angle  $\phi$  as displayed in Figure 14.3. The rotating of the coordinates is done according to Equation 14.9. In which  $\mathbf{r}^r$  and  $\mathbf{r}^i$  are the position vectors in the rotating frame and inertial frame in m.  $\mathbf{U}_z$  is the rotation matrix as displayed in Equation 14.10.<sup>1</sup>

$$\mathbf{r}^r = \mathbf{U}_z \mathbf{r}^i \quad (14.9) \quad \mathbf{U}_z = \begin{bmatrix} \cos(-\phi) & -\sin(-\phi) & 0 \\ \sin(-\phi) & \cos(-\phi) & 0 \\ 0 & 0 & 1 \end{bmatrix} \quad (14.10)$$

The rotating of the velocity vector from the inertial to the rotating frame is done using Equation 14.11. In which  $\mathbf{v}^r$  and  $\mathbf{v}^i$  are the velocity vectors in the rotating and inertial frame in m.  $\mathbf{r}^i$  is the position vector in inertial frame in meter and  $\mathbf{U}_z$  is the rotation matrix displayed in Equation 14.10. The time derivative of  $\mathbf{U}_z$  is displayed in Equation 14.12.<sup>1</sup>

$$\mathbf{v}^r = \mathbf{U}_z \mathbf{v}^i + \frac{d\mathbf{U}_z}{dt} \mathbf{r}^i \quad (14.11) \quad \frac{d\mathbf{U}_z}{dt} = \begin{bmatrix} \omega \sin(-\phi) & \omega \cos(-\phi) & 0 \\ -\omega \cos(-\phi) & \omega \sin(-\phi) & 0 \\ 0 & 0 & 1 \end{bmatrix} \quad (14.12)$$

### 14.2.3. VERIFICATION

To verify the tool the inputs of a two point system are given. Point 1 rotates with the x-axis of the rotating frame on the x-axis and the location of point 2 is fixed in the inertial frame. This gives the following inputs:

$$\mathbf{r}_1^i = \begin{bmatrix} 0 \\ 1 \\ 0 \end{bmatrix} \text{ m}, \mathbf{v}_1^i = \begin{bmatrix} -\omega \\ 0 \\ 0 \end{bmatrix} \text{ ms}^{-1}, \mathbf{r}_2^i = \begin{bmatrix} 0 \\ 2 \\ 0 \end{bmatrix} \text{ m}, \mathbf{v}_2^i = \begin{bmatrix} 0 \\ 0 \\ 0 \end{bmatrix} \text{ ms}^{-1}.$$

The expected and real outputs for the inputs above, for an angular velocity  $\omega$  of  $3.0 \text{ rad s}^{-1}$ , are displayed in Table 14.2. With a maximum deviation in terms of position of  $1.22 \times 10^{-16} \text{ m}$ , and a maximum deviation in terms of velocity of  $3.67 \times 10^{-16} \text{ ms}^{-1}$ , this tool is considered verified.

Table 14.2: Comparison of the expected and real outputs of the rotating frame tool.

	Expected output point 1	Real output point 1	Expected output point 2	Real output point 2
$r_x^r$ [m]	1	1	2	2
$r_y^r$ [m]	0	$6.1232 \times 10^{-17}$	0	$1.2246 \times 10^{-16}$
$r_z^r$ [m]	0	0	0	0
$v_x^r$ [ms <sup>-1</sup> ]	0	0	0	$3.6739 \times 10^{-16}$
$v_y^r$ [ms <sup>-1</sup> ]	0	0	-6	-6
$v_z^r$ [ms <sup>-1</sup> ]	0	0	0	0

<sup>1</sup> [https://ocw.mit.edu/courses/aeronautics-and-astronautics/16-07-dynamics-fall-2009/lecture-notes/MIT16\\_07F09\\_Lec08.pdf](https://ocw.mit.edu/courses/aeronautics-and-astronautics/16-07-dynamics-fall-2009/lecture-notes/MIT16_07F09_Lec08.pdf) Accessed on 26.06.2017

14.2.4. VALIDATION

To validate this tool, one of the possible partial trajectories of the low-energy transfer is used. This trajectory in a Sun-centred rotating frame is displayed in Figure 14.4.

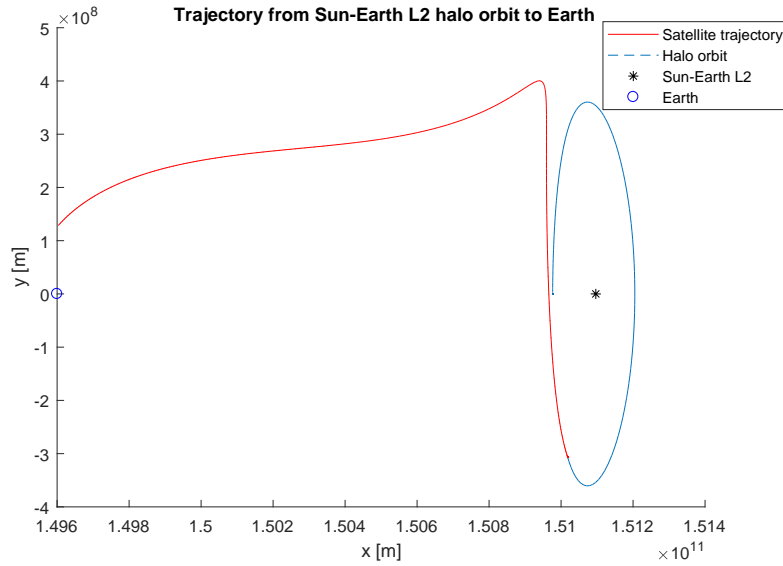


Figure 14.4: Possible trajectory from Sun-Earth L2 halo orbit to Earth in a Sun-centered rotating frame.

The positions and velocities of this trajectories in the rotating frame are displayed in Figure 14.5. It is shown that the positions correspond to the plot in Figure 14.5. Furthermore, the velocities correspond to the development of the positions. Therefore, this tool is considered validated.

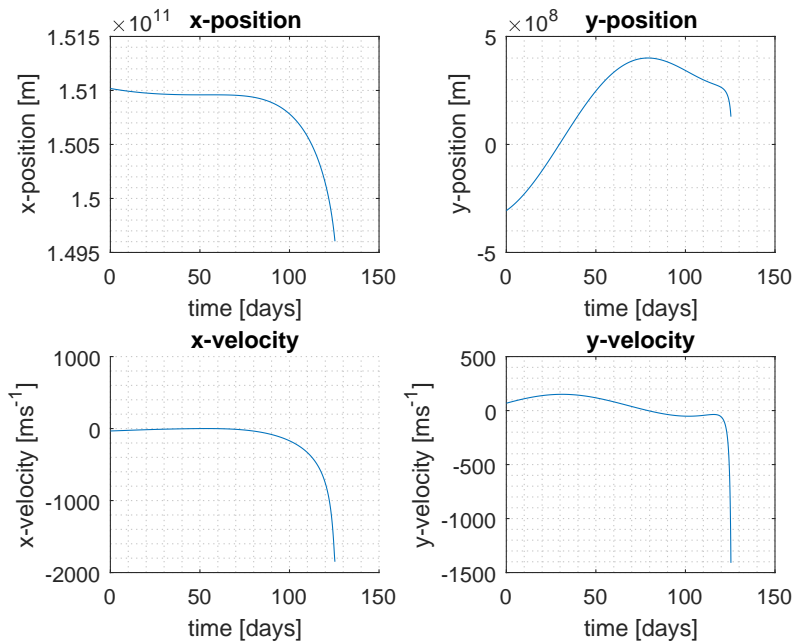


Figure 14.5: Positions and velocities in Earth-fixed rotating frame of a trajectory compared to inertial frame.

14.3. PLANE CHANGE TOOL

This tool is used to calculate the  $\Delta V$ 's and positions of orbital plane change manoeuvres.

14.3.1. ASSUMPTIONS

**Restricted two-body orbital model** Orbits are assumed to only be influenced by the gravity of the Moon, which is modelled as a point mass. Furthermore, the mass of the spacecraft is neglected. This allows the use of analytic

formulas to calculate the geometry of orbits about the Moon. The real orbit is also affected by the gravity of the Earth and the Moon's uneven gravity field. The effect of this assumption has been quantified in [subsection 14.3.4](#).

**Impulsive manoeuvres** Manoeuvres are modelled as an instant change in velocity. Real manoeuvres will be less efficient for a lower thrust level. This loss can be minimised by splitting manoeuvres in stages, at the cost of a waiting time of one orbit revolution per stage.

### 14.3.2. TOOL DESCRIPTION

The plane change tool calculates the manoeuvre needed to change the orientation of an orbital plane. Its inputs are the Keplerian orbit elements of the initial orbit and the target inclination and argument of ascending node of the final orbit. The manoeuvre consists of a single impulse, and changes the orbital plane while keeping the semi-major axis and eccentricity the same. The manoeuvre takes place at the highest altitude along the intersection axis. The outputs of the tool are the manoeuvre position, thrust direction,  $\Delta V$  and argument of periapse of the new orbit. It is also possible to calculate these outputs for a series of manoeuvres by inputting the target plane orientations in the required order.

Two right-handed frames of reference are defined to perform vector operations. Both frames are centred at the Moon. The 'Final' reference frame has its x-axis aligned to the ascending node of the final orbit and y-axis parallel to the reference plane. The 'Initial' reference frame has its y-axis pointing towards the apoapse of the initial orbit and its x-axis parallel to the initial orbit plane. By representing the the normal vector of the final orbit in the 'initial' reference frame, the intersection geometry can be computed. Reference frame transformations are made using Euler rotation matrices<sup>1</sup>.

Firstly, the unit vector normal to the final plane, in the 'final' reference frame ( $\mathbf{n}_F^F$ ) is defined and translated to the 'Initial' frame ( $\mathbf{n}_F^I$ ). This transformation is shown in [Equation 14.13](#) and [Equation 14.14](#), where ' $\Delta\Omega$ ' is the difference in RAAN between each plane and ' $\omega_{p_I}$ '. The higher-altitude intersection true anomaly (' $\theta_{int_2}$ ') is then calculated from [Equation 14.16](#), where ' $\theta_{int_1}$ ' is the low intersection true anomaly. The relative inclination between the planes (' $\phi_r$ ') is known by [Equation 14.17](#). The radius length at intersect can now be calculated from [Equation 14.18](#) [11, p. 205]. To calculate the argument of periapse of the new orbit, the lower intersect argument for the initial orbit (' $A_I$ ') is first calculated from [Equation 14.19](#), where ' $\omega_{p_I}$ ' is the initial argument of periapse. Then, the unit vector pointing to the lower intersect (' $\mathbf{u}_{int_1}^F$ ') is represented in the 'Final' frame by [Equation 14.20](#) and the final argument of periapse is found from [Equation 14.21](#) and [Equation 14.22](#), where ' $A_F$ ' is the lower intersect argument for the final orbit.

$$\mathbf{n}_F^F = [0 \quad -\sin(\phi_F) \quad \cos(\phi_F)]^T \quad (14.13) \quad \mathbf{n}_F^I = \mathbf{U}_z(-\omega_{p_I})\mathbf{U}_x(\phi_I)\mathbf{U}_z(\Delta\Omega)\mathbf{n}_F^F \quad (14.14)$$

$$\theta_{int_1} = \arctan\left(\frac{|\mathbf{n}_F^I|_i}{|\mathbf{n}_F^I|_j}\right) \quad (14.15) \quad \theta_{int_2} = \pi - \theta_{m_1} \quad (14.16)$$

$$\phi_r = \arccos\left(\frac{\mathbf{n}_F^I \cdot \hat{\mathbf{k}}}{|\mathbf{n}_F^I|}\right) \quad (14.17) \quad \mathbf{r}_{int_2} = \frac{a(1-e^2)}{1+e\cos(\theta_{int_2})} \quad (14.18)$$

$$A_I = \begin{cases} \omega_{p_I} - \theta_{int_1}, & (\mathbf{n}_F^I)_j > 0 \\ \omega_{p_I} + \theta_{int_1}, & (\mathbf{n}_F^I)_j < 0 \end{cases} \quad (14.19) \quad \mathbf{u}_{int_1}^F = \mathbf{U}_z(-\Delta\Omega)\mathbf{U}_x(-\phi_I)\mathbf{U}_z(-A_I)\hat{\mathbf{i}} \quad (14.20)$$

$$A_F = \arccos(\mathbf{u}_{int_1}^F \cdot \hat{\mathbf{i}}) \quad (14.21) \quad \omega_{p_F} = \begin{cases} -A_F + \theta_{int_1}, & (\mathbf{n}_F^I)_j > 0 \\ A_F - \theta_{int_1}, & (\mathbf{n}_F^I)_j < 0 \end{cases} \quad (14.22)$$

Given the relative inclination between two orbital planes and the tangential velocity at which the manoeuvre takes place ( $V_\theta$ ), the  $\Delta V$  can be calculated using [Equation 14.23](#) [53] and [Equation 14.24](#) [11, p. 229], where ' $V_\theta$ ' is the circumferential velocity, ' $r$ ' is the radius ' $a$ ' is the semi-major axis and ' $e$ ' is the eccentricity.

$$V_\theta = \frac{1}{r}(\mu(2a(1-e) - (1-e)^2))^{1/2} \quad (14.23) \quad \Delta V = 2V_\theta \sin(\phi_r/2) \quad (14.24)$$

Since Keplerian orbital elements are used as inputs, several singularities exist for some input combinations. If the inclination of the orbit is zero, the orbit's angular momentum axis is not fully defined. The orbit could be rotating in a prograde or retrograde direction. For this, another optional input exists to define the orbit as prograde or retrograde. This input is only used when the inclination is zero, and is automatically changed to its correct value otherwise. Another singularity exists when two orbits are in the same plane. In this case, each orbit's rotation direction (prograde or retrograde) is checked to determine whether the manoeuvre  $\Delta V$  is zero or twice the orbital speed.

### 14.3.3. VERIFICATION

The relative inclination results are verified by comparing results computed for known cases. When the argument of ascending node is the same for both orbits, the relative inclination between the planes is equal to the difference inclination between them. The  $\Delta V$  can then quickly be calculated by hand and compared to the tool's value. The position of the manoeuvre can also be checked to lie in the x-y plane in Cartesian coordinates. When the inclination is 90 degrees, the relative inclination is equal to the difference in arguments of ascending node, as shown in [Figure 14.9](#). The same verification method can be applied, where the manoeuvre location lies in the z-axis.

To verify a more general set of results, 3D plots were made. The relative inclination axis can be checked to touch both orbits and both orbits are checked to touch in this axis. The manoeuvre position is also displayed and checked to touch both orbits and the inclination axis, as well as being located in the highest point in the axis. This is checked

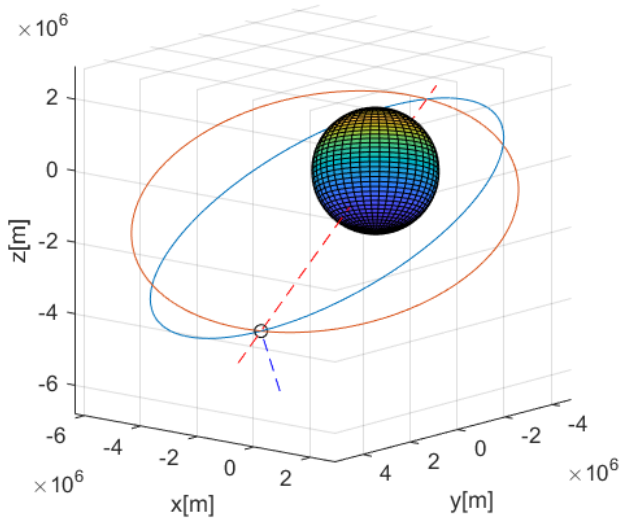


Figure 14.6: Example plot showing the initial (blue) and final (red) orbits after a 20 degree RAAN and 15 degree inclination manoeuvre. The black circle shows the manoeuvre location, the red dashed line shows the relative inclination axis and the blue dashed line shows the thrust vector.

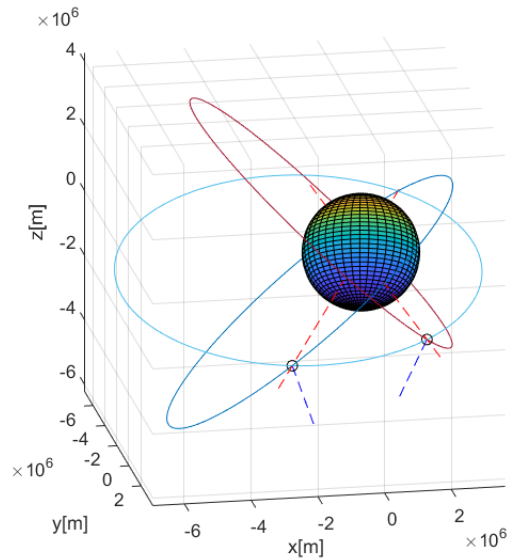


Figure 14.7: Example plot showing 2 consecutive 60 degree RAAN change manoeuvres. The initial orbit is coloured dark blue; the final orbit is coloured red.

for a sequence of manoeuvres as well, to make sure the change in argument of periapee is correctly calculated. An example plot for a single manoeuvre is shown in Figure 14.6. An example plot for 2 consecutive manoeuvres is shown in Figure 14.7.

To check for exceptions not properly handled by the code, different output variables are plotted for inputs spanning over the expected domain of each input variable. An example of this is shown in Figure 14.8.

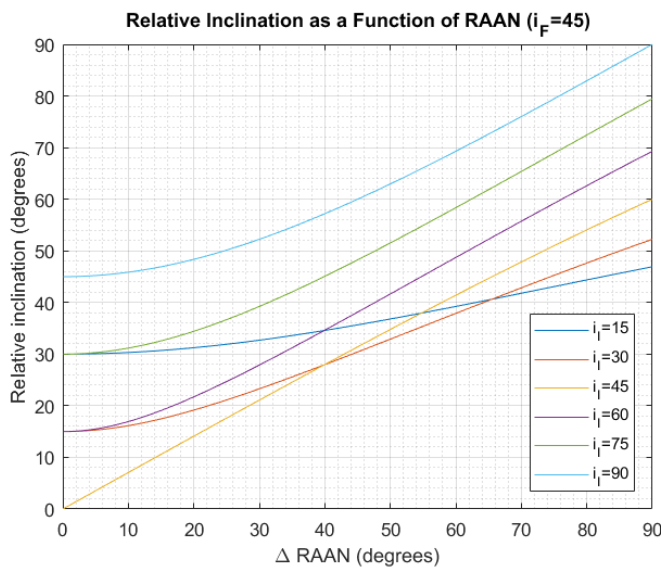


Figure 14.8: Relative inclination between the initial and final planes after a manoeuvre, plotted against the RAAN difference between the two planes for different initial inclinations. The final inclination is 45 degrees.

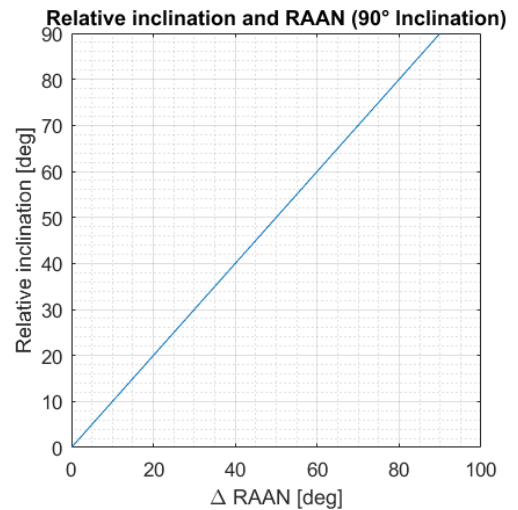


Figure 14.9: Relative inclination plotted against the RAAN difference between the initial and final planes. The Initial and final inclination is 90 degrees.

#### 14.3.4. VALIDATION

To validate the insertion tool, its results are checked to work within a reasonable accuracy in the trajectory simulation tool. The results to be validated are the manoeuvre positions,  $\Delta V$ s, thrust directions and orbital parameters of each plane.

The direct transfer is propagated from LEO to the first insertion manoeuvre. After this, the spacecraft is very close to the target initial orbit. This target orbit is assumed as the initial condition for the insertion tool. The trajectory is then propagated until it reaches the closest point to the next manoeuvre position. At this point, the  $\Delta V$  and thrust

direction of the manoeuvre is used to compute an instant velocity change. This process is repeated for the rest of the manoeuvres.

Finally, the orbital parameters resulting from each manoeuvre are compared to those assumed for the insertion tool. The velocity and position of the spacecraft is transformed from Cartesian coordinates to Keplerian orbital elements using Equation 14.30, Equation 14.25, Equation 14.26, Equation 14.27 and Equation 14.25<sup>2</sup>. Here,  $\mathbf{v}$ ,  $\mathbf{r}$  and  $\mathbf{n}$  are the spacecraft's velocity and position vectors and the orbit's normal vector respectively in Cartesian coordinates.  $\mathbf{e}$  is the orbital eccentricity vector. Figure 14.10 shows the orbital elements simulated in the 3-body model as a function of time compared to the target values. Errors with respect to the target elements can be seen to generally increase with every manoeuvre on a very small scale, which can be seen most in the semi-major axis plot. However, the size of this error is comparable to the errors caused by perturbations from the Earth's gravity alone.

$$\mathbf{h} = \mathbf{r} \times \mathbf{v} \quad (14.25) \quad e = \left| \frac{\mathbf{v} \times \mathbf{h}}{\mu} - \frac{\mathbf{r}}{|\mathbf{r}|} \right| \quad (14.26) \quad i = \arccos\left(\frac{h_z}{|\mathbf{h}|}\right) \quad (14.27)$$

$$a = \frac{1}{\frac{2}{|\mathbf{r}|} - \frac{|\mathbf{v}|^2}{\mu}} \quad (14.28) \quad \Omega = \arccos\left(\frac{-h_y}{|\mathbf{h}|}\right) \quad (14.29) \quad A_{TA} = \begin{cases} \arccos\left(\frac{\mathbf{e} \cdot \mathbf{r}}{e|\mathbf{r}|}\right) - 2\pi, & \mathbf{r} \cdot \mathbf{v} < 0 \\ \arccos\left(\frac{\mathbf{e} \cdot \mathbf{r}}{e|\mathbf{r}|}\right), & \text{otherwise} \end{cases} \quad (14.30)$$

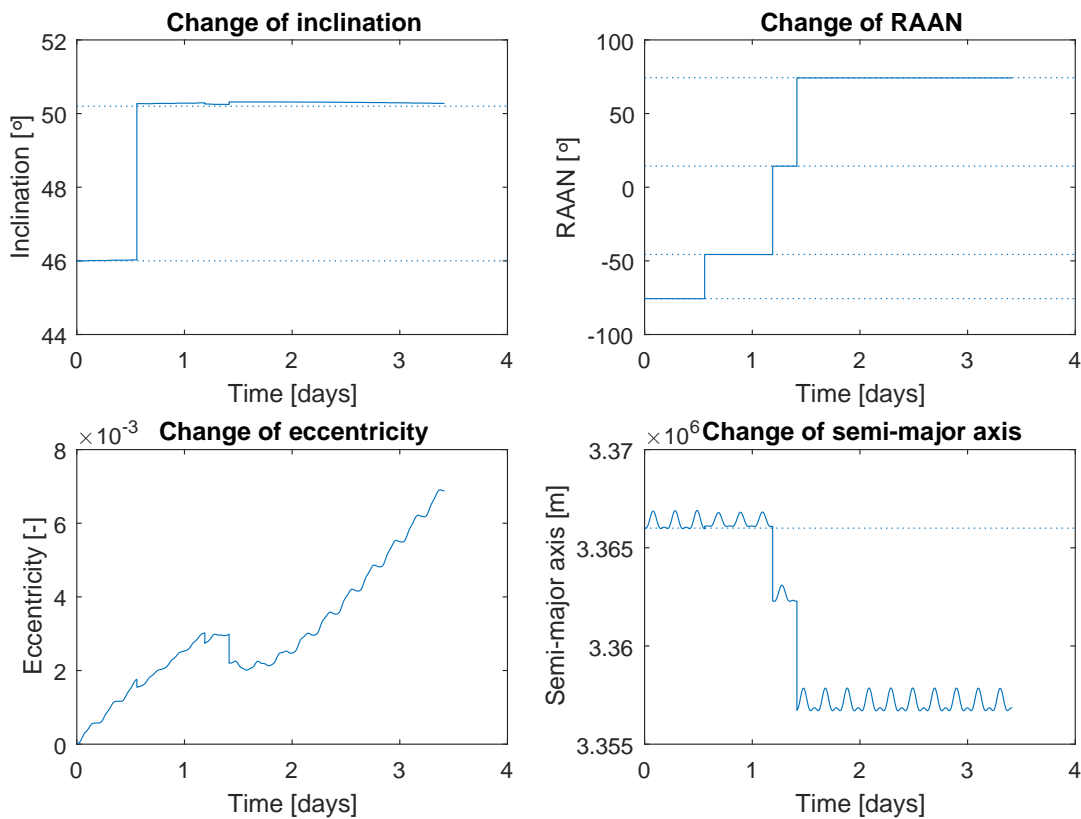


Figure 14.10: Kepler elements during insertion simulated over time. Instant velocity changes are applied to change the orbital planes. The dashed lines show the target elements for each orbit of the constellation.

## 14.4. DEPLOYMENT MOVEMENT SIMULATION

The aim of this tool is to model the orbital motion of the satellites after deployment to ensure that no collisions take place.

### 14.4.1. ASSUMPTIONS

The following assumptions were used to develop this simulation:

- The stiffness of the deployment springs is considered constant. For large deflections, real springs have varying stiffness. However, the deflections here are quite small (on the order of centimeters). This will have a negligible effect on the forces.

<sup>2</sup>[https://downloads.rene-schwarz.com/download/M002-Cartesian\\_State\\_Vectors\\_to\\_Keplerian\\_Orbit\\_Elements.pdf](https://downloads.rene-schwarz.com/download/M002-Cartesian_State_Vectors_to_Keplerian_Orbit_Elements.pdf) Accessed on 26.06.2017

- The satellites are treated as point masses. Since only collision is of importance in this simulation, the specific attitude is not important, as long as their relative distance is not below a minimum safety distance.
- It is assumed that the rotation of the DeVe is not affected by the deployment of the satellites. This assumption does not have an effect on the results, if the attitude control system is used to control the rotational speed of the deployment vehicle.
- All perturbations from the irregular mass distribution of the Moon and the influence from Sun, Earth and other bodies are neglected. As the orbit only needs to be modelled for a few orbital revolutions, the perturbations are not large enough to cause significant differences between the satellites. As they are very close together immediately after deployment, the perturbations affect the individual bodies almost equally.

#### 14.4.2. TOOL DESCRIPTION

The aim of this tool is to model the orbital motion of the satellites after deployment to ensure that no collisions take place. The script takes the following inputs:

- The number, mass and dimensions of the satellites to be deployed at once.
- The stiffness and initial compression of the springs.
- The length of the guiding rails.
- The rotational speed of the deployment vehicle.
- The position and speed in the Moon centred reference frame.
- The delay in deployment of separate satellites.

From this, the tool can be split into two main parts: the phase where the satellites are still constrained by the guiding rails of the DeVe and the phase where they separate and their orbits are modelled to check for collision.

##### DEPLOYMENT

At the start of the simulation, the clamping holding the springs is released, exerting a force on the satellite. This force is determined using Hooke's law:  $F = -k \cdot x$  [54, p. 56]. Where  $F$  is the force produced by the spring in N,  $k$  is the spring constant in  $\text{Nm}^{-1}$  and  $x$  is the deflection of the spring from its neutral state in m. The acceleration can then be determined from Newton's second law of motion. This is then integrated in time to receive the position of the satellite. Once the spring is extended beyond its neutral point, the force exerted on the satellites is zero.

The satellites will still be guided by the guiding rails and are therefore subject to the same rotation as the DeVe. Only once they leave the guiding rails, they are separated and the second part begins.

##### ORBIT MODELLING

The last satellite position and velocity in the DeVe body frame are taken as inputs to this unit. They are then converted to a Moon centred reference frame and then set as starting conditions for an orbit propagator. The "ode113" function of the Matlab toolkit was used to solve the resulting differential equation. This function utilises a variable-step, variable-order (VSVO) Adams-Bashforth-Moulton PECE algorithm [51, p.1-22].

#### 14.4.3. VERIFICATION

##### DEPLOYMENT PHASE

There are three main units that need to be verified: the force calculation unit, the numerical integration unit and the conversion of the state in radial coordinates to Cartesian coordinates.

Two forces need to be computed in order to properly simulate the motion of the satellites within the DeVe: the force due to the spring mechanism and the centrifugal force due to the rotation of the vehicle. The spring force is simply calculated by Hooke's law, given the spring constant and the deflection. In case the deflection of the spring is positive (i.e. the spring is extended), no force is exerted on the satellite, due to them not being connected.

The centrifugal force is calculated by  $F_{cent} = m \cdot \omega_r^2 \cdot r$ , where  $m$  is the mass of the body in kg,  $\omega_r$  is the rotation rate of the reference frame with respect to an inertial frame in  $\text{rad s}^{-1}$  and  $r$  is the distance to the centre of rotation in m [55, p.343]. The other fictitious forces (Coriolis force and Euler's force) are neglected as the supporting structure restricts the motion of the satellite in the directions of these forces and because it is assumed that the rotation rate is constant. These two components of the force calculation unit were tested by simple cases: The spring force calculator was given two test inputs, both with a spring constant of  $500 \text{ Nm}^{-1}$ . For a deflection of  $-0.1 \text{ m}$ , the spring force is  $50 \text{ N}$ . For a deflection of  $0.1 \text{ m}$ , the returned value is zero, as expected. The centrifugal force calculated by the unit was tested similarly. For inputs of  $m = 10 \text{ kg}$ ,  $\omega = 3 \text{ rad/s}$  and  $r = 1 \text{ m}$ , the returned value is  $90 \text{ N}$ , as expected.

In order to determine the correct behaviour of this system of units, two tests were considered: a change in the rotation rate of the DeVe and a change in the spring stiffness.

For an increase in rotation rate the expected behaviour is an increase in the velocity of the satellites as they leave the body of the DeVe due to the increased centrifugal force. Additionally, even though the time spent inside the DeVe is shorter, the angle traversed due to its rotation should be higher.

For an increased spring stiffness, the expected behaviour is similar as the exit velocity will be higher. However, due to the fact that the satellites get pushed out faster, the traversed angle should be smaller.

The results of these tests can be seen in Figure 14.11 and Figure 14.12. The graphs show the path taken by the individual satellites over a time-span of three seconds. In each path, Two distinct phases are visible, one curved and one linear path. The former takes place inside of the DeVe, while the latter occurs when the satellites have left the vehicle.

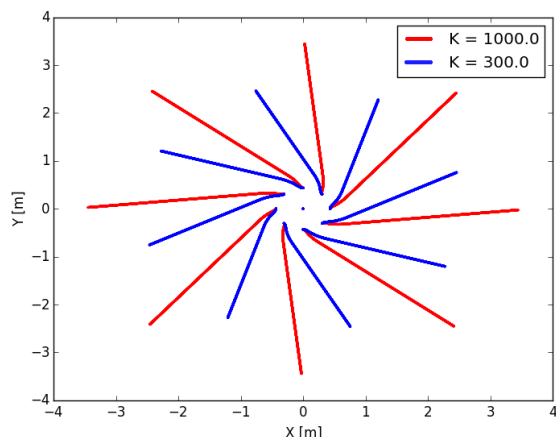


Figure 14.11: The path of the deployment vehicles for two different spring constants ( $K=1,000 \text{ N m}^{-1}$  and  $K=300 \text{ N m}^{-1}$ ) with a rotational speed of 45 degrees/s, simultaneous deployment.

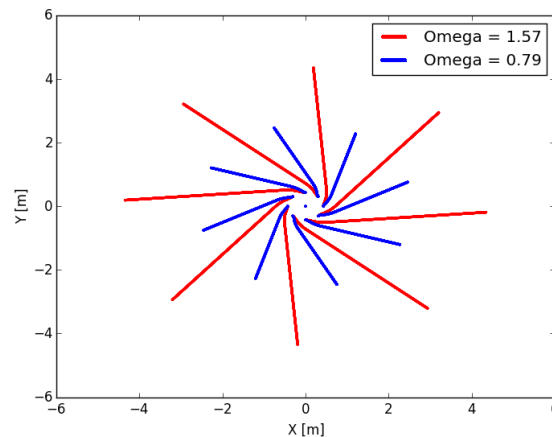


Figure 14.12: The path of the deployment vehicles for two different rotational speeds ( $\Omega=90^\circ \text{ s}^{-1}$  and  $\Omega=45^\circ \text{ s}^{-1}$ ) with a spring constant of  $300 \text{ N m}^{-1}$ , simultaneous deployment.

As can be seen, the behaviour is exactly as expected.

#### ORBIT PROPAGATION PHASE

The orbit propagation phase contains many of the same aspects as the tools used to model the trajectory and therefore was not tested extensively.

The acceleration unit was tested by specifying an input of a position of  $\mathbf{x} = [1, 2, 3,]$  and velocity of  $\mathbf{x} = [4, 5, 6,]$ . The output acceleration of  $-9.36 \text{ m s}^{-2}$  matched exactly with hand calculations.

#### 14.4.4. VALIDATION

At this stage of the design, no validation of this simulation has been performed. Due to the uniqueness of the situation, no data on real positions after deployment is available. If the project is to be realised, the deployment tool should be validated or another (validated) tool should be used to simulate their trajectories after deployment instead of this one.

### 14.5. STRUCTURAL SIZING NSAT (SUPPORT) STRUCTURE

The tool used for structural sizing of the deployment vehicle in the midterm report assumed a supporting structure mass that was 25 % of the mass of the satellites [1, p.29]. This was a large assumption, which this tool aims to rectify by sizing the guiding rails and their connections.

#### 14.5.1. ASSUMPTIONS

- The guiding rails are modelled as beams, clamped to the main column. This neglects the stresses which occur near the connection. Due to the clamping the stresses close to the wall are higher than expected.
- The loads on the rails are modelled as a distributed load across their length.
- The material is uniform and isotropic. In reality, the actual stress will in some locations be slightly higher, in others slightly lower.
- There are no out of plane stresses. Out of plane stresses exist in the structure, but they are very small ( $< 1 \text{ MPa}$ ) and therefore the results will slightly underestimate the actual stress.
- Plane sections remain planar under deformation. It is possible that planar sections warp under the applied stresses, which will increase the stresses experienced by the structure.
- Plane sections remain perpendicular to the beam axis after deformation. The stresses in the real structure are higher due to this assumption because of the additional bending that is neglected.
- The structure is considered thin-walled for the shear analysis. The actual stress will be slightly higher due to the actual thickness, especially at sharp bends and corners.

#### 14.5.2. TOOL DESCRIPTION

The tool sizes the guiding rails which act as the main structural element transferring the loads from the main structure of the DeVe to the satellites. The rails are attached perpendicularly to the main structure and experience the same launch loads as the main structure. The overall tool is therefore very similar to the deployment vehicle structural sizing tool described in the Midterm Report [1, p.29].

Given the loading case, the material and dimensions of the guiding rails, the script first calculates the loading diagrams. These consist of bending, shear and axial force diagrams. The axial force can only be in tension as the individual satellites are not clamped to the guiding rails, therefore they can only pull on the outside plate.

From the diagrams, the most critically loaded cross-section is determined and analysed further. The axial stress is simply  $\sigma_{axial} = F/A$  [56, p.5], where  $F$  is the axial force in N and  $A$  is the cross-sectional area in  $\text{m}^2$ . The bending stress can be calculated to be  $\sigma_{bend} = My/I$  [56, p.486], where  $M$  is the applied bending moment in Nm,  $I$  is the second moment of area of the cross-section in  $\text{m}^4$  and  $y$  is the distance to the neutral axis in m. The most complex stress calculation is due to shear, the general equation of which is given in Equation 14.31 [56, p.540].

$$q_b = -\frac{I_{xx}S_x - I_{xy}S_y}{I_{xx}I_{yy} - I_{xy}^2} \cdot \int t_D x ds - \frac{I_{yy}S_y - I_{xy}S_x}{I_{xx}I_{yy} - I_{xy}^2} \cdot \int t_D y ds \quad (14.31)$$

Where  $I_{xx}$ ,  $I_{yy}$  and  $I_{xy}$  are the moments of inertia in  $m^4$ ,  $S_x$  and  $S_y$  are the shear forces in x and y direction in N,  $x$  and  $y$  are the respective coordinates in m and  $t_D$  is the thickness of the structure at that point in m. This general equation is simplified due to the fact that the product of inertia  $I_{xy}$  is zero, as there two axes of symmetry. Additionally, the discretisation of the structure leads to the integral becoming a cumulative sum. This results in Equation 14.32 [56, p.508].

$$q = -\frac{S_y}{I_{xx}} \cdot \sum_N t_D y_N \Delta s_N - \frac{S_x}{I_{yy}} \cdot \sum_N t_D x_N \Delta s_N \quad (14.32) \quad P_{crit} = \frac{\pi^2 EI}{L^2} \quad (14.33)$$

Once both axial, bending and shear stresses are known, the Von Mises Stress is calculated using equation Equation 14.34.

$$\sigma_{VonMises} = \sqrt{\frac{1}{2}[(\sigma_x - \sigma_y)^2 + (\sigma_x - \sigma_z)^2 + (\sigma_y - \sigma_z)^2] + 3(\tau_{xy}^2 + \tau_{xz}^2 + \tau_{yz}^2)} = \sqrt{\sigma_y^2 + 3\tau_{xy}^2} \quad (14.34)$$

This results in the maximum stress in the structure, for which it can be sized. Furthermore, the guiding rails which are in compression are checked for column buckling using Equation 14.33 [56, p.271].

Where  $P_{crit}$  is the critical load at which the column will buckle in N,  $E$  is the Young's modulus of the material in Pa,  $I$  is the second moment of area of the cross-section in  $m^4$  and  $L$  is the length of the column in m. This critical buckling load is compared to the average stress in the rails (at the location of the highest bending moment) multiplied by the area of one rail. Additionally, the natural frequency of the guiding rail construction is analysed using Equation 14.35 [17, p.454].

$$f_{lon} = 0.25 \cdot \sqrt{\frac{AE}{mL}} \quad f_{lat} = 0.56 \cdot \sqrt{\frac{EI_{min}}{mL^3}} \quad (14.35)$$

Where  $f_{lon}$  and  $f_{lat}$  are the natural frequencies in the longitudinal and lateral direction respectively in Hz,  $A$  is the cross-sectional area in  $m^2$ ,  $E$  is the Young's modulus of the material in Pa,  $m$  is the mass of the beam in kg,  $L$  is its length in m and  $I_{min}$  is the lower of the two moments of inertia of the cross-section in  $m^4$ .

### 14.5.3. VERIFICATION

As there are no new units added to this tool compared to the midterm (all units from the main structural tool were adapted for the guiding rails), no unit tests are performed.

To confirm that this new system works properly, the loading diagrams are checked and compared to hand calculations. If the correct forces and moments are passed to the stress calculation units, the resulting stresses will also be correct. The resulting forces and moments given a satellite mass of 13.73 kg and a loading case of 6 g in the longitu-

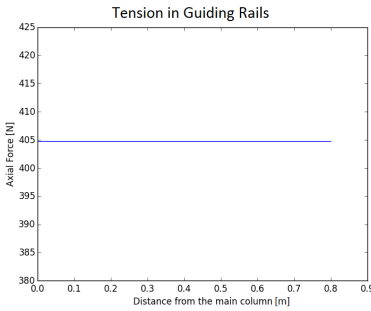


Figure 14.13: Tensile force in the guiding rails, satellite mass of 13.73 kg, 3 g loading

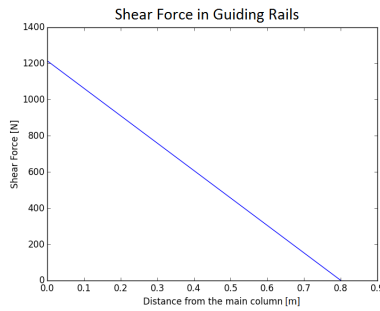


Figure 14.14: Shear force in the guiding rails, satellite mass of 13.73 kg, 9 g loading

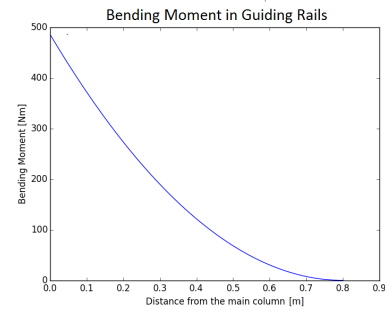


Figure 14.15: Bending moment in the guiding rails, satellite mass of 13.73 kg, 9 g loading

dinal direction of the launcher (the lateral direction of the satellites) and 2 g in the lateral direction of the launcher (longitudinal direction of the satellites). A safety factor of 1.5 is applied to all loads.

The tensile force is simply the lateral loading  $l_f$  factor multiplied with the mass of the satellites  $F_T = m \cdot g \cdot l_f \approx 405$  N, the same as seen in Figure 14.13. Due to the distributed vertical load, the shear force is decreasing linearly. The root shear force is simply the weight of the satellite under the longitudinal loading factor. This turns out to be  $S_{root} = m \cdot g \cdot l_f = 1,212.22$  N. The script calculates a value of 1,214.15 N which is only a difference of 0.15 %.

The root bending moment in this case can be calculated as the weight of the satellites under the loading condition, applied at a moment arm of half the length of the guiding rails. For a guiding rail length of 0.8 m, this results in a moment of  $M_{root} = m \cdot g \cdot l_f \cdot l_{rail}/2 = 484.9$  N m. The difference between this hand calculation and the script results is approximately 0.5 N m or 0.1 %. This can be considered small enough to be verified

#### 14.5.4. VALIDATION

Validation proves to be difficult for the structural design of spacecrafts. Most structures used in industry are custom made and are companies are unforthcoming with their testing data. It is therefore impossible to obtain proper validation data for the structural analysis of a something as novel as a deployment vehicle. This holds as well for the structural design of the ring deployment vehicle (section 14.6).

### 14.6. STRUCTURAL SIZING OF DEPLOYMENT RING

This tool is used in the design of the deployment ring used in the low-energy transfer

#### 14.6.1. ASSUMPTIONS

The following assumptions were used in the structural sizing of the deployment ring:

- The driving loading conditions are the launch loads. This includes vertical and lateral accelerations, as well as induced vibrations. This is an accurate assumption, as the forces experienced during operation are on the order of a few N, whereas the launch will subject the structure to up 6.5 times its own weight hundreds of N).
- There are no out of plane stresses. This will slightly underestimate the stresses.
- Plane sections remain planar under deformation.
- Plane sections remain perpendicular to the beam axis after deformation.
- Uniform, isotropic material. In reality, the actual stress will in some locations be slightly higher, in others slightly lower.
- When the thickness is less than 10 mm, higher order terms such as  $t^2$ ,  $t^3$ , ... can be neglected.
- Minimum thicknesses will be capped at 1 mm to reflect constraints in manufacturing accuracy.
- Loads between the satellite and deployment ring are not dampened by the interface adapter.
- All static loads act through the shear centre of the ring. This insinuates that there is no angle of twist on the ring, which might induce additional shear stresses.

#### 14.6.2. TOOL DESCRIPTION

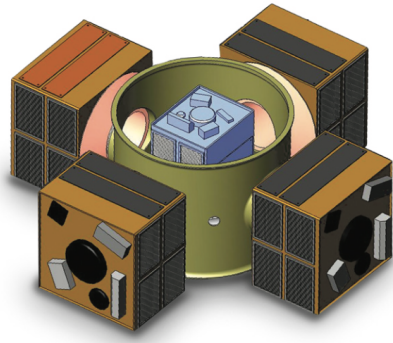


Figure 14.16: Example of a deployment ring: the ESPA Grande by MOOG [57].

Table 14.3: List of inputs required for the structural sizing of the deployment ring.

Required input	Symbol
Outer radius of deployment ring (m)	R
Height of deployment ring (m)	h
Thickness of deployment ring (m)	t
Maximum longitudinal acceleration ( $m/s^2$ )	$S_y$
Maximum lateral acceleration ( $m/s^2$ )	$S_x$
Mass of relay satellites (kg)	$m_{Rsat}$
Material density ( $kg/m^3$ )	$\rho$
E-modulus (Pa)	E
Compressive yield stress (Pa)	$\sigma_c$
Tensile yield stress (Pa)	$\sigma_t$
Shear yield stress (Pa)	$\tau_c$
Location of Rsat's c.o.g. (height, width, depth) (m)	a, b, c

Figure 14.16 shows an example of a deployment ring. This structural tool helps in determining the required variable thickness of the deployment ring in order to withstand the launch loads while remaining light as possible. An overview of the required inputs are listed in table Table 14.3.

Orbital launch vehicle companies provide customers with a user manual in which they indicate the launch loads of their vehicle. These are given in the form of longitudinal and lateral acceleration ( $a_y$ ,  $a_x$ ). The loading situation in Newtons can be derived by multiplying these quantities by the mass of the payload. Therefore, the chosen height, radius, thickness, and material density, along with the mass of of the relay satellites determine the overall loading situation that the structure has to endure. For instance, the force in the longitudinal direction, equals:  $F_{long} = a_y(\rho h \pi (R^2 - (R - t)^2) + 4m_{Rsat})$ . Similarly, the force in the lateral direction,  $F_{lat}$ , is the same except with  $a_x$  instead of  $S_y$ , which is explained in the previous section.

Using these loads, the structure is now checked for various modes of failure. The first of which is failure in bending. The lateral loads from the launch vehicle can induce a bending moment in the deployment ring. The latter is assumed to take the behaviour of a clamped beam and therefore, the experienced stress is shown in Equation 14.36 [56, p.486].  $\sigma_y$  represents the stress experienced in the longitudinal direction due to the bending moment in Pa.  $I$  denotes the moment of inertia, in  $m^4$ , which for a thin-walled ring is approximately  $I = \pi R^3 t$  [58, s. 9].  $x_{max/min}$  represents the distance in the x-direction where the stress experienced by the bending moment is the highest in m. These will occur on the edges of the ring, therefore when  $x_{max/min} = R$ .  $M$  is the overall bending moment that the ring experiences which is  $M = F_{lat}h$ . The resulting stress is then compared against the tensile and yield stress of the material. In most cases, the compressive yield stress is slightly higher than the tensile one, hence it will be used to determine whether the chosen dimensions are resilient to failure in bending.

$$\sigma_y = \frac{Mx_{max/min}}{I} = \frac{MR}{\pi R^3 t} \quad (14.36)$$

$$\sigma = \frac{F}{A} = \frac{F_{long}}{\pi(R^2 - (R-t)^2)} \quad (14.37)$$

Regarding failure in buckling, since it is impossible to conceive of a perfect beam, flawless loading condition and boundary conditions, it is only assumed that the beam will buckle in the first mode. Furthermore, the ring will be modelled as a beam. From this, it is possible to determine the the critical force ( $P_{crit}$ ) at which the ring will buckle in N, which is shown in Equation 14.33.  $E$  represents the elastic modulus of the material used in Pa, and  $L$  denotes the length of the column in m, which in this case is equal to  $h$ . The resulting critical load is compared to the maximum longitudinal force induced by the launcher:  $F_{long}$ . If the latter is lower than the critical load, then the chosen material and dimensions for the ring do not fail in buckling.

Compression is another mode of failure which is considered as the structure could yield simply fail due to the longitudinal acceleration of the launch vehicle. The experienced compressive stress is shown in Equation 14.37 [56, p.5]. This quantity is evaluated against the compressive yield stress of the material to determine whether the chosen dimensions are suitable.

Shear is the final static mode of failure for structural sizing that is considered. As the considered structure is a closed one, it has to be "cut" in order to determine the internal shear flows. This will occur where the axis of symmetry aligns with the load as may be seen in Figure 14.17. The internal shear flows can then be determined using Equation 14.31 [58, s. 9-13].  $q_s$  represents the internal shear flow in  $Nm^{-1}$ , and since the ring has more then one axis of symmetry,  $I_{xy} = 0$ . Furthermore, the thickness may be taken out of the integral as it is constant. After all internal shears have been determined, the cut can be closed by applying a constant shear flow ( $q_{s0}$ ) which balances the torque around the section, shown in Equation 14.38 [56, p.550]. The maximum shear flow in the section may then be determined and divided by the local thickness to determine the shear stress:  $\tau = q/t$  [56, p.536]. This is then compared to the material's shear yield stress to determine whether it fails in shear.

$$\oint p q_s ds + 2Aq_{s0} = 0 \quad \rightarrow \quad q_{s0} = -\frac{R \oint q_s ds}{2\pi(R^2 - (R-t)^2)} \quad (14.38)$$

The loading of the relay satellites on the ring is also considered. The mass and weight they impose on the structure is translated into shear and moment forces as seen in Figure 14.18. Their weight acts directly through their centre of gravity, and is hence heavily dependent on their dimensions and mass distribution. The moments that the satellites impose on the structure are broken down into a set of coupled forces  $F_c$  represented by Equation 14.40 [56, pp.591-593]. Where  $M$  denotes the moment load on the ring by the relay satellite in Nm, and  $L$  is the height of the satellite in m (either  $a$ ,  $b$ , or  $c$  from Table 14.3). This force is then divided over the associated area of the ring to obtain the stress, which is then compared to the yielding values of the material.

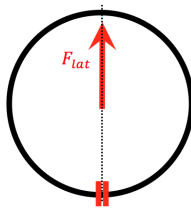


Figure 14.17: Location of cut to determine shear flows in ring.

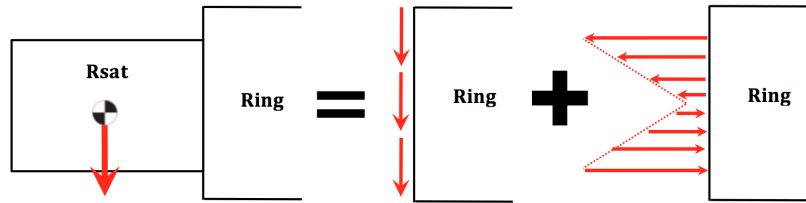


Figure 14.18: Loading considerations from Rsats on deployment ring.

The final structural analysis that is conducted on the ring is vibration and frequency analysis. If the natural frequencies of the ring in the lateral and longitudinal directions are lower than the specified ones in the launcher, then the structure will not fail due to resonance. Equation 14.39 shows the natural frequencies in the lateral and longitudinal directions ( $f_{lat}$  and  $f_{long}$ ) [17, p.454]. Where  $m$ ,  $A$ , and  $h$  denote the mass in kg, area in  $m^2$ , and height in m of the ring respectively. In-plane bending is the final frequency analysis that is conducted and proves to be quite sensitive for thin-walled rings. This analysis considered that the ring is free-floating and not fixed which isn't entirely accurate as it will be attached to the launcher therefore will not be as susceptible to resonating in this mode. The frequency for in-plane bending ( $f_{IPB}$ ) is shown in Equation 14.41 [59, p.3], and will be evaluated against the launcher's maximum lateral frequency of vibration.

$$f_{lat} = 0.560 \sqrt{\frac{EI}{mh^3}} \quad f_{long} = 0.250 \sqrt{\frac{EA}{mh}} \quad (14.39)$$

$$F_c = \frac{M}{L} \quad (14.40) \quad f_{IPB} = \frac{6}{\pi 4R^2 \sqrt{5}} \sqrt{\frac{Et^3}{3\rho}} \quad (14.41)$$

If the chosen dimensions for the deployment ring are such that the structure does not fail, then it can concluded that the dimensions are adequate.

### 14.6.3. VERIFICATION

Most of the considered structural loading scenarios may be simply verified by hand calculations, especially in the cases of bending, buckling, and compression. The case of shear is a unique one because the singular shear force acts

through the shear centre which is the geometrical centre of the ring, and the cut is made along the vertical axis. Because of this situation, there is no induced moment on the entire structure and the constant shear flow that has to be applied at the end to balance said moment is equal to zero:  $q_{s0} = 0$ . This proves to be a simple verification method for the case of shear, which the program abides to.

As the ring will likely be a short and stubby structure meaning that  $h$  is small ( $< 1$  meter), it is more likely to fail in compression before it fails in buckling since  $P_{crit} \propto \frac{1}{h^2}$  (Equation 14.33). Therefore if the model suggests that the considered structure fails in buckling but not compression, then there is likely an error.

The location and magnitude of the maximum Von Mises stress can also prove to be an apt method of verification. The latter is defined in Equation 14.34 [56, p.9]. Since the considered loading case only results in direct stresses in the longitudinal direction ( $\sigma_y$ ), and shear stresses in the lateral direction ( $\tau_{xy}$ ), the expression for the Von Mises stresses may be simplified accordingly. The model may now be verified by comparing its maximum Von Mises stress to that generated by a FEM in Catia (Figure 14.19). The chosen parameters and results may be seen in Table 14.4. With a relative error of only 3.26%, the developed model is considered verified.

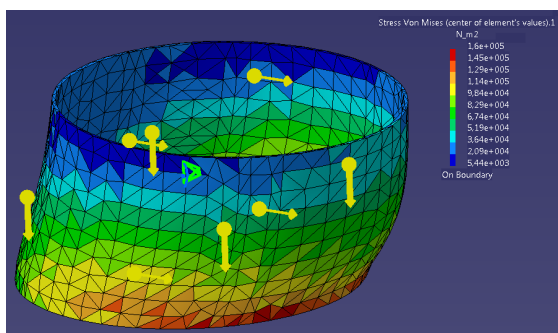


Figure 14.19: Catia FEM analysis

Table 14.4: Parameters used in ring verification.

Entity	Value
Outer radius of deployment ring	0.5 m
Height of deployment ring	0.6 m
Thickness of deployment ring	0.01 m
Maximum longitudinal acceleration	6.6g
Maximum lateral acceleration	1.1g
Mass of relay satellites	0.0 kg
Material density	$2,810.0 \text{ kg/m}^3$
E-modulus	71.7 GPa
Maximum Von Mises from Model	$1.53 \times 10^5 \text{ Pa}$
Maximum Von Mises from FEM	$1.58 \times 10^5 \text{ Pa}$
<b>Relative error</b>	<b>3.26 %</b>

#### 14.6.4. VALIDATION

Please refer to the Validation section of section 14.5.

### 14.7. STRUCTURAL SIZING OF THE NSAT PRIMARY STRUCTURE

This tool is developed to analyse the stresses in the primary structure of the network satellite and therefore size it accordingly. This is done so it does not fail when the limit load case is applied to it. Furthermore, this tool sizes the structure for stiffness and strength. In the following paragraphs the main assumptions are listed and then the tool is described in terms of the equations used and the necessary inputs needed for it to function.

#### 14.7.1. ASSUMPTIONS

- It is assumed that there are no out of plane stresses.
- Thin walled structures assumed and hence all the higher terms of thickness such as  $t^2, t^3$  can be considered to be approximately zero.
- While analysing the cylindrical primary structure of the satellite, all the thickness variations are neglected and the structure is assumed to have a constant thickness 't' along the entire cross section.
- The entire structure is isotropic and uniform. In reality minor defects are present causing stress concentrations. This causes the tool to slightly underestimate the stresses.
- Plane sections remain plane and perpendicular to the beam neutral axis after it has been deformed.
- The applied load on the cylindrical primary structure of the network is assumed to be distributed over the entire length of the structure.

#### 14.7.2. TOOL DESCRIPTION

##### COORDINATE SYSTEM AND STRUCTURE RESTRAINS

In Figure 14.20 a coordinate system is displayed to define the stresses in. Moreover, the figure also shows the chosen structural constraints. It is assumed that the structure is clamped at 0.1 m intervals. This is where the structure is supported by the rigid structure to the rest of the satellite.

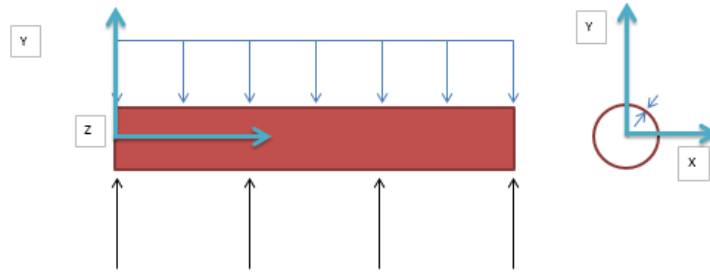


Figure 14.20: Coordinate system of the Nsat primary structure tool

### SHEAR AND BENDING DIAGRAMS

The developed tool begins by analysing the internal loads in the structure. This is done after the limit load case parameters are input in the tool as is the length of the structure. The results are then given in terms of shear and moment diagrams like the ones shown in the the example [Figure 14.21](#). This gives a first indication to where the most critical locations of the structure are.

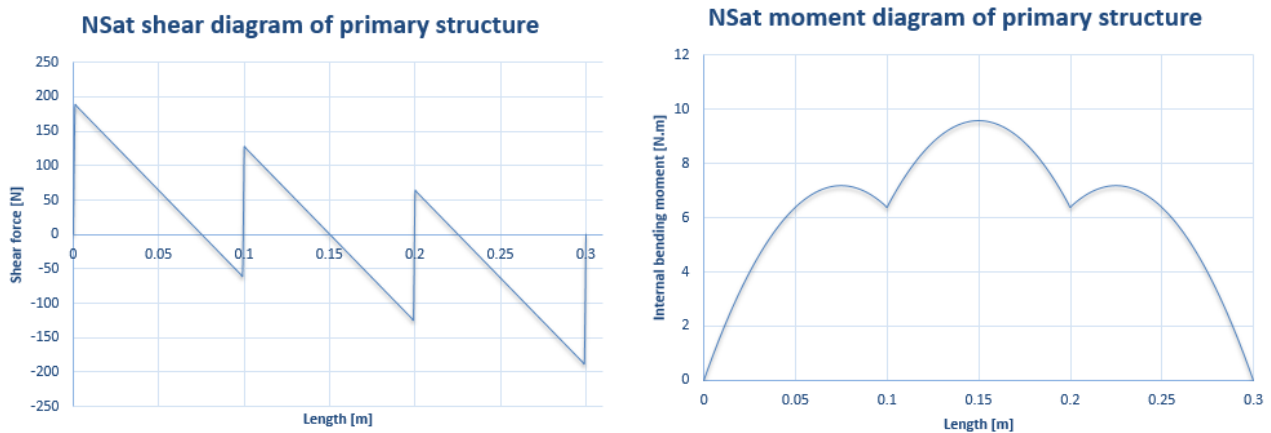


Figure 14.21: An example of the Shear and moment diagrams of the primary structure at a given load case

### SIZING FOR STRENGTH

After the load case has been defined, the shear and moment diagrams are generated. The tool computes the bending stress at different locations along the entire length of the structure. This is done using [Equation 14.36](#), which is defined earlier. The same formula ( $I = \pi R^3 t$ ) is also applicable for the area moment of inertia of the cross-section as the thin wall assumption still holds. This stress is then compared to the tensile/compressive yielding stress of the selected material to see if the structure fails under bending. The shear stress is then calculated throughout the cross section of the structure, using the same method as described in [section 14.6](#).

### SIZING FOR STIFFNESS

After the structure has been sized for strength, it is sized for stiffness by performing a vibrational and frequency analysis to make sure that the natural frequency of the primary structure is not reached in the lateral direction nor the longitudinal direction during the limit load case. This can be assured by inputting the structure's dimensions and the material's characteristics in the tool, which then uses [Equation 14.39](#) and [Equation 14.41](#) to compute the natural frequencies of the structure. If these frequencies are lower than that of the limit load case, it is concluded that the structure is sized for stiffness.

### 14.7.3. VERIFICATION

The entire verification of the tool is done by unit testing, this means that every sub-component of the tool is checked by doing hand calculations. To start with, the shear and moment diagrams are constructed by hand after deriving the necessary equations to do so and then it is checked if the tool developed gives the same results. As a second verification step, the diagrams are compared with results from already existing online tools and the results match. Moreover, the bending stress calculator part of the tool is verified, by randomly choosing a position on the primary cylindrical structure and calculating the bending stress at that location by hand to find if the results match. The same is done for the shear stresses and therefore it is concluded that the unit is verified. After all the units are verified, the entire tool is system tested to make sure that the flow of inputs and outputs is running the correct way. Only then it is possible to conclude that the entire tool is verified. This verification process is quite similar to the one discussed in [subsection 14.6.3](#).

#### 14.7.4. VALIDATION

Please see the validation section of [section 14.5](#).

### 14.8. WEIBULL PROCESSOR

This tool is used in the reliability analysis of the satellites.

#### 14.8.1. ASSUMPTIONS

Over a span of five years, a sampling rate of once per day will result in sufficiently accurate results. With this sampling rate, 1825 data points are present. This leads to smooth curves and a negligible discretisation error.

#### 14.8.2. TOOL DESCRIPTION

Before a constellation reliability analysis can be conducted, the probability of a satellite failing at a certain point has to be known for each point in time. This can be done in the form of a hazard function. The hazard function displays the probability of the failure of a satellite that has functioned up to a certain time. The inverse of this function gives the probability that this satellite survives. The input of this function is the lifetime to be analysed and a reliability curve. Various reliability curves are obtained from statistical data compiled from several databases [16, 60]. For this function, statistical data on small satellites (10 kg to 500 kg) is used, which have a successful orbit insertion. From the statistics, a Weibull function can be fitted, representing the reliability distribution of a single satellite over its lifetime. Together with the derivative of this function (the failure probability density function), the hazard function can be determined as shown in [Equation 14.42](#) [61, p. 2]. Here,  $R$  is the reliability function,  $t$  is the time in days,  $f$  is the probability density function, the derivative of  $R$  and  $h$  is the hazard function. In [Table 14.5](#), the values of the 2-Weibull mixture can be found with their meaning. The first term is responsible for the infant failure with a negative exponential shape ( $\beta_1 > 1$ ). This term has a very high weight compared to the second term, causing the infant failure to be strongly visible in [Figure 14.22](#). The second term is responsible for the wear-out stage. The influence of this term can be seen close to the end of life of the satellites, where the hazard curve decreases a bit and the slope of the Weibull curve becomes more negative. The value of the inverse hazard function at each day during the constellation lifetime is given as a final output.

$$R = \alpha \cdot e^{-\left(\frac{t}{\eta_1}\right)^{\beta_1}} + (1 - \alpha) \cdot e^{-\left(\frac{t}{\eta_2}\right)^{\beta_2}}$$

$$f = \frac{dR}{dt} = \alpha \cdot \frac{\beta_1}{\eta_1} \cdot \left(\frac{t}{\eta_1}\right)^{\beta_1-1} \cdot e^{-\frac{t}{\eta_1}^{\beta_1}} + (1 - \alpha) \cdot \frac{\beta_2}{\eta_2} \cdot \left(\frac{t}{\eta_2}\right)^{\beta_2-1} \cdot e^{-\frac{t}{\eta_2}^{\beta_2}} \quad (14.42)$$

$$h = \frac{f}{R}$$

Table 14.5: Parameters of the 2-Weibull mixture used in the reliability analysis [16].

Parameter		Values
Relative weight parameter	$\alpha$	0.9607
First term shape parameter	$\beta_1$	0.2101
Second term shape parameter	$\beta_2$	2.754
First term scale parameter	$\eta_1$	$10^7 \cdot 365$ days
Second term scale parameter	$\eta_2$	$7.3 \cdot 365$ days
Regression fit quality	$R^2$	0.9757
Sum of the squares of errors	SSE	0.9438

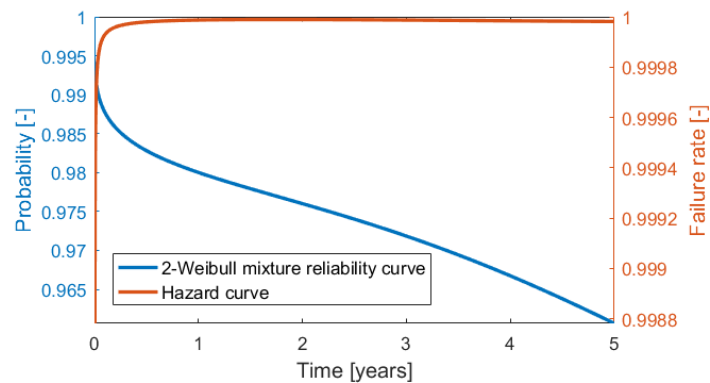


Figure 14.22: Weibull probability curve with hazard function

#### 14.8.3. VERIFICATION

The only calculation that the Weibull processor does, is the creation of the Weibull curve and hazard function shown in [Equation 14.42](#). This is verified by calculating the values of specific points on these curves manually and comparing them to the output of the function. The results of this can be seen in [Table 14.6](#). No errors are observed, so it can be concluded that the manual and automatic calculation corresponds.

#### 14.8.4. VALIDATION

Validation for this function is not considered, since this function on its own does not have any practical application. The fact that this function is mathematically sound, is deemed sufficient to use its output for other functions.

### 14.9. MONTE CARLO SIMULATION: ADJACENT PLANE FAILURE ANALYSIS

This tool is used in the reliability analysis of the constellation. To quantify the reliability of the constellation, a Monte Carlo simulation is conducted. For each satellite, a value between zero and one determines the probability that the

Table 14.6: Verification data of the Weibull processor

t [days]	Reliability function			Inverse probability distribution function		
	manual calculation	tool output	difference	manual calculation	tool output	difference
1	0.99064	0.99064	0	0.99804	0.99804	0
75	0.97697	0.97697	0	0.99994	0.99994	0
400	0.96722	0.96722	0	0.99998	0.99998	0
1000	0.95811	0.95811	0	0.99999	0.99999	0
1825	0.94381	0.94381	0	0.99998	0.99998	0

satellite has survived up to then, and fails in that time instance: the hazard rate. Then a random number is taken from a random number generator. If this number is higher than the inverse of the hazard rate, the satellite has failed. Expanding this for the entire constellation and drawing a random sample for each satellite for each day in the constellation operational lifetime, results in one lifetime sample. Increasing the amount of samples and averaging the outcome, results in a Monte Carlo simulation.

### 14.9.1. ASSUMPTIONS

The following assumptions are made for this tool development:

- Over a span of five years, a sampling rate of one day will give in accurate results. This results in 1825 datapoints which have a negligible discretisation error.
- Satellite failure is instantly detected. If this were not the case, it would take longer for the constellation to reestablish N-1 redundancy, increasing the probability of a system failure. Since communication goes with the speed of light, detection of a non-communicating satellite should be done in the order of seconds at maximum. Since the sampling rate is in days, this is negligible.
- A spare satellite can replace a broken satellite within 10 days (maximum phase change of 180°). If this were longer it would take longer to restore N-1 redundancy, increasing the probability of a potential system failure. The Nsats are capable of doing a phasing manoeuvre within 10 days.
- Infinitely many spares are present. This part of the reliability analysis does not take into account the fact that the amount of spares is actually limited. This reduces the amount of system failures observed since spares are always present. This assumption is only valid if in another part of the analysis, the influence of the fact that the amount of spares is limited, is taken into account.
- Each satellite starts in fully functional conditions. This is an assumption that originates from the Weibull dataset that is used for this analysis. If a satellite failure before deployment does occur, this will increase the likelihood of a system failure occurring since the amount of spares is reduced.
- N-1 coverage redundancy in the entire constellation. This is proven during the constellation design. Single satellite failures have no impact on the performance.
- Only adjacent satellite failures in adjacent planes affect the constellation performance, adjacent in-plane failures have no impact. This eliminates the detection of some system failures. This is done since this part of the analysis is responsible for detecting a particular type of system failures. The other type of failure is taken into account in a later stage of the reliability analysis.

### 14.9.2. TOOL DESCRIPTION

In this analysis, the Monte Carlo simulation goes over each day in the lifetime of the constellation, which consists of six orbit planes with 6 active satellites in each plane. For each day a random sample between zero and one is drawn for each active satellite in the constellation. If this sample is larger than the value from the hazard function for that day, the satellite has failed. The lifetime cycle of the constellation is simulated for  $n$  times, creating  $n$  samples for each day of the constellation lifetime. This data can then be analysed to quantify the reliability of the constellation.

The adjacent plane failure analysis consists of a Monte Carlo simulation for the full constellation (6x6 satellites). This is then constrained to only register adjacent plane failures as system failures to analyse this particular type of failure. The final output will show the probability of a satellite failing next to another failed satellite in another plane. Additionally, the amount of time that adjacent failure occurred and the area affected by this failure is determined. An example of the output of this function can be seen in [Figure 14.23](#).

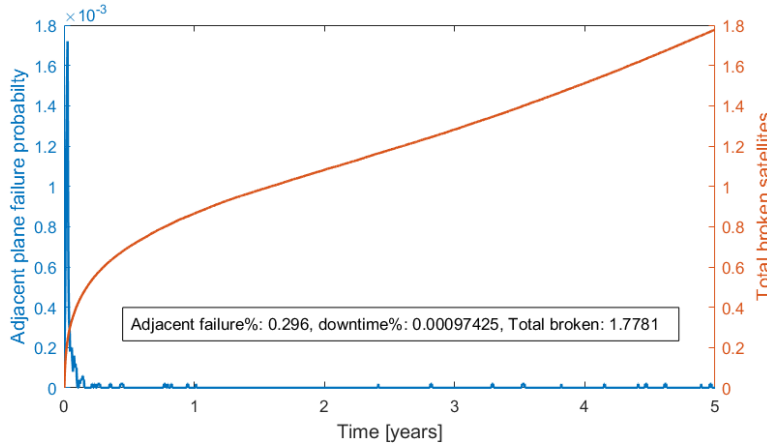


Figure 14.23: Output example of the adjacent plane satellite failure analysis.

Samples	Adjacent failure %	Downtime %	Total broken satellites
10	0	0	2
100	0	0	1.74
1,000	0.2	0.00049315	1.802
10000	0.31	0.0011507	1.7818
50000	0.296	0.00097425	1.7781

Table 14.7: Convergence of outputs.

### 14.9.3. VERIFICATION

A simple check whether the data is handled properly is conducted by running the simulation multiple times with different amount of samples. Some inconsistency in results is expected since the results are based on the Matlab random number generator. However, when using a large amount of samples, a convergence in values should be seen according to the law of large numbers [62, p. 184]. If the output results vary significantly, there is an error in the data manipulations. The results of this can be found in Table 14.7. Due to the low failure probability and the fact that only adjacent plane failures are observed, no downtime is observed for a lower amount of samples. It can be seen that all the values converge for a higher amount of samples. Here one sample equals one run through the lifetime of the constellation. Furthermore, if the Monte Carlo simulation is properly implemented, a direct correlation of the failure probability and average number of failed satellites should be found if a large amount of samples is taken (law of large numbers). This fact is used as a verification method for the Monte Carlo simulation using Equation 14.43. The results of this can be found in Table 14.8. Here the average amount of satellites is calculated directly by integrating the hazard function over time and multiplying it by the number of satellites in the simulation. It can be clearly seen that the Monte Carlo simulation gives the expected overall results.

Table 14.8: Verification results of the adjacent plane failure Monte Carlo analysis

$$N_{fail} = N_{sat} \cdot \int_t h(t) dt \quad (14.43)$$

Average satellites failed after 5 years		
Simulation (50,000 samples)	Calculated	Difference
1.7781	1.78364	-5.54E-3

### 14.9.4. VALIDATION

Satellite failure statistics are used as an input for this Monte Carlo simulation. Since no other validation data is available, validation of this tool is not possible.

## 14.10. MONTE CARLO SIMULATION: IN-PLANE FAILURE ANALYSIS

This tool is used in the reliability analysis of the satellites.

### 14.10.1. ASSUMPTIONS

- Over a span of five years, a sampling rate of one day will result in sufficiently accurate results. Again, this results in 1825 datapoints per sample which produces smooth results with negligible discretisation errors.
- A satellite failure is instantly detected. Since the signals between the satellites travel with the speed of light, a failure can be detected and confirmed in a matter of seconds. The sampling rate is in the order of days, making the failure detection time negligible.
- A spare satellite can replace a broken satellite within 10 days (maximum phase change of 180°). If this were longer it would take longer to restore N-1 redundancy, increasing the probability of a potential system failure. The N<sub>sats</sub> are capable of doing a phasing manoeuvre within 10 days.
- N-1 coverage redundancy in the entire constellation. This is proven during the constellation design. Single satellite failures have no impact on the performance.
- Sending new spares to the constellation from Earth to a desired network orbit takes 182 days or 6 months maximum. This is conform the requirement of maximum constellation element replacement time. The maximum is assumed although it is expected that faster delivery of satellites is possible.
- Each launch of new spares can deliver an amount of satellites to each orbital plane if desired. This allows for flexibility in the amount of satellites added to each plane based on the satellite failures in each plane.

**14.10.2. TOOL DESCRIPTION**

The in-plane failure analysis uses a similar Monte Carlo simulation as the adjacent plane failure plane tool described in section 14.9. This time only one plane consisting of 6 satellites is simulated, rather than the entire constellation. Also, this tool no longer works under the assumption of unlimited spares present and therefore has to keep track of the amount of spares available in the orbital plane. The relevant inputs are the amount of spare satellites present per plane after constellation deployment and the threshold of amount of spares when a new spares launch from Earth is requested. The outputs are the average broken satellites, launches required and spares in orbit throughout the constellation lifetime. Also the in-plane system failure probability is given over the constellation lifetime. This can be seen in Figure 14.24. Furthermore, histograms are made for the probability of occurrence of an amount of failed satellites and launches after 5 years. Also the occurrence probability of a minimum amount of spares present in the plane throughout the constellation lifetime is given. These outputs are shown in Figure 14.25. This tool can also be used to optimise the spares configuration per plane. This is done by looping the Monte Carlo simulation itself with different input parameters.

A data storage optimisation has been conducted to allow higher amount of samples with the available amount of RAM memory by reducing the amount of data stored per sample without losing information.

Table 14.9: Convergence data in-plane Monte Carlo simulation (2 initial spares, 2 new spares are launched when 0 spares remain)

Samples	Avg spares	Avg launches	Avg satellite failures	Any system failure in lifetime%	Downtime %
10	1.9	0	0.1	0	0
100	1.71	0	0.29	0	0
1,000	1.793	0.039	0.290	0	0
10,000	1.759	0.0306	0.3036	0.02	1.6438E-5
50,000	1.7636	0.03096	0.29944	0.066	2.2795E-4
100,000	1.7666	0.03027	0.29517	0.044	1.726E-4

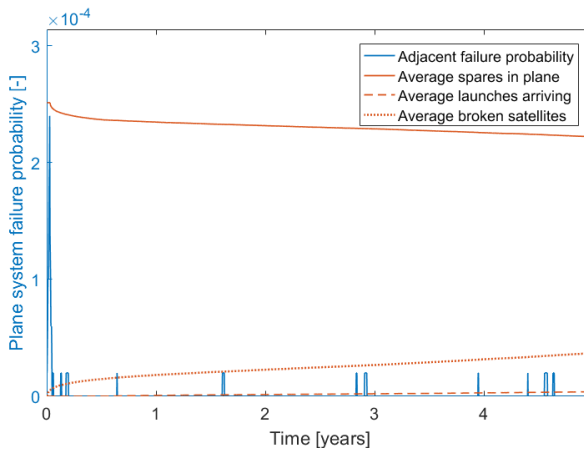


Figure 14.24: Averaged in-plane analysis data from 50,000 lifetime cycles (2 initial spares, 2 new spares are launched when 0 spares remain)

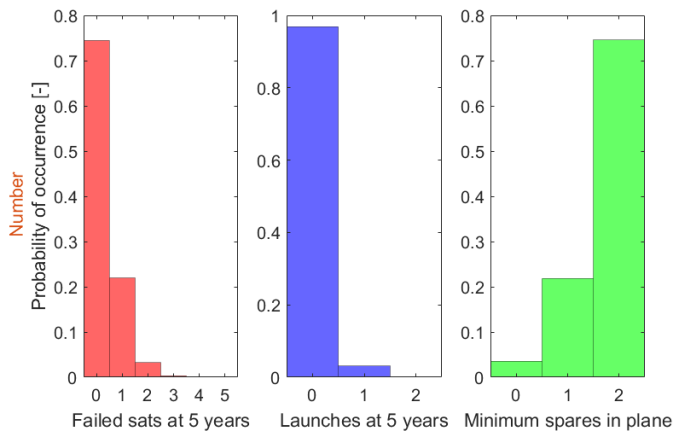


Figure 14.25: In-plane analysis statistics from 50,000 lifetime cycles (2 initial spares, 2 new spares are launched when 0 spares remain)

**14.10.3. VERIFICATION**

Similarly to the adjacent plane Monte Carlo simulation, the convergence of this tool is checked with increasing samples. The results of this can be seen in Table 14.9.

**14.10.4. VALIDATION**

Satellite failure statistics are used as an input for this Monte Carlo simulation. Since no other data has been found, this tool can not be validated.

**14.11. DISTURBANCE TORQUES CALCULATOR**

Identifying the disturbance torques acting on the spacecraft during its operations is an essential step that has to be taken. This will enable the sizing of a reliable control system to counteract these disturbance and achieve a controlled attitude.

**14.11.1. ASSUMPTIONS**

- It is assumed that both of the relay and network satellites are not influenced by Earth’s magnetic field. This is a safe assumption to make as both orbits are out of the magnetic sphere of influence of Earth.
- Considering the size of the relay satellite, its fairly symmetric geometry and its distance away from Earth and the Moon at an L1 halo orbit, it is safe to assume that the gravity gradient induced torques on the relay satellites are negligible.
- Induced torques due to atmospheric drag are not applicable to both the relay satellite and network satellite. This is an accurate assumption to make because of the absence of atmosphere at these orbits.

- The distance between both satellites and the Sun is assumed to be 1 AU at all times while calculating the disturbance torques. This is a safe assumption to make because the orbits considered are periodic and the changes in orbital altitude are negligibly small when compared to the distance from the Sun.
- When considering the gravity gradient induced torques acting on the network satellite, an angle of  $1^\circ$  can be assumed to be the misalignment between the centre of gravity and centre of mass, due to the satellite's small size and symmetry. This assumption was retrieved from SME [11, p.572].

### 14.11.2. TOOL DESCRIPTION

#### BODY-AXIS SYSTEM

Before determining the disturbances acting on the spacecraft, a body axis system has to be defined. By doing so the characteristics of the spacecraft can be defined. It will also later be used to describe the orientation and the attitude of the spacecraft with respect to another fixed frame. The body axis used for both the Rsats and Nsats is illustrated in Figure 14.26. For the Nsats the Z-axis is pointing towards the surface of the Moon while the Y-axis is parallel to the longitudinal axis of the solar arrays.

#### SOLAR RADIATION PRESSURE INDUCED TORQUES

To calculate the disturbance torques exerted on the satellites due to the solar radiation, the factors affecting this torque have to be identified. The momentum transferred by the solar radiation is dependent on the solar flux  $\Phi$  which in turn is dependent on the relative position of the spacecraft with respect to the Sun. This means that the higher the solar flux, the stronger the disturbance torque will be. It is also important to take into account the reflectivity  $q$  of the satellite, the higher that factor is, the greater the disturbance torques will be on the spacecraft. In addition to these factors, the disturbance torque is also dependent on incident angle  $\varphi$  of the solar radiation and the distance between the radiation centre of pressure of the illuminated area and the centre of pressure ( $cp_s - cm$ ). The relation between all these factors and the overall solar pressure disturbance torque is given by Equation 14.45 which is extracted from SME [11, p.571]. The developed tool requires the user to input the maximum radiated area possible which is normal to Sun's radiation during the satellite's orbit and the maximum solar flux at the satellite's orbit. The tool then computes the solar radiation pressure induced torques for different reflectivity factors and different shifts between the centre of mass and the centre of pressure of the radiated surface and generates graphs of the results. An example output of the tool is shown in Figure 14.27.

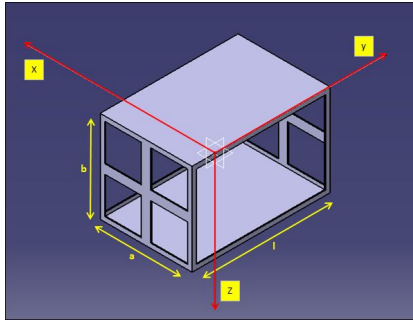


Figure 14.26: Body-axis system of the satellites

$$\begin{aligned} T_{gx} &= \frac{3\mu}{2R} |I_z - I_y| \sin(2\theta) \\ T_{gy} &= \frac{3\mu}{2R} |I_z - I_x| \sin(2\theta) \\ T_{gz} &= \frac{3\mu}{2R} |I_x - I_y| \sin(2\theta) \end{aligned} \quad (14.44)$$

$$T_s = \frac{\Phi}{c} A_s (1 + q) (cp_s - cm) \cos\varphi \quad (14.45)$$

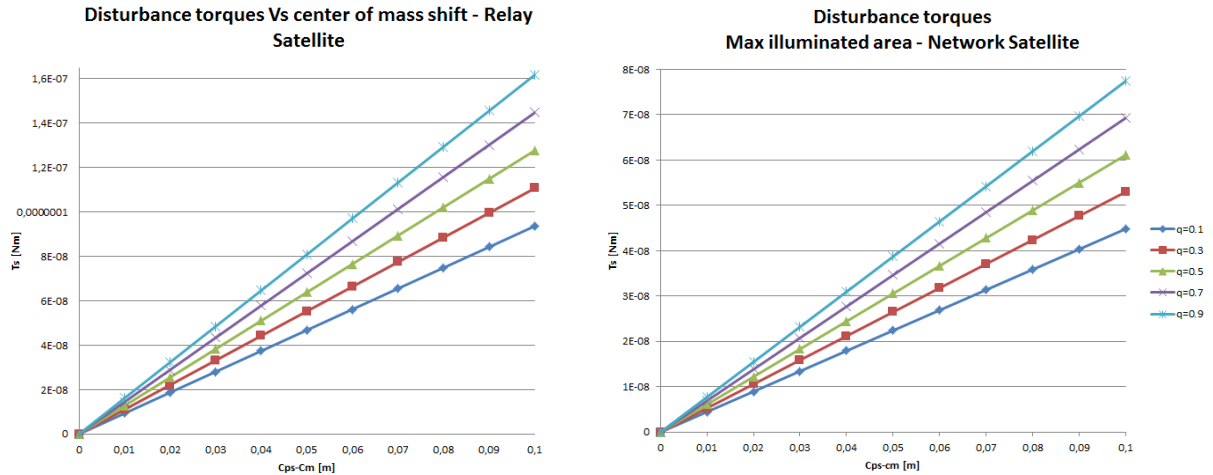


Figure 14.27: Solar pressure disturbance torques vs the shift in centre of mass at different reflectivity factors, (right) relay satellite, (left) network satellite

### GRAVITY GRADIENT INDUCED TORQUES

The disturbance torques generated by the gravity gradient are caused when the centre of gravity of the satellite is not aligned with the centre of mass with respect to the local vertical. This part of the tool requires the geometrical characteristics and the estimated mass of the satellite where it uses them to calculate the mass moment of inertia. It also needs the orbital altitude and gravitational constant of the Moon. It then uses all these inputs to compute the gravity gradient induced disturbance torques by applying the relation given by Equation 14.44, adapted from SME [11, p.573].

#### 14.11.3. VERIFICATION

The verification of this tool is straight forward, as it only uses simple mathematical relations. The tool is unit tested by using two hypothetical satellite parameters acquired from SME[11] as inputs. These geometric and orbital parameters are given to the tool and the disturbance torques are computed. The results match the results from [11], which indicates that the tool is functioning properly. Just to be sure, every sub-component of the tool is checked by doing hand calculations. After all that proves successful, it is safe to conclude that the tool is verified.

#### 14.11.4. VALIDATION

Since this mission is unique and nothing similar has ever been achieved, finding data to compare with the current findings is not possible. So it is impossible to validate this tool at the time being. As for the future, it is recommended to simulate the disturbances torques acting on the satellite with more refined and detailed models to get a better estimate of their magnitude.

## 14.12. REACTION WHEELS AND THRUSTERS SIZING TOOL

This tool is used to size the different components of the ADCS of the different vehicles.

### 14.12.1. ASSUMPTIONS

- The reaction wheels are used to slew the spacecraft when needed and to counteract the disturbance torques, this means that the thrusters are only used to dump the momentum built up by the reaction wheel.
- While estimating the amount of momentum stored in the reaction wheels due to solar disturbances, it was assumed that the maximum momentum accumulates every  $\frac{1}{4}$  of an orbit. This is a simplification adapted from SMAD [11, p.581].
- Equation 14.46 assumes no resisting momentum for max acceleration slews. But since the spacecraft considered in this mission does not require sudden changes of attitude, it is assumed that there will be no resisting momentum and hence it is safe to use this equation.

### 14.12.2. TOOL DESCRIPTION

#### REACTION WHEELS

As mentioned in the assumptions the reaction wheels are used to slew the spacecraft and therefore they should be able to supply the necessary torque to do so. The developed tool requires the slew rate as an input and then it calculates the slewing torque using Equation 14.46 which is adapted from [11, p.581].

$$T = 4 \cdot \theta \cdot \frac{I}{t^2} \quad (14.46) \quad h_{rw} = T_D \cdot P \cdot \frac{0.707}{4} \quad (14.47)$$

It is then checked if the chosen reaction wheel can provide that torque and then it is sized for its momentum storage capabilities. The amount of momentum stored in a reaction wheel is calculated by this tool using Equation 14.47 after inputting the orbital period of the spacecraft. It also requires the magnitude of the dominant disturbance torque which is an output of the disturbance calculator tool.

The tool then generates the graphs in Figure 14.28. The graphs illustrates the amount of momentum building up in the reaction wheels over the number of orbits due to the disturbance torques. When choosing the reaction wheel it can be decided how often is it necessary to fire the thrusters to dump the momentum.

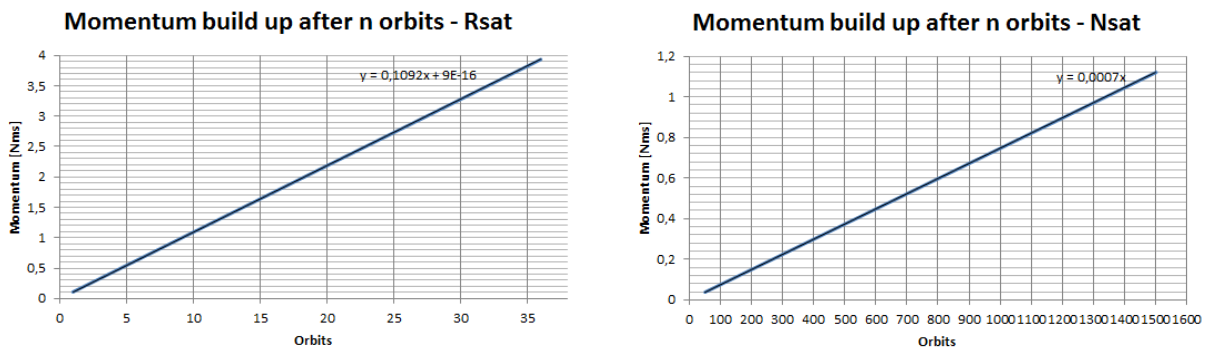


Figure 14.28: Solar pressure disturbance torques vs the shift in centre of mass at different reflectivity factors, (left) relay satellite, (right) network satellite.

### THRUSTERS

After using the previously described tool to size the reactions wheels, the thrusters needed to complete the active control process of both satellites have to be sized. The tool developed to do so is described below.

The chosen thrusters should be able to provide a thrust level that is able to counter the worst-case disturbance, this is simply done by dividing the torque by the moment arm of the thruster  $F = \frac{T_D}{L}$ . It is important to note that this thrust level won't be used to size the thrusters, but the momentum dumping requirements will. This is because the ADCS thrusters are mainly used for momentum dumping during normal operations. For this tool to function it requires certain inputs which can be obtained from the reaction wheel sizing tool. It requires the total momentum stored in the reaction wheels before dumping. It also requires the burn time of the thrusters, It then calculates the thrust level needed for momentum dumping using Equation 14.48[11, p.583]. The tool also uses the same inputs to generate graphs in Figure 14.29[11, p.583] that describes the necessary thrusting level for different burn times. These graphs allow for choosing the optimum thrusting level and burn time according to the thruster specifications.

$$F = \frac{h}{L \cdot t_{burn}} \quad (14.48) \quad m = F \cdot \frac{t_{burn}}{g \cdot I_{sp}} \quad (14.49)$$

Furthermore, the tool requires the fuel's specific impulse as an input, it then uses Equation 14.49[11, p.583] to calculate the fuel mass needed to dump the reaction wheel's momentum during the life time of the satellite.

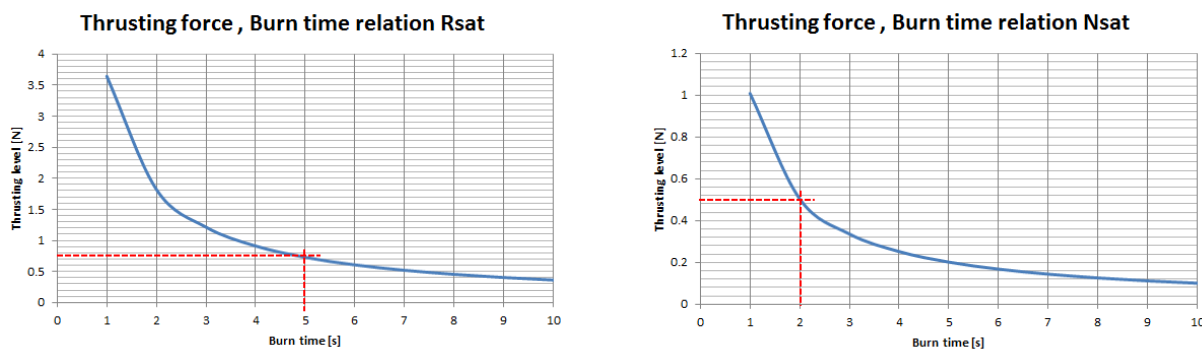


Figure 14.29: Momentum build up in a reaction wheel due to the disturbance torques after n-orbits.

#### 14.12.3. VERIFICATION

This tool was verified by unit testing each sub-component of it. Each unit was verified by checking if its output matches the results achieved by doing hand calculations. Moreover [11], has sized the reaction wheels and thrusters of two hypothetical satellites. The overall tool was concluded to be verified when the results of the tool matched the results from [11].

#### 14.12.4. VALIDATION

It is not possible to validate the findings of this tool at the current time. This is because of the non existence of data of similar missions to compare with. There has not been a single deep space mission conducted using Cubesats before.

### 14.13. POWER SIZING AND MONITORING TOOL

This tool is used to size the electric power subsystem of the different vehicles.

#### 14.13.1. ASSUMPTIONS

- Solar panel degradation is assumed to be 3% [36, p. 371] per year for GaAs based solar cells around the Moon. This causes a reduction in incoming power over time.
- GaAs junctions in multi-junction solar cells are most sensitive to radiation degradation and thus have largest impact on degradation [63].
- The network satellite orbit is circular. This allows for a simplistic eclipse time calculation. If the orbit would be slightly elliptic, this could lead to a longer eclipse time which is not taken into account in this tool.
- The relay satellites in halo orbit always receive sunlight. This means that the relay satellite EPS is not designed for operation during eclipse.
- Only first order temperature influence on the solar cells. Higher order performance changes are not taken into account in this tool.
- No Earth eclipse/Earth penumbra effects (less than 0.2% occurrence). This means that the network satellites will not be designed for operations during Earth eclipse.
- The power requirement is equal to the average power requirement at all time. This adjusts the power generation level to the average power requirement. The battery will act as a buffer to accommodate very low and high power loads.

- The solar panel is operating at the maximum power point at all time. If this is not the case, the solar panels deliver less power than expected. However, maximum power point trackers are present to ensure maximum power point operations.

### 14.13.2. TOOL DESCRIPTION

This tool consists of two parts, the power subsystem sizing and the power simulation.

The initial power subsystem sizing is explained in [1, p. 25]. The eclipse time is calculated using the satellite orbital parameters. With the day and night power requirements, depth of discharge and power efficiency, the battery capacity and solar panel power output can be determined.

Another approach is to set up an energy balance at each time interval during one orbit. The energy requirement for this balance is the average power requirement from the power budget.

The incoming energy comes from the solar panels, which are affected by solar cell temperature, degradation, solar panel absorptivity and Sun-pointing angle. Taking all this into account, the solar panel power output can be calculated using Equation 14.50. Here  $V_{mp}$  and  $EC_{mp}$  are the voltage and electrical current at the maximum power point,  $i$  is the inclination,  $t$  is time in years,  $A_{sol}$  is the solar absorptivity and  $L_f$  is the yearly degradation. Usually an increase in temperature leads to an increase in current and a decrease in cell voltage. Since the decrease in voltage is significantly larger, the overall power output goes down with increasing temperature.

With the power input and output known throughout the orbit, the energy balance can be established for each point in time. The power surplus or shortage is stored in the satellite energy storage. The difference between the last and first value of the energy storage is used to adjust the solar panel size by adding or removing a solar cell, to make sure that a sufficient amount of energy is produced by the solar panels. After the solar panels are sized, the difference between the maximum and minimum energy stored is used to calculate the required battery capacity with the chosen depth of discharge. Using this method guarantees that the state of charge will always be in the desired range constrained by the depth of discharge and full charge.

An example of this energy balance is plotted for one orbit in Figure 14.30. The orbit starts at the moment the satellite leaves eclipse. After this a slight decrease in solar panel power output can be seen, which is caused by the fast increase in solar cell temperature. Furthermore it should be noted that the battery starts at a state of charge of 60 %, but ends slightly above this at 62.5 %. Although this tool sizes the solar panels, the choice of solar cell size discretises the total solar panel area since an integer number of solar cells is required. This causes the total solar cell area to always be slightly larger than required.

This tool also contains a peak power analysis, where a peak wattage, duration, allowable depth of discharge and recovery time are given as inputs. The output is the required battery capacity and the continuous power generation that has to be dedicated to recharging the battery within the recovery time.

$$P_{sol} = \left( V_{mp} + \frac{dV}{dT} \cdot dT \right) \cdot \left( EC_{mp} + \frac{dEC}{dT} \cdot dT \right) \cdot \cos(i) \cdot (1 - L_f)^t \cdot A_{sol} \quad (14.50)$$

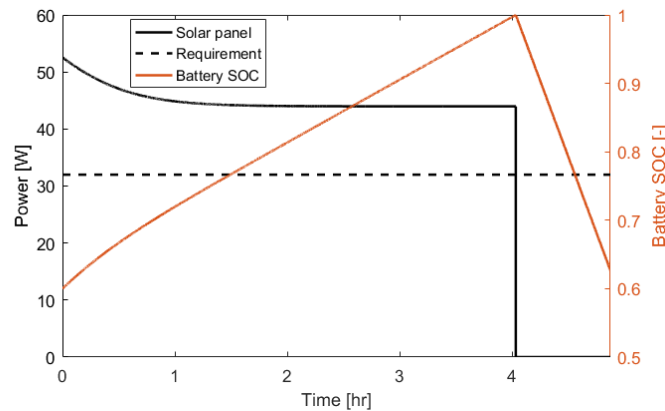


Figure 14.30: Example of a power balance graph showing the power requirement, power generated and battery state of charge throughout one orbit time.

### 14.13.3. VERIFICATION

The verification of the first part of this tool containing the initial power subsystem sizing can be found in the midterm report [1]. For the simulation, the efficiency of the solar cells is manually calculated at various points and compared to the efficiency used in the simulation. This is done using the following equation:  $\eta = P_{sol} / A_{cell}$  where  $P_{sol}$  is calculated with Equation 14.50. The results of this are shown in Table 14.10. It can be clearly seen that the manually calculated efficiency and the efficiency determined by the tool correlate. The small difference is caused by rounding off the values.

Table 14.10: Verification results for the power monitoring tool.

Time (s)	1	2000	5000	9000	14509
Manual solar panel efficiency calculation	0.171654	0.151032	0.142532	0.141471	0.141419
Simulation solar panel efficiency	0.171654	0.151032	0.142532	0.141471	0.141419

#### 14.13.4. VALIDATION

For validation, the Lunar Reconnaissance Orbiter (LRO) case will be used. The results can be found in Table 14.11. The battery capacity is quite close to the lower bound for the battery capacity from the LRO and is considered acceptable. The required solar cell area shows a large difference compared to the previously computed area and the LRO data. Upon investigation is the solar efficiency in the simulation higher than the solar efficiency assumed for the LRO and the initial estimation. This is mainly caused by the low temperatures of the solar panels, which increases the power output. The temperature varies between  $-65^{\circ}\text{C}$  to  $15^{\circ}\text{C}$ , while for the LRO temperature ranges of  $-120^{\circ}\text{C}$  to  $120^{\circ}\text{C}$  are assumed. This allows the solar panels in the model to work more efficiently, reducing the required area. The worst case that the solar panels are constantly  $120^{\circ}\text{C}$  is simulated, giving a value close to the LRO data. When using this tool it should be kept in mind that the output values are ideal values without any margin. As such, a conservative design should be considered when using this tool.

Table 14.11: Validation data for the power subsystem sizing tool.

	Solar cell area	Area difference %	Battery capacity	Capacity difference %
LRO Data	8.5	0 %	>1760 (at 22V)	0 %
Initial estimation	8.889	4.58 %	1675	-4.83 %
Simulation	5.965	-29.8 %	1817	3.24 %
Simulation with $120^{\circ}\text{C}$ solar panels	8.293	-2.44 %	1817	3.24 %

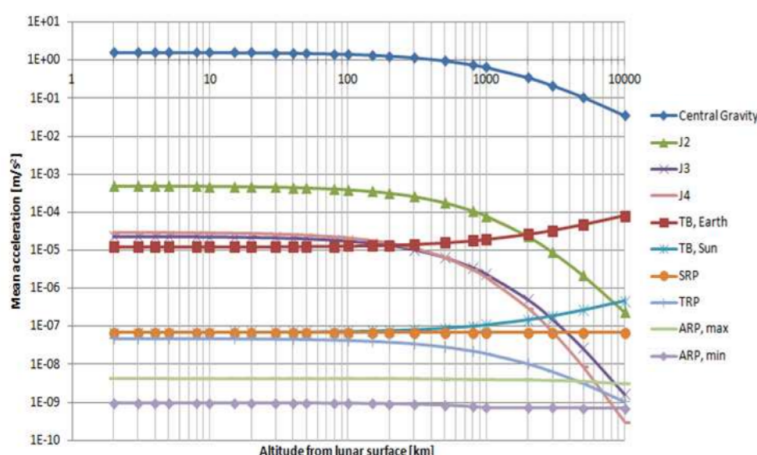
#### 14.14. ORBIT PERTURBATION SIMULATION

This orbit perturbation tool is used to determine the required orbit maintenance for the Nsats in frozen orbits around the Moon.

##### 14.14.1. ASSUMPTIONS

Many of the same assumptions are made in the creation of this tool as in the creation of the trajectory simulation tool described in section 14.1. Deviating assumptions are discussed below.

- Only the irregular gravity field of the Moon and the third body perturbation of the Earth is considered. Other perturbations are neglected as they are several orders of magnitude smaller according to Figure 14.31. This does introduce an error in the order of  $10^{-7}$ , which is acceptable for the conceptual design phase.
- The used model for the gravity spherical harmonics is LP165P provided by Matlab. While updated models exist, these new models are only important for low lunar orbits. In Figure 14.32, the data from the grail mission is compared to the lunar prospector mission for the altitude of the Nsats at 1,629 km. It is seen that the differences in gravity field are smaller than  $1 \times 10^{-7} \text{ ms}^{-2}$ , while perturbations of magnitudes lower than  $1 \times 10^{-6} \text{ ms}^{-2}$  are neglected (smaller than Earth's third body perturbation). Due to the significantly lower runtime, it is chosen to use the LP165P model, even though it is slightly less accurate.<sup>3</sup>

Figure 14.31: Magnitude of the acceleration due to different perturbations as a function of altitude from the lunar surface.<sup>4</sup>

Far side of the Moon - Degree: 100, Altitude: 1629 km

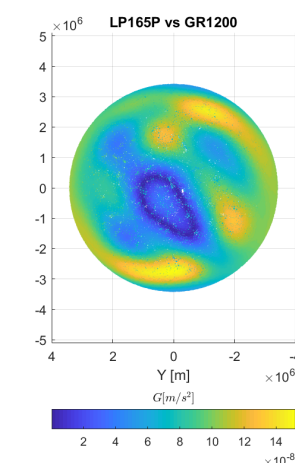


Figure 14.32: Difference between the LP165 and the GR1200 gravity field models.

<sup>3</sup>[http://pds-geosciences.wustl.edu/grail/grail-1-lgrs-5-rdr-v1/grail\\_1001/shadr/gggrx\\_1200a\\_sha.tab](http://pds-geosciences.wustl.edu/grail/grail-1-lgrs-5-rdr-v1/grail_1001/shadr/gggrx_1200a_sha.tab) Accessed on 26.06.2017

### 14.14.2. TOOL DESCRIPTION

This tool takes initial conditions for a satellite in orbit around the Moon and models its movement under the influence of the Moon's gravity and third-body perturbation by the Earth. The orbits are modelled as described in [subsection 14.1.2](#). However, the state vector of this tool contains only the state of the satellite. The total acceleration vector used to model the forces on the satellites consists of the Moon's gravity and Earth's third body perturbation:  $\mathbf{a} = \mathbf{a}_M + \mathbf{a}_E$ .

#### PERTURBATIONS

**Moon gravity Field** The Moon's gravitational field is represented using spherical harmonics. Spherical harmonics represent the complete system by a superposition of multiple simpler functions. The degree of a spherical harmonics model represents the level of detail in the representation of the system. A built-in function in Matlab is used, which requires the coordinates, the gravitational model and the degree of the spherical harmonics model are to be specified. The function outputs the gravitational accelerations in Cartesian coordinates at the specified coordinates<sup>5</sup>.

**Third body acceleration** Equation 14.51 is used for calculating the third body acceleration ( $\mathbf{a}_{TB}$ ) on the satellite in  $\text{m s}^{-2}$ .  $\mathbf{R}$  is the vector from the Moon to the third body in m,  $\boldsymbol{\rho}$  is the vector from the satellite to the third body in m and  $\mu_{TB}$  is the standard gravitational parameter of the third body in  $\text{m}^3 \text{s}^{-2}$ . In Equation 14.52 [12, p. 31], the third body accelerations due to the Earth is shown.

$$\mathbf{a}_{TB} = \mu_{TB} \left( \frac{\boldsymbol{\rho}}{\|\boldsymbol{\rho}\|^3} - \frac{\mathbf{R}}{\|\mathbf{R}\|^3} \right) \quad (14.51) \quad \mathbf{a}_E = GM_E \left( \frac{(\mathbf{u}_E - \mathbf{u}_s)}{\|\mathbf{u}_E - \mathbf{u}_s\|} - \frac{(\mathbf{u}_E)}{\|\mathbf{u}_E\|} \right) \quad (14.52)$$

#### REFERENCE FRAMES

The orbits are modelled in a right-handed Moon-centred inertial frame. Its axes are aligned with the axes of the seleno-centric reference frame at the time when the simulation starts. The seleno-centric reference frame is a Moon surface-fixed reference frame. Its x-axis points to the intersection between the equator and the prime meridian. The z-axis points along the Moon's axis of rotation [64, p.5].

The orientation of the seleno-centric reference frame with respect to the ICRF (International Celestial Reference Frame) can be determined by the Moon's 'libration angles'. These are hereby referred to as ' $\phi_m$ ', ' $\theta_m$ ' and ' $\psi_m$ '. ' $\phi_m$ ' is the angle between the x-axis and the intersection of the Moon's equator with the x-y plane. ' $\theta_m$ ' is the angle between the Moon's equator plane and the x-y plane. ' $\psi_m$ ' is the angle between the intersection of the x-y plane with the equator and the prime meridian. [65, p.6]. The libration angles for a given time have been determined using Matlab's Aerospace Toolbox, 'MoonLibration' function.

The initial position and velocity of the Earth at the are taken using JPL's 'DE430' Ephemeris model [66], using Matlab's Aerospace Toolbox, 'planetEphemeris' function.

#### MOON'S ROTATION

Since the satellite positions are determined in the inertial Moon centred-frame, the satellite position is rotated about the Z-axis in the opposite direction of the rotation of the Moon. Then the gravitational accelerations in x, y and z are retrieved for that position. Finally, these components are rotated back to the actual position of the satellite within the inertial frame. The Moon's rotation rate is 27.32 days (Table 5).

#### EARTH POSITION

This section describes the procedure to model the Earth's position with respect to the Moon inertial reference frame. For a fixed period of time, the Moon is assumed to be in a restricted two-body orbit about the Earth. The initial conditions of this orbit are obtained from Ephemeris data, and are updated with a fixed frequency. The position of the Earth depends on three angles and the absolute distance. These three angles are:

- $\psi_e$ : The angle along the x-y plane between the x-axis and the ascending node of Earth's orbit.
- $\phi_e$ : The inclination angle (angle between velocity and the x-y plane at the ascending node).
- $\theta_e$ : The angle along the Earth's orbital plane between the ascending node and Earth's position vector.

' $\psi$ ' and ' $\phi$ ' dependent on Ephemeris data. ' $\theta$ ' depends on the initial angle (' $\theta_0$ '), the initial true anomaly of the orbit of the Moon about the Earth (' $A_0$ ') and the current true anomaly (' $A$ '). In order to reduce run time, the rate at which Ephemeris data is extracted needs to be limited. ' $\psi$ ', ' $\phi$ ', ' $A_0$ ' and ' $\theta_0$ ' are extracted for a set of times (from the start of the simulation) with a fixed interval. 'i' refers to a step in the set, ' $\Delta t$ ' is the time passed from that step's time. Ephemeris data consists of the velocity and position of the Moon with respect to the Earth in the ICRF with respect to the Earth's mean equator plane. The unit vector normal to the Earth-Moon orbital plane is represented in the seleno-centric frame using Equation 14.53, where  $\mathbf{r}_m$  and  $\mathbf{v}_m$  are the Moon's position and velocity vectors in the ICRF. ' $\mathbf{n}^S$ ' is the unit vector normal to the Earth-Moon plane in the selenocentric reference frame. ' $\psi_e$ ' and ' $\phi_e$ ' are then found from Equation 14.54 and Equation 14.55. ' $\theta_0$ ' is found from Equation 14.56. The Moon's orbital eccentricity and semi-major axis are found using Equation 14.26 and Equation 14.28. The initial true anomaly (' $A_0$ ') is found from equation Equation 14.30. The current true anomaly ' $A$ ' is found by iteration. The Earth position vector in the Moon inertial frame is represented in Cartesian coordinates using Equation 14.57<sup>2</sup>, where  $\omega_m$  is the Moon's angular velocity about its rotation axis.

<sup>4</sup><http://www.aerospacengineering.net/?p=537> Accessed on 26.06.2017

<sup>5</sup><https://nl.mathworks.com/help/aerotbx/ug/gravitysphericalharmonic.html> Accessed on 26.06.2017

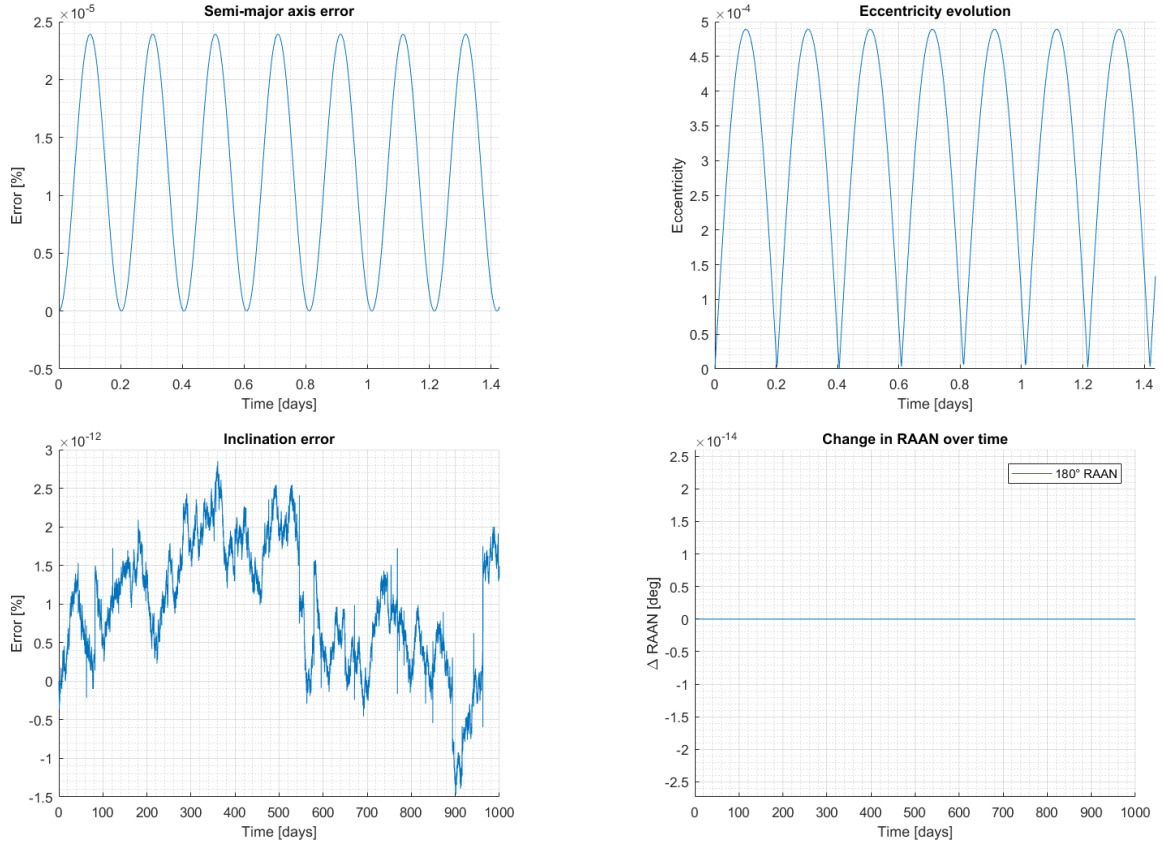


Figure 14.33: Simulation of a trajectory with initial conditions for a circular orbit of 3,366 km, 50.2° inclination and 180° RAAN. Only the gravity of the Moon is taken into account. The Moon's gravity is assumed a point mass.

$$\mathbf{n}^S = T_z(\psi_m)T_x(\theta_m)T_z(\phi_m) \frac{\mathbf{r}_m \times \mathbf{v}_m}{|\mathbf{r}_m \times \mathbf{v}_m|} \quad (14.53)$$

$$\phi_e = \arccos(\mathbf{n}^S \cdot \hat{\mathbf{k}}) \quad (14.55)$$

$$\psi_e = \arccos((\hat{\mathbf{k}} \times \mathbf{n}^S) \cdot \hat{\mathbf{i}}) \quad (14.54)$$

$$\theta_0 = \arccos(\mathbf{u}_{E_0}^S \cdot \mathbf{u}_{an}^S) \quad (14.56)$$

$$\mathbf{u}_e^{MI} = T_z(-\omega_m t_i)T_z(-\theta_{0_i} + A_{0_i} - A(\Delta t))T_x(-\phi_{m_i})T_z(-\psi_{m_i})\hat{\mathbf{i}} \quad (14.57)$$

### CORRECTION $\Delta V$

Correction manoeuvres are modelled by three instant velocity changes that change the perturbed orbit into the required orbit. The first manoeuvre changes the orientation of the orbital plane to the initial inclination and the target RAAN. The target RAAN is such that the difference in RAAN between each orbital plane is the same. The out of plane manoeuvre  $\Delta V$  is calculated using the plane change tool described in section 14.3. The next manoeuvres take place at the apocenter and pericenter, and correct the eccentricity and semi-major axis to the initial value. It is assumed that the three manoeuvres take place within a very short period of time, and the orbital Kepler elements therefore are not perturbed from one manoeuvre to the next. The correction  $\Delta V$  is defined as the period between each orbit correction event. An event refers to the three manoeuvres taking place. Total maintenance  $\Delta V$  dependent on correction period is estimated by dividing each  $\Delta V$  estimate by the time at each propagation step, as seen in Figure 4.15 and Figure 14.36.

### 14.14.3. VERIFICATION

The first verification test consists of running the simulation without including perturbations. This simulation should result in a Keplerian orbit. Figure 14.33 shows the evolution of the semi-major axis, eccentricity, inclination and RAAN over 1000 days. The initial conditions are those for a circular orbit. The numerical errors with respect to the initial Kepler elements are checked. The semi-major axis and eccentricity errors show a periodic trend with a constant amplitude within  $2.5 \times 10^{-5} \%$  and  $5 \times 10^{-4}$  respectively. Inclination errors are within  $1.5 \times 10^{-10} \%$ . These errors are determined to originate from the orbit propagation using the ode113 functionality.

The next test concerns the computation of the position of the Earth with respect to the inertial frame as a function of time. To verify this, the Earth position resulting from these calculations is plotted over time. An example is shown in Figure 14.34. It is checked that there are no clear discontinuities at the points where the Moon's orbital elements are updated. The Moon's orbital elements are checked to be within the right range. The Earth's distance is within the range of  $3.57 \times 10^8$  m to  $4.07 \times 10^8$  m, which complies with the eccentric orbit of the Moon.

For verifying the Moon's irregular gravity field it is checked whether using only degree 1, only the central gravity of the Moon is modelled. The Matlab LP165P source file is checked for the stored gravitational constant of the

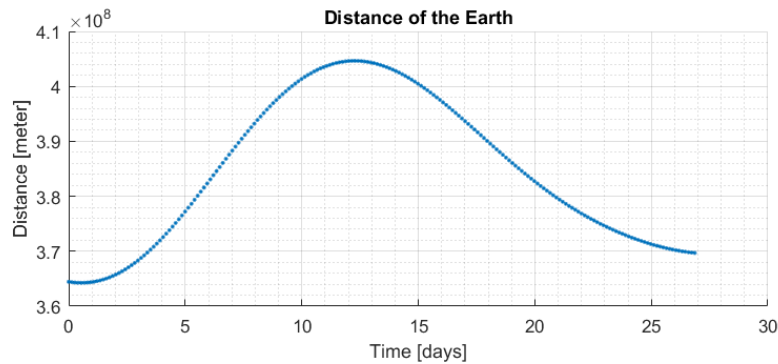


Figure 14.34: Earth's distance with respect to the Moon inertial reference frame calculated by the tool at each time step.

Moon. In particular, if they are equal to the spherical harmonics coefficients. This is the case, the compared files are: 'aerolp165p.mat' located in the aero toolbox in Matlab and the file 'jgl165p1.sha' found on<sup>6</sup> under LP/RSS/LP-L-RSS-5-GRAVITY-V1.0 /LP\_1001. Then, the implementation of the Moon's rotation is verified, by checking if the acceleration vector due to the gravity points towards the centre of the Moon.

For verifying the effect of the irregular gravity field, a simulation is run for a lunar polar orbit at 100 km. The reference data is for a lunar polar orbit at 100 km, with a RAAN of 0° using a model with LP165P using order 50x50. In Figure 14.35 the graph resulting from the simulation is superimposed. It can be seen that the general trend line is almost equal and that the simulated data for less than 40 days the errors are less than 5 km.

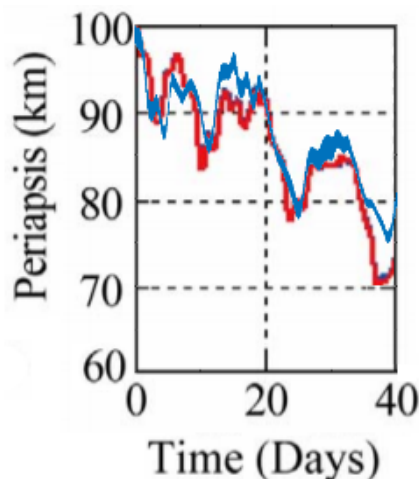


Figure 14.35: Lunar polar orbit at 100 km: Reference data [15, p. 157] (RAAN = 0°) (red), (RAAN = 0°) Simulated data (blue)

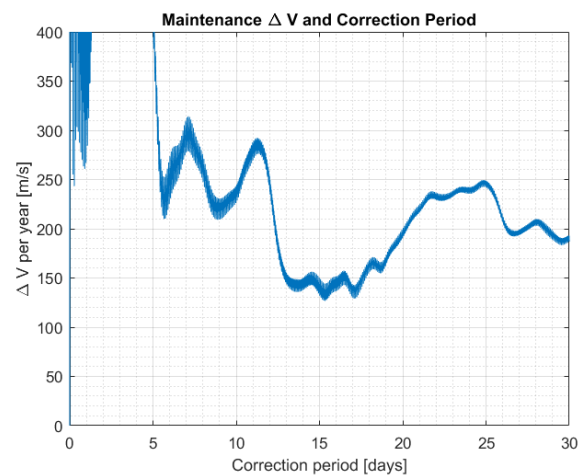


Figure 14.36: Yearly maintenance  $\Delta V$  dependent on correction period estimated for the Lunar Reconnaissance orbiter.

#### 14.14.4. VALIDATION

The paper used for performing the system tests has performed validation on its own. Therefore, by verifying the model using their results, this model is implicitly validated.

To validate estimated orbit maintenance  $\Delta V$ , the estimation process is applied to the orbit of the Lunar Reconnaissance Orbiter. This is a polar 50 km orbit. Orbit maintenance budget was designed to be about  $150 \text{ m s}^{-1}$  for maintaining this orbit [67, p. 6]. Since the RAAN does not need to be controlled in this case, the out of plane correction manoeuvre is applied only to change the inclination. The simulation results can be seen in Figure 14.36. For a correction period spanning from 12 to 20 days the  $\Delta V$  is about  $160 \text{ m s}^{-1}$  to  $140 \text{ m s}^{-1}$ .

### 14.15. THERMAL ANALYSIS TOOL

In this section the tool for the thermal analysis is discussed. The basics of the tool were taken from the thermal tool in the midterm report [1, p. 22]. However a more detailed analysis of the internal components is made.

#### 14.15.1. ASSUMPTIONS

- The Sun, Earth and Moon are modelled to radiate as black bodies, in reality the radiation is not uniform. Also the intensity of the radiation is not as uniform as black body radiation. This will make the simulation an over-estimation.

<sup>6</sup><http://ode.rsl.wustl.edu/moon/indexDatasets.aspx> Accessed on 26.06.2017

- The spacecraft is modelled as a series of nodes. Each node has a conduction path to adjacent nodes. The result is more accurate as more nodes are used. This discretisation will cause the simulation to deviate both up and down from reality.
- Each node is modelled to have one temperature. This will have an impact on the temperature of the part, if it is a large node there will most likely be temperature difference across the node.
- Each node has one specific heat capacity. If the node is made up of several different materials the heat capacity will be estimated, introducing a small error.
- The internal radiation is small compared to thermal conductivity and can be neglected. Calculated to be at an order of  $10^{-6}$  change in temperature and thermal conductivity is calculated at  $10^{-4}$  change in temperature. The final temperature will be estimated inaccurately. Therefore, an uncertainty of  $\pm 1^\circ\text{C}$  is included in the final temperature.

### 14.15.2. TOOL DESCRIPTION

The incoming radiation is calculated as described in the thermal tool in the midterm report [1, p. 22]. Also the angle for the irradiated area is calculated the same way however a mistake in the formula was found. The corrected one is given in Equation 14.58. Where  $A_{irradiated}$  is the effective area irradiated by radiation in  $\text{m}^2$ .  $A_{surface}$  is the surface area of the area illuminated in  $\text{m}^2$ . The big change between the two tools is splitting up the spacecraft into nodes. This is done to get an analysis of the inside of the spacecraft. The angle  $\theta$  will be the inclination of the orbit with respect to the Sun.  $\phi$  is a variable angle as the spacecraft goes around the orbit. It is the angle of the spacecrafts orbit with respect to a starting point.

$$A_{irradiated} = \cos(\theta)\cos(\phi)A_{surface} \quad (14.58)$$

$$m_i C_i \frac{dT_i}{dt} = Q_{external,i} + Q_i - \sigma_b \epsilon_i A_{space,i} T_i^4 - \sum_{j=1}^n h_{ij} (T_i - T_j) \quad (14.59)$$

Equation 14.59 is used to calculate the temperature change of node i. Where  $m_i$  is the mass of the node in kg,  $C_i$  is the specific heat of node i in  $\text{Jkg}^{-1}\text{K}^{-1}$ ,  $\frac{dT_i}{dt}$  is the temperature change of node i over a time step  $dt$  in K,  $Q_{external,i}$  is the external heat added to node i from radiative sources like the sun in J,  $Q_i$  is the internal heat generation of element i in J,  $\sigma_b$  is the Stefan–Boltzmann constant  $5.67036713 \times 10^{-8} \text{Wm}^{-2}\text{K}^{-4}$ ,  $\epsilon_i$  is the emissivity of node i,  $A_{space,i}$  is the Area node i has exposed to space in  $\text{m}^2$ ,  $T_i$  is the temperature of node i in K,  $h_{ij}$  is the effective conductance between node i and j in S,  $T_j$  is the temperature of node j in K,  $A_i$  is the surface area of node i in  $\text{m}^2$ ,  $F_{ij}$  is the view factor between element i and j and  $\epsilon_{ij}$  is the effective emittance between node i and j. All elements of Equation 14.59 are described in detail in [47, p. 357-390]. An example of the temperature calculation is shown in Figure 14.37.

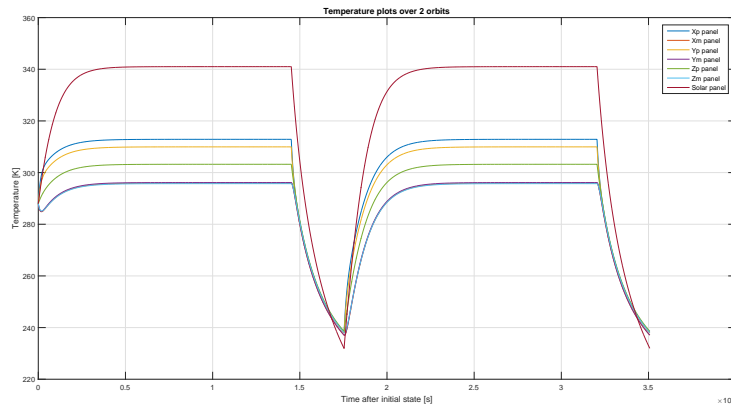


Figure 14.37: Example plot of temperatures over 2 orbits of an example satellite

The Xp, Yp, Mp are the outside panels illuminated by the Sun. The Xm, Yp, Zp are the outside panels in the shadow. The solar panel is also modelled. It can be seen that the temperature fluctuates heavily. This is due to the fact that the simulation only models the outside panels in this example. They are only 2 mm thick and this makes the satellite very light. The simulation runs over 2 orbits. The more detailed simulation will be run in the design phase.

### 14.15.3. VERIFICATION

The verification was done by calculating the equilibrium temperature of the satellite during day and night. Then run the program for a case where there is no eclipse and one where there is only eclipse. The formula used for the equilibrium temperature is given by Equation 14.60 [47, p. 357-390].

$$T_{equilibrium} = \left( \frac{A_{\alpha} J_{incident}}{A_{\epsilon}} \frac{\alpha}{\sigma_b \epsilon} \right)^{1/4} \tag{14.60}$$

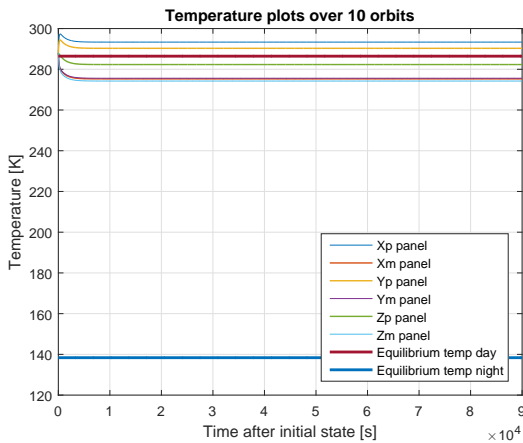
Where  $A_{\alpha}$  is the irradiated area and  $A_{\epsilon}$  is the radiating area. The equilibrium temperature is calculated for a 1,629 km high orbit with the following incoming radiation shown in Table 14.12. The temperatures from the simulation and the equilibrium temperatures are shown in Figure 14.38a and Figure 14.38b. In the figure it is seen that the temperatures of the simulation gets really close to the equilibrium temperature. The equilibrium temperature is marked as the bold line. The difference in Figure 14.38a is due to the simplification in Equation 14.60. The largest difference is 2.35 % for the day and 1.85 % for the night. These are reasonable values and hence the model is verified. The values for the panels and angles are listed in Table 14.13.

Table 14.12: Radiation intensities in Moon orbit

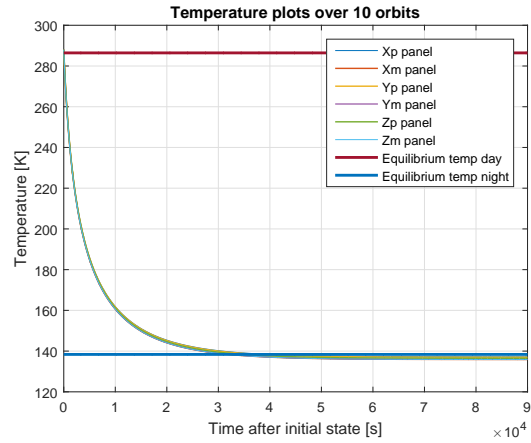
Radiation type	Intensity [ $W/m^2$ ]	Intensity in example orbit 700 km [ $W/m^2$ ]
Solar	1361	1361
Earth IR	$236 \left( \frac{R_{Earth}}{R_{orbit}} \right)^2$	0.065
Moon IR	$303 \left( \frac{R_{Moon}}{R_{orbit}} \right)^2$	80.69
Moon reflection	$150 \left( \frac{R_{Moon}}{R_{orbit}} \right)^2$	39.87
Earth reflection	$408 \left( \frac{R_{Earth}}{R_{orbit}} \right)^2$	0.114

Table 14.13: Values used in calculations

Item	Value	Unit
Xp	0.06	m
Xm	0.06	m
Yp	0.06	m
Ym	0.06	m
Zp	0.04	m
Zm	0.04	m
$\theta$	39	degrees
$\phi$	20	degrees



(a) Simulation graph and equilibrium temperature during day.



(b) Simulation graph and equilibrium temperature during night.

#### 14.15.4. VALIDATION

For validation data from the Delfi N3xt mission was used. The Delfi N3xt spacecraft was modelled in the simulation tool around Earth. The simulation assumes constant dissipated power of 3 W. The temperature ranges given in [68] are 29.5 °C to -26.1 °C. From the model the spacecraft has a temperature range of 27 °C to -30 °C. These two numbers are very close to each other and the temperature range is only 2.5 % different. This makes the model validated.

### 14.16. VISIBILITY CHECK TOOL

The visibility checker is a tool that determines if the full coverage of the Moon requirement (IRIS-CON-01) is met.

#### 14.16.1. ASSUMPTIONS

- It is assumed the Moon is a perfect sphere, thus craters are ignored. In order to account for surface roughness a minimum elevation angle of 10° is used. In [69, p. 892] it is said that it could be even as low as 5° however the aforementioned value assures some margin in case the rover is within a crater. Thus in reality, locally there could be more satellites in view.

#### 14.16.2. TOOL DESCRIPTION

Within the visibility tool there are several angles that are computed between vectors. Equation 14.61 is used in Matlab to retrieve the smallest angle between two vectors, whereas in Equation 14.62 it is proven([70, p.7], where  $v_1$  and  $v_2$  are vector 1 and 2 respectively).

$$angle = atan2(norm(cross(vector1, vector2)), dot(vector1, vector2)) \tag{14.61}$$

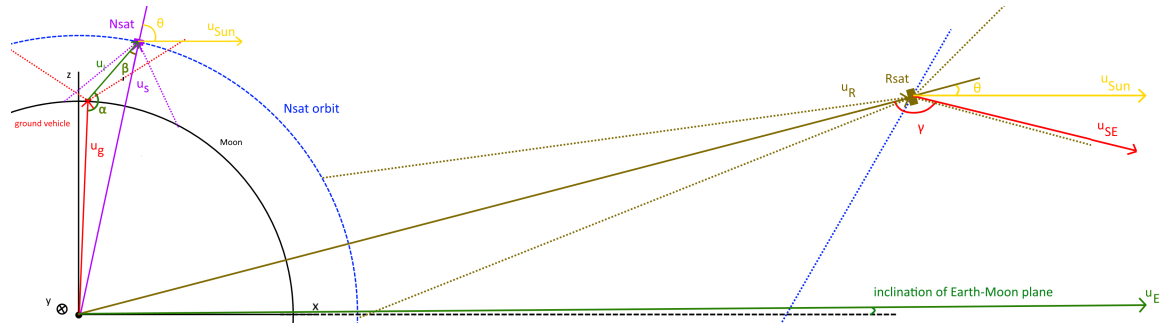


Figure 14.39: Visibility tool reference frame  $(x, y, z)$ ,  $u_g$ : ground vehicle position,  $u_s$ : satellite position,  $u_l = u_s - u_g$ ,  $u_R$ : Rsat position,  $u_E$ : Earth position,  $u_{RE} = u_E - u_R$ ,  $u_S$ : Sun position,  $\alpha$ : angle between  $u_g$  and  $u_l$ ,  $\beta$ : angle between  $u_l$  and  $u_s$ ,  $\gamma$ : angle between  $u_R$  and  $u_{RE}$  and  $\theta$ : solar incidence angle

$$angle = atan\left(\frac{\|v_1 \times v_2\|}{v_1 \cdot v_2}\right) = atan\left(\frac{\|v_1\| \|v_2\| \sin angle}{\|v_1\| \|v_2\| \cos angle}\right) = atan\left(\frac{\sin angle}{\cos angle}\right) \quad (14.62)$$

All antennas are either pointed towards the centre of the Moon or pointed straight upwards as seen in Figure 14.39. For Rsats the same assumption is made. In Figure 14.39 the following vectors are defined in the Cartesian Moon fixed Moon centred reference frame:  $u_g$  is the position vector of the ground vehicle on the Moon.  $u_s$  is the position vector of the Nsat.  $u_l$  is defined such that  $u_g + u_l = u_s$ . Angle  $\alpha$  is the smallest angle between  $-u_g$  and  $u_l$ . Angle  $\beta$  is the smallest angle between  $-u_s$  and  $-u_l$ . The ground vehicle has a cone (Field of View = FOV) where the antenna can be used, it is assumed to be pointing upwards away from the Moon. The Nsat also has a cone for its antenna which is pointed directly at the Moon as seen by the dotted lines in the enlarged portion in the frame

For the two vehicles to communicate with each other, the link vector  $u_l$  must be within these cones.  $\alpha$  should therefore be larger than  $180^\circ - FOV_{rover}/2$  to ensure the satellite is in view of the rover while  $\alpha$  should also be larger than  $90^\circ + elevation$ , to ensure the signal is above the horizon.  $\beta$  should be smaller than  $FOV_{Nsat}$ . The distance between the two vehicles must be smaller than the maximum distance for which the link budget can be closed. ( $\|u_l\| < d_{max}$ )

The simulation generates a mesh of a sphere with a radius equal to the length of the  $u_g$  vector. The simulation runs through all the satellite vectors and then runs through the whole sphere mesh where the above conditions are checked. For each ground location a "Nsat" value is stored, this indicates with how many Nsats a link can be established. If all conditions are satisfied then the ground vehicle is in view of the satellite and then the value of the number of Nsats in view is increased by one.

The Nsat counter can be used to check whether a constellation services the whole Moon and how much redundancy is present. These values are also used to check the percentage of the Moon that is covered. A resulting 3D plot containing the Nsat locations and the 2D longitude latitude plot is given in Figure 14.40 and Figure 14.41 respectively.

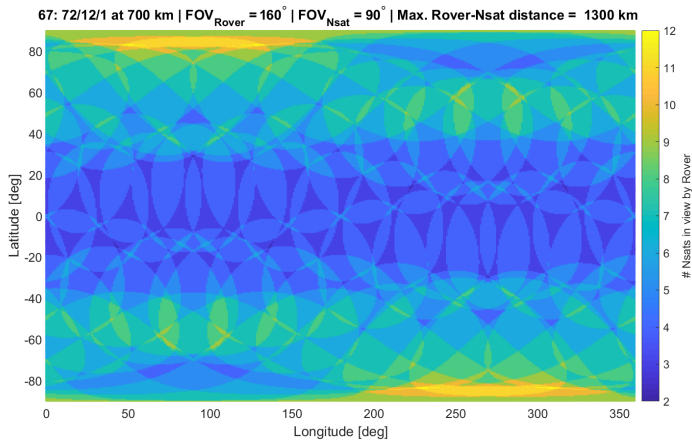


Figure 14.40: Example of a 2D visibility map generated by the tool, the walker configuration is given using the walker configuration i: t/p/f, the used field of views for both the rover and Nsat are given as well as the maximum distance for which the link budget can be closed.

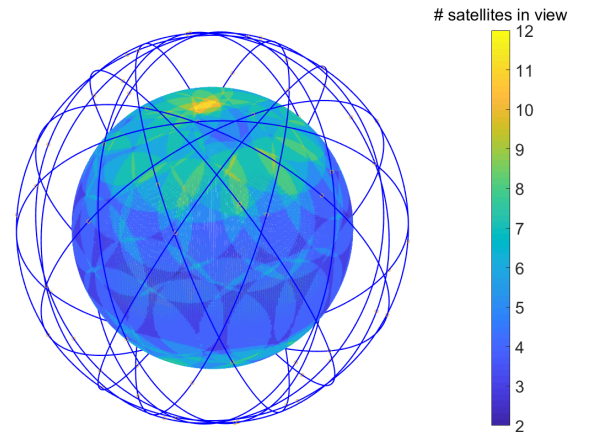


Figure 14.41: Example of a 3D visibility map generated by the tool for the inputs as specified in Figure 14.40.

Compared to the tool in the midterm report [1, p. 18] a number of additions have been made. These are described below

**Relay visibility tool** This visibility tool can also be used to check whether links between the Nsats and Rsats can be established. Thus redefining  $u_g$  as the position vector of the Nsat around the Moon and  $u_s$  as the position vector of

the Rsat. The assumptions on how the antennas are pointed still hold. Using these new definitions, the Nsats now also have an Rsat counter, which shows how many Rsat links it can make.

**Earth antenna angle** The Rsats must have a continuous link with the Earth, thus the Earth must be in the field of view of the Earth pointing antenna. By creating the Earth vector:  $\mathbf{u}_E$  as seen in Figure 14.39 the required FOV for the Earth pointing antenna can be determined by calculating the angle  $\gamma$  between the Rsat vector and the vector from the Rsat to the Earth ( $\mathbf{u}_{RE}$ ).  $\gamma$  should be larger than  $180^\circ - FOV_{RsatsE}/2$ . The Earth vector is located within the xz-plane since the frame is a Moon-fixed frame. Its z component increases and decreases according to the inclination of the Earth Moon plane and the assumed position of the Moon in the static case.

**Sun incidence angle** Since the orientation of the Nsats is determined by their requirement to be Moon pointing, the resulting solar incidence angles for the Nsats must be determined using the Nsat orientation and position. This also assumes the solar panels are located as specified in section 6.1 and are able to rotate about their longitudinal axis. The Sun is in the ecliptic plane, thus it is offset from the Moon centred inertial frame by  $1.54^\circ$  (Figure 4.3). In the same way the solar incidence angles of the Rsats are determined.

**Number of Nsats-Rsat link in total** Since the Nsats are designed to send one rover signal, and the requirement that 10 rovers must be serviced, at least 10 Nsats must be able to establish a link with the Rsats. For a given configuration the visibility tool counts the number of Nsats that have an Rsat count of 1 or higher. Thus this performance parameter should always be higher than 10 for a viable constellation.

**Number of Nsats-Rsat link per plane** Since inter-Nsat communication can only happen within each orbital plane as chosen in section 4.2, it is desired to have at least one Nsats per plane in view of an Rsat. This extension determines the number of Nsats in view of an Rsat per plane.

**All constellation configurations of the constellation** The tool only considers static cases for the constellation, thus extra loops have been added to evaluate the constellation for the Nsats moving within their orbit and the Rsats within their halo orbit. Normally one Rsat configuration and one Nsat configuration is analysed, now all possible Nsat and Rsat configurations are tested. This is to ensure the constellations has the desired performance for all possible configurations. In order to model the rotation of the Moon around the Earth, to get the evolution of the solar incidence angle, it is assumed that the Sun rotates at a constant rate in the Moon centred fixed frame. This rotation rate is  $360^\circ$  in 29.5 days. Note that the solar incidence angle is only the angle between vectors in the xz plane as the solar panels are able to rotate around their longitudinal axis to compensate for angles in the xy-plane.

**Nsat-Rsat link time** In order to determine the duty cycle of the Nsats for transmitting data to the Rsat, the time a link between Rsat and Nsat can be established is counted. This tool determines the available link time per Nsat (in percentage of orbit). It is desirable that the link time is as high as possible, this ensures that not a lot of switching between transmitting Nsats needs to occur, thus reducing the complexity of the communication flow.

**Averaged number of Nsats-Rsat link per plane** Now that all configurations of the Nsat and Rsats are evaluated, the number of Nsat-Rsat links per plane can be counted in percentage of all combinations, thus it is able to represent the characteristics of the constellation. It is desired that this number is as high as possible as this means the system itself is more adaptable to failures of Nsats.

### 14.16.3. VERIFICATION

This tool and angle calculator has been already verified in the midterm report [1, p. 19] however some extensions have been added which need to be verified. Both the Earth and Sun angles are checked in implementation of the Earth vector and the Sun vector. The Earth vector should be aligned with the x-axis and then rotated about the y-axis. this has been checked by verifying the used rotation matrix. The Sun vector coincides with the x-axis, this is verified by looking at its components.

### 14.16.4. VALIDATION

Since the extensions are very specific no validation data is available, thus no validation can be performed.



## VERIFICATION AND VALIDATION PROCEDURE

This chapter outlines the verification procedure of the product. Due to the sheer number of requirements on the system, there is no verification procedure outlined for every single one. Instead, the procedures for the key and driving requirements are specified in [section 15.1](#). A complete list of all the requirements is included in [Appendix D](#).

### 15.1. KEY AND DRIVING REQUIREMENT VERIFICATION

#### KEY REQUIREMENTS

- *IRIS-01: The cost of the mission shall not exceed 1 billion Euros.*  
This requirement can be verified by demonstration. Of course, the mission will be designed in such a way to meet this requirement. However, it is only once the mission is complete, that the exact cost of the entire mission is known.  
However, the cost is estimated to be 791 million euros (see [section 16.1](#)) and this cost can be continuously updated during the design process after the DSE is completed.
- *IRIS-02: The system shall be operational before the start of 2030.*  
Again, this requirement can be verified by demonstration. With a precise schedule in place the design is made such that the constellation can start performing its function before 2030. However, only after it is functional it can be shown that this requirement is met.

#### DRIVING REQUIREMENTS

The procedure for the driving requirements is as follows:

- *IRIS-NCON-01: The constellation shall provide full coverage of rovers on the Moon's surface without any system failure in five years with a reliability of at least 97.5 %.*  
This requirement shall be verified by simulation. The trajectory of all satellites is modelled in a circular orbit in their respective planes. The attitude of the satellites is modelled based on the function of the satellites attitude control system. The simulation integrates the position and attitude of all satellites over time. For each time instance, it is checked that a link can be achieved between the ground station and any satellite in the constellation. For this, first visibility is checked between Rsats and any Nsat. If this check fails for a Nsat, it is checked that it can communicate to a Nsat that can see the relay satellite. If this check is failed, the system cannot perform its function. The up-link and down-link performance between each network satellite and the ground station is now known for a time instance. From this, the ground coverage of all satellites can be computed. The simulation is carried out for an orbit period. A certain probability distribution of failure is implemented for the satellites and the satellite failure is incorporated in the simulation. With the probability distribution implemented, the chance can be checked of the constellation losing coverage as a result of a satellite failure.
- *IRIS-04: The system shall comply with international space laws.*  
This requirement will be verified by review of the design. The relevant aspects of the Law will be reviewed and shown that the design complies with regulations.
- *IRIS-01: The cost of the mission shall not exceed 1 billion Euros.*  
This requirement will be verified by demonstration (see above).
- *IRIS-NSAT-TT-02: Intra-network communication shall be possible with a datarate of  $1,000 \text{ kbit s}^{-1}$*   
This requirement will be verified by test. The Nsats are equipped with additional antennas which can be tested in a setup simulating lunar orbit. To assure their functionality as internal relays, simulated data will be given to a test satellite and the output of the relay antennas will be measured. This output can be fed to another satellite unit to test the correctness of the internal relay.
- *IRIS-05: The system shall ensure a lag time of equal or less than 3 seconds between Earth operators and objects on the Moon's surface.*  
To verify that the product fulfils this requirement both a test and analysis are performed. The analysis will determine how many satellites the signal has to travel through in the worst case scenario and the path the signal takes. From this, the time the signal spends in space and therefore the amount of available processing time can be determined. The actual processing time can then be determined by passing a testing signal through a relay satellite, stationed in a laboratory on Earth. The on board computer will be set up in such a way that it resembles its operating conditions as closely as possible. The processing time is then measured and the procedure is repeated for a network satellite unit. Additionally, the processing time of the ground station needs to be known. This can be determined from another test, in which the ground station is passed a test signal and the processing time is measured. If all processing times are within the appropriate limit, this requirement is verified.
- *IRIS-DEVE-03: The deployment vehicle shall remain stable under the influence of the disturbance loads due to the deployment of the satellites.*  
This requirement will be verified by simulation. The precise external and internal layout of the deployment vehicle and the Nsats will be inputs and a numerical model of this system will be constructed. With this model, the stability of the deployment vehicle can be demonstrated.

- *IRIS-NSAT-PROP-02: The propulsion subsystem shall be able to supply a total  $\Delta V$  of at least  $391 \text{ m s}^{-1}$ .*  
This requirement can be verified by analysis. Together with the design of the Nsats, Tsiolkovsky's rocket equation can be applied to determine the amount of  $\Delta V$  available once the satellite is in orbit. The needed  $\Delta V$  for orbit maintenance can be calculated from orbital perturbations, which can be computed by simulation. The satellite orbits can be propagated accurately (over a certain amount of time) by including many disturbing effects of the Earth and the Moon's irregular gravity.
- *IRIS-RSAT-TT-05: The Rsats shall have a bit error rate of  $10E-6$  and IRIS-NSAT-TT-07: Nsats shall have a bit error rate of  $10E-6$*   
This requirement will be verified by testing. The test setup will consist of one Nsat communication subsystem, one Rsat communication subsystem, a receiver connected to a computer and a noise simulator. A predefined data stream will be passed through the Rsat and Nsat communication subsystems. This data stream will be modulated according to the chosen modulation scheme. The noise simulator is going to generate the expected noise level for the different phases of the mission, this way transmitter and receiver can be placed closely together. The principle of the test is straightforward but its implementation is more involved. The principle consists of comparing the data-stream pre-modulation and after its been transmitted and demodulated, determining how many of the bits arrived with errors. The main issue is the fact that bit errors are random errors and to have an accurate measurement of their rate, theoretically, one would need the transmission of infinite bits. To reduce the time needed the data stream will consist of pseudo random code. A first order approximation for the test to have a confidence level of 95% one would need to send  $3 \times 10^7$  bits.
- *IRIS-NDEVE-02: The deployment vehicle shall fit in the Falcon 9 launch bay in the two payload configuration and IRIS-RDEVE-02: The deployment vehicle shall fit in the PSLV launch bay.*  
These two requirements will be verified by review of design. Once the design is complete, the outer dimensions can be compared to the payload volume of the respective launchers. The current design can be seen in [Figure 15.1](#) and [Figure 15.2](#).

## 15.2. VALIDATION OF REQUIREMENTS

This section describes the process of validating the requirements.

### 15.2.1. VALIDATION PROCESS

The requirements are validated in a two step process. First, the original author of the requirement applies the VALID criteria to rephrase it. Then, the requirement is added to a list where it is checked again by another member of the group before it added to the actual list of requirements. Below, two examples of requirements and their new phrasings are given:

- *Nsats shall be able to receive rover data, from a rover with a transmitter power of 40 Watts*  
This requirement from an earlier design stage is not valid due to it neither being verifiable nor definite. It would be impossible to verify if an Nsat is actually able to receive data as neither distance to, nor gains of the rover are specified. This requirement was replaced by:  
*The Nsat antenna for receiving rover data shall have a receiver gain of at least 13 dB.*  
This requirement is much more suitable: it is easily verifiable and definite.  
The other part of the requirement (specifying the power of the rover) was taken up as another requirement, but not on the satellite but on the rovers: *The rovers on the lunar surface shall transmit with an EIRP of 17 dBW.*
- *The primary structure shall be able to withstand up to TBD Hz +/- TBD Hz of vibrations in The longitudinal direction.*  
This requirement is not valid as it is not logical. It does not make sense to "withstand vibrations", without an indication of the acceleration in the specified frequency. Furthermore, vibrations during launch do not only occur at a small range of frequencies, as indicated in the requirement. The vibrations form a spectrum ranging from a few Hz to multiple thousands. Without knowing the exact vibration profile, it is impossible to verify this requirement. It was replaced by:  
*The structure shall be able to withstand the vibrational loads as specified in the Falcon 9 launch catalogue*  
This requirement is more specific and verifiable. It does require that the vibrational loads of the Falcon 9 are adequately re-created, but in essence it is verifiable.

### 15.2.2. VALIDATION OF DRIVING REQUIREMENTS

The verifiability of the driving requirements is specified above and other considerations for the validity of the driving requirements are elaborated on in this section.

- *IRIS-NCON-01: The constellation shall provide full coverage of rovers on the Moon's surface without any system failure in five years with a reliability of at least 97.5 %.*

As specified by the customer, the coverage of the constellation should be global, continuously. However, it is not possible to guarantee is 100 % of the time. Therefore, a requirement on the reliability of the system (defined as the change of no system failure occurring) is necessary. 97.5 % was found to be an acceptable and achievable value.

- *IRIS-04: The system shall comply with international space laws.*  
It is vital for the success of the mission that compliance with space laws is assured as otherwise neither a launch nor continuous operation are possible.

- **IRIS-01:** *The cost of the mission shall not exceed 1 billion Euros.*  
The investors money is a very valuable resource which should not be squandered.
- **IRIS-NSAT-TT-02:** *Intra-network communication shall be possible with a datarate of 1,000 kbits<sup>-1</sup>.*  
The network satellites need to be able to send the rover's signal through the constellation to reach a satellite in view of the relays. As it will occur that a single satellite has to relay two rover signals, this requirement is necessary.
- **IRIS-05:** *The system shall ensure a lag time of equal or less than 3 seconds between Earth operators and objects on the Moon's surface.*  
The customer specified a 3 s lag time to have (almost) real-time control over rovers on the lunar surface.
- **IRIS-DEVE-03:** *The deployment vehicle shall remain stable under the influence of the disturbance loads due to the deployment of the satellites.*  
An instability in the deployment vehicle under the influence of the deployment force could seriously hinder the mission, if it leads to improper deployment. This could lead to collision of satellites. Even under less severe circumstances, an improper deployment will decrease the functionality of the constellation (potentially no coverage in certain parts) and the satellites (expend more fuel to correct the deviation due to the DeVe).
- **IRIS-NSAT-PROP-02:** *The propulsion subsystem shall be able to supply a total  $\Delta V$  of at least 391 ms<sup>-1</sup>.*  
Without proper orbit maintenance, the orbits would quickly change to the point where inter satellite communication might no longer be possible. Furthermore, the satellites have to perform phasing manoeuvres which require a certain amount of  $\Delta V$ .
- **IRIS-RSAT-TT-05:** *The Rsats shall have a bit error rate of 10E-6 and IRIS-NSAT-TT-07: Nsats shall have a bit error rate of 10E-6.*

It is important for establishing a fast and secure connection that the bit error rates are very small. Furthermore, the bit error rate determines how many packages need to be re-sent and therefore influences the lag time between rover and operator.

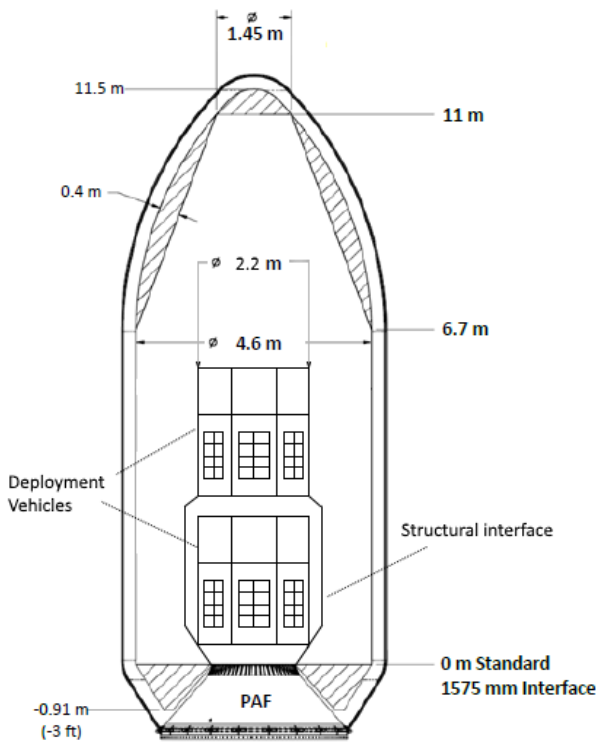


Figure 15.1: Relay deployment vehicle located in the launch bay of the Falcon 9 launch bay (to scale)[8].

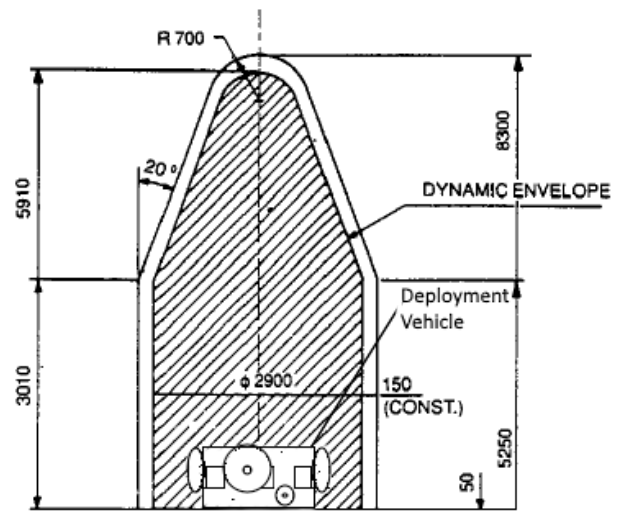


Figure 15.2: Relay deployment vehicle located in the launch bay of the PSLV (to scale)[9].



This chapter discusses the financial analysis of Project IRIS. Where the cost estimation of the system and its breakdown is discussed in [section 16.1](#). Special focus will be on changes of the estimation method with respect to the Midterm Report [1, p.54]. An update on the market analysis of the system will be given in [section 16.2](#). Lastly in [section 16.3](#) the Return On Investment (ROI) will be discussed.

### 16.1. COST ESTIMATION

During the Midterm Report [1, p.54] a cost estimation model was presented to estimate the cost of the three concept. For this Final Report this model is updated to make more accurate estimations. These alternations to the model are discussed below:

**Cost Estimation Relations** The Cost Estimation Relations (CERs) used to perform the cost estimation of the IRIS system are obtained from Table 11-11 from the new SMAD [11, p.301]. These relations are meant for estimating Earth orbiting total non-recurring cost (development plus one protoflight unit, including manufacturing), whereas the IRIS system will be operating around the Moon. It is assumed that these relations can still be used as the change in design between Earth and Moon vehicles is incorporated in the masses of the subsystems of the vehicles, which are inputs for the CERs.

**Deployment Vehicles** During the Midterm Report the cost of the deployment vehicles was estimated to be 50 million Euros [FY2017] for all three concepts. Due to the fact that the design of the deployment vehicles has become more detailed and the masses of the different subsystems are now known a cost estimation can be performed based on them. The same CERs as for the Nsats and Rsats are used for this. These relations are not meant for estimating the cost of deployment vehicles, but due to the a lack of statistical data of similar deployment vehicles this decision is made.

**Learning Curves** On advise of ir. B.T.C. Zandbergen (TU Delft) different values of learning curves are investigated, due to the nature of the different elements of Project IRIS. There are different types of spacecrafts (Nsats, Rsats & DeVe's) and they have different numbers of units produced. From slides of Prof. David W. Miller (MIT), it is found that for production of less than 10 units, a learning curve of 95%<sup>1</sup> can be applied and for production of 10 to 50 units a learning curve of 90%<sup>1</sup> can be used. A learning curve of 95% was used during the Midterm Report.

**Application of Learning Curves** The learning curves mentioned above will be used on the earlier mentioned development plus one protoflight unit cost. In fact the learning curve should only be applied to the manufacturing cost of the satellites. However, there is a lack of CERs on the manufacturing cost of satellites similar to the ones used by Project IRIS. Furthermore, there is a lack of information on sub-components from possible suppliers. Therefore, the learning curve is applied on the development cost including one protoflight unit. This means that in fact the cost of IRIS's system will be overestimated.

**Internal Redundancy** The estimated cost of the Rsats was increased by 50% during the Midterm, because they would need internal-redundancy of their subsystems. With the more detailed design of the Rsats, this internal-redundancy is taken into account in the subsystem masses, which are being used for the cost estimation. Therefore, this additional 50% increase is not needed anymore.

**Multiple Payloads** The payload of the direct transfer will consist of multiple payloads (two DeVe's with Nsats in them). The Falcon 9 launcher will be used, in the Falcon 9 Launch Vehicle Payload User's Guide it is specified that SpaceX can include multi-payload systems, but this is a nonstandard service [8]. To obtain a price for this contact should be made with SpaceX. At this moment is it assumed that this multi-payload system will cost 1% of the total launch cost, which is € 620000 .

**Launch Insurance** A conservative launch insurance of 20% was used in the Midterm, taken from the New SMAD [11, p.347]. On recommendation of ir. B.T.C. Zandbergen insurance rates based on the reliability of the chosen launchers (PSLV XL and Falcon 9) are investigated. It is found that the PSLV-XL has had 17 launches from which 17 were successful<sup>2</sup>. The Falcon 9 family has had 35 launches, from which 33 were successful<sup>3</sup>. It is therefore chosen to set the insurance of the launch on 10% of the payload value, this is considered to be on the conservative side when looking at the success rate of the launchers.

**Ground Segment Costs** The ground segment and operational costs (GS&C) were set to be 5% of the total cost of the system in the Midterm. After investigation, this number is increased to 8% for the operational cost for 5 years, this includes the cost of using ground stations on Earth. A percentage of 2.6% is used for the Ground Cost, both percentages are given with respect to the total system cost [71]. This is done because the ground segment is very important in the IRIS system and therefore higher percentages are used to obtain a more conservative estimation.

<sup>1</sup> <https://pdfs.semanticscholar.org/2874/ef735125a99c31abac09c17490319114277d.pdf> Accessed on 26.06.2017

<sup>2</sup> <http://www.isro.gov.in/launchers/list-of-pslv-launches> Accessed on 26.06.2017

<sup>3</sup> [https://en.wikipedia.org/wiki/List\\_of\\_Falcon\\_9\\_and\\_Falcon\\_Heavy\\_launches](https://en.wikipedia.org/wiki/List_of_Falcon_9_and_Falcon_Heavy_launches) Accessed on 26.06.2017

**Standard Error** The used relations of Table 11-11 of the new SMAD [11, p.301] give an indication of the absolute value of the standard error of estimate. Unfortunately no insight is given on how these numbers are obtained, nor is explained how these numbers should be used. Therefore it is decided to use the standard error as percentage of the total cost of 2 sample cost estimation cases (FireSat II % SCS Space), which are worked out in the new SMAD [11, p320 & p322]. These percentages are 8.2% and 6.8 % of the total cost of the system, respectively. It is chosen to use a conservative standard error of estimated percentage of 8% for the cost estimation of the IRIS system.

The cost estimation breakdown of the total cost of the IRIS system is given in Table 16.1. Where the individual cost (development + one protoflight unit) of the vehicles are found to be \$7.010 Million for the Nsat, \$8.429 Million for the Rsat, \$36.631 Million for the Nsat DeVe and \$11.312 Million for the Rsat DeVe, all given in Financial Year 2010 (FY2010).

Table 16.1: Cost estimation breakdown of the IRIS system in FY2010 in Millions of dollars (unless specified otherwise)

Cost Estimation Breakdown	
Nsats cost (including 90% learning curve)	186.8
Rsats cost (including 95% learning curve)	44.3
Nsat DeVe's cost (including 95% learning curve)	69.6
Rsat DeVe cost (including 95% learning curve)	11.3 +
Total space vehicles cost	312.0
Integration, Assembly & Test	43.4
Program Level	71.4
Launch & Orbital Operations Support	19.0
Ground Support Equipment	20.6 +
Total Space Segment (TSS) cost to contractor	466.4
10% contractor fee	46.6 +
Total Space Segment(TSS) cost to customer	513.1
Insurance on Launch (10%)	51.3 +
TSS cost (incl insurance) [FY2010, \$M ]	564.4
↓ change in financial year	
TSS cost (incl insurance) [FY2017, \$M ]	645.2
Flight software cost [FY2017, \$M ]	70.0
Launcher cost [FY2017, \$M ]	77.6 +
TSS (incl. flight software) cost + launcher [FY2017, \$M ]	792.8
↓ change from dollar to Euro	
TSS (incl. flight software) cost + launcher [FY2017, €M ]	708.0
Ground segment cost [FY2017, €M ]	84.0 +
Total system cost [FY2017, €M ]	791.9
↓ add standard error of estimate of 8%	
Total system cost [FY2017, €M ]	<b>791.9 ± 63.4</b>

As comparison, during the Midterm [1, p.9+56] the total cost of the system was estimated to be €552 Million [FY2017]. This increase of 43.5% is mostly due to the fact that the number of satellites has increased, from 24 to 48 for the Nsats and from 2 to 6 for the Rsats. Where the estimated cost of the space vehicles is input for most of all the other costs in Table 16.1. The increase in the total cost of the DeVe's should also be noted, this changed from €50 Million to approximately €80 Million.

## 16.2. MARKET ANALYSIS

During the Market Analysis in the Baseline Report [5, p.33] the current market and its future prospects were discussed, also potential customer were identified. Furthermore, the economic feasibility of IRIS's system was checked and a target cost of the service was given. In this market analysis update the focus will lie on those two last subjects.

In the Baseline Report [5, p.34] it was found that the reduction of dry mass for the average Lunar satellite mission by using the IRIS system is 46.25kg, which is approximately equal to a cost saving of €51 Million. This reduction in mass is obtained in terms of communication and power subsystem masses. In Table 16.2 the used missions for this estimation are displayed including the used values. As can be seen in the table the designed mission lifetime is added, which will be used to make an estimation on the cost reduction per day. The designed mission duration/lifetime will be used instead of the actual operations time of the satellites. This is done because future mission will mainly make the decision of using IRIS's service based on how much the service will cost during its designed lifetime and how much it would cost to implement a communication system themselves.

From Table 16.2 it is obtained that the designed mission lifetime data of the average Lunar satellite mission is 457 days. Using this average cost saving of €51 Million, the average cost saving was found to be €116,000 per day.

Table 16.2: Recent Moon mission data. <sup>4</sup>

Moon Orbiters	Operator	Launch year	Total mass [kg]	Dry mass [kg]	Designed mission duration/ lifetime [days]
GRAIL	NASA	2011	307	202	270
LRO	NASA	2009	1846	949	365
Chang'e 2	CNSA	2010	2480	1175	183
LADEE spacecraft	NASA	2003	383	248.2	160
SELENE	JAXA	2007	2914	1729	365
SMART-1	ESA	2003	367	287	1095
THEMIS / ARTEMIS	NASA	2003	128	79	760
<b>Average</b>			<b>1204</b>	<b>737</b>	<b>457</b>

Up until now, only satellite missions to the Moon have been discussed. However, during the Baseline, Moon miners and rovers were identified as possible customers as well. Especially Moon rovers which go to the 'far' side of the Moon should be considered. They would need to have a dedicated satellite orbiting the Moon to assure communication with the Earth. Research has been done on these type of missions with a rover and dedicated orbiter. Reference missions which were identified were the SELENE-2 mission<sup>5</sup>, the Chang'e 3 mission with the Yutu rover<sup>6</sup> and the Indian Chandrayaan-2 mission<sup>7</sup>. Unfortunately only from the Chandrayaan-2 mission financial information was disclosed. The allocated project cost for the Chandrayaan-2 mission are around €83 million<sup>8</sup>. The mission consists of a 1,400 kg orbiter, a 1,260 kg lander and a rover of 20 kg<sup>9</sup>. Where the design lifetime of the orbiter is 2 years and that of the lander and rover just 15 days<sup>9</sup>. Assuming that each kilogram of the system costs the same, the orbiter would cost approximately €43 Million. If this orbiter is only used as communications relay satellite for the rover, communication between the rover and Earth would cost around €2.9 Million per day. In fact the orbiter is carrying scientific instruments which also require communication, so the cost would need to be divided by them, but this illustrates what the cost could be for a dedicated relay satellite around the Moon for communications of a rover.

A possible collaboration between DSE group 26 was considered, as they are designing a Lunar habitat which needs communication with Earth. Unfortunately their operations start somewhere between 2035-2045, as specified by one of the group members. From a business standpoint of view this is unfortunate, because IRIS is designed to be operational from 2030 onwards for 5 years. Only after this period, with an extension of the mission duration a possible collaboration might be established.

### 16.3. RETURN ON INVESTMENT

In the Baseline Report [5, p.35] a first estimate of the target cost of the service of the IRIS system was obtained, which turned out to be €54,800 per day for a continuous data rates of at least 500 kbits<sup>-1</sup>. This was based on a Life Cycle Costs of €1 Billion, 10 lunar rovers (customers) and a break-even point in 5 years.

With the new found total system cost for 5 years of approximately €792 Million, an updated minimum price per day is found of roughly €43,400 per day. It is assumed that the market share of the IRIS system will be 100%, because no competitors with a similar system have been identified during the Baseline report [5, p.33]. This would mean that the price for the service is highly influenced by what it would cost for the customers to provide the service themselves. In section 16.2 it was found that for the average Lunar satellite mission this would roughly be €116,000 per day and that for Lunar rovers this number would lie significantly higher. This gap of approximately €73,000 per day gives room enough for a significant profit without customers being doubtful of using IRIS system based on financial grounds.

If a price of service of €86,800 per day is asked, which is still more than €29,000 per day less than providing it yourself, a ROI of 100% is obtained. That means that the break-even point is met in 2.5 years. The found ROI is incredibly high compared to companies with similar communications systems around the Earth. Take for example Iridium Communications Inc, which has a ROI of 3.66%<sup>10</sup> and Globalstar Inc, which has a ROI of -12.5%<sup>11</sup>.

In case extension of the mission is considered after 5 years, the cost for replenishment of the system should be taken into account. Here a conservative approach is used by assuming that the decreasing cost per satellite, due to the learning curve, has reached its minimum at 48 Nsats and 6 Rsats. This would mean that the individual cost of a new Nsat would approximately be \$ 3.306 Million and a new Rsat would cost \$ 6.881 Million [FY2010]. The cost for complete or partial replenishment of the system would be based on how many new satellites would be needed, what kind and how many DeVe's would be used and which launchers would be selected. In case a total replenishment of the system for a new period of 5 years operational time would be needed, a cost of roughly €651 Million [FY2017] would be present. This is based on the same procedure as given in section 16.1, using the 'minimum' cost of the vehicles and excluding the cost of flight software.

<sup>4</sup><https://directory.eoportal.org/web/eoportal/satellite-missions> Accessed on 26.06.2017

<sup>5</sup><https://repository.exst.jaxa.jp/dspace/bitstream/a-is/560425/1/SA6000046252.pdf> Accessed on 26.06.2017

<sup>6</sup>[https://en.wikipedia.org/wiki/Chang%27e\\_3](https://en.wikipedia.org/wiki/Chang%27e_3) Accessed on 26.06.2017

<sup>7</sup><http://www.isro.gov.in/update/30-aug-2010/payloads-chandrayaan-2-mission-finalised> Accessed on 26.06.2017

<sup>8</sup><http://www.business-standard.com/article/current-affairs/successful-commercial-launches-boost-isro-s-reputation-in-2015-115122901.html> Accessed on 26.06.2017

<sup>9</sup><https://sites.google.com/site/indianspaceprojects/moon-exploration/chandrayaan---2#TOC-Lander> Accessed on 26.06.2017

<sup>10</sup><https://markets.ft.com/data/equities/tearsheet/financials?s=IRDM:NSQ&mhq5j=e3> Accessed on 26.06.2017

<sup>11</sup><https://markets.ft.com/data/equities/tearsheet/financials?s=GSAT:ASQ> Accessed on 26.06.2017



## TECHNICAL RISK IMPACT ANALYSIS

In this chapter, the technical risk assurance system is updated based on the one outlined in the Midterm report [1, p.52-54]. At this stage, a detailed risk analysis is crucial since it is the criteria that the selected concept performs the worst in. With an overall risk level of 71.5%, it is by far the riskiest concept in the trade-off (Table 1.1). The reason for this was mainly due to the nature of one of the trajectories employed, namely the low-energy transfer. Even the slightest deviations can prevent the relay satellites from establishing their halo orbits, which would be detrimental to the overall mission. As such, the RDeVe and Rsats have been designed with extensive redundancies to cope with the risks of the low-energy transfer. The risks are concurrently updated over the duration of the project in accordance with the engineers designing the various subsystems and phases of the mission. Following identification, risk interdependencies are established and mitigation procedures are devised based on importance ratings. The risk assurance system is essentially tailored to the most at-risk areas by means of a simplified probabilistic risk analysis (PRA).

Technical risks are assessed in terms of their probability of occurrence and potential impact on performance, schedule and cost. The impact can take the form of negligible, marginal, critical, or catastrophic [11, p.771]. This is a generic classification of the impact of a risk in space applications. The probability of occurrence of a risk is however not as evident as it is a function of the state of technology and/or its maturity. It is therefore directly related to its TRL<sup>1</sup>. These qualitative terms provide the names of the bins used in the fever charts and are further quantified based on typical values for space missions. An overview of the used probabilities may be seen in Table 17.1, and an extensive description can be found in Table 24-11, Example 2 of the new SMAD [11, p.772].

Table 17.1: Qualitative and quantitative definitions and limits of the employed likelihood ratings.

Qualitative definition	Probability of occurrence	Description
Negligible	<1%	A negligible probability of occurrence stems from flight proven systems/ technologies that have been successful time and time again (TRL = 9).
Unlikely	1% - 5%	Risks are unlikely to occur since the considered technology is based on existing flight data (TRL = 7 - 8).
Moderate	5% - 15%	Risks that are moderately likely to occur since the considered technology based on existing, non-flight engineering (TRL = 5 - 6).
Likely	15% - 25%	This is related to technologies for which there is a working laboratory model, but no other existing engineering data (TRL = 3 - 4).
Very likely	>25%	The probability of occurrence is almost inevitable. The technology around which this revolves is only deemed to be feasible in theory (TRL = 1 - 2).

After solidifying the definitions of likelihood and impact ratings, a general system familiarisation is carried out, which is a fundamental step to developing a PRA. This will in turn help develop effective mitigation strategies depending on the path of the concerned risk. When contemplating a subsystem failure, one should not devise mitigation measures without considering other subsystem interactions. For instance, a failure in the propulsion subsystem might be caused by a failure in the electrical power subsystem, which might in turn be caused by a failure in the thermal subsystem. A dependency table of all mission subsystems is shown in Table 17.2 [72, p.70-71]. The table is read by column, where the system at the top of the column is supported by all those marked with an "X" in the rows beneath. For example, PROP is supported by EPS and STR. A failure in either of the latter two may cause a failure in the propulsion subsystem. Therefore, a risk in the propulsion subsystem might be effectively mitigated by applying specific measures on the EPS and STR subsystems as well.

Using these relations, all identified risks can now be classified in terms of likelihood, impact, and appropriate mitigation strategy and are structured in a risk register in Appendix C. To facilitate categorisation, the risks are broken down into various groups each representing a stage of the mission: launch (L), transfer/trajectory (T), deployment of satellites (D), phasing of satellites (P), and operations (O). Trajectory risks have subscripts to denote to which trajectory they apply ( $T_1$ : low-energy transfer,  $T_2$ : direct transfer,  $T_{12}$ : low-energy and direct transfer). Furthermore, combined codes are used for risks that apply in multiple phases of the missions. For instance, a risk with a PO-code is applicable in the phasing and operation stages. Risks with an A-code apply to the trajectory, deployment, phasing, and operation phases. Figure 17.1 shows the placement of all risks in a fever chart. The green, yellow, and red regions represent areas of low, moderate, and high risk respectively. Figure 17.2 shows how the risks move after the mitigation strategies are applied. The goal is to remove all risks from the high-risk region, and shift them towards the bottom left corner of the fever chart.

Table 17.2: Subsystem dependency table of all satellites and deployment vehicles.

	PROP	COM	EPS	STR	ADCS	THR	C&DH	TRK
PROP								
COM							X	X
EPS	X	X			X		X	X
STR	X				X	X		
ADCS		X	X					
THR			X	X				
C&DH		X						
TRK		X			X			

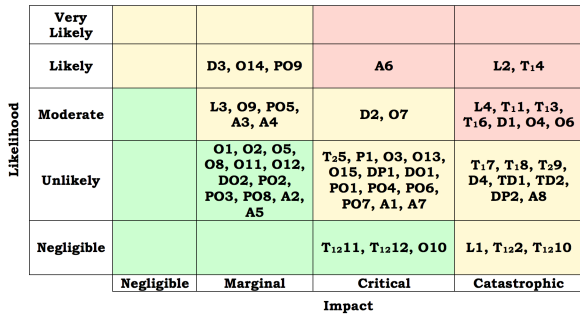


Figure 17.1: Fever chart before mitigation. Green region = low risk, yellow region = moderate risk, and red region = high risk.

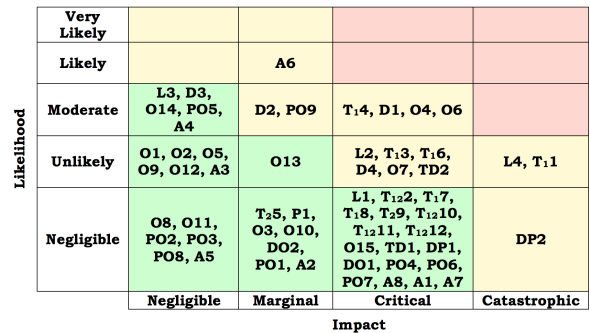


Figure 17.2: Fever chart after mitigation with same colour scheme.

The focus of the mitigation strategies are the risks in high-risk region of Figure 17.1, as those are the ones that pose the greatest threat to the success of the mission. Launch risks are only present in the first 30 minutes and can be mitigated to a limited extent. As trajectory risks occupy 50% of those in the high-risk region and are present for over a year, they will be of primary focus. A fault tree can be developed to help visualise the risks which might cause a trajectory failure, which is shown in Figure 17.3. There are three identified cut-sets which lead to trajectory failure: attitude control failure, transfer/insertion manoeuvre failure, and miscalculated trajectory model. Each of these are divided into minimal cut-sets, which has the potential to cause mission failure. For example, if risks A1 and A5 occur, then the trajectory fails because the DeVe cannot control its attitude and hence cannot properly perform the required manoeuvres. Using the probabilities defined in Table 17.1, it is possible to calculate the probability of these minimal cut-sets. Even more pertinent is establishing the precedence of all considered risks. Brinbaum importance measures (BIM) help in reducing the largest impact risks by assessing their importance and will be employed to determine which trajectory risks should be monitored more than others [11, p.775]. The BIM of a risk "A", is defined in Equation 17.1 where  $I_{Brinbaum}$  is the percentage importance measure and  $P_{Failure}$  denotes the probability of failure.

$$I_{Brinbaum}(A) = \frac{\partial P_{Failure}(total)}{\partial P_A} = (P_{Failure}(total)|P_A = 1) - (P_{Failure}(total)|P_A = 0) \quad (17.1)$$

BIM values are calculated for every risk in Figure 17.3, and it is found that every risk has a negligible relative importance ( $BIM < 0\%$ ) with the exception of those listed in Table 17.3.  $T_{16}$ ,  $T_{25}$ , and  $T_{122}$  all have extremely high importance measures and should be carefully monitored and dynamically mitigated.  $T_{16}$  displays the highest BIM and can therefore be considered as one of the most destructive risks of the mission.

<sup>1</sup><https://www.nasa.gov/sites/default/files/tr1.png> Accessed on 26.06.2017

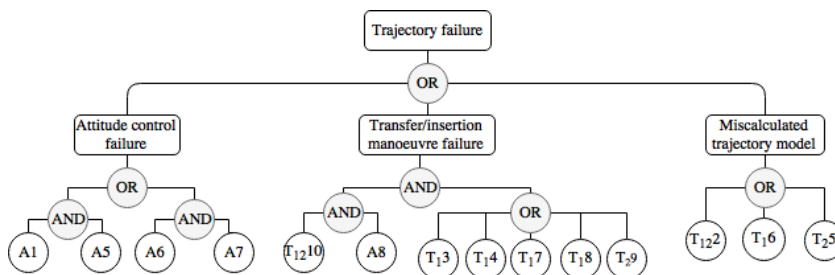


Table 17.3: Brinbaum importance measures.

Risk	BIM (%)
$T_{122}$	78.47
$T_{25}$	82.47
$T_{16}$	92.47

Figure 17.3: Trajectory fault tree.

## SUSTAINABLE DEVELOPMENT STRATEGY

The system's sustainability is assessed according to the P5 Standard (people, planet, prosperity, product and process). To achieve this, the impact of the mission on the social, environmental and financial categories needs to be evaluated. As the financial aspect is estimated in detail in [chapter 16](#), only the first two impact categories are investigated. The full analysis is displayed in [Figure 18.1](#). Events with an impact are identified and rated on a scale of +3 (highly negative impact) to -3 (highly positive impact). If a mitigation strategy is necessary, it is stated and the reduced impact is mentioned. It is seen that the average score goes from +1.125 to -0.333(-0.444). During the design regular checks with the design groups were made. The chosen components, materials and methods are checked for sustainability using the criteria mentioned below. As sustainability checks were regularly made, some design decisions could be made that positively influence the sustainability aspect of the mission and are presented below.

#	Category	Sub category	Event	Impact	Mitigation Strategy	Impact after Mitigation
S1	Social	Labour Practices	Working with toxic gases	+2	Safety measures will be implemented in manufacturing to avoid accidents & Make use of green propellants for the vehicles	+1/0
S2	Social	Labour Practices	Manufacturing will be performed by certified companies or institutions	-1	N/A	-1
S3	Social	Public Policy and Compliance	Project follows International Space Law	-1	Extra care is taken to follow advice from ITU regarding frequency usage	-2
S4	Social	Ethical Behaviour	Customer privacy is compromised and data is stolen	+2	The data is encrypted before sending and therefore harder to acquire by third parties	0
E1	Environmental	Contamination & Pollution	Launcher produces harmful exhaust products	+1	No mitigation possible	+1
E3	Environmental	Contamination & Pollution	Rare Earth materials are used	+2	Only make use of rare Earth materials if no other feasible solution is possible	+1
E2	Environmental	Energy Consumption	All types of energy sources are used	+2	Renewable energy sources are used	-2
E4	Environmental	Waste & Disposal	Space debris is created after mission is performed	+2	A specific end-of life strategy is implemented for each vehicle.	-1

Figure 18.1: P5 Impact analysis of project IRIS up to the final phase. Events with an impact are identified and rated on a scale of +3 (highly negative impact) to -3 (highly positive impact).

### 18.1. SOCIAL IMPACT

The social aspect consists of all elements which affect society. In the context of this project and design stage, the relevant sections described in the P5 standard are labour practices, public policy & compliance, and ethical behaviour.

**S1 Toxic gasses** Originally all vehicles used hydrazine as a propellant, which is highly toxic and could be the cause of accidents during manufacturing. In order to mitigate the risks induced by this event, safety measures will be implemented and trained personnel will be employed for the processes involving these fuel tanks. During the design of both the Nsat and Rsat it is found that a new 'green' non-toxic mono propellant can be used. This new mono propellant is already incorporated into the second iteration of the Nsat and Rsat, however not for the deployment vehicles. The proposal for the application into the DeVes is in [chapter 20](#).

**S2 Manufacturing by certified companies** The manufacturing of all parts will be performed by companies or institutions which are certified for space equipment. The companies that are used for the components that have been selected so far are presented in [Table 18.1](#) as well as the certifications they have. As for the components which have yet to be chosen, no outsourcing to companies with inhumane labour practices will take place. Three common certifications were checked and definitions taken from the source are given. "The **ISO 9000** family addresses various aspects of quality management and contains some of ISO's best known standards. The standards provide guidance and tools for companies and organizations who want to ensure that their products and services consistently meet customer's requirements, and that quality is consistently improved."<sup>1</sup> "The **ISO 14000** family of standards provides practical tools for companies and organizations of all kinds looking to manage their environmental responsibilities."<sup>2</sup> "Standard **AS9100** includes ASQ 9001:2000 quality system requirements and specifies additional requirements for the quality system of the aerospace industry."<sup>3</sup> In [Table 18.1](#) all the companies for which certifications are available to

<sup>1</sup><https://www.iso.org/iso-9001-quality-management.html> Accessed on 26.06.2017

<sup>2</sup><https://www.iso.org/iso-14001-environmental-management.html> Accessed on 26.06.2017

<sup>3</sup><http://standards.sae.org/as9100/> Accessed on 26.06.2017

view online have either ISO9001 or AS9000, which is enough in terms of certifications. ISO14000 is always appreciated as it deals with the environment. The companies for which no certifications could be found are in orange, although this could be retrieved by contacting the companies for these certifications. Note that some of these companies like YT-Space are featured on Cubesatshop.com which indicates they would have these certifications. Furthermore, NASA JPL is well known for its quality.

**S3 Following International Space Laws** No international law relating to the use of the space environment is violated by the project. Specifically, no radio-thermal generators will be used as energy sources. On top of the international space law, the recommendations by the ITU[20] on which frequencies to use are taken into account, this can be seen in subsection 5.1.1, where a certain frequency option was discarded for use by Project IRIS.

**S4 Customer Privacy** The data of customers is vulnerable to interception and therefore theft if no preventative measures are taken. The intercepted data might be confidential and could be used for malicious purposes. Therefore, the data will be encrypted before being transmitted to its destination. This heavily increases the effort for third parties to access the data and therefore negates this impact. This encryption is implemented and highlighted briefly in section 5.2.

## 18.2. ENVIRONMENTAL IMPACT

**E1 Launcher exhaust products** The exhaust of the launcher negatively impacts the environment. In the launchers considered (Falcon 9, Falcon Heavy and PLSV-XL), the gasses which are emitted include CO, CO<sub>2</sub>, NOX amongst others. However, as the design of a launcher is out of the scope of this project, there is no alternative to use a launcher which produces harmless exhaust gases.

**E2 Use of Rare Earth materials** During the final phase it was ensured no components in the mission use rare Earth elements (REE) if other feasible options are available. These are defined as the 15 elements in the lanthanide group as well as scandium and yttrium [73]. Iridium is used as catalyst for the propulsion system in all the vehicles, this is however in minute amounts (<1 g).

**E3 Energy sources** In space there are many options for power generation. In project IRIS it is chosen to only use renewable energy sources. This is also safer for the environment when building the satellites. Thus in case of the satellites and vehicles, solar energy is chosen together with rechargeable batteries.

**E4 Space debris** Even though the space around the Moon is not a protected region according to the "European Code of Conduct Space Debris Mitigation", the generation of space debris is an issue that should be avoided. To this end, mitigation measures are put in place with specific end of life strategies for each vehicle. For both the NDeVe this consists of an additional burn to impact the satellite on the surface of the Moon. The Nsats are put in a disposal orbit where they will decay into a Moon-collision orbit. This will take 14 years. Therefore, this solution requires some extra tracking to ensure the Nsats don't pose problems for future missions. For the RDeVe there is the possibility of putting it in a heliocentric orbit as the Rsats are deployed in the Sun-Earth L2 point, thus only a small burn is required. For the Rsats a similar plan is made except, it will need 50 m s<sup>-1</sup> more to go from the Moon-Earth L1 to the Sun-Earth L2. In these heliocentric orbits it will pose no danger to any existing satellites and the chances of colliding with future missions are very low.

Table 18.1: Certification of companies from which components have been selected.

Company	ISO9001	ISO14000	AS9100	Company	ISO9001	ISO14000	AS9100
Spectrolab	X	X	X	Optolink			
Azurspace	X		X	Honeywell	X	X	X
CESI	X			Honeybee	X	X	
Saft	X			Busek			
Aerojet	X	X		BCT			
Rocketdyne	X	X	X	YT-Space			
EnerSYS	X	X		SEAKR	X	X	
GS Yuasa	X		X	IMT	X		
NSS				NASA JPL			
SST	X		X				

This final phase of the project will be concluded with a review, this review can be considered equivalent to the Critical Design Review of the ESA standards on project management. The most important aspects that are going to be reviewed in this milestone are: the project status with regards to schedule, budget and performance, the compatibility and producibility of chosen hardware/software and the risk management practises. After this milestone, preparation activities for the final and symposium presentations will take place. These activities are indicated in Appendix C of the Midterm report [1]. During this time an internal review of the team performance will be conducted and an updated SWOT analysis of the team will be performed. The reason for this is to identify weaknesses of the team or resources that will be needed in further phases. Once the symposium has been completed, the team will be free for a couple of months to get some well deserved rest and try to think of value that we can add to the system.

The team will reconvene in the third week of September 2017. This phase will start with a review of the final objectives, where the team members and the main customer will have a discussion of possible additions or omissions. This discussion will initially start internally and after important changes identified the project manager will inform the main customer and get his opinion on the possible changes.

Once that is done, a review of the organisational structure will occur. During this review the performance of the main team in the assigned responsibilities will be reviewed. As the number of activities during this phase is expected to rise so will the number of required human resources. Also it may be required that new divisions within the project organisation are created. Such divisions may include one dedicated to legal aspects of the project. The production of the satellites will most likely be done from several contractors, a contractual strategy should be developed. Furthermore during production different suppliers will be needed, as such the legal division can also deal with managing the supply chain. Another possible division can be a project financing division. As it was mentioned the number of people involved in the project is expected to rise, all this added human resources, contractors and suppliers will need regular payments to perform their jobs. This results in a need of an office keeping track of all expenditures and in case of low budgets attract investors and prepare proposals for them.

The above mentioned steps are expected to be finished before the end of the fiscal year 2017. At the new fiscal year 2018 the pre-qualification and pre-production phase will take place. During this phase an extensive market research will be performed. The result of this research will be the identification of the market needs, potential customers, potential investors and the state of the contractor market. Following the market research, proposals for contractors and investors will be prepared. At the same time the proposals are being prepared, the additional human resources will be slowly brought in, starting from the most needed elements. Once the proposals are deemed ready they will be made public. Concurrently with the market research the detail design will be performed.

After the public proposals a long phase of judging and grading the potential contractors will take place. The end result is selecting a contractor that will assure delivery of a product up to specification, in the required schedule on the lowest amount of budget. After the selection of the contractors, work on the hardware and software needed for the mission elements can begin. Thus the phases of qualification and production will start at the same time so that an implementation of the V model can be assured.

Qualification is the phase expected to last the longest as everything that will go on the satellite will have to be tested on a component, subsystem and system level to ensure functionality. Several test will need to occur and some of these test will require special facilities to be performed (such as radiation and vacuum chambers). Besides the hardware, each line of code of the on board software will need to be debugged, verified and validated.

Once production has finished and the qualification phase is half-way, the ground segment of the mission can be set up and the software required for nominal operations can be created. At the same time close contact with the launch providers will be established and a periodical status updated from both the project organisation and launch provider will be held. As mentioned the pre-launch and launch activities will be undertaken by the launch provider. The first launch window is in July 2028, by then every component and subsystem should be qualified and every line of code checked for mistakes. In [Appendix E](#), a Gantt chart of the post DSE planning is given.



The final design as achieved in this paper, albeit being detailed, is not a final one. There are still many areas which can and should be improved if Project IRIS is to be implemented in reality.

#### GENERAL RECOMMENDATIONS

**Validation Data** A number of tools, including the structural sizing tools described in [section 14.5](#) and [section 14.6](#), are not properly validated as no proper validation data is available. If this design is to be implemented, a way should be found to properly validate these tools.

**Cost Estimation Statistics** In order to estimate the cost of the different system elements, statistics-based relations from the new SMAD [11] are used. However, these relations are established using data from missions to Earth-centred orbits. To better estimate the costs, data should be used which is better applicable to the IRIS mission. Especially, the estimation of the cost for the deployment vehicles can be improved.

**Probabilistic Risk Analysis** In this conceptual design, NASA's probabilistic risk analysis (PRA) method is implemented in a simplified way. If this design is to be developed, it is paramount that a better understanding of the risks is achieved by implementing NASA's full PRA. This includes generating fault trees for all failure modes that would lead to mission failure, individually evaluating all minimal cut-sets, and determining importance measures for all risks in order to optimise their mitigation strategies.

**Deployment Reliability Analysis** The constellation reliability analysis assumes that each satellite is deployed successfully. To make the reliability analysis more complete, it can be extended to include the deployment procedure and deployment vehicles.

**Manufacturing, Assembly and Integration Plan** The manufacturing, assembly and integration plan should be improved by setting definitive dates for the relevant tasks.

#### RECOMMENDATIONS FOR TRAJECTORY DESIGN

**Burn Time** In the design and simulation of both transfer trajectories, the velocity changes were instantaneous. In reality, the velocity changes are over a certain burn time. In future design iterations the effect of these burn times should be incorporated in the simulation, and the design, of the transfer trajectories.

**Inclination of the Moon** The relative inclination of the orbital plane of the Moon is not incorporated in the design of both the direct transfer and the low-energy transfer. This does have an influence on the required manoeuvres for the transfer and on the trajectories themselves. Therefore, this should be investigated in future design iterations.

**Planning of Transfer** An advanced ephemeris tool should be used to combine the planning and designs of the trajectories with the relative positions of the relevant celestial bodies.

**Sun-Earth L2 Halo Orbit** The design of the low-energy trajectory is made using one specific halo orbit around the Sun-Earth L2. However, there are multiple of such halo orbits possible. It should be investigated if the transfer can be optimised by using a different L2 halo orbit.

**More Efficient Low-Energy Transfer** The design of the low-energy transfer incorporates getting into a halo orbit around the second Sun-Earth Lagrangian point. However, the duration of the trajectory can be drastically reduced by not getting in this halo orbit, but merely "touching" it [74]. This should be investigated in future design efforts.

**Matching parts 2 and 3 of low-energy transfer** During the matching of parts 2 and 3 of the low-energy transfer in the current design, the displacement and velocity in z-direction are disregarded. In order to implement this design in reality, this aspect of the transfer should be included.

**Phasing of Earth-Moon L1 Halo Orbits** The phasing of halo orbits is not investigated in this report due to the complex interaction of the different bodies. It is assumed that this phasing can be done by applying different burns after part 2 of the low-energy transfer or partially incorporated in the deployment procedure of the Rsats. However, this should be confirmed by investigating it in future design efforts.

**Varying Kick Magnitude and Direction** The current low-energy transfer involves a kick in the halo orbit around Sun-Earth L2. This kick is currently  $10 \text{ m s}^{-1}$  and aligned with the velocity. Changing the magnitude and direction of this kick can have favourable consequences on the trajectory in terms of time and  $\Delta V$ .

**Different Earth-Moon L1 Halo Orbit Insertion** The insertion into the two different Earth-Moon L1 halo orbits is assumed to be done by different kicks when entering the Earth-Moon system. This injection should be further investigated to ensure that this is possible. Furthermore, it should be checked if this is the most efficient way to do so, or rather getting into one halo orbit and then manoeuvring into the other is more efficient in terms of  $\Delta V$ .

**Orbit Insertion by Satellites** During the direct transfer, the orbit insertion is done by the deployment vehicles. The favourable effects of letting the Nsats do this themselves, at large apocentre, can be investigated. Especially, the launch payload mass could be decreased.

**Addition of Insertion Manoeuvre** The possibility of adding a manoeuvre after injection, during the direct transfer, can be investigated. This manoeuvre changes the plane orientation of the Moon fly-by trajectory so that it is aligned with the first plane of the constellation. Consequently, this could reduce the amount of  $\Delta V$  needed for orbit insertion.

**Different Direction of Burn** The design of the direct transfer incorporates a first burn in the direction of the velocity. However, it is also possible to burn in other directions. It should be investigated if the trajectory can be optimised in terms of time or  $\Delta V$  by burning in a different direction.

#### RECOMMENDATIONS FOR CONSTELLATION DESIGN

**Weibull Curve** The Weibull curve used in the reliability analysis of the constellation is taken from a reliability study [16]. To make the reliability analysis more realistic, relevant satellite failure data could be gathered. This can be done by either selecting relevant data from databases or using the reliability of the individual components of the satellites over time

**Perpendicular Halo Orbit** Due to time constraints, and limited knowledge, only a slanted halo orbit (22°) around the Earth-Moon L1 point is found. If a halo orbit can be found with a slant less than 5°, the amount of Rsats could be reduced to three, instead of six.

**Orbit Maintenance Strategy** The orbit maintenance strategy as implemented in this design should be validated in terms of  $\Delta V$ . It has to be checked if this strategy is suitable, accounting for orbit determination and manoeuvre errors. Furthermore, the strategy should be improved to account for these errors.

#### RECOMMENDATIONS FOR DEPLOYMENT DESIGN

**Storing of Nsats in DeVe** Different ways of storing the Nsats within the DeVe, besides using a ring-like structure as in the current design, can be investigated.

**Deployment Procedures as Phasing Manoeuvre** The deployment procedure changes the velocity of the satellites. By using a clever design, this could be used in the phasing manoeuvre. This would reduce the phasing  $\Delta V$ .

#### RECOMMENDATIONS FOR VEHICLE DESIGN

**Frequency Response to Acoustic Noise and Launcher Vibrations** The only dynamic load consideration currently taken in the structural design is in calculating the fundamental frequency of the vehicle which should be higher than the fundamental frequency of the launcher. However, the vibration profile of the launcher as well as the acoustic noise can also cause critical loads to occur in the structure. Therefore, the response to the frequencies of the launcher of the structure should be investigated.

**In-plane Concentrator Solar Cells** The use of in-plane concentrator solar cells can be investigated instead of the normal solar cells, which are currently used. This could improve the performance in terms of power generated.

**Beam-width and Power** A better coverage of the Moon by the Rsats can be obtained by increasing the beam-width of the Rsats, but this reduces the gain. It can be investigated if this could be compensated by increasing the power of the Rsats and its influences on the design. This could result in one less Rsat being required.

**Internal Radiation** To have a more realistic thermal analysis of the satellites, the internal radiation can be included in the thermal analysis tool.

**Specific Thrust Vectoring Mechanism** To properly implement the design of this mission, a design should be made for the thrust vectoring mechanism.

**Day and Night Efficiency** In the design of the electrical power subsystem, general spaceflight statistics are used to determine the day and night efficiency instead of calculating the actual operating efficiency. When more details about the components used throughout the vehicles is known, the actual operating efficiency can be calculated.

**Structural Analysis Solar Array** The structural elements of the solar array are sized using Catia estimates and statistics. This should be improved by performing a structural analysis, using for example FEM.

**Size Reduction Rsats** In the current design of the Rsats, there is approximately 7U of free space. It can be investigated if it is advantageous to reduce the size of these Rsats.

**Rotational Actuator for Solar Array Pointing** The one-axis rotational actuator for the solar array pointing should be designed to obtain the final parameters.

**Radiation Shielding** An aspect of the satellite design which is not investigated thoroughly, due to time constraints, is the radiation shielding. To implement this design the radiation shielding should be properly designed and its effect on the received radiation dose of the different subsystems should be researched.

**Structural Modelling** To gain a better understanding of the structural elements of the vehicles, as well as the stresses and strains in these structures, finite element methods can be used. These methods are time consuming leading to the decision to leave this for future design efforts.

**Fuel Deployment Vehicle** In the current design, the deployment vehicles use hydrazine as fuel. However, the satellites use a more efficient, green, alternative. It should be investigated if this green fuel is also an option for the deployment vehicles.

# 21

## CONCLUSIONS

Project IRIS aims to conceptually develop an economically viable 24/7 communication system between at least 10 Lunar vehicles anywhere on the Moon and Earth-based operators simultaneously, within a budget of 1 billion Euros, by 10 students in 10 weeks. This paper makes up the final report of that process. The report builds on and further develops the selected concept from the midterm report [1].

An overview of the mission provides a framework for the design efforts. The design of the low-energy trajectory takes 347 days and a total  $\Delta V$  of  $3,382 \text{ ms}^{-1}$ . The direct transfer takes almost eight days to place the network satellites into their required orbits. This transfer requires  $4,418 \text{ ms}^{-1}$  to get into the orbit around the Moon with the required inclination.

The design of the constellation ensures 100%, fully redundant coverage. This design makes use of six relay satellites in two halo orbits around the first Earth-Moon Lagrangian point and 36 network satellites in a frozen Walker-Delta constellation at 1,629 km altitude above the Moon.

The link design makes use of phased arrays to mitigate the risks of pointing mechanisms and reduce requirements on the ADCS. The data rates for all link segments are at least 500 kbit for the science and rover uplink, and at least 100 kbit for deployment communicative purposes. Furthermore all these links are able to close with a margin of at least 3 dB.

The network satellites are projected to use  $75 \text{ m s}^{-1}$  for orbit maintenance over the five-year lifetime which is achieved using green fuel. A fully passive system using only coatings is used to ensure thermal stability. Three axis control stabilisation is required due to attitude requirements. This is ensured with the use of reaction wheels and momentum-dumping thrusters which allow for translation. An on-board oscillator enables the satellites to perform tracking and down-link in one go through one-way tracking. The total weight of one network satellite amounts to 15 kg.

The relay satellites themselves are approximately 31.13 kg in total mass. These satellites are projected to require  $250 \text{ m s}^{-1}$  for orbit maintenance. Green fuel is used for propulsion and a fully passive system using coatings is used to ensure that the temperature of the subsystems stay within their boundaries.

In terms of deployment, the network satellites will be carried by two separate octagonal vehicles, each with a total mass of 1,393 kg. These vehicles will perform orbit insertion manoeuvres with a 4 kN bi-propellant engine with thrust vector control and sequentially deploy the satellites in the orbital plane, leading to a minimum distance after deployment of 360 m. These manoeuvres require a total  $\Delta V$  of  $2,328 \text{ m s}^{-1}$  per deployment vehicle. After the deployment, the network satellites perform a phasing manoeuvre requiring a maximum of  $35 \text{ m s}^{-1}$ . The whole transfer, including subsequent manoeuvres, takes almost 8 days.

The relay satellites are carried by a ring-like adaptor structure with a weight of 87 kg. The ring is connected to the relay satellites with explosive bolts which are activated once the vehicle reaches a halo orbit around the Sun-Earth Lagrange point.

The robustness of the design was tested by performing a sensitivity analysis. Increasing the orbital altitude would decrease the required  $\Delta V$  for orbit insertion. The power needed to close the link budgets would increase due to increased distances. Increasing the number of rovers would not have a large effect on the trajectory design. However, the number of satellites would need to increase or the mass per satellite would need to increase.

The total cost of the system was estimated to be  $\text{€}791.9 \pm 63.4$  Million in Financial Year 2017. An analysis of the market showed that  $\text{€}86,800$  per day is a feasible price of the service IRIS provides (continuous data rate of  $500 \text{ kbits}^{-1}$ ). Combined with a minimum of 10 lunar rovers or satellites (customers), this resulted in an expected return on investment of 100% in 5 years, where the break even point is met 2.5 years.

All the risks associated with the design of Project IRIS were identified and risk mitigation strategies were implemented to minimise the likelihood and impact of said risks. Furthermore, the design was analysed in terms of sustainability. The social impact, as well as the environmental impact were analysed. Any negative impact was minimised by implementing counter-measures.

As the aim of Project IRIS is to create a conceptual design. There are still a number of phases to go through before Project IRIS can become a reality for that reason, future development phases have been outlined. Furthermore, general recommendations, as well as specific recommendations to improve the design in terms of trajectory, constellation and vehicles, were provided to further optimise the various mission elements.



## BIBLIOGRAPHY

- [1] DSE Group 06 - Project IRIS, *Midterm report*, (Spring 2017).
- [2] L. David, *China outlines new rockets, space station and moon plans*, [space.com](#) (2015).
- [3] Google, *The race is on*, [XPrize Foundation](#) (2017).
- [4] DSE Group 06 - Project IRIS, *Project Plan*, (Spring 2017).
- [5] DSE Group 06 - Project IRIS, *Baseline report*, (Spring 2017).
- [6] O. ATK, [Minotaur v fact sheet](#), (2017).
- [7] M. Xiang and L. Tongyu, *The new generation launch vehicles in china*, (accessed 2017).
- [8] SpaceX, [Falcon 9 user's guide](#), (2015).
- [9] I. S. R. Organization, *Polar Satellite Launch Vehicle user manual*, Tech. Rep. (ISRO, 2016).
- [10] J. S. Parker, *Low-Energy Ballistic Lunar Transfers*, diploma thesis, University of Colorado (2003).
- [11] D. F. E. James R. Wertz and J. J. Puschell, *Space Mission Engineering: The New SMAD* (Microcosm Press, Hawthorne, 2011).
- [12] E. Cardoso Vilana, *Study of spacecraft orbits in the gravity field of the moon*, (2012).
- [13] R. B. Roncoli, *Lunar constants and models document*, JPL D-32296, Sept (2005).
- [14] D. Folta, M. Woodard, and D. Cosgrove, *Stationkeeping of the first earth-moon libration orbiters: The artemis mission*, (2011).
- [15] G. Shradha and S. Ram Krishan, *Effect of altitude, right ascension of ascending node and inclination on lifetime of circular lunar orbits*, International Journal of Astronomy and Astrophysics **2011** (2011).
- [16] G. F. Dubos, J.-F. Castet, and J. H. Saleh, *Statistical reliability analysis of satellites by mass category: Does spacecraft size matter?* Acta Astronautica **67**, 584 (2010).
- [17] W. J. Larson and J. R. Wertz, *Space Mission Analysis and Design* (Kluwer Academic Publishers, 1992).
- [18] D. D. Morabito, W. Imbriale, and S. Keihm, *Observing the moon at microwave frequencies using a large-diameter deep space network antenna*, IEEE Transactions on Antennas and Propagation **56**, 650 (2008).
- [19] D. D. Morabito, *Dynamic telemetry link advantage when tracking a lunar orbiter with a 34-m antenna at 2.3 ghz and 8.4 ghz*, Interplanetary Network Progress Report **200**, 1 (2015).
- [20] I. T. Union, *Recommendation itu-r ra.479-5: Protection of frequencies for radioastronomical measurements in the shielded zone of the moon*, (2003).
- [21] J. R. B. Robert E. Wallis and P. M. Malouf, *Testing of the messenger spacecraft phased-array antenna*, IEEE Antennas and Propagation Magazine **47**, 208 (2005).
- [22] R. E. W. Sheng Cheng, *Phased-array antenna system for the messenger deep space mission1*, Aerospace Conference, 2001, IEEE Proceedings. (2001).
- [23] K. Dang, *Phased array antenna investigation for CubeSat size satellites*, Ph.D. thesis, Morehead State University (2016).
- [24] D. T. Jonathan Klein, Joe Hawkins, *Improving cubesat downlink capacity with active phased array antennas*, Aerospace Conference, IEEE (2014).
- [25] C. O. NASA Glenn Research Center, *Ka-band technologies for small spacecraft communications via relays and direct data downlink*, in *CubeSat Workshop – 30th Annual AIAA/USU Conference on Small Satellites* (2016).
- [26] D. of Defense (DoD), *Strategic Spectrum Plan*, Tech. Rep. (Department of Defense, 2008).
- [27] D. E. Whiteman, L. M. Valencia, and R. B. Birr, *Ku-and ka-band phased array antenna for the space-based telemetry and range safety project*, (2005).
- [28] A. G. Aguilar, J. M. I. Alonso, J. M. F. González, and M. S. Pérez, *Printed antenna for satellite communications*, (2010).
- [29] A. Cervone, *Lecture 11 spacecraft: Recap, practical examples and exercises*, (2015), aE 2111-II ,Aerospace Design and Systems Engineering Elements II.
- [30] P. Fortescue, G. Swinerd, and J. Stark, *Spacecraft systems engineering* (John Wiley & Sons, 2011).
- [31] N. S. Fatemi, H. E. Pollard, H. Q. Hou, and P. R. Sharps, *Solar array trades between very high-efficiency multi-junction and si space solar cells*, in *Photovoltaic Specialists Conference, 2000. Conference Record of the Twenty-Eighth IEEE* (IEEE, 2000) pp. 1083–1086.
- [32] green rhino energy ltd., [Concentrating photovoltaics \(cpv\)](#), (2013).
- [33] M. R. Reddy, *Space solar cells—tradeoff analysis*, Solar energy materials and solar cells **77**, 175 (2003).
- [34] G. Pistoia, *Lithium-ion batteries: advances and applications* (Newnes, 2013).
- [35] C. Pearson, C. Thwaite, and N. Russel, *The use of small cell lithium-ion batteries for small satellite applications*, (2004).
- [36] V. Badescu, *Moon: Prospective Energy and Material Resources* (Springer Science & Business Media, 2012).
- [37] A. M. Watt and S. Pellegrino, *Tape-spring rolling hinges*, in *Proceedings of the 36th Aerospace Mechanisms Symposium* (2002) pp. 15–17.
- [38] N. Femia, G. Petrone, G. Spagnuolo, and M. Vitelli, *Optimization of perturb and observe maximum power point tracking method*, IEEE transactions on Power Electronics **20**, 963 (2005).

- [39] M. Gaboriault and A. Notman, *A high efficiency, noninverting, buck-boost dc-dc converter*, in *Applied Power Electronics Conference and Exposition, 2004. APEC'04. Nineteenth Annual IEEE*, Vol. 3 (IEEE, 2004) pp. 1411–1415.
- [40] N. A. (US) *et al.*, *Evaluation of the Multifunction Phased Array Radar Planning Process* (National Academies Press, 2008).
- [41] P. Bender, D. Currie, S. Poultney, C. Alley, R. Dicke, D. Wilkinson, D. Eckhardt, J. Faller, W. Kaula, J. Mulholland, *et al.*, *The lunar laser ranging experiment*, *Science* **182**, 229 (1973).
- [42] H. Yong, H. Xiao-gong, H. Cheng, J. Dong-ro, Z. Wei-min, and Z. Xiu-zhong, *Orbit determination of satellite “tance 1” with vlbi data*, *Chinese Astronomy and Astrophysics* **30**, 318 (2006).
- [43] J. S. B. Catherine L. Thornton, *Radiometric tracking techniques for deep-space navigation*, (Deep-Space Communications and Navigation Systems Center of Excellence Jet Propulsion Laboratory California Institute of Technology, 2000) Chap. Range and Doppler Tracking Observables.
- [44] J. B. Berner, P. W. Kinma, and J. M. Layland, *Regenerative pseudo-noise ranging for deep space applications*, (2001).
- [45] J. S. B. Catherine L. Thornton, *Radiometric tracking techniques for deep-space navigation*, (Deep-Space Communications and Navigation Systems, Jet Propulsion Laboratory, California Institute of Technology, 2000) Chap. Future Directions of Radiometric Tracking.
- [46] A.-M. P. S. A. . Improvements, *Robert K. Masse, May Allen, Elizabeth Driscoll, Ronald A. Spores, Lynn A. Arrington, Steven J. Schneider, Thomas E. Vasek*, Tech. Rep. (Aerojet Rocketdyne, NASA Glenn Research Center, 2016) <https://ntrs.nasa.gov/archive/nasa/casi.ntrs.nasa.gov/20170001286.pdf> accessed on 25.06.2016.
- [47] P. Fortescue, G. Swinerd, and J. Stark, *Spacecraft systems engineering* (John Wiley & Sons, 2011).
- [48] D. J. J. D. R. B. Noll, J. Zvara, *Spacecraft Attitude Control During Thrusting Maneuvers*, Tech. Rep. (JPL NASA, Washington, DC, United States, 1971).
- [49] A. Mehrparvar, D. Pignatelli, J. Carnahan, R. Munakat, W. Lan, A. Toorian, A. Hutputanasin, and S. Lee, *Cubesat design specification rev. 13*, The CubeSat Program, Cal Poly San Luis Obispo, US (2014).
- [50] M. List, S. Bremer, B. Rievers, and H. Selig, *Modelling of solar radiation pressure effects: parameter analysis for the microspace mission*, *International Journal of Aerospace Engineering* **2015** (2015).
- [51] L. F. Shampine and M. W. Reichelt, *The matlab ode suite*, *SIAM journal on scientific computing* **18**, 1 (1997).
- [52] F. Topputo, *On optimal two-impulse earth-moon transfers in a four-body model*, *Celestial Mechanics and Dynamical Astronomy* **117**, 279 (2013).
- [53] M. Ceriotti, *Lecture notes on space flight dynamics*, (2017).
- [54] I. S. Sokolnikoff, R. D. Specht, *et al.*, *Mathematical theory of elasticity*, Vol. 83 (McGraw-Hill New York, 1956).
- [55] J. R. Taylor, *Classical mechanics* (University Science Books, 2005).
- [56] T. H. G. Megson, *Aircraft structures for engineering students* (Elsevier, 2012).
- [57] M. C. Engineering, *The eelv secondary payload adapter*, .
- [58] D. C. Kassapoglou, *Lecture 7 - AE2135 Structural analysis & design* (TU Delft, 2016).
- [59] T. Irvine, *Ring vibration modes, revision e*, (January 2015).
- [60] J. Guo, L. Monas, and E. Gill, *Statistical analysis and modelling of small satellite reliability*, *Acta Astronautica* **98**, 97 (2014).
- [61] Stanford, *Bio 244: Unit 1 survival distributions, hazard functions, cumulative hazards*, (accessed on June 9, 2017).
- [62] F. M. Dekking, *A Modern Introduction to Probability and Statistics: Understanding why and how* (Springer Science & Business Media, 2005).
- [63] T. Sumita, M. Imaizumi, S. Matsuda, T. Ohshima, A. Ohi, and H. Itoh, *Proton radiation analysis of multi-junction space solar cells*, *Nuclear Instruments and Methods in Physics Research Section B: Beam Interactions with Materials and Atoms* **206**, 448 (2003).
- [64] *A Standardized Lunar Coordinate System for the Lunar Reconnaissance Orbiter*, White Paper 451-SCI-000958 (NASA, Goddard Space Flight Center, 2008).
- [65] J. G. W. Myles Standish, *Orbital Ephemerides of the Sun, Moon, and Planets*, Explanatory supplement (Jet Propulsion Laboratory, 2010).
- [66] W. Folkner, *Jpl planetary and lunar ephemerides: Export information*, (2014).
- [67] R. S. S. J. Martin B. Houghton, Craig R. Tooley, *Mission design and operations considerations for nasa's lunar reconnaissance orbiter*, IAC (2007).
- [68] T. Delft, *Cubesat workshop data sheets*, (2015), aE3534.
- [69] R. B. Marsten, *Communication Satellite Systems Technology: A Collection of Technical Papers Drawn Mainly from the AIAA Communications Satellite Systems Conference, May 2-4, 1966*, Vol. 19 (Academic Press, 2014).
- [70] M. Spiegel, *Schaum's outlines: Complex variables*, (1964).
- [71] E. S. L. C. E. M. I. of Technology, *Communications satellite constellations: Unit 1 “technical success and economic failure”*, MIT Industry Systems Study (2003).
- [72] P. Michael Stamatelatos and P. Homayoon Desfuli, *Probabilistic Risk Assessment Procedures Guide for NASA Managers and Practitioners*, Tech. Rep. (NASA, 2011).
- [73] S. B. Castor and J. B. Hedrick, *Rare earth elements*, Industrial minerals volume, 7th edition: Society for mining, metallurgy, and exploration, Littleton, Colorado, 769 (2006).
- [74] J. S. Parker and R. L. Anderson, *Low-Energy Lunar Trajectory Design*, Deep Space Communications and Navigation Series (Wiley, 2013).

## FUNCTIONAL FLOW DIAGRAM

The functional flow diagram aims to provide an in-depth overview of all mission functions and their precedence. It also ensures that all design choices meet the required mission functions. Project IRIS is segmented into four general stages which are shown in Figure A.1. These cover the two trajectories, the operational duration of the mission, and the disposal phase. The full FFD is distributed over the four following pages further elaborating the functional procedures of the mission, with the fourth phase shown below in Figure A.3. Furthermore, two repeated paths A and B are shown in Figure A.2. A functional breakdown structure is also developed concurrently with the FFD to modularly assess the various functions which need to be completed for mission success, which is shown in Appendix B.

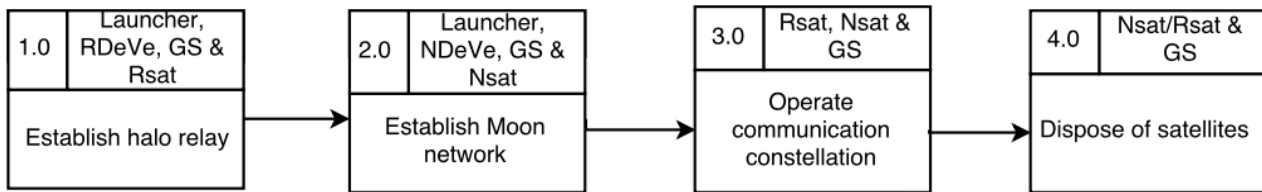


Figure A.1: General overview of the defined functional stages of the mission.

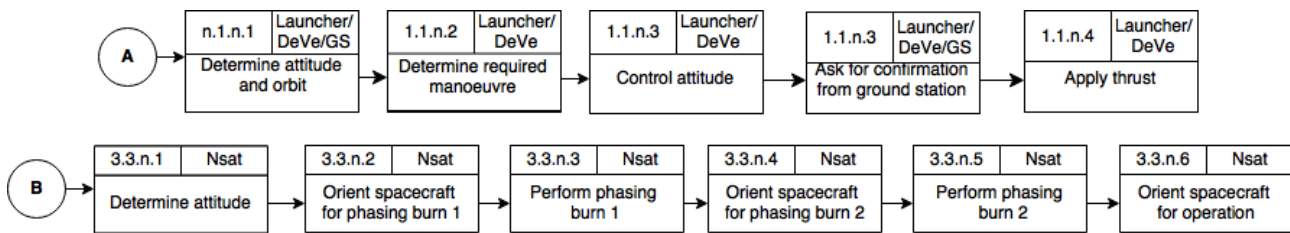


Figure A.2: Repeated sub-functional flows A and B.

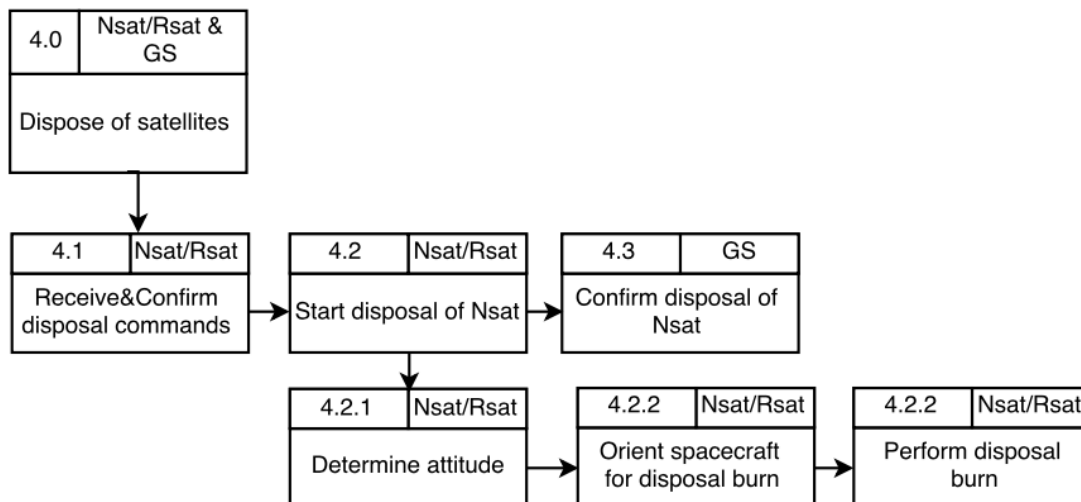


Figure A.3: FFD of phase 4: Disposal of satellites.

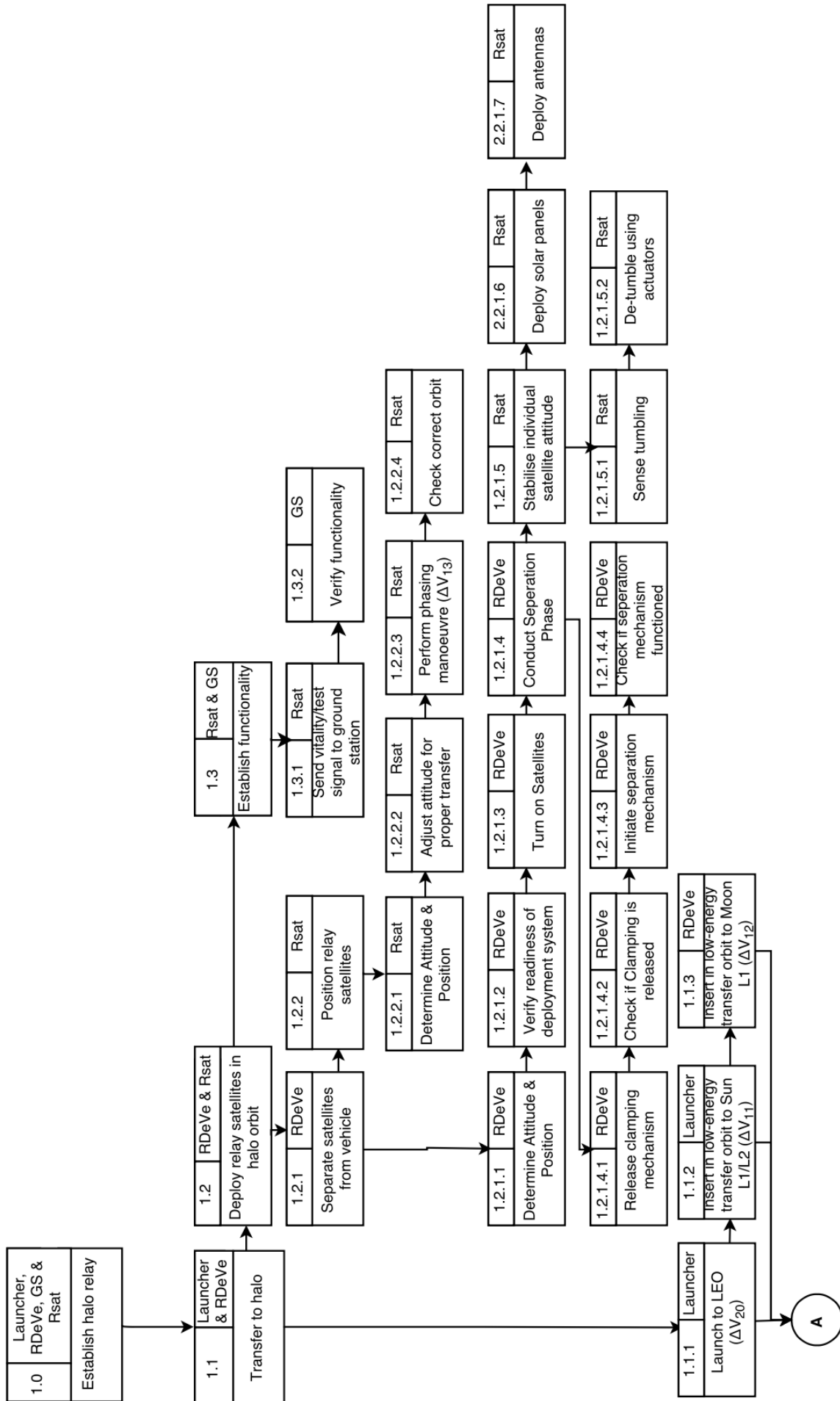


Figure A.4: FFD of phase 1: Establish halo relay.



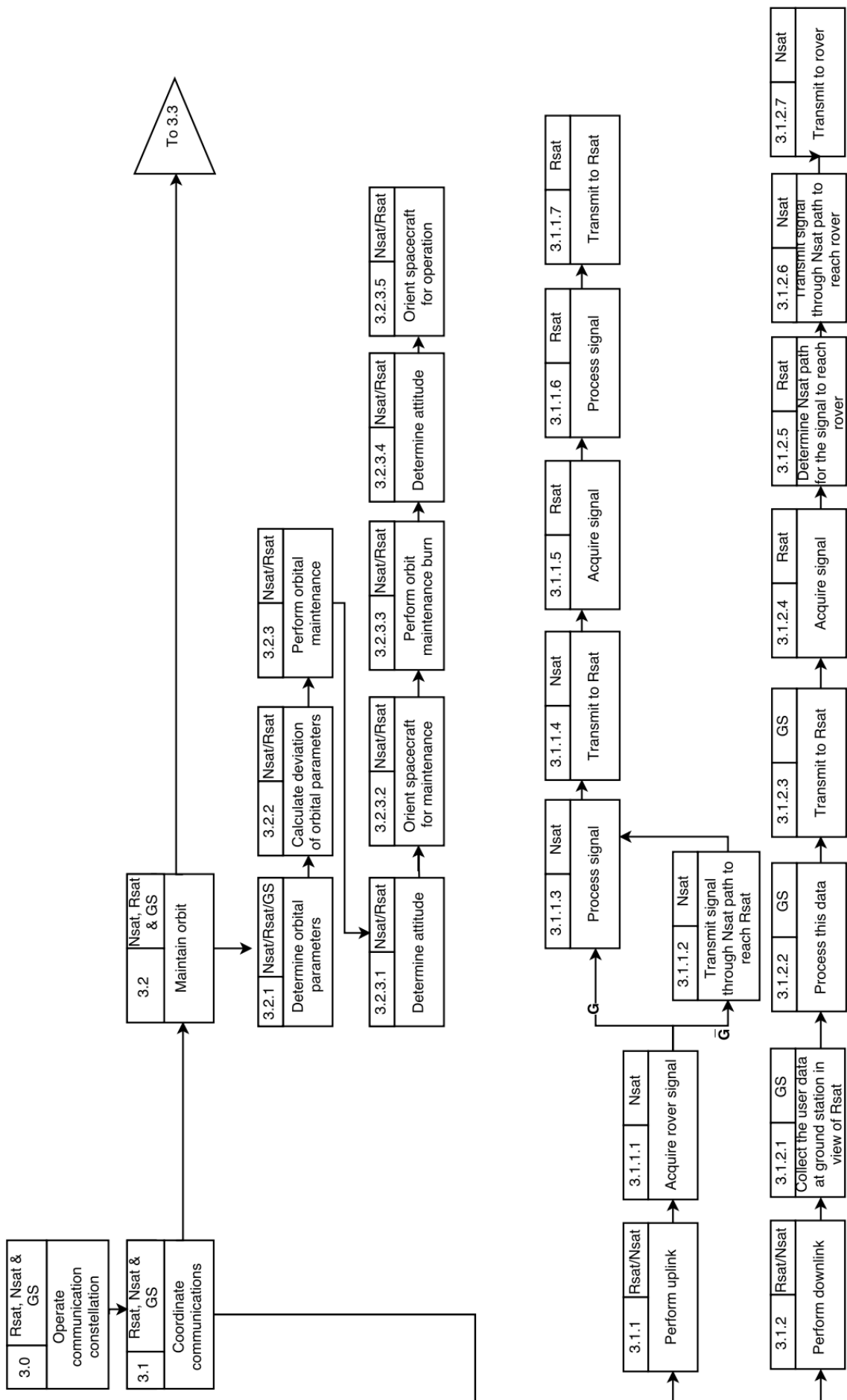


Figure A.6: FFD of phase 3: Operate communication constellation.

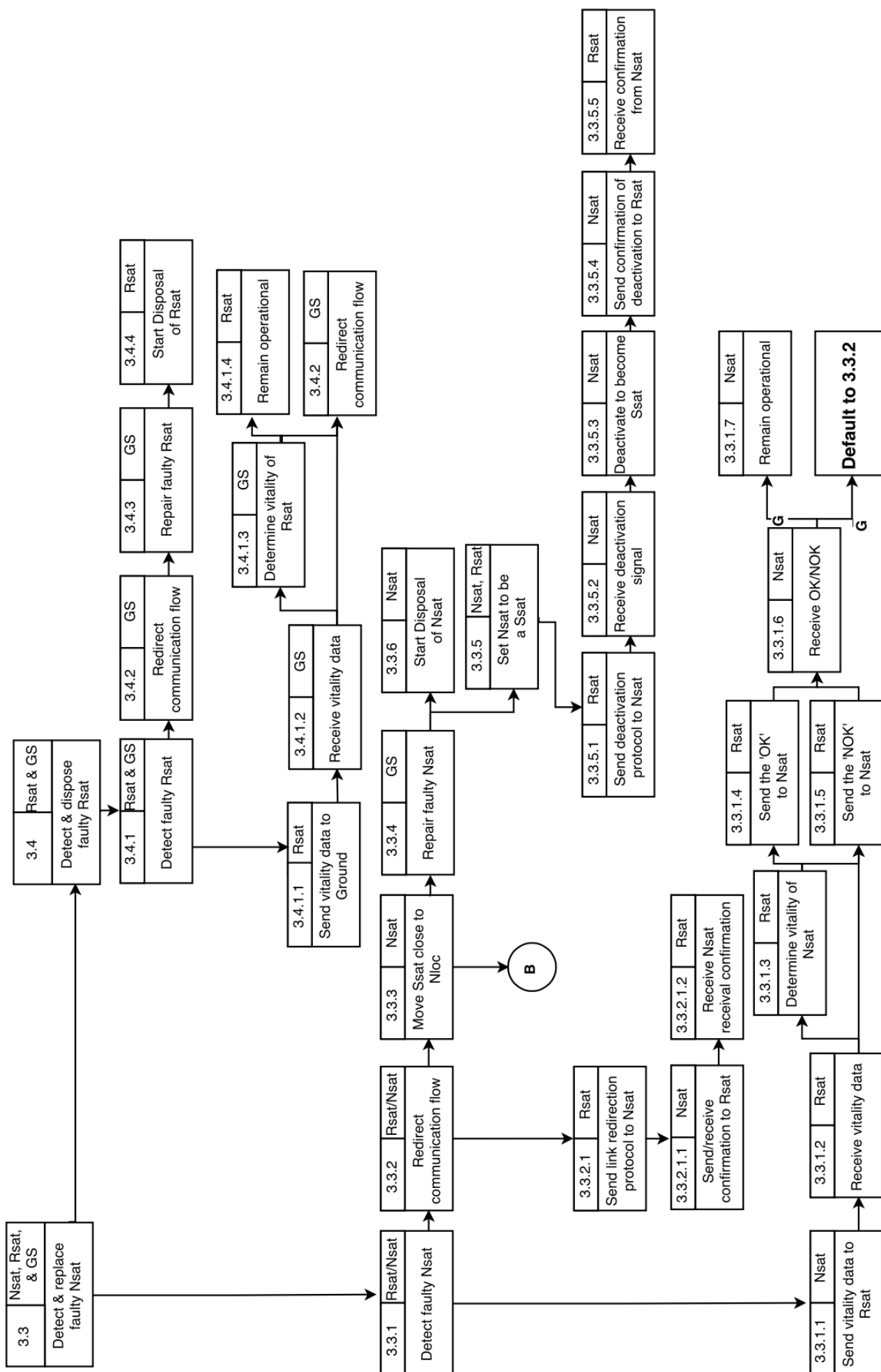


Figure A.7: Phase 3 continued.



## FUNCTIONAL BREAKDOWN STRUCTURE

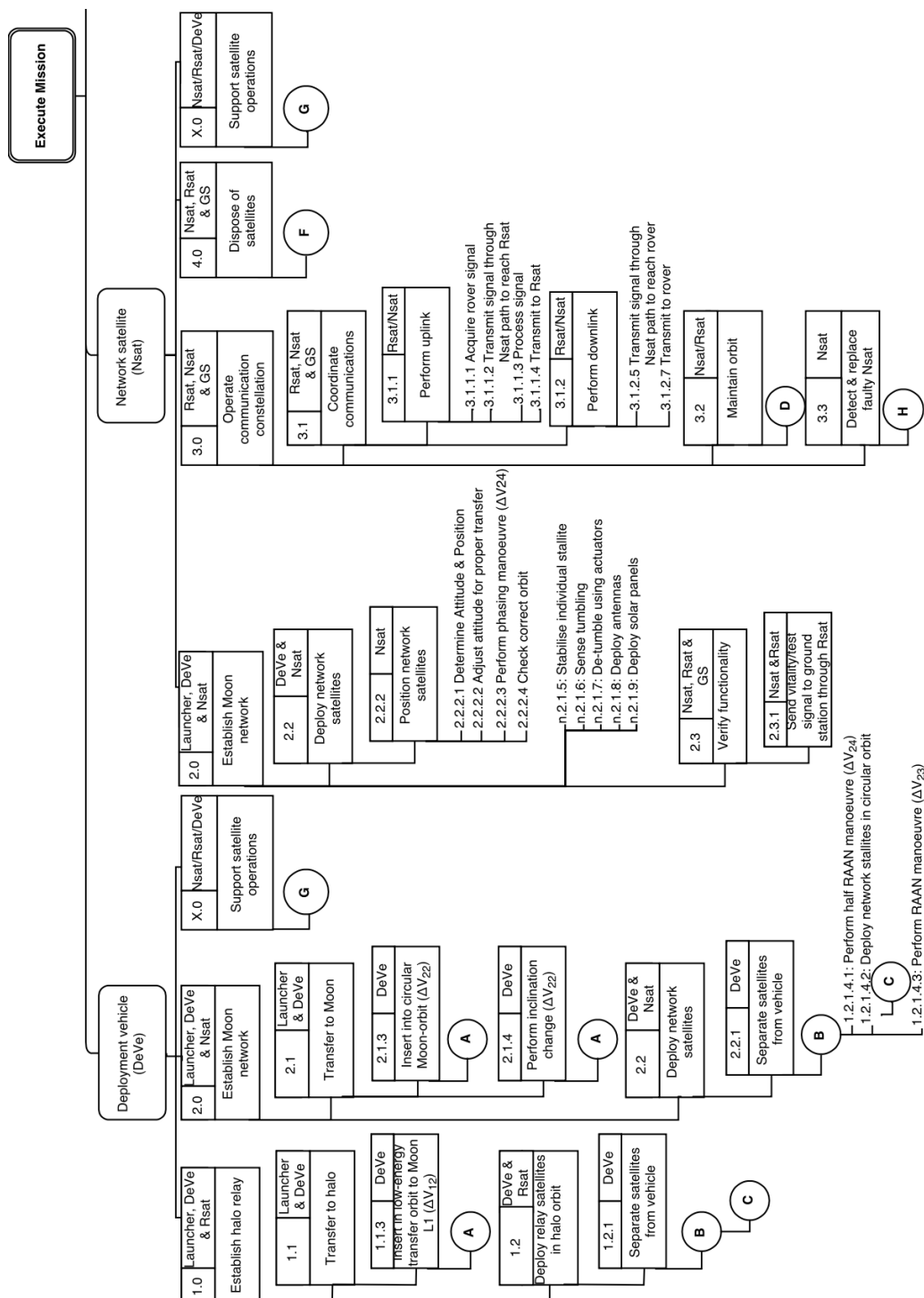


Figure B.1: Functional breakdown structure. Part 1 of 3.

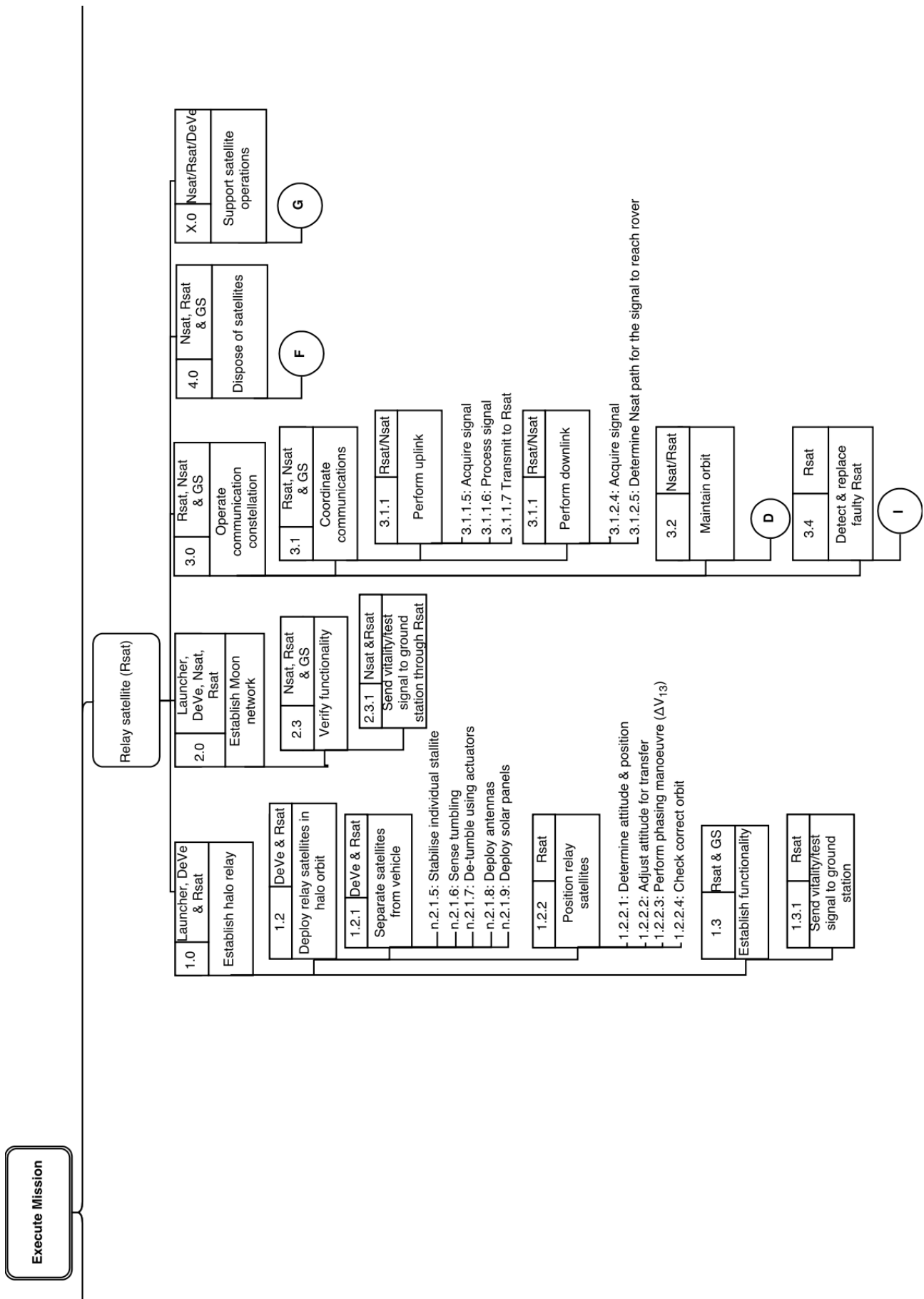


Figure B.2: Functional breakdown structure. Part 2 of 3.



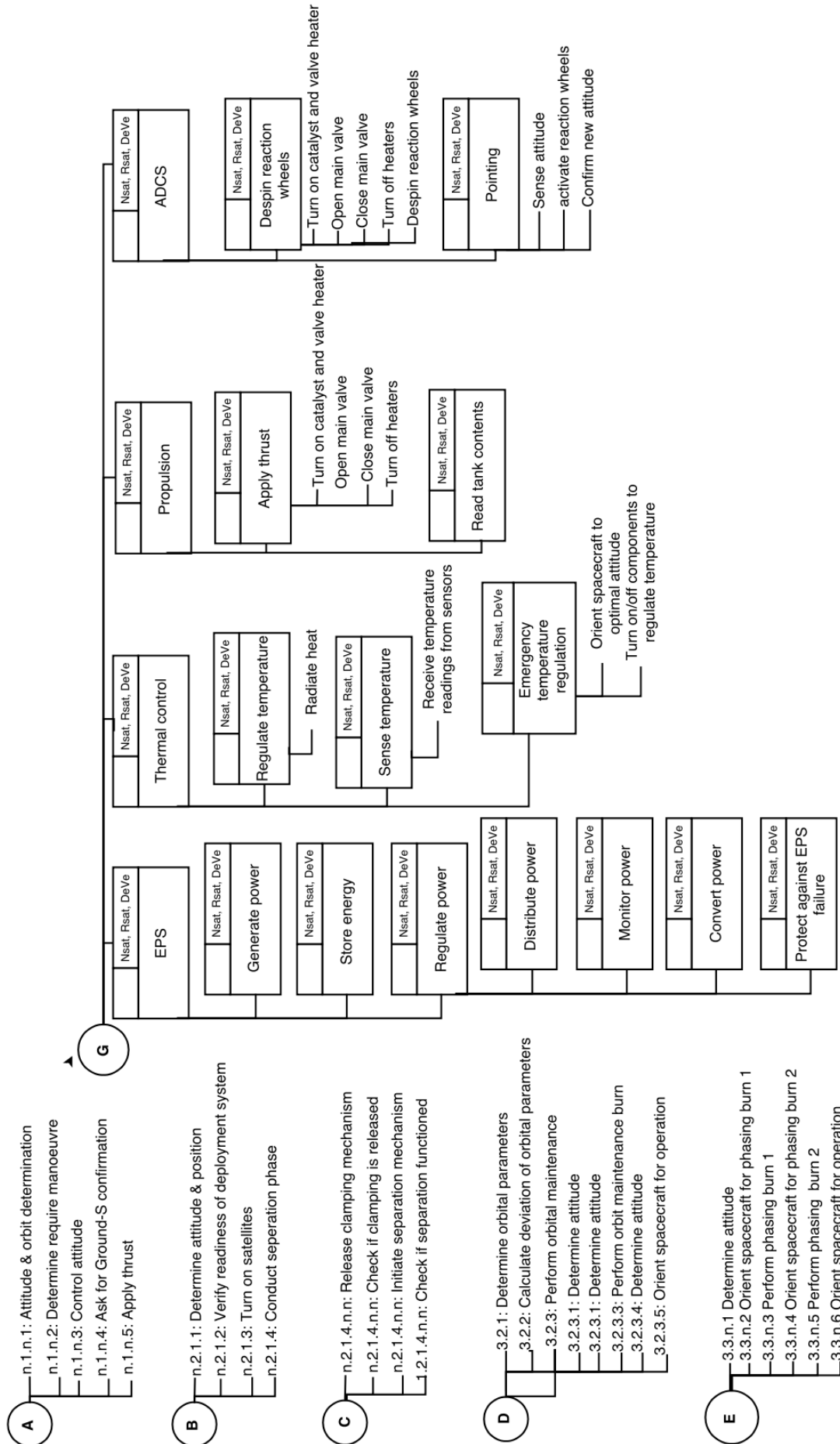


Figure B.4: Functional breakdown structure sub-groups. Part 1 of 2.

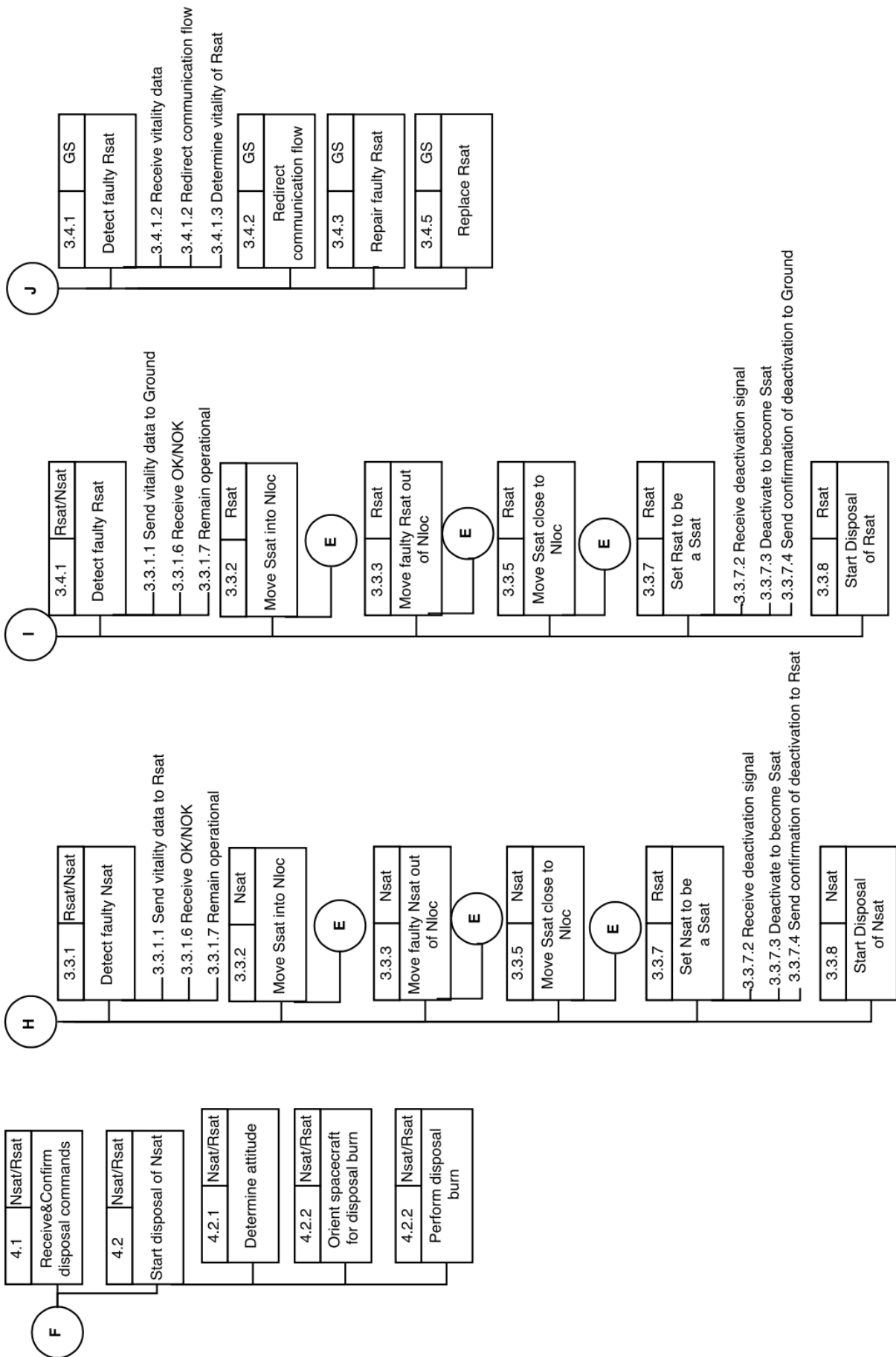


Figure B.5: Functional breakdown structure sub-groups. Part 2 of 2.



TECHNICAL RISK REGISTER

#	Risk Event	Consequence	Likelihood	Effect	Mitigation Strategy
L1	Launcher fails/ explodes.	Mission failure.	Negligible	Catastrophic	Insure payload through space insurance contract.
L2	Structural failure of payload due to launch loads.	Mission failure.	Likely	Catastrophic	Assess the structural limitations of the payload and redesign if necessary. Insure payload through space insurance contract.
L3	Launch window missed.	Launch and time to establish operational communication network delayed. Project costs will increase and time to ROI increases.	Moderate	Marginal	Insure project for costs associated to launch delays. Determine multiple launch dates /window ahead of schedule to increase flexibility.
L4	Gapping in deployment structure due to an incorrect balance between preloading and launch loads.	Induced vibrations and axial loads on satellites and DeVe with the potential to cripple payload and damage subsystems.	Moderate	Catastrophic	Use a deployment mechanism that minimizes the chance of gapping such as a V-band.
T1.1	Subsystems significantly damaged by space radiation.	Payload and other systems are more susceptible to malfunction.	Moderate	Catastrophic	Design DeVe to provide additional protection from the harsh environment on long trajectories.
T1.2	Miscalculated trajectory models.	DeVe overshoots specified destination.	Negligible	Catastrophic	Establish corrective measures in case of trajectory deviation.
T1.3	Miss maneuver window.	New transfer trajectory needs to be determined, requiring more $\Delta V$ and mission is delayed.	Moderate	Catastrophic	
T1.4	Slight deviations in the trajectory.	Increased amount of $\Delta V$ required for proper orbital insertion.	Likely	Catastrophic	Design alternate trajectories in case maneuver window is missed such to minimize the required $\Delta V$ . Dynamically update the trajectory of vehicle during the transfer if/when needed. Account for extra propellant onboard the DeVe in the case of additional corrective maneuvers. The sizing of the propellant subsystem will thus be altered and should be accounted for when sizing other subsystem, which might be affect as well as the internal layout of the DeVe.
T1.5	Trans-Lunar-insertion missed.	The DeVe will have to correct for the trajectory deviation.	Unlikely	Critical	
T1.6	Relay satellites miss their insertion.	Relay satellites and their DeVe will have to correct the trajectory. The entire communication network will be unstable.	Moderate	Catastrophic	
T1.7	Risk of missing the Earth-Moon system.	A large amount of $\Delta V$ will be needed for correction.	Unlikely	Catastrophic	
T1.8	Missing Sun-Earth L2 halo orbit.		Unlikely	Catastrophic	
T1.9	Orbit insertion from direct transfer missed.	New transfer trajectory needs to be determined, requiring more $\Delta V$ and mission is delayed.	Unlikely	Catastrophic	
T1.10	DeVe's propellant valve closes.	Insertion burn results in lower $\Delta V$ . Relay satellites will not end up in a halo orbit.	Negligible	Catastrophic	Ensure there is a dedicated power supply for this specific maneuver.
T1.11	Asteroid impact.		Negligible	Critical	Constantly monitor potentially hazardous asteroids and space debris.
T1.12	Damage due to space debris.	Physical damage to the system	Negligible	Critical	
D1	Deployment mechanism is blocked.	Satellites cannot be deployed.	Moderate	Catastrophic	Implement redundant deployment mechanism.

<b>D2</b>	Deployment mechanism activates ahead of schedule.	Satellites deploy prematurely.	<b>Moderate</b>	<b>Critical</b>	Design satellites and alternate trajectories such that they can still reach their destination on their own.
<b>D3</b>	Software malfunction in DeVe.	Satellites cannot be deployed until software bug is rectified.	<b>Likely</b>	<b>Marginal</b>	Create bug-detecting software so the problem can be quickly resolved, perhaps even automatically.
<b>D4</b>	Satellites fail to activate.	Satellites cannot be deployed and form communication system.	<b>Unlikely</b>	<b>Catastrophic</b>	Include redundant power system in the DeVe to hard-start the satellites.
<b>P1</b>	Solar array cannot deploy.	Lack of power to other satellite systems.	<b>Unlikely</b>	<b>Critical</b>	Use multiple power sources such as batteries as redundancy as well as additional deployment mechanisms.
<b>O1</b>	Thermal foil is damaged.	Required thermal environment cannot be easily maintained	<b>Unlikely</b>	<b>Marginal</b>	Use passive thermal control amount others to ensure sufficient thermal redundancy.
<b>O2</b>	Lost communication packages.	Cannot reassemble received signal.	<b>Unlikely</b>	<b>Marginal</b>	Ensure that the satellite keeps a copy of the signal for a set time to communicate it again later or relay it to another satellite in the constellation, which can pass it on.
<b>O3</b>	Inaccurate attitude and orbit determination.	Orbital positioning and pointing accuracy are conceded. Communication network is not as reliable.	<b>Unlikely</b>	<b>Critical</b>	Ensure that the calibration of the ADCS is verified once in space. Ensure sufficient sensor redundancy of the ADCS.
<b>O4</b>	Relay malfunction.	Entire communication network becomes inert.	<b>Moderate</b>	<b>Catastrophic</b>	Ensure that there are sufficient redundant relay satellites in place.
<b>O5</b>	Higher-than-anticipated lag time between mission control and DeVe.	Satellites deploy with a minute delay.	<b>Unlikely</b>	<b>Marginal</b>	Design deployment models that take into account slight delays such that the satellites can compensate accordingly.
<b>O6</b>	Multiple satellite failure in view of rover on surface.	Broken communication between rover on Lunar surface and constellation (and hence Earth).	<b>Moderate</b>	<b>Catastrophic</b>	Ensure there is sufficient satellite redundancy in sight of the rover.
<b>O7</b>	Solar interference from relay to Earth	Communication signal disrupted when sent to and from Earth.	<b>Moderate</b>	<b>Critical</b>	Design communication system to utilize frequencies that won't be heavily disrupted the Sun's charged particles.
<b>O8</b>	Excessive solar cell degradation.	No sufficient power supply for the designed operation.	<b>Unlikely</b>	<b>Marginal</b>	Size EPS using conservative power margins.
<b>O9</b>	Overall EPS system has more losses than expected.		<b>Moderate</b>	<b>Marginal</b>	
<b>O10</b>	Only Nsat in view relay fails & the adjacent orbital plane has 1 Nsat in view of relay that is already servicing a rover.	System is not able to service the rover	<b>Negligible</b>	<b>Critical</b>	Phase-in spare satellites to make them assist in operations/communications.

<b>O11</b>	Nsat not placed into correct disposal orbit.	Rsat cannot be controlled and poses risk of collision with other Rsats. Extra required effort in tracking.	<b>Unlikely</b>	<b>Marginal</b>	Design alternate disposal orbits and account for extra $\Delta V$ for correction.
<b>O12</b>	Rsat not put in proper disposal orbit.	Rsat cannot be controlled and poses risk of collision with other Rsats.	<b>Unlikely</b>	<b>Marginal</b>	Track disposed satellites such that they can be maneuvered to avoid collisions.
<b>O13</b>	An Nsat in disposal orbit collides with an active or spare Nsat.	Loss of 2 Nsats and creation of debris in disposal & Nsat orbits.	<b>Unlikely</b>	<b>Critical</b>	Maintenance $\Delta V$ is designed as the worst-case over a 10 day period. Plan alternative maneuvers as contingency.
<b>O14</b>	Orbit maintenance maneuver is delayed.	Maneuver is made at a different time (less efficient). Required $\Delta V$ increases.	<b>Likely</b>	<b>Marginal</b>	The orbits will be designed to ensure that collisions to not occur.
<b>O15</b>	Spare Nsat collides with Nsat.	Loss of 2 Nsats + creation of Debris in two Nsat orbits.	<b>Unlikely</b>	<b>Critical</b>	Split battery physically in cell groups with one redundant group to reduce risk.
<b>TD1</b>	Battery catches fire/explodes in DeVe.	Communications cut: mission failure.	<b>Unlikely</b>	<b>Catastrophic</b>	Actively monitor the current to disconnect any short circuit behavior before damage.
<b>TD2</b>	Short circuits in DeVe.	Subsystem failure or EPS failure.	<b>Unlikely</b>	<b>Catastrophic</b>	Add an angular velocity component during the deployment to help separate the deployed satellites.
<b>DP1</b>	DeVe sets satellites on collision path.	2-6 satellites are destroyed	<b>Unlikely</b>	<b>Critical</b>	Implement sequential deployment procedures and according phasing strategies to ensure collisions will not occur.
<b>DP2</b>	DeVe collides with deployed satellites.	2 to 24 satellites are destroyed.	<b>Unlikely</b>	<b>Catastrophic</b>	Use Nano-conductive materials to shield the structure from space radiation.
<b>DO1</b>	Structural degradation due to radiation (including composite delamination).	Satellite structure will become weakened	<b>Unlikely</b>	<b>Critical</b>	Use tried-and-true propellant tanks that have shown a high reliability in cubesat applications.
<b>DO2</b>	Propulsion tank ruptures.	Satellite damaged through pressurized rupture leading to potential satellite failure.	<b>Unlikely</b>	<b>Marginal</b>	Assess constellation design and make (constellation relative RAA) changes when needed.
<b>PO1</b>	Nsat finds itself in an orbit with $\beta = 0$ .	No incoming power. Maximum operation of ~2 orbits.	<b>Unlikely</b>	<b>Critical</b>	Use flight-proven batteries with appropriate insulation/shielding.
<b>PO2</b>	Battery catches fire/explodes in Nsat/Rsat.	Batteries become unusable with possible damage to other subsystems.	<b>Unlikely</b>	<b>Marginal</b>	Actively monitor the current to disconnect any short circuit behavior before damage infliction if needed.
<b>PO3</b>	Short circuit in satellite.	Subsystem failure or EPS failure.	<b>Unlikely</b>	<b>Marginal</b>	Ensure sufficient subsystem redundancy in Rsat.
<b>PO4</b>	An Rsat fails.	Not every orbital plane can be serviced. 1 or more rovers are not serviced. Long downtime.	<b>Unlikely</b>	<b>Critical</b>	

<b>PO5</b>	An Nsat fails.	There is one less satellite available for sending signals to Rsats and/or other Nsats.	<b>Moderate</b>	<b>Marginal</b>	Ensure that there are 2 Nsats in view as well as spares. There will be a downtime of a few minutes to re-path the new link.
<b>PO6</b>	Nsat collides with an Nsat.	Loss of 2 Nsats + creation of Debris in two Nsat orbits.	<b>Unlikely</b>	<b>Critical</b>	The orbits will be designed to ensure that collisions do not occur.
<b>PO7</b>	Rsat collides with an Rsat.	Loss of 2 Rsats and creation of debris in disposal & Nsat orbits.	<b>Unlikely</b>	<b>Critical</b>	
<b>PO8</b>	Thruster malfunctions.	Can no longer fire thruster. If main engine system is affected: harder to complete maneuvers.	<b>Unlikely</b>	<b>Marginal</b>	Implement redundant thrusters and use flight proven thrusters. Also make sure to have extra propellant onboard
<b>PO9</b>	1 attitude thruster fails.	Dumping momentum of reactions wheels becomes more difficult and time-consuming.	<b>Likely</b>	<b>Marginal</b>	Implement and position redundancy thrusters to assist with the dumping of the momentum and lack of maneuverability.
<b>A1</b>	Misalignment of thrusters.	Increased amount of $\Delta V$ required while conducting appropriate maneuvers.	<b>Unlikely</b>	<b>Critical</b>	Ensure that the design of the satellite is such that the thrusters are protected from potential external loads, which could lead to their misalignment.
<b>A2</b>	EPS battery degrades faster than anticipated.	No sufficient power supply for the designed operation.	<b>Unlikely</b>	<b>Marginal</b>	Size EPS using conservative power margins.
<b>A3</b>	Solar cell or its bypass diode malfunctions.	Reduced solar array performance or disruption of power supply.	<b>Moderate</b>	<b>Marginal</b>	Apply redundant circuitry in solar array and account for solar cell margin.
<b>A4</b>	Wire/component burnout.	Some subsystem will no longer work.	<b>Moderate</b>	<b>Marginal</b>	Ensure redundancy in wire system.
<b>A5</b>	Thruster misfires.	Maneuver is made at a different time. Required $\Delta V$ increases & vehicle can start spinning if only 1 thruster misfires.	<b>Unlikely</b>	<b>Marginal</b>	Implement redundant thrusters and use flight proven thrusters. Also make sure to have extra propellant onboard
<b>A6</b>	1 reaction wheel fails.	Extra work has to be done by the other 2 reaction wheels in cooperation.	<b>Likely</b>	<b>Critical</b>	Install at least 1 redundant reaction wheels.
<b>A7</b>	2 reaction wheels fail.	Reduction in pointing accuracy of the satellite, which might cause the link to be lost. Need to switch to coarse pointing mode.	<b>Unlikely</b>	<b>Critical</b>	Install at least 1 redundant reaction wheels. Implement measures to handle dual wheel failure from flight control.
<b>A8</b>	Failure to reignite engines.	The satellites are not able to achieve their designed orbits. Insertion maneuvers are no longer possible.	<b>Unlikely</b>	<b>Catastrophic</b>	Implement redundant thrusters and use flight proven thrusters with a high TRL.

# D

## REQUIREMENTS

The table below shows the requirement identification, a description of the requirement, how it will be verified that the design meets this requirement and a compliance check, including a reference to a relevant section of the report, where the design is shown to comply with the requirement. If the requirement compliance is not investigated yet or cannot be proven at this time, the compliance box contains a "u".

Table D.1: List of requirements

Requirement ID	Description	Verification Method	Compliance
IRIS-01	The system cost shall not exceed 1 billion Euros .	Demonstration	✓ (16.1)
IRIS-02	The system shall be operational before the start of 2030.	Demonstration	✓ (12.2)
IRIS-03	The system shall only make use of rare Earth materials if there is no feasible alternative is available.	Review of design	✓ (18)
IRIS-04	The system shall comply with international space laws.	Review of design	u
IRIS-05	The system shall ensure a lag time of equal or less than 3 seconds between Earth operators and objects on the Moon's surface.	Review of design	✓ (5)
IRIS-06	The system shall be able to service at least 10 rovers at the same time.	Review of design	✓ (4)
IRIS-NLAU-01	The launcher shall be able to carry at least 3,600 kg of payload mass into a trans lunar injection orbit.	Similarity check	✓ (2.3)
IRIS-NLAU-02	The launcher shall be available for launch from in September 2029.	Review of design	✓ (2.3)
IRIS-NLAU-03	The launcher shall have an injection accuracy resulting in a maximum correction needed of $40 \text{ ms}^{-1}$ over the whole trajectory.	Similarity check	✓ (2.3)
IRIS-NLAU-04	The launcher shall be able to apply a total $\Delta V$ of at least $13,000 \text{ ms}^{-1}$ .	Similarity check	✓ (2.3)
IRIS-NLAU-05	The launcher shall be able to store two seperate payloads in the payload bay.	Similarity check	✓ (2.3)
IRIS-RLAU-01	The launcher shall be able to carry at least 300 kg of mass into a low energy ballistic transfer to The L1 point of the Earth-Moon system.	Similarity check	✓ (2.3)
IRIS-RLAU-02	The launcher shall be available for launch in July 2028.	Review of design	✓ (2.3)
IRIS-RLAU-03	The launcher shall have an injection accuracy resulting in a maximum correction needed of $40 \text{ ms}^{-1}$ over the whole trajectory.	Similarity check	✓ (2.3)
IRIS-RLAU-04	The launcher shall be able to apply a total $\Delta V$ of at least $13,000 \text{ ms}^{-1}$ .	Similarity check	✓ (2.3)
IRIS-NDEVE-01	The deployment vehicle shall be able to carry at least a 358 kg kg payload.	Review of design	✓ (8.8)
IRIS-NDEVE-02	The deployment vehicle shall fit in the Falcon 9 launch bay in the two payload configuration.	Review of design	✓ (8.1)
IRIS-NDEVE-03	The deployment vehicle shall remain stable under the influence of the disturbance loads due to the deployment of the satellites.	Analysis	✓ (8.6)
IRIS-NDEVE-04	The deployment vehicle shall be capable of de-orbiting from the selected orbit.	Analysis	✓ (8.5)
IRIS-NDEVE-ADCS-01	The ADCS shall have a pointing accuracy of at least $0.94^\circ$ .	Simulation	✓ (8.6)
IRIS-NDEVE-ADCS-02	The ADCS shall have an attitude determination accuracy of at least $0.94^\circ$ .	Simulation	✓ (8.6)
IRIS-NDEVE-ADCS-03	The ADCS shall be able to provide a slew rate of at least $10^\circ$ in 60 s during normal mission operating mode.	Simulation	✓ (8.6)
IRIS-NDEVE-ADCS-04	The ADCS shall not consume more than 88 W in idle mode.	Test	✓ (8.6)
IRIS-NDEVE-ADCS-05	The ADCS shall not consume more than 420 W during slew manoeuvres.	Test	✓ (8.6)
IRIS-NDEVE-ADCS-06	The ADCS shall have a mass less than or equal to 36 kg.	Test	✓ (8.6)

IRIS-NDEVE-EPS-01	The EPS shall provide 79.13 W continuously at end of life.	Analysis	✓ (8.2)
IRIS-NDEVE-EPS-02	The EPS shall be able to store 66 Wh, at end of life.	Analysis	✓ (8.2)
IRIS-NDEVE-EPS-03	The EPS shall have an overall efficiency of 85 %.	Analysis	✓ (8.2)
IRIS-NDEVE-EPS-04	The EPS shall provide 79.13 W continuously during safe mode.	Test	✓ (8.2)
IRIS-NDEVE-EPS-05	The EPS shall be able to regulate the voltage from 0 V to 28 V.	Test	✓ (8.2)
IRIS-NDEVE-EPS-06	The EPS shall be able to facilitate the power needs of every subsystem.	Test	✓ (8.2)
IRIS-NDEVE-EPS-07	The EPS shall protect other subsystems from EPS failure.	Test	u
IRIS-NDEVE-EPS-08	The EPS shall have a mass less than 10 kg.	Test	✓ (8.2)
IRIS-NDEVE-TT-01	The position of the deployment vehicle shall be determined with an accuracy of less than 50 m.	Analysis	✓ (6.4)
IRIS-NDEVE-CD-01	The communication rate shall be at least 100 kbits <sup>-1</sup> .	Analysis	✓ (5.3)
IRIS-NDEVE-THRM-01	The deployment vehicle shall be able to operate under temperatures from 253 K to 313 K.	Test	✓ (8.7)
IRIS-NDEVE-THRM-02	The thermal control subsystem shall have a mass less than or equal to 22.8 kg.	Test	✓ (10.2)
IRIS-NDEVE-THRM-03	The thermal control subsystem shall not use any power for temperature regulation.	Test	✓ (8.7)
IRIS-NDEVE-PROP-01	The propulsion system shall be able to fit at least 1,130 kg of propellant MMH/MON-3	Test	✓ (8.8)
IRIS-NDEVE-PROP-02	The propulsion system shall be able to apply a total $\Delta V$ of 6,200 ms <sup>-1</sup> .	Analysis	✓ (10.2)
IRIS-NDEVE-PROP-03	The propulsion system shall be able to apply a thrust of at least 4,000 N.	Similarity check	✓ (8.5)
IRIS-NDEVE-PROP-04	The propulsion system shall have a mass less than 29 kg.	Review of design	✓ (8.5)
IRIS-NDEVE-PROP-05	The propulsion system shall use less than 90 W.	Test	✓ (10.2)
IRIS-NDEVE-STR-01	The structure shall be able to withstand loads up to 6 gs of acceleration in longitudinal direction.	Test	✓ (8.8)
IRIS-NDEVE-STR-02	The structure shall be able to withstand loads up to 2 gs of acceleration in lateral direction.	Test	✓ (8.8)
IRIS-NDEVE-STR-03	The structure shall be able to withstand the shock loads as specified in the Falcon 9 launch catalogue.	Test	✓ (8.8)
IRIS-NDEVE-STR-04	The structure shall be able to withstand the vibrational loads as specified in the Falcon 9 launch catalogue.	Test	✓ (8.8)
IRIS-NDEVE-STR-05	The structure shall have a mass less than or equal to 95.9 kg kg.	Test	✓ (8.8)
IRIS-NCON-01	The constellation shall provide full coverage of rovers on the Moon's surface without any system failure in five years with a reliability of at least 97.5 %.	Simulation	✓ (4.9)
IRIS-NCON-02	A Nsat shall not collide with other satellites after deployment.	Simulation	✓ (8.9, 4.3)
IRIS-NCON-03	The Nsat orbit shall require an orbit maintenance of no more than 75 ms <sup>-1</sup> $\Delta V$ per year.	Simulation	✓ (4.6)
IRIS-NCON-04	A non-functioning Nsat shall be replaced within 6 months.	Analysis	✓ (4.7)
IRIS-NCON-05	Debris originating from Nsats shall be removed from its orbit around the Moon within 50 years.	Simulation	✓ (4.7)
IRIS-NCON-05	The constellation shall allow Slocs for each Nsat without compromising the constellation performance.	Analysis	✓ (4.3)
IRIS-NSAT-01	A Nsat shall not collide with other satellites during deployment.	Simulation	✓ (8.9)
IRIS-NSAT-ADCS-01	The ADCS shall have a pointing accuracy of at least 8 arcsec during normal mission operating mode.	Analysis	✓ (6.6)
IRIS-NSAT-ADCS-02	The ADCS shall not consume more than 47 W as peak consumption.	Test	✓ (10.2)
IRIS-NSAT-ADCS-03	The ADCS shall have a mass less than or equal to 3.00 kg.	Review of design	✓ (10.2)
IRIS-NSAT-ADCS-04	The ADCS shall be able to provide a slew rate of at least 7.5 deg/s during normal mission operating mode.	Analysis	✓ (6.6)
IRIS-NSAT-ADCS-05	The ADCS shall be able to determine attitude with an accuracy of at least 7 arcsec during normal mission operating mode.	Analysis	u
IRIS-NSAT-EPS-01	The EPS shall provide continuous 28.5 Wat end of life.	Analysis	✓ (6.2)
IRIS-NSAT-EPS-02	The EPS shall be able to store 172.7 Wh at end of life.	Analysis	✓ (6.2)
IRIS-NSAT-EPS-03	The EPS shall have an overall efficiency of 65 % .	Test	✓ (6.2)
IRIS-NSAT-EPS-04	The EPS shall have a mass less than 4 kg.	Test	✓ (6.2)
IRIS-NSAT-EPS-05	The EPS shall provide 28.5 W during safe mode.	Test	✓ (6.2)
IRIS-NSAT-EPS-06	The EPS shall be able to regulate the voltage up to 28 V.	Test	✓ (6.2)

IRIS-NSAT-EPS-07	The EPS shall be able to facilitate the power needs of the remaining subsystems.	Review of Design	✓ (6.2)
IRIS-NSAT-TT-01	The field of view of the Moon pointing antenna shall be at least 90°.	Simulation	✓ (5.1)
IRIS-NSAT-TT-02	Intra-network communication shall be possible with a datarate of 1,000 kbits <sup>-1</sup> .	Analysis	✓ (5.3)
IRIS-NSAT-TT-03	Nsat shall be able to send data to a Rsat with a datarate of 550 kbits <sup>-1</sup> .	Analysis	✓ (5.3)
IRIS-NSAT-TT-04	Nsats shall be able to receive control data from Rsats at a datarate of 100 kbits <sup>-1</sup> .	Analysis	✓ (5.3)
IRIS-NSAT-TT-05	Nsat shall be able to send control data to a vehicle on the Moon's surface with a datarate of 100 kbits <sup>-1</sup> .	Analysis	✓ (5.3)
IRIS-NSAT-TT-06	Nsat shall be able to receive data from a vehicle on the Moon's surface with a datarate of 500 kbits <sup>-1</sup> .	Analysis	✓ (5.3)
IRIS-NSAT-TT-07	Nsats shall have a bit error rate of $10 \times 10^{-6}$ or lower.	Test	✓ (5.3)
IRIS-NSAT-TT-08	The rovers on the lunar surface shall transmit with an EIRP of 17 dBW.	Analysis	✓ (5.3)
IRIS-NSAT-TT-09	The Rsat pointing antenna shall have a beamwidth of at least 5°.	Simulation	✓ (5.1)
IRIS-NSAT-TT-10	The Nsat antenna for receiving rover data shall have a receiver gain of at least 13 dB.	Test	✓ (5.3)
IRIS-NSAT-TT-11	The Nsats shall be able to send housekeeping data to other Nsats.	Analysis	✓ (5.3)
IRIS-NSAT-CDH-01	The C&DH subsystem shall be able to process at least 220000 instructions per second.	Test	✓ (6.3)
IRIS-NSAT-CDH-02	The C&DH subsystem shall be equipped with a CPU of at least 10 MHz processing speed.	Test	✓ (6.3)
IRIS-NSAT-CDH-03	The Nsat shall have a clock with a Allan deviation of $10 \times 10^{-9}$ at 1 s.	Test	✓ (6.4)
IRIS-NSAT-THRM-01	The thermal control subsystem shall keep the spacecraft in the range of 253 K to 323 K. Excluding solar panels.	Simulation	✓ (6.7)
IRIS-NSAT-THRM-02	The thermal control subsystem shall not use any power for temperature regulation.	Analysis	✓ (6.7)
IRIS-NSAT-THRM-03	The thermal control subsystem shall have a mass less than 1 kg.	Test	✓ (6.7)
IRIS-NSAT-THRM-04	The thermal control subsystem shall be able to operate in low-energy mode.	Test	✓ (6.7)
IRIS-NSAT-PROP-01	The propulsion subsystem shall perform each orbit correcting burn within a burn time of 1,000 s throughout its lifetime.	Test	✓ (6.5) (4.6)
IRIS-NSAT-PROP-02	The propulsion subsystem shall be able to supply a total $\Delta V$ of at least 230 m s <sup>-1</sup> .	Test	✓ (6.5)
IRIS-NSAT-PROP-03	The propulsion subsystem shall be able to give a thrust of at least 1 N.	Test	✓ (6.5)
IRIS-NSAT-PROP-04	The propulsion subsystem shall have a specific impulse in vacuum larger than 200 s.	Test	✓ (6.5)
IRIS-NSAT-PROP-05	The propulsion subsystem shall not use more than 40 W of power during operations.	Test	✓ (6.5)
IRIS-NSAT-PROP-06	The propulsion subsystem shall have a mass less than or equal to 2 kg.	Test	✓ (6.5)
IRIS-NSAT-PROP-07	The propulsion subsystem shall be able to relight after the satellite has been in low-energy mode.	Test	u
IRIS-NSAT-STR-01	The primary structure shall be able to withstand up to 2 gs of acceleration in the longitudinal direction.	Test	✓ (6.8)
IRIS-NSAT-STR-02	The primary structure shall be able to withstand up to 6 gs of acceleration in the lateral direction.	Test	✓ (6.8)
IRIS-NSAT-STR-03	The structure shall be able to withstand the shock loads as specified in the Falcon 9 launch catalogue.	Test	✓ (6.8)
IRIS-NSAT-STR-04	The structure shall be able to withstand the vibrational loads as specified in the Falcon 9 launch catalogue.	Test	✓ (6.8)
IRIS-NSAT-STR-05	The structure shall have a radiation shielding around the C&DH subsystem with a minimum area density of 0.5 g cm <sup>-2</sup> .	Review of Design	✓ (6.3)
IRIS-NSAT-STR-06	The Nsat structure shall have mass less than 2.87 kg.	Test	✓ (10.2)
IRIS-RCON-01	A Rsat shall not collide with other satellites during operation.	Simulation	✓ (4.4)

IRIS-RCON-02	The Rsat orbit shall have a maximum orbit maintenance of $250 \text{ ms}^{-1} \Delta V$ per year.	Simulation	✓ (4.6)
IRIS-RCON-03	Debris originating from Rsats shall be removed from its orbit within 50.	Simulation	✓ (4.7)
IRIS-RCON-04	A Rsat shall not collide with other satellites after deployment.	Simulation	u
IRIS-RDEVE-01	The deployment vehicle shall be able to carry at least a 186.8 kg payload.	Review of design	✓ (9.8)
IRIS-RDEVE-02	The deployment vehicle shall fit in the PSLV launch bay.	Review of design	✓ (9)
IRIS-RDEVE-03	The deployment vehicle shall remain stable under the influence of the disturbance loads due to the deployment of the satellites.	Analysis	✓ (9.6)
IRIS-RDEVE-ADCS-01	The ADCS shall have a pointing accuracy of at least $0.243^\circ$ .	Simulation	✓ (9.6)
IRIS-RDEVE-ADCS-02	The ADCS shall have an attitude determination accuracy of at least $0.243^\circ$ .	Simulation	✓ (9.6)
IRIS-RDEVE-ADCS-04	The ADCS shall not consume more than 46.3 W in idle mode.	Test	✓ (10.2)
IRIS-RDEVE-ADCS-05	The ADCS shall not consume more than 65 W during slew manoeuvres.		✓ (9.6)
IRIS-RDEVE-ADCS-06	The ADCS shall have a mass less than or equal to 11.1 kg.	Test	✓ (9.6)
IRIS-RDEVE-EPS-01	The EPS shall provide 76.30 W continuously at end of life.	Analysis	✓ (9.2)
IRIS-RDEVE-EPS-02	The EPS shall be able to store 20 Wh at end of life.	Analysis	✓ (9.2)
IRIS-RDEVE-EPS-03	The EPS shall have an overall efficiency of 85 %.	Analysis	✓ (9.2)
IRIS-RDEVE-EPS-04	The EPS shall provide 76.30 W during safe mode.	Test	✓ (9.2)
IRIS-RDEVE-EPS-05	The EPS shall be able to regulate the voltage from 0 V to 28 V.	Test	✓ (9.2)
IRIS-RDEVE-EPS-06	The EPS shall be able to facilitate the power needs of the remaining subsystems.	Test	✓ (9.2)
IRIS-RDEVE-EPS-07	The EPS shall protect other subsystems from EPS failure.	Test	✓ (6.2)
IRIS-RDEVE-EPS-08	The EPS shall have a mass less than or equal to 4 kg.	Test	✓ (9.2)
IRIS-RDEVE-TT-01	The position of the deployment vehicle shall be determined with an accuracy of less than 50 m.	Analysis	✓ (6.4)
IRIS-RDEVE-TT-02	The communication rate shall be at least $100 \text{ kbit s}^{-1}$ .	Analysis	✓ (5.3)
IRIS-RDEVE-TT-03	The operation lag time shall be less than 3 s.	Analysis	u
IRIS-RDEVE-THRM-01	The deployment vehicle shall be able to operate under temperatures from 253 K to 313 K.	Test	✓ (10.2)
IRIS-RDEVE-THRM-02	The thermal control subsystem shall have a mass less than or equal to 12.7 kg.	Test	✓ (10.2)
IRIS-RDEVE-THRM-03	The thermal control subsystem shall not use any power for temperature regulation.	Test	✓ (10.2)
IRIS-RDEVE-PROP-01	The propulsion system shall be able to fit at least 20.7 kg of hydrazine.	Test	✓ (9.8)
IRIS-RDEVE-PROP-02	The propulsion system shall be able to apply a total $\Delta V$ of at least $240.23 \text{ m s}^{-1}$ .	Analysis	✓ (9.5)
IRIS-RDEVE-PROP-03	The propulsion system shall be able to apply a thrust of at least 88 N.	Similarity check	✓ (9.5)
IRIS-RDEVE-PROP-04	The propulsion system shall have a mass less than or equal to 7.7 kg.	Review of design	✓ (9.5)
IRIS-RDEVE-PROP-05	The propulsion system shall use less than or equal to 120 W.	Test	✓ (9.5)
IRIS-RDEVE-STR-01	The structure shall be able to withstand loads up to 6.5 gs of acceleration in longitudinal direction.	Test	✓ (9.8)
IRIS-RDEVE-STR-02	The structure shall be able to withstand loads up to 1.1 gs of acceleration in lateral direction.	Test	✓ (9.8)
IRIS-RDEVE-STR-03	The structure shall be able to withstand the shock loads as specified in the PSLV launch catalogue.	Test	✓ (9.8)
IRIS-RDEVE-STR-04	The structure shall be able to withstand the vibrational loads as specified in the PSLV launch catalogue.	Test	✓ (9.8)
IRIS-RDEVE-STR-05	The structure shall have a mass less than or equal to 21.07 kg.	Test	✓ (9.8)
IRIS-RSAT-01	A Rsat shall not collide with other satellites.	Simulation	u
IRIS-RSAT-ADCS-01	The Rsat shall have a pointing accuracy of at least $0.1^\circ$ during normal mission operating mode.	Analysis	u
IRIS-RSAT-ADCS-02	The ADCS shall use less than 57 W at any operating mode.	Test	✓ (10.2)
IRIS-RSAT-ADCS-03	The ADCS shall provide a torque of 0.025 N m along each axis in normal mission operating mode.	Test	
IRIS-RSAT-ADCS-04	The ADCS shall have no single points of failure.	Review of Design	✓ (7.6)

IRIS-RSAT-ADCS-05	The ADCS shall be able to determine attitude with an accuracy of at least 7 arcsec along each axis in normal mission operating mode.	Test	u
IRIS-RSAT-ADCS-06	The ADCS shall have a mass less than 5 kg.	Test	✓ (10.2)
IRIS-RSAT-EPS-01	The EPS shall provide 94 W at end of life.	Test	✓ (7.2)
IRIS-RSAT-EPS-02	The EPS shall be able to store at least 500 Wh at end of life.	Analysis	✓ (7.2)
IRIS-RSAT-EPS-03	The EPS shall have an overall efficiency of 85 %.	Test	✓ (7.2)
IRIS-RSAT-EPS-04	The EPS shall have a mass less than 8 kg.	Test	✓ (7.2)
IRIS-RSAT-EPS-05	The EPS shall provide 94 W during safe mode.	Test	✓ (7.2)
IRIS-RSAT-EPS-06	The EPS shall be able to facilitate the power needs of the remaining subsystems.	Simulation	✓ (7.2)
IRIS-RSAT-EPS-07	The EPS shall protect other subsystems from EPS failure.	Test	u
IRIS-RSAT-TT-01	The Rsat shall be able to send data to Earth at a datarate of 2,000 kbits <sup>-1</sup> .	Analysis	✓ (5.3)
IRIS-RSAT-TT-02	The Rsat shall be able to receive data from Earth at a datarate of 500 kbits <sup>-1</sup> .	Analysis	✓ (5.3)
IRIS-RSAT-TT-03	The Rsat shall be able to send data to a Nsat with a data rate of at least 100 kbits <sup>-1</sup> .	Analysis	✓ (5.3)
IRIS-RSAT-TT-04	The Rsat shall be able to receive data from a Nsat with a datarate of at least 550 kbits <sup>-1</sup> .	Analysis	✓ (5.3)
IRIS-RSAT-TT-05	The Rsats shall have a bit error rate of $10 \times 10^{-6}$ or less	Test	✓ (5.3)
IRIS-RSAT-TT-06	The Rsats shall have pointing losses no more than 1 dB.	Analysis	✓ (5.3)
IRIS-RSAT-CDH-01	The C&DH subsystem shall be able to process at least 361,000 instructions per second.	Test	✓ (7.3)
IRIS-RSAT-CDH-02	The C&DH subsystem shall be equipped with a CPU of at least 20 MHz processing speed.	Test	✓ (7.3)
IRIS-RSAT-CDH-03	The Rsat shall have a clock with an Allan deviation of $10 \times 10^{-9}$ at 1 s or less.	Test	✓ (6.4)
IRIS-RSAT-THRM-01	The thermal control subsystem shall keep the spacecraft between 253 K to 313 K. Excluding solar panels.	Simulation	✓ (7.7)
IRIS-RSAT-THRM-02	The thermal control subsystem shall have a mass less than 1 kg.	Test	✓ (7.7)
IRIS-RSAT-THRM-03	The thermal control subsystem shall not use any power for temperature regulation.	Review of Design	✓ (7.7)
IRIS-RSAT-PROP-01	The propulsion sub-system shall be able to apply a total $\Delta V$ of at least 400 m s <sup>-1</sup> .	Test	✓ (7.5)
IRIS-RSAT-PROP-02	The propulsion sub-system shall be able to deliver a thrust of at least 1 N.	Test	✓ (7.5)
IRIS-RSAT-PROP-03	The propulsion subsystem shall deliver a specific impulse larger than 200 s in vacuum.	Test	✓ (7.5)
IRIS-RSAT-PROP-04	The propulsion subsystem shall not use more than 40 W of power during operations.	Test	✓ (7.5)
IRIS-RSAT-PROP-05	The propulsion subsystem shall perform all correcting burns within a burn time of 1,000 s throughout its lifetime	Simulation	✓ (7.5)
IRIS-RSAT-PROP-06	The propulsion subsystem shall have a mass less than 2 kg.	Test	✓ (7.5)
IRIS-RSAT-STR-01	The Rsat primary structure shall be able to withstand up to 2.0 gs of acceleration in the longitudinal direction of the satellite without failure.	Test	u
IRIS-RSAT-STR-02	The Rsat primary structure shall be able to withstand up to 6.2 gs of acceleration in the lateral direction without failure.	Test	u
IRIS-RSAT-STR-03	The Rsat structure shall be able to withstand the shock loads as specified in the PSLV launch catalogue.	Test	u
IRIS-RSAT-STR-04	The Rsat structure shall be able to withstand the vibrational loads as specified in the PSLV launch catalogue.	Test	u
IRIS-RSAT-STR-05	The Rsat structure shall have a radiation shielding around the C&DH subsystem with a minimum area density of 0.5 g cm <sup>-2</sup> .	Review of Design	u
IRIS-RSAT-STR-06	The Rsat structure shall weigh no more than 6 kg.	Test	✓ (10.2)



## POST-DSE GANTT CHART

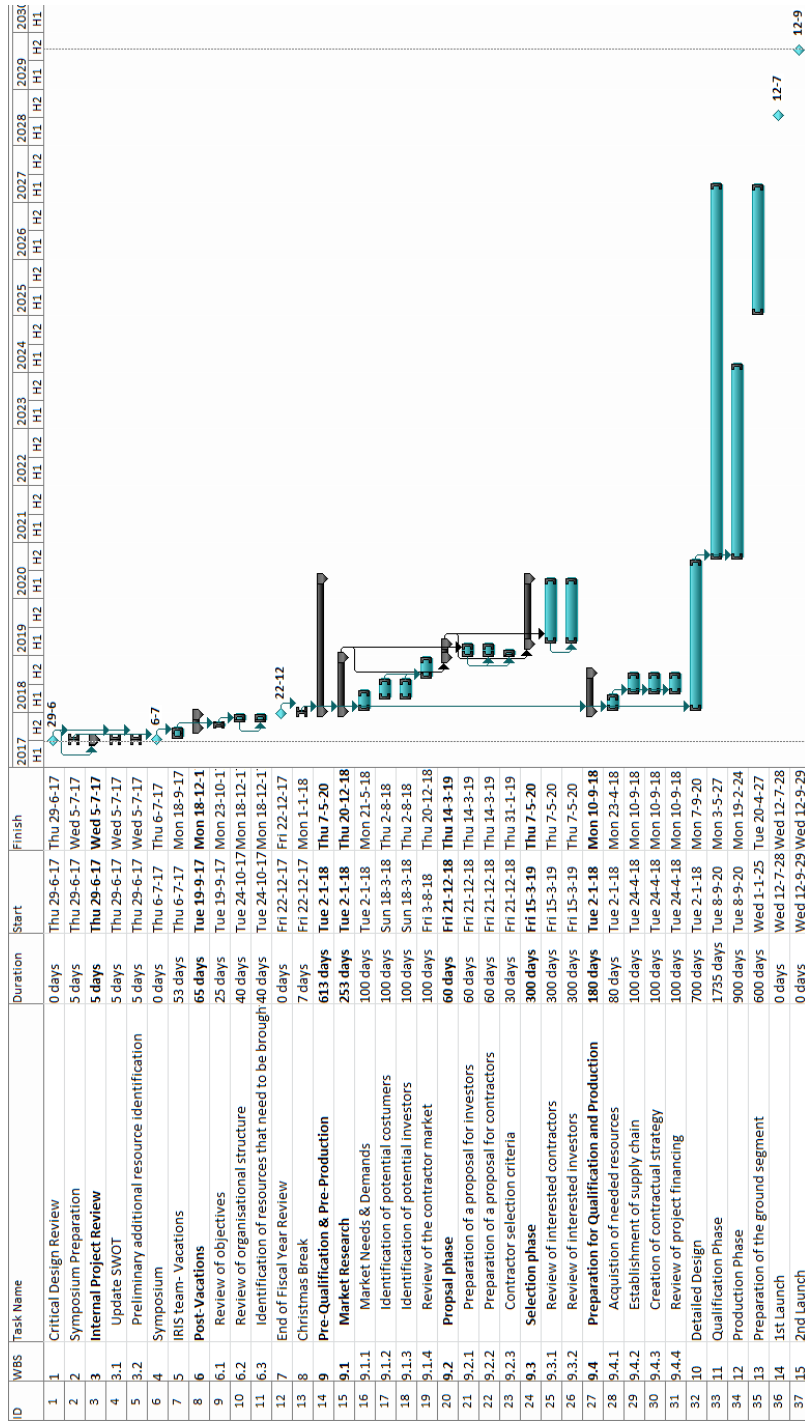


Figure E.1: Gantt chart for the post DSE process